Study of Parameters Influencing Surface Distress of Gears.

By

M. P. Alanou.

Thesis submitted to Cardiff University
For the degree of
Doctor of Philosophy

School of Engineering
Cardiff University

January 2006

ProQuest LLC
789 East Eisenhower Parkway
P.O. Box 1346
Ann Arbor, MI 48106-1346

DECLARATION

This work has not been previously been accepted in substance for any degree and is not being concurrently submitted in candidature for any degree.

Signed..... 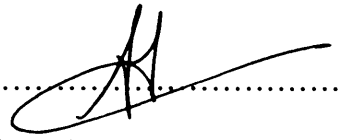 .....(candidate)

Date.....08.05.06.....

STATEMENT 1

This thesis is the result of my own investigations, except where otherwise stated.

Other sources are acknowledged by footnotes giving explicit references. A bibliography is appended.

Signed..... 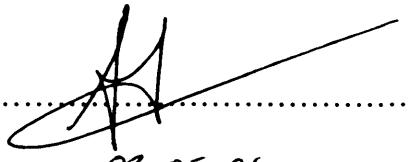 .....(candidate)

Date.....08.05.06.....

STATEMENT 2

I hereby give consent for my thesis, if accepted to be available for photocopying and for inter-library loan, and for the title and summary to be made available to outside organisations.

Signed..... 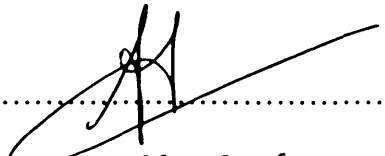 .....(candidate)

Date.....08.05.06.....

Summary.

This thesis aims to provide a better understanding of the influence of various parameters on surface distress in gears. The types of gears of concern in this study are the ones found in gas turbine engines and helicopter gearboxes where tooth contacts are particularly heavily loaded. The work is concerned with the influence of surface roughness, gear material and hard coatings and their effect in reducing the occurrence of scuffing, which is a form of surface distress that can occur under severe conditions of sliding and high temperature. An extensive experimental programme has been carried out using a two-disc machine developed to simulate gas turbine gearing and micro-elastohydrodynamic lubrication (micro-EHL) contacts under realistic conditions of load, speed, surface finish and temperature.

The project involved a large number of disc tests with the aim of quantifying the effects of: a significant improvement in surface finish; the use of a different gear material and surface hardening; and the use of different hard coatings on the resistance to scuffing. This work was conducted using an existing disc machine to extend the work carried out by Patching (1994) who used a single material. The scuffing performance of axially ground (roughness average, Ra = 0.4 μm) case-carburised steel discs was used as a benchmark against which the performance of alternative materials/surfaces could be measured. Different materials and surface conditions were investigated as follows. The ground discs were superfinished to better than Ra = 0.1 μm using a proprietary polishing method. A nitriding steel was used. Two different super-hard coatings were investigated. The main conclusions to be drawn from the work are: the scuffing resistance of nitrided surfaces is superior to case-carburised surfaces, but it is essential to remove the compound layer ("white layer") to achieve durability at high sliding speeds. The benefits of superfinishing are clearly demonstrated; better finish improves the scuffing performance and also gives lower friction and bulk temperatures during operation. Hard coatings show promise, and the triple combination of nitriding, superfinishing and hard coatings gave particularly impressive scuffing resistance in this investigation.

A micro-EHL solver was used to simulate the conditions of the various tests. The solver, which was developed at Cardiff by Professor H P Evans and his associates, can be used to simulate the lubrication of rough surfaces in contact under realistic thin film conditions in which there is significant asperity interaction including momentary "dry" contact. Surface profiles acquired from the discs used in the tests were used as input to the solver. Using the solver a number of objective performance parameters were obtained including high pressure cycling and occurrences of thin or zero film within the nominal contact between the discs. The results of the simulations confirmed the distinct advantages of using smoother surfaces and contributed to an understanding of the way in which hard coatings can lead to surface improvement.

In addition to work on scuffing the project included the design and manufacture of a test rig, complete with data acquisition and control system, for research on contact fatigue and micropitting in particular.

Preface.

This work has been carried out under the supervision of Professor R. W. Snidle to whom the author is most grateful. Without his constant support and enthusiasm and also in my case his patience, this project would not have come to a successful conclusion.

I am also very grateful to Professor H. P. Evans for his constant support and suggestions that kept me going through the darkest hours.

The project was made possible by funding from the U.S. Army Research Laboratory, Glenn Research Center, Cleveland, Ohio to whom I am very grateful especially Dr T. L. Krantz. Manufacture of the discs and the building of the pitting rig were carried out by the workshop staff at the School of Engineering and I particularly want to thank Mr Goff Jordan and Mr Dave Taylor for their expertise and invaluable skills.

Finally I would like to express my gratitude to my family who encouraged me to carry on despite the many changes that were taking place.

Contents.

Notation.

(N.B. Notation is given here for symbols that occur throughout the thesis. Other symbols are defined as they appear.)

α	pressure exponent of viscosity
a	semi-major axis of the contact ellipse
β	angle between the start of the involute curve and the angular position of the base circle
b	semi-minor axis of the contact ellipse
Ca	tooth relief width
CVD	Chemical Vapour Deposition
dw	pitch circle diameter
E'	reduced elastic modulus $\frac{2}{E'} = \left(\frac{1-\nu_1^2}{E_1}\right) + \left(\frac{1-\nu_2^2}{E_2}\right)$
E*	reduced elastic modulus (as used by Johnson) $E^* = \left(\frac{1-\nu_1^2}{E_1} + \frac{1-\nu_2^2}{E_2}\right)^{-1}$
Φ	pressure angle
ϕ	rough surface profile height function in Eq. (6.5)
f	influence coefficients in Eq. (6.5)
$\Phi(h)$	fraction of dry contact area whose film thickness *is less than* h
$\Phi(p)$	fraction of dry contact area whose *pressure exceeds* p
FS	Fast Shaft of a rig
γ	pressure coefficient of compressibility for the lubricating oil
h	height or thickness
$\eta(p)$	pressure dependent viscosity
η_0	viscosity of lubricant at atmospheric pressure

h_{cen}	central EHD smooth body film thickness	
h_{min}	minimum EHD smooth body film thickness	
HV	Vickers Hardness	
j,k	mesh point indices in Eq. (6.5)	
λ	lambda ratio	$\lambda = \frac{h_{min}}{\sqrt{R_{q_1}^2 + R_{q_2}^2}}$
λ	pressure coefficient of compressibility for the lubricating oil	
μ	coefficient of friction	
m_n	gear module (normal)	
n	rotational speed	
ν	Poissons ratio	
p	hydrodynamic pressure	
p_0, P_{max}	maximum Hertzian pressure	
PVD	Physical Vapour Deposition	
θ	angular position at the start of the involute curve	
r	current radius	
R	pitch circle radius	
R	radius of relative curvature of contacting cylinders or radii R_1 and R_2	$R = \left(\frac{1}{R_1} + \frac{1}{R_2}\right)^{-1}$
$\rho=\rho(p)$	pressure dependent density	
ρ_0	density at atmospheric pressure	
r_a	addendum circle radius	
R_a	centreline average roughness	
R_b	base circle radius	
R_c	radius of curvature	
R_q	root mean square roughness	

S	non-Newtonian flow factor
SS	Slow Shaft of a rig
σ_Y	yield stress
t	time
τ_0	Eyring shear stress
TAN	Total Acid Number
u	surface speed of body
V	tangential velocity
V_s, U_s	sliding speed
w'	load per unit length
ω, Ω	angular velocity
z	number of teeth
Z	parameter in oil viscosity formula

CHAPTER 1.

The engineering problem and review of past work

1.1 Introduction

The principal objective of this work is to contribute to a better understanding of the various parameters influencing surface distress of gears with particular reference to heavily loaded gear tooth contacts as found in aerospace applications such as those in gas turbine engine accessory gearboxes or helicopter gearboxes. This thesis is concerned with scuffing and the influence of surface finish, hardening process and coatings.

Helicopter gearboxes and gas turbine engine accessory gearboxes span the full range of gearbox transmission challenges facing the engineer. For example in the case of helicopter main gearboxes (MGB), design features usually include high speed multi-engined input, helical stages, spiral bevel and epicyclic reduction stages with a low speed high torque rotor output. The very high rotor head moments of a helicopter impose particular structural challenges in achieving a highly reliable transmission system, where for example the gear box casing has to be designed to minimise the effects of the head deflection in order to achieve better gear life. The helicopter gearbox also incorporates a high power, high integrity tail rotor drive and a low power drive for the accessories. Figure 1.1 is a cross-section drawing of a helicopter MGB for a five metric tonne type helicopter which transmits 850 KW to the main rotor and 300 KW (maximum) to the tail rotor. One could also cite the case of an extreme design solution for the heaviest helicopter in the world where the MGB is driven by two engines capable of delivering 8.5 MW each! Looking at accessory gearboxes (AGB) as found in gas turbine engine and as illustrated in Figure 1.2, their role includes typically two different functions. On the one hand the AGB has to transmit a high static torque in order to start the engine itself. This torque if of the order of 2100 Nm in the case of the Rolls Royce high by-pass ratio Trent engine (500 series), for example. Its other function includes the driving of a number of accessories such as

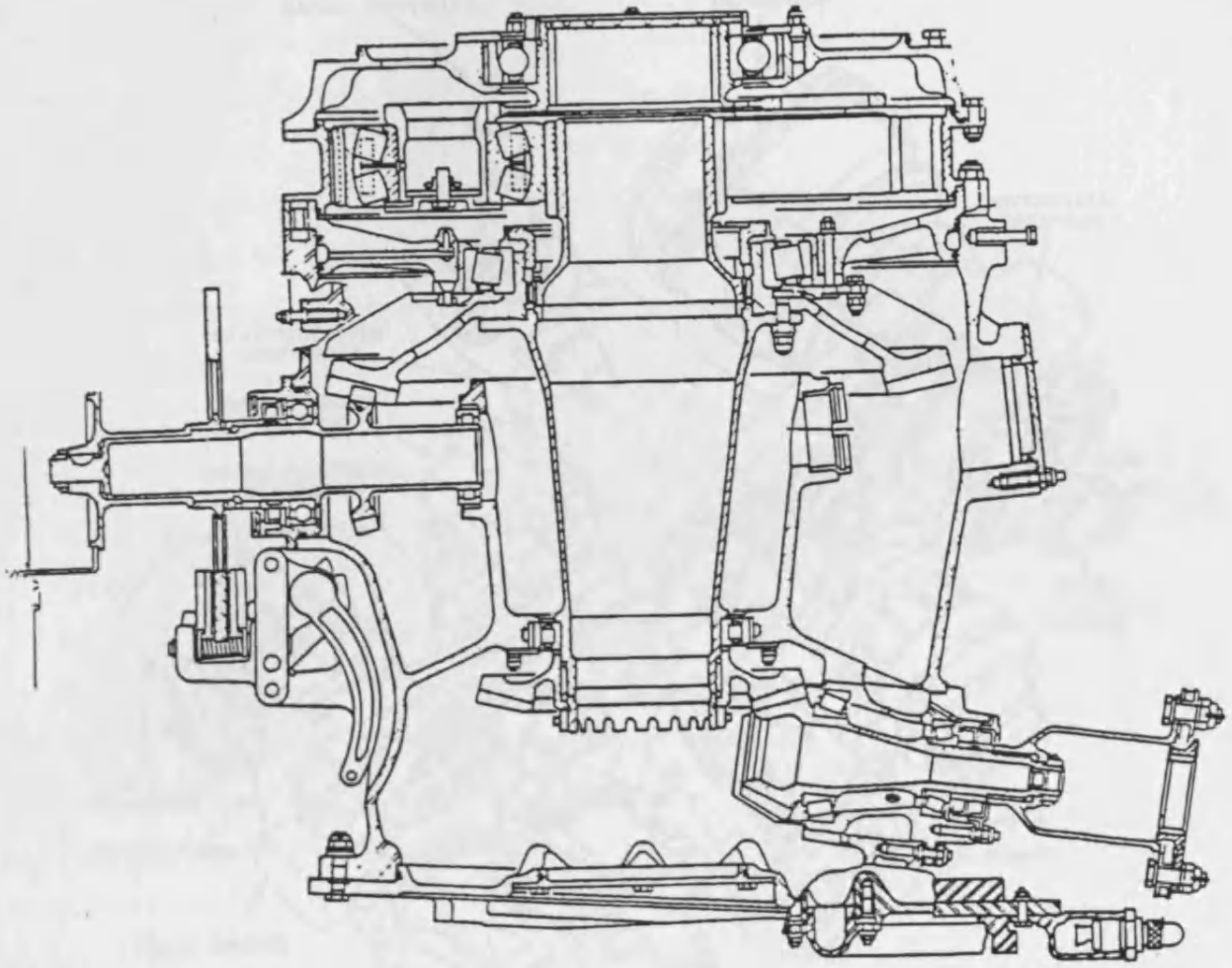

Figure 1.1: **Cross-section of a five metric ton helicopter Main Gearbox (MGB) (personal collection)**

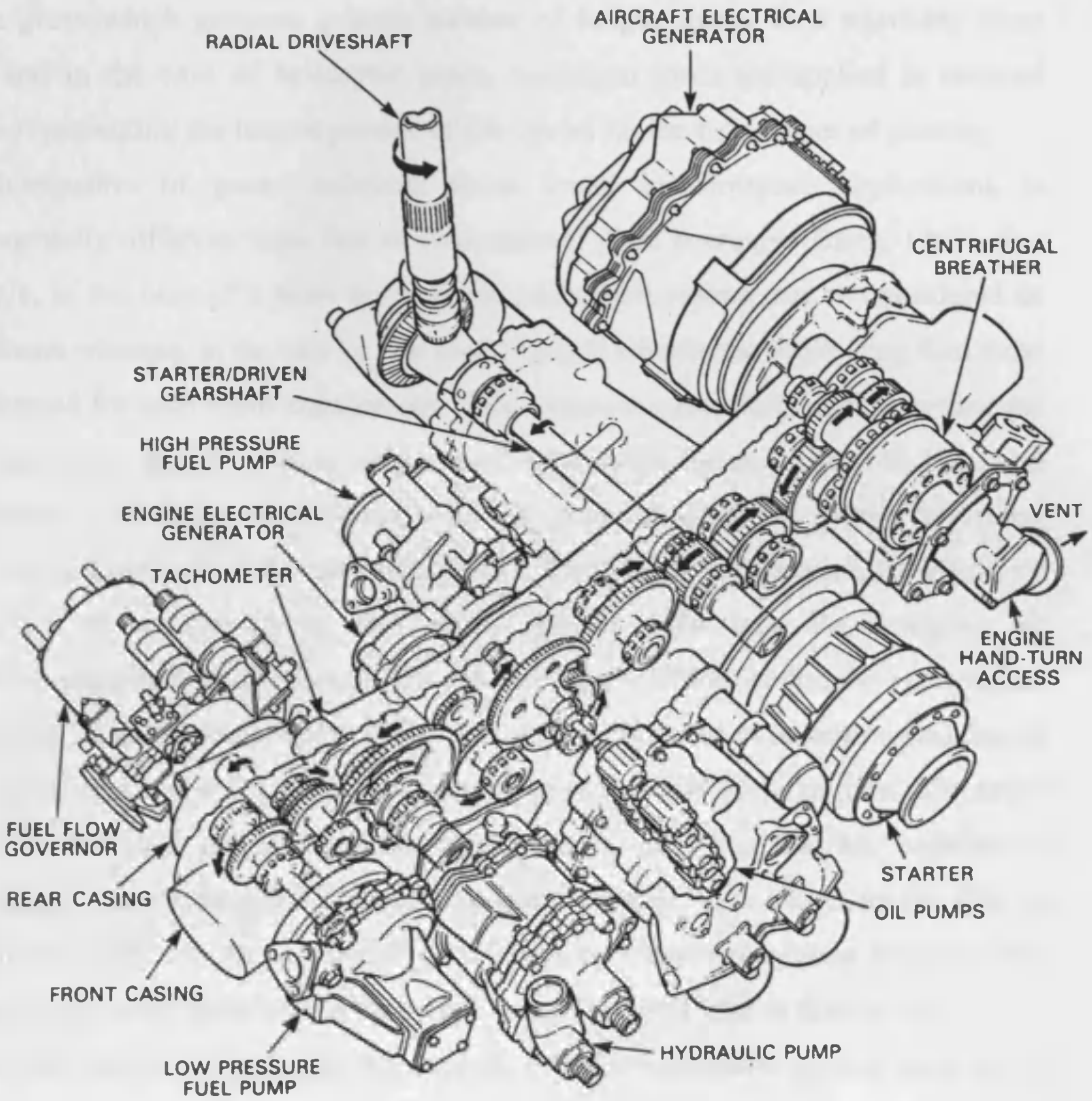

Figure 1.2: Cutaway drawing of a typical gas turbine engine Accessory Gearbox (AGB) (from Rolls Royce)

hydraulic pumps and alternators. In the case of the Trent 800 series engine, the power extracted can be as much as 300 KW at take-off with 150 KW extracted by one accessory alone (IDG: Integrated Drive Generator). Again the design of these gearing assemblies requires a very high level of integrity and reliability with minimum direct operating costs (DOC).

Aerospace gearing therefore involves high torques and loads, high speeds of turbine driven gears which generate a large number of fatigue cycles in a relatively short time, and in the case of helicopter gears, maximum loads are applied at reduced speeds representing the largest portion of life cycles for the final stages of gearing.

The lubrication of gears including those found in aerospace applications is fundamentally different from that of conventional plain bearings. (Bartz, 1993). For example, in the case of a plain bearing, the lubrication regime can be considered as continuous whereas, in the case of two meshing gear wheels, the lubricating film must be reformed for each tooth engagement. This feature is particularly crucial in the case of a high-speed gear set where only a short time exists for an oil film to form and separate the gear flanks. Nonetheless, a heavily pressurised oil film usually forms and transmits at least part of the transmitted load. The lubrication regime for the type of oil films as considered in this work usually falls into the category of elastohydrodynamic lubrication (EHL). In this regime of lubrication the geometrical conformity of the surfaces is low which causes very high contact pressures, and this in turn increases the viscosity of the lubricant by several orders of magnitude. The latter effect is beneficial and enables the generation of oil films that are capable of separating the surfaces given a reasonably smooth finish. In cases where the film is insufficient there will be penetration of the film by surface roughness features; this aspect of gear lubrication will be discussed in greater detail later in this thesis.

Apart from the heavy loads and high speeds found in aerospace gearing there is the tendency to use relatively low viscosity oils (typically 5 cSt at 100°C), particularly in cases where the oil services both gears and high speed turbine bearings. This has a negative effect on oil film formation. High sliding speeds encountered at the tips of gear teeth cause high temperatures and this can lead to scuffing failure of the surfaces. The combination of these adverse factors means that in many cases the oil film that can be generated is significantly less than the average roughness of the surfaces involved. The typical surface roughness Ra level of ground aerospace gears is about 0.4μm and the EHL oil film thickness predicted using the classical equation is

typically 1 μm or less. It is therefore clear that surface roughness effects are of importance in these demanding applications.

It is commonly accepted that gears can suffer from three main gear failure modes, which are tooth bending fatigue, pitting and scuffing. Tooth bending fatigue is now well understood. For unidirectional bending, the gear tooth rotates through a mesh from a zero stress condition to a maximum stress condition, and back again to a zero stress condition on each revolution, and the critical area for bending is at the base of the tooth (root). Tooth bending stresses generally are calculated using the methods outlined by the American Gear Manufacturers Association (AGMA), and allowable bending stresses are based on this one-way bending mode. Allowable bending stresses clearly take account of the steel, its heat treatment and its cleanliness. These allowable stresses are based on the material mean endurance limit curve of load versus cycles (S/N curve). Helicopter gears usually are designed in bending for infinite life at the highest expected operating condition. Current high cleanliness gear steels produced using the Vacuum Induction Melted – Vacuum Arc Remelted (VIM-VAR) process have greatly reduced the number of such failures by limiting the number of metallurgical inclusions.

On the other hand both micropitting and scuffing remain a major concern for aerospace type gears. Micropitting (also called grey staining) is defined by the ISO standard ISO 10825:1995 "Wear and damage to gear teeth – Terminology", as a "degradation of gear tooth working surfaces under lubrication conditions where the film is too thin for the load. It appears under magnification as dense patches of micropits or microcracks". It is believed to be the result of a surface fatigue phenomenon similar in nature to macro pitting, but at the asperity scale. In its advanced stages, micropitting can lead to removal of metal and the formation of large cavities on the flank of the gear which in turns can lead to the complete loss of the drive. Scuffing as also defined in ISO 10825:1995 is considered as banded roughness "running in the direction of sliding, varying in degree from mild to severe scuffing". Severe scuffing, as described in the standard, causes an increase of noise and vibration leading eventually to tooth breakage.

Micropitting and scuffing are very complex problems as they include a large number of variables induced by the operating environment of the contacting surfaces such as operating temperature, contact stress, amount of sliding, surface hardness, surface

roughness, type of lubricant, lubricant viscosity, material chemistry and microstructure, etc.

A number of ways of solving these two surface distress problems have been discussed for quite a long time but with no real consensus achieved so far. For example as outlined in ISO standard ISO 6336-1:1996 Calculation of load capacity of spur and helical gears: "at the present time, there is insufficient agreement concerning the method for designing cylindrical gears to resist scuffing failure". The same applies to micropitting where in this case full comprehension of the phenomenon, in particular its initiation and its development, needs to be fully established.

Some measures have proved helpful in reducing scuffing, for example a reduction in surface roughness using superfinishing techniques has proved very beneficial as confirmed by Patching (1995). Other measures like the use of different thermo-chemical treatments for the surface layer like nitriding instead of carburising may prove successful as demonstrated by a number of manufacturers such as the Eurocopter Company, or Allen Gears (part of the Rolls-Royce Company). In the same way, ultra hard thin coatings deposited using physical or chemical vapour deposition have appeared in the last twenty years mostly for tooling applications. They have shown promise due to their high hardness and durability.

The question of surface roughness effects remains, however, and it is believed that the problems of scuffing and micropitting cannot be fully cured without first gaining a thorough understanding of the part played by surface roughness effects. Some progress is being made in this respect as a result of recent work performed at Cardiff University on the development of a novel rough surface EHL solver. This technique will be used in this work to assess the effects of different finishes on the lubrication performance under scuffing conditions.

1.2 Fundamental properties of involute gears

In order to approach the problem of gear distress, it is important to review the relevant key features defining gear geometry and gear meshing. Although, surface distress is encountered in all kinds of gears notably in spiral bevel gears commonly used in the aerospace industry, this presentation will be limited to spur gears.

It has been established for at least 150 years that the most versatile gear tooth profile is that based on the involute curve. Its relatively simple generation from a straight rack has made this shape the most universally used profile for power transmission applications. Involute gears satisfy the fundamental property of gearing which is to have a constant velocity ratio between the two gear shafts. Geometrically, the involute curve is obtained as illustrated in Figure 1.3 as the path generated by a tracing point on a cord as the cord is unwrapped from a circle called the base circle. The base circle completely defines the involute profile. The locus of the points of contact between two involute teeth is a fixed straight line (line of action) which is the common tangent to the two base circles. This line crosses the line of centres of the gears at the pitch point P. The sliding velocity between two meshing gears as defined by Buckingham (1988) corresponds to the difference in the tangential speed at the ends of the generating lines of the involute profiles. The angular velocity of these generating lines will be the same as the angular velocities of the gears themselves. The length of these generating lines corresponds to the local radius of curvature of the involute profile for the radius of the driving (or driven) gear considered (see illustration in Figure 1.4). Hence, the respective tangential speeds can be expressed as follows:

$$V_1 = R_{c1} \cdot \omega_1 \qquad \text{and} \qquad V_2 = R_{c2} \cdot \omega_2$$

The sliding speed V_s will then be expressed as:

$$Vs = R_{c1} \cdot \omega_1 - R_{c2} \cdot \omega_2$$

Radii of curvature can themselves be expressed as a function of the radius on the gear considered and the base radius, hence:

$$R_{c1} = \sqrt{r_1^2 - R_{b1}^2} \quad \text{and} \quad R_{c2} = \sqrt{r_2^2 - R_{b2}^2}$$

With consideration to pitch circle dimensions R_1, R_2 and pressure angle Φ:

$$R_{b1} = R_1 \cdot \cos\Phi \qquad R_{b2} = R_2 \cdot \cos\Phi$$

Hence the final expression of the sliding speed can be established as:

$$Vs = \sqrt{r_1^2 - R_1^2 \cos^2\Phi} \cdot \omega_1 - \sqrt{r_2^2 - R_2^2 \cos^2\Phi} \cdot \omega_2 \qquad (1.1)$$

As an illustration of the severity in terms of the level of sliding encountered in real aerospace gearing, the case of the high speed input stage of a 10 tons class helicopter has been chosen. Its gearing characteristics are summarised in table 1.1.

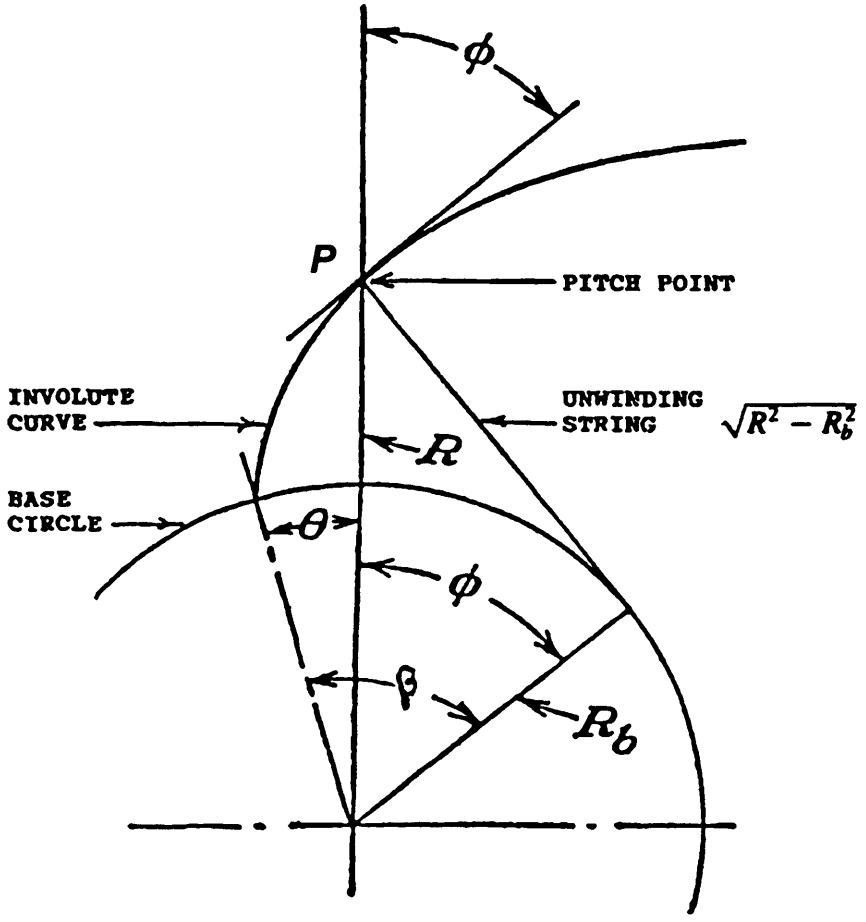

Figure 1.3: **Description of the involute curve obtained from the base circle of radius R_b and including pressure angle ϕ and pitch point P (from Buckingham)**

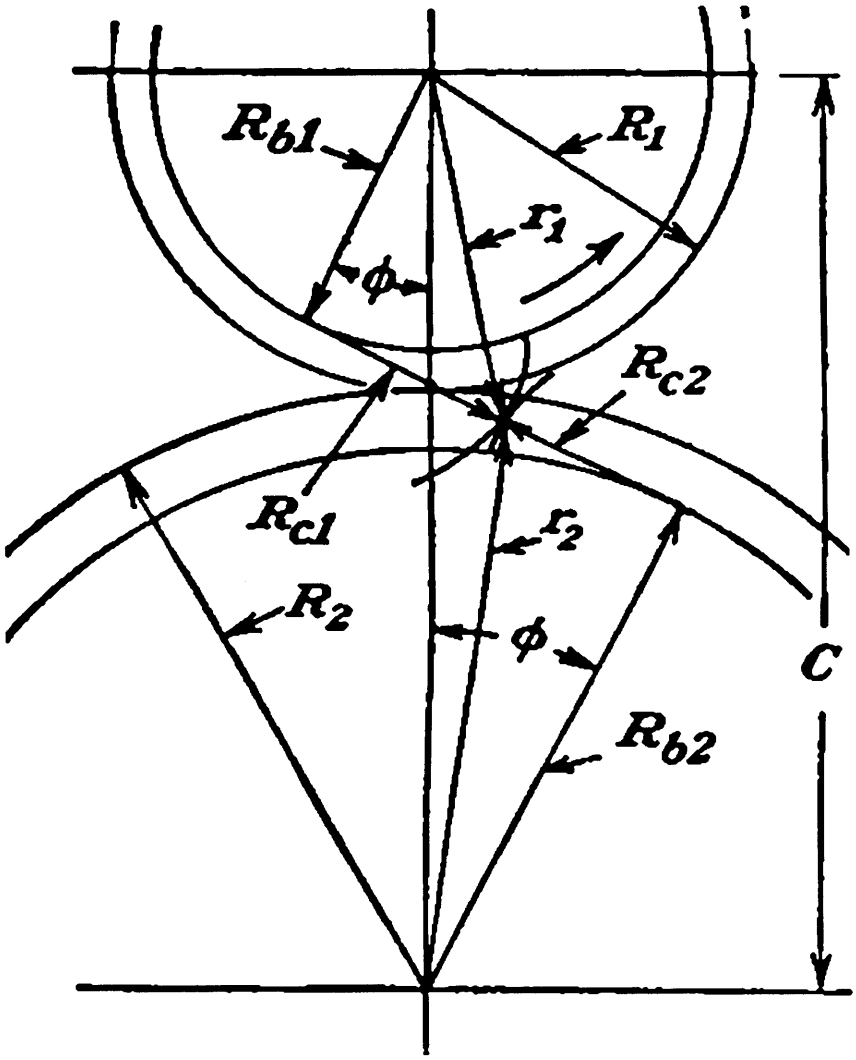

Figure 1.4: **Description of the radii of curvature R_{c1} and R_{c2} at any point on a pair of involute gear teeth. The point is positioned by r_1 on the first gear and r_2 on the second. Involute profiles are obtained from base circles of radii R_{b1} and R_{b2}, having a respective pitch circle radius R_1 and R_2 (from Buckingham).**

Table 1.1

Gearing characteristics of the high speed input stage of a helicopter main gearbox

	pinion	wheel
z (teeth)	31	89
m_n (mm)	2.337	2.337
Φ(degrees)	22	22
Pitch Diameter (mm)	73.346	210.574
Tip Diameter (mm)	79	212.5
Root Diameter (mm)	68	202.2
Face Width (mm)	65	65
n (rpm)	22841	7956

Presented in Figure 1.5 is the variation of the sliding speed versus radial position *r* on the pinion gear. In this case it can be seen that the sliding speed at the tooth tip reaches about 22 m/s and is about 12 m/s at the root. These high sliding speeds make the teeth susceptible to surface distress as outlined by numerous authors and standards (e.g. Dudley, 1994). The sliding speed is zero at the pitch point (pure rolling) and the direction of sliding motion changes at the pitch point. These two features have an influence on the contact behaviour. The presence of pure rolling at the pitch point will have a direct influence on the rheological response of the lubricant and especially on non-Newtonian effects that will be described in section 1.5.3. The change of direction of sliding motion has been found to have a direct effect on the development of micropitting as described by Olver (1984).

Another important aspect that needs to be taken into account when considering surface distress of gears is the way the load is introduced into the gear mesh. According to classical EHL theory for smooth surfaces load has little influence on the thickness of the oil film, but the effect on local contact stresses is, of course, significant and this will affect the onset of surface distress (Seager, 1976, Wilkinson, 1998).

The length of the path of contact as illustrated in Figure 1.6 corresponds to the distance XY. This distance can be expressed with reference to the pitch point as the sum XZ (arc of approach) and ZY (arc of recess). This length can then be expressed as a function of the addendum, base and pitch circle radii as follows:

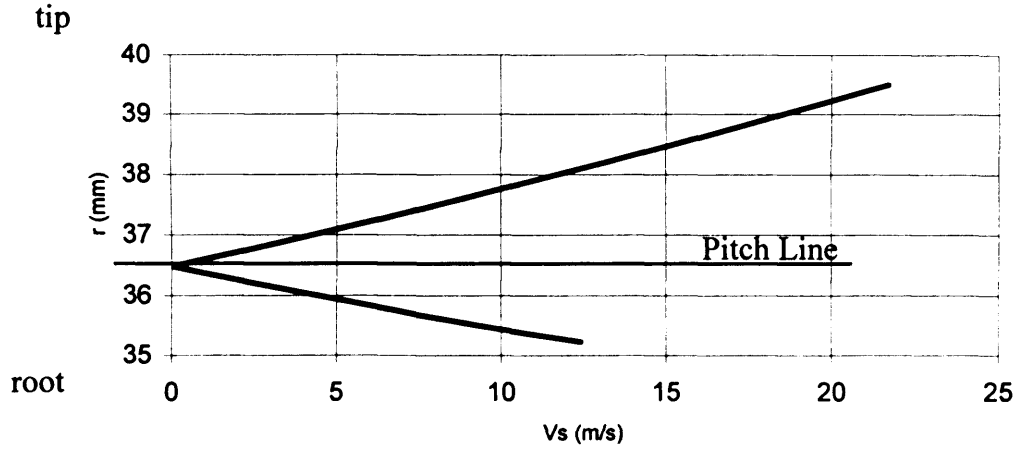

Figure 1.5: **Evolution of sliding speed as a function of the radial position on the pinion gear.**

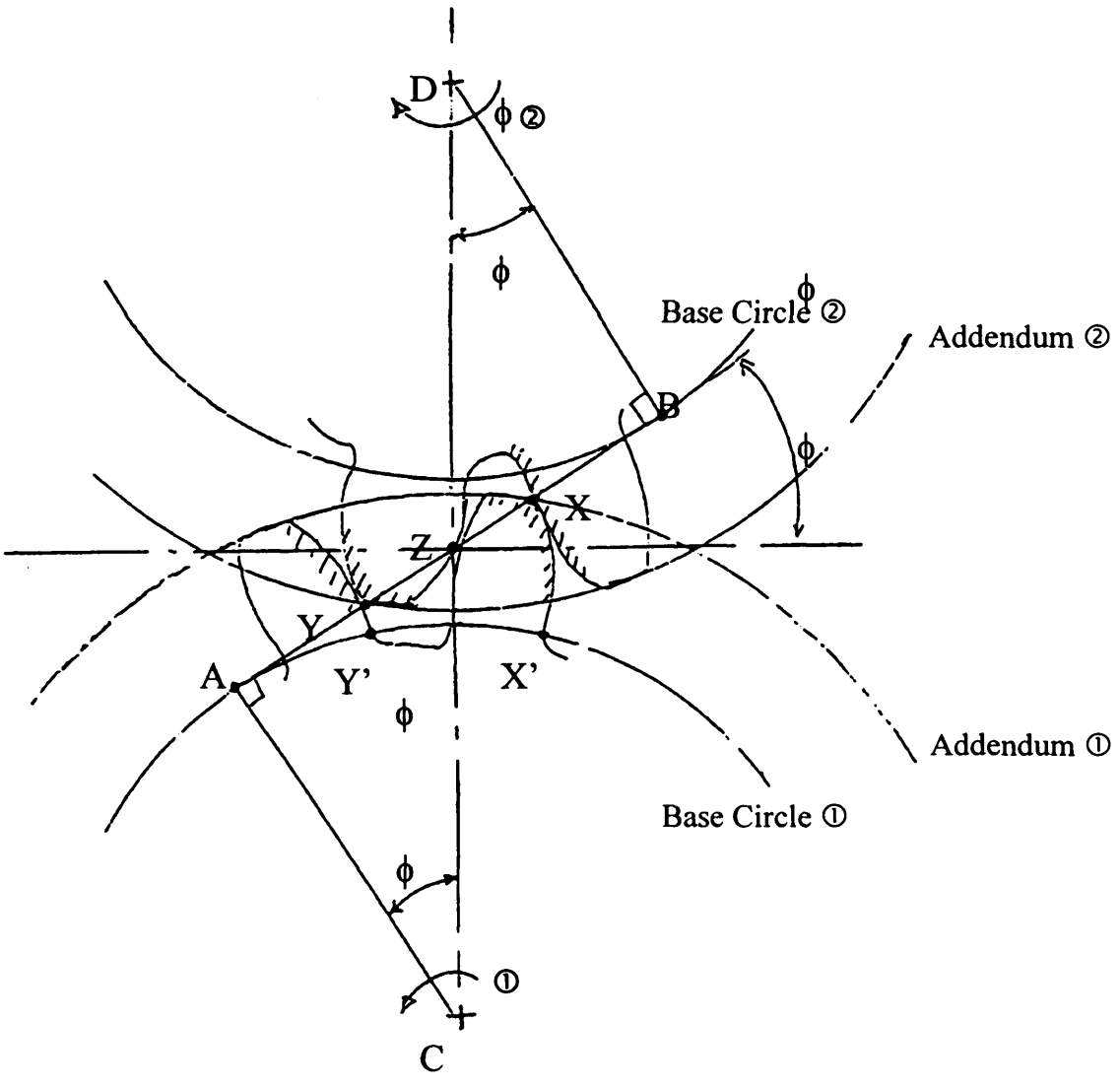

Figure 1.6: **Path of contact for a gear mesh (from Snidle).**

$$XY=\sqrt{r_{a1}^2-r_{b1}^2}-r_{b1}\cdot\tan\phi+\sqrt{r_{a2}^2-r_{b2}^2}-r_{b2}\cdot\tan\phi$$

The ratio of the length of the contact path to the base circular pitch defines the contact ratio. This is taken as a measure of the degree of overlap of tooth contacts. Good practice requires having a contact ratio greater than 1.2 (Coy *et al.*1985). From the load point of view, contact ratios greater than unity will correspond to two pairs of teeth sharing the applied load for a percentage of the meshing time. Figure 1.7 shows an illustration from Höhn *et al.* (2001) of the variation of the normal tooth force along the path of contact between points A and E. In this case, two teeth share the load for approximately half of the meshing time (contact ratio $\approx$ 1.5). The same teeth would carry the fully applied load between point B and D, C being the pitch point.

This theoretical approach does not allow for dynamic and elastic deformation effects taking place during gear meshing. Because the loaded teeth of the *driven* member are deflected in the direction of motion, every unloaded tooth of that gear will be slightly behind its correct position in relation to the loaded teeth. In the same way, every unloaded tooth of the *driving* member is slightly ahead of its correct position in relation to the loaded teeth. As a result, two unloaded teeth that are about to enter the mesh will be out of step. The amount of offset will correspond to the sum of the deflections of a pair of loaded teeth. This results in tooth engagement occurring with a certain amount of shock, possibly on the corners of the teeth rather than the true involute arc. This is detrimental both in terms of stress and lubrication effects, particularly since it is at tooth tips that the maximum sliding occurs. In order to avoid this effect the profile of the involute is modified to include so-called *tip relief*. Figure 1.8a gives an illustration of a typical tip relief defined by parameters *Ca* (width) and *h* (height) corresponding to a linear alteration of the tooth tip ("thinning"). The net result is a much smoother operation with the "build-up" of load taking place in a much more progressive way. Figure 1.8b shows the theoretical effect along the path of contact of optimal profile modification. It is customary to decide upon the quantity of relief to be applied by considering the total amount of anticipated deflection of a pair of loaded teeth. This latter quantity is itself influenced by two main quantities. On the one hand, we have the stiffness of the gear mesh, which can be rather difficult to

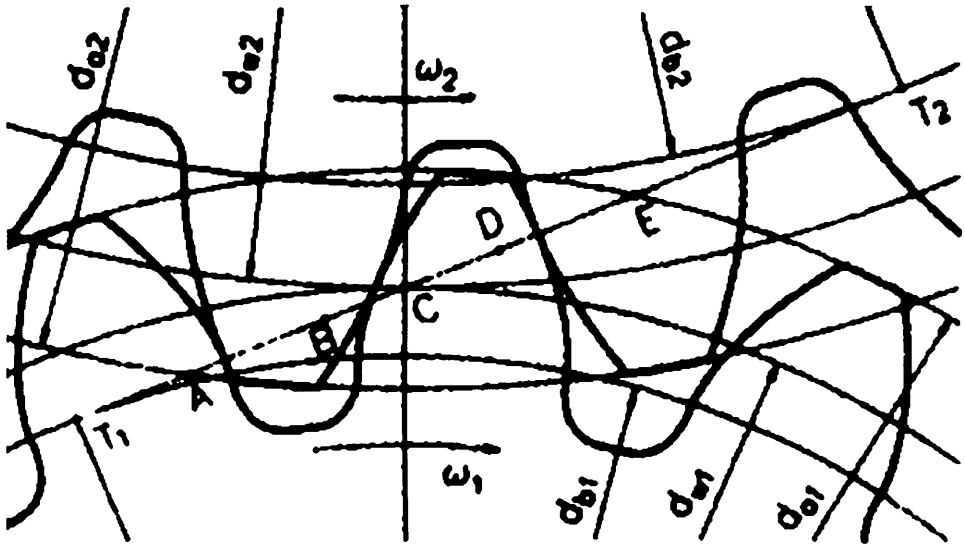

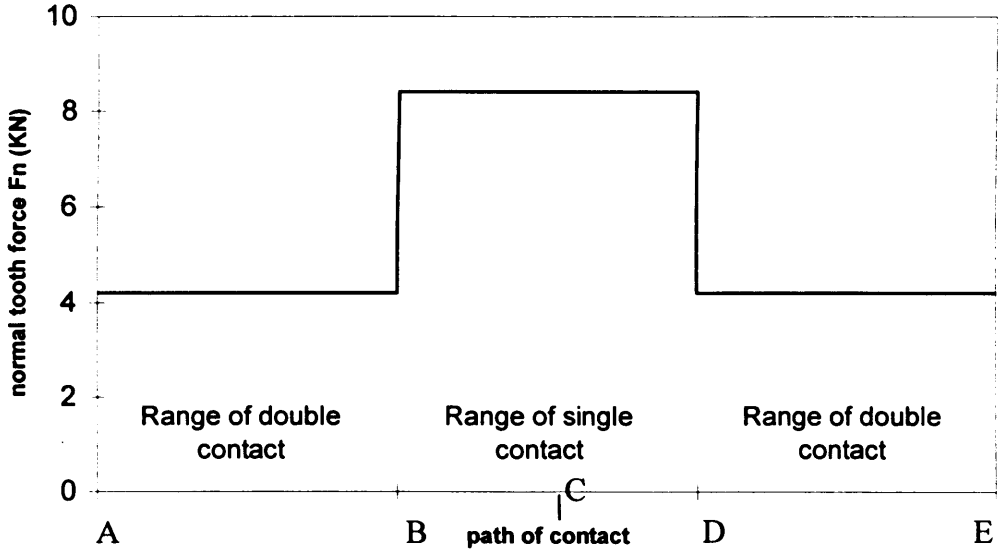

Figure 1.7: **Load sharing due to contact ratio greater than 1. The path of contact starts in A and finishes in E. C is the pitch point. Between B and D is the case of the single contact (from Höhn *et al.*, 2001).**

(a)

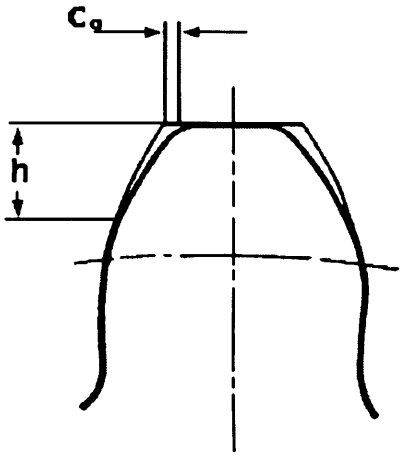

(b)

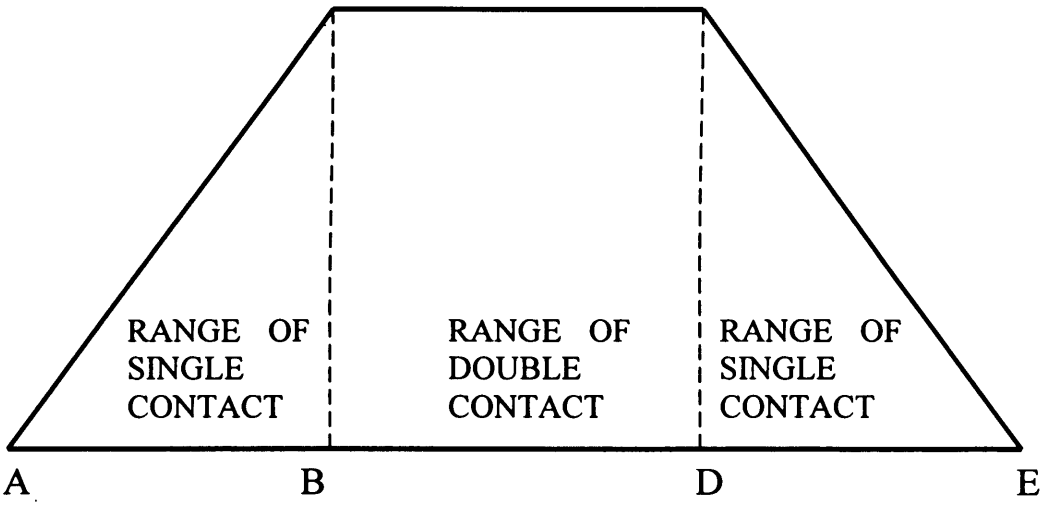

Figure 1.8: **(a): Representation of a typical tip relief as performed on spur gears defined by its *width* Ca and its *height* h (from AGMA). The original involute tooth profile is shown with the thinner line. (b) Net effect on the load along the meshing path of with an optimal profile modification (same notations as for Figure 1.7.**

establish, and on the other hand the actual load applied on the teeth considered. This last parameter inevitably means that there is unfortunately no real optimum profile modification, as in most gearing, the load fluctuates with time.

From the foregoing we may conclude that the contact between gear teeth represents a uniquely demanding lubrication situation, particularly when considering aerospace conditions.

1.3 Power transmissions

Two main types of power transmission systems are found in the aerospace industry. First, we find systems that are designed to transmit mechanical power from turbo-engine(s) to propulsion devices. These systems are usually speed reducers and are used in helicopter rotor drives (main, intermediate and tail Gearboxes) and as turboprop reduction gearboxes (see Figure 1.9). All helicopter gearboxes include a change in motion direction. This is usually achieved using spiral-bevel gears performing a 90° angle change of direction or more in the case of certain MGB input stages or IGBs. Gear ratios in these applications are relatively high. Typical output speeds from turbo-engines can reach 23,000 rpm, and in the case of heavy weight helicopters the main rotor would be rotating at about 260 rpm. This corresponds to an overall reduction ratio of nearly 90 to 1. In the case of turboprops, this ratio is not as dramatic but can reach typically 10 to 1. Such reduction ratios require a number of stages and usually involve a final epicyclic gear stage for reasons of compactness. In the case of a turboprop gearboxes speed reduction, Figure 1.9, for example, shows a twin compound layshaft design as used in the Pratt and Whitney 100 series engine. In most turboprops, however, the epicyclic reducer is used.

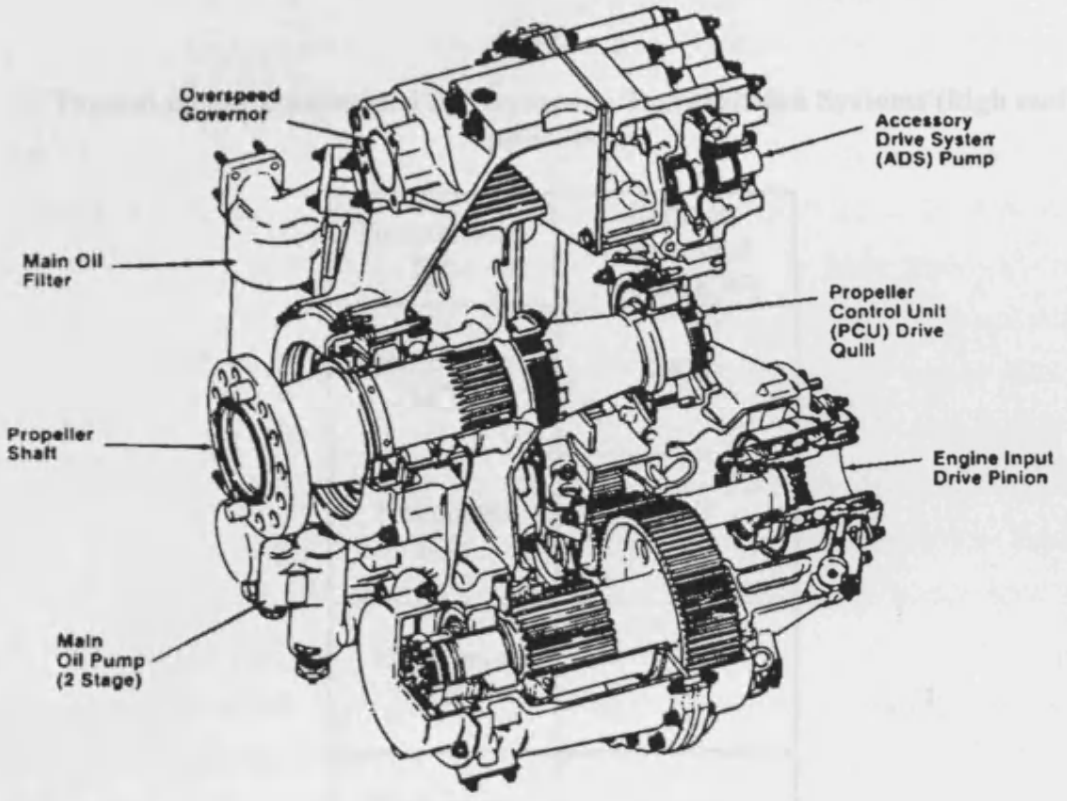

Figure 1.9: Cutaway drawing of a Turboprop reduction gearbox using twin-compound gear technology (from Pratt & Whitney)

The second function fulfilled by aerospace transmission systems is the drive of a number of accessories necessary for the flight of the aircraft (or rotorcraft). These assemblies are usually called an accessory gearbox (AGB) as illustrated in Figure 1.2. Typical driven accessories include electrical generators, hydraulic pumps, and fuel pumps. The minimum power that these assemblies transmit in the case of high end (heavy) applications is summarised in Table 1.2.

Table 1.2

Typical power transmitted by Aerospace Transmission Systems (high end applications)

Transmission Type	Minimum Transmitted Power (KW)
Helicopter MGB	2000
Helicopter IGB	500
Helicopter TGB	500
Turboprop Gearbox	3000
Jet Engine AGB	250 / 2000 Nm*

(* :maximum static torque at start-up)

These values correspond to very demanding applications particularly when taking into consideration the extremely stringent weight limitations that need to be applied to any mechanical assemblies mounted on board. As a result, levels of power density (power/unit of mass) are extremely high and can reach in the case of helicopters 6 kW/kg. Light materials like magnesium are normally selected for the casings supporting the gearing, shafting and bearings. The intrinsic low rigidity of such

materials coupled with minimum practical thickness used for casing walls results in significant displacements of shaft lines under load. This has a direct influence on the alignment of the gears and can induce less than optimum meshing conditions which further exacerbate surface distress.

The typical operating temperature for these assemblies follows usual aerospace requirements which corresponds to an outside temperature of – 45°C to + 50°C (possible storage up to +70°C). Such a wide range of possible operating temperature has serious consequences in terms of lubricant viscosity selection. The normal, stabilized bulk operating temperature within the gearbox is usually between 90 to 100°C. The lubricant normally used in these assemblies meets the United States Military specification MIL-L-23699, which was developed in the mid 1960s. It is a synthetic type lubricant (di-ester). Shown in Table 1.3 are the basic characteristics of lubricant Mobil Jet Oil II which meets specification MIL-L-23699. This lubricant was originally tailored for jet engine applications therefore has high thermo-chemical stability with a maximum operating temperature of 204°C (400°F) and a very low viscosity at high temperature (5 cSt at 100°C). The basic advantage of using a jet engine lubricant to lubricate gearbox assemblies is the resulting commonality between engine and gearbox, which is very beneficial from the logistics and maintenance point of view. Nonetheless this philosophy has a serious penalty from the lubrication point of view. Ideally, gears would be lubricated with an oil of higher viscosity grade which would give a more effective oil film thickness under EHL conditions.

Table 1.3

Characteristics of lubricant Mobil Jet Oil II with reference to spec. MIL-L-23699C (from the Mobil Company)

	Mobil Jet Oil II	MIL-L-23699C Requirements
Viscosity		
cSt at 100° C (212° F)	5.0	5.0 - 5.5
cSt at -40° C (102° F)	25.3	25.0 min
cSt at -40° C (-40° F)	11,000	13,000 max
% change at -40° C after 72 hr.	3.7	±6
Flash Point, °C (°F), min	268 (515)	246 (475)
Fire Point, °C (°F)	285 (545)	--
Autogenous Ignition Temp, °C (°F)	404 (760)	--
Pour Point, °C(°F)	-54 (-65)	-54 (-65) max

Table 1.3 (continued)

	Mobil Jet Oil II	MIL-L-23699C Requirements
Specific Gravity, 15/15 °C (60/60 °F)	1.0035	--
TAN (mg KOH/g sample)	0.08	0.50 max
Evaporation Loss, %		
6.5 hr at 204° C (75° F), 29.5" Hg	5.0	10 max
6.5 hr at 232° C (450° F), 29.5" Hg	10.9	--
6.5 hr at 232° C (450° F), 5.5" Hg	33.7	--
Foam, ml		
Sequence 1, 24° C (75° F)	25 max	10 max
Sequence 2, 93° C (200° F)	25 max	--
Sequence 3, 75° C (after 200° F test)	25 max	--
Foam Stability, after 1 min settling, ml	0	0 max
Rubber Swell		
F Rubber, 72 hr at 204° C (400° F), %	19	5 – 25
H Rubber, 72 hr at 70° C (159° F), %	16	5 – 25
Silicone, 96 hr at 121° C (250° F), %	9	5 – 25
Tensile Loss, %	17	30 max
Sonic Shear Stability		
KV at 39 °C (100° F), change, %	0	4 max
Ryder Gear		
Average lb/in	2750	--
% Hercolube A	115	112 min

Although the bulk-stabilized oil operating temperature has been described as being below 100°C, this temperature can be substantially exceeded in epicyclic gearing stages. This is due to the relative confinement of epicyclics within a small volume which encloses a large number of gears (planets – typically up to eight, sun and annulus). The oil jet lubrication is problematic and numerous surface distress problems tend to appear in these drives.

For most aerospace gearing systems (apart from helicopter tail and intermediate gearboxes), the lubrication system uses pressurized oil jets. The oil is re-circulated via a sump with a pump driven itself by the gear assembly. The level of filtration of the lubricating oil is typically 8μm. Finer levels of filtration are generally considered impractical because of the problem of clogging and consequent higher frequency of maintenance. It is therefore inevitable that debris of a size much greater than the oil films present between the gear teeth will be in circulation. This debris can ingress into

the various gear meshes and bearing contacts and create premature surface distress. Debris contamination can be a serious problem as a typical oil change with MIL-L-23699 lubricant is usually performed only every 1200 hours of operation and Time Between Overhaul (TBO) with aerospace gearboxes is about 3000 hours. All these factors add to the challenge of preventing surface distress in aerospace gears.

1.4 Current trends in aerospace transmissions

After having considered the general features of Aerospace type transmissions and their potential influence on surface distress of gears, it is important to consider the current trends in this sector to better justify the relevance of the current work. A recurring theme in today's economic climate is affordability of products and costs of ownership. Both parameters must be kept to a minimum for a company to maintain its market share. There has also been a much greater emphasis on environmental issues notably the limiting of use of natural resources. This situation has resulted in a number of initiatives from a number of governmental bodies in order to guide the aerospace industry towards these objectives. Hence a number of large research programmes have emerged both in the U.S.A and Europe.

For the past ten years or so, Europe has supported via the Brite Euram framework a number of projects in the aerospace sector clearly geared towards reducing acquisition costs, lowering the cost of ownership and inducing lower environmental impact. For example, the Brite Euram III framework programme on Aeronautics Technologies, covering the period 1994 – 1998, included as general objectives reductions of 30% in engine fuel consumption, a 20% reduction in airframe, engine and systems weight and 40 % in maintenance cost. More specifically, the program called for the need to develop and validate the technologies required for the realisation of new and improved mechanical transmission systems for rotorcraft and engines, including advanced designs concepts, new material and process applications and enhanced diagnostic systems. The current framework programme, covering the period 2001 – 2002 (Fifth Framework), stresses, in its statement on perspectives for aeronautics, the need to develop technologies to improve operational safety and efficiency. In particular the objective is to reduce fuel consumption by 20% with a general improvement on reliability and direct operating costs. In the same way, maintenance

costs should be reduced by 25% with a reduction of accident rates by the same factor as the growth of traffic. Already, the European Community has indicated its vision for the future in aeronautics (Vision 2020 report) indicating the need to further reduce direct operating costs by 20% in the short term and 50% in the long term. This vision insists specifically on the need to focus the research effort on mechanical systems to meet this very ambitious objective.

In the U.S.A, a number of research programmes have been developed specifically on helicopter mechanical transmission systems. Most of these programmes have been defined and are supported by military users and particularly the U.S. Army, which is a large user of rotorcraft. For example, one can cite two recent dedicated programmes like the ART (Advanced Rotorcraft Transmission) programme and the RDS-21 (Rotorcraft Drive System for the 21st Century) programme. The former was initiated in the mid nineties with the aim of improving specifically reliability and the power-to-weight ratio. Objectives were set for a two times increase in the Mean Time Between Unscheduled Removals (MTBUR) and a 25% improvement in power density. Another specific aim brought in by the programme was loss of lubrication tolerance. In other words, it should be possible to return to base even after having lost lubrication in the Main Gearbox. In the same way but for normal operation, the programme insists on having a lubrication system capable of operating at elevated temperature and reduced flow rates for weight reduction. The RDS-21 programme, which is currently being implemented and which follows the ART programme, takes again as a primary objective the improvement in the power-to-weight ratio. The requirement in this case is a 35% improvement in power density along with a 25% reduction in operating and support cost. The promoters of the programme suggest that the objectives can only be achieved by using high load capacity gear stages.

Apart from the various government agencies setting the trends in terms of required enhancements in order to maintain either competitiveness or mission efficiency, civil certification bodies like the Federal Aviation Administration (FAA) (answering for all safety aspects) have recently imposed new regulations having a direct effect on gear surface performance. For example, in the Federal Aviation Regulation part 29 dealing with helicopter airworthiness, for rotorcraft with a maximum weight greater than 20,000 pounds (9000 kg) and 10 or more passenger seats, "it must be shown by test that any failure which results in loss of lubricant in any normal use lubrication system will not prevent continued safe operation, although not necessarily without damage, at

a torque and rotational speed prescribed by the applicant [manufacturer] for continued flight, for at least 30 minutes after perception by the flight crew of the lubrication system failure or loss of lubricant." (FAR Part 29 Sec. 29.927, extract). Hence, such a requirement induces inevitably the necessity for the gear surface to be able to operate without any distress under very poor lubrication conditions including mixed lubrication conditions and extremely high bulk temperature.

Generally speaking, each of the trends set by these various programmes and certification bodies imply a direct specific improvement at gear surface level. For instance, an increase in the power-to-weight ratio or power density will necessitate for example reduced gear face widths therefore increasing surface contact stress, which in turn may influence surface distress. In the same way, reducing maintenance costs will require increasing the times between overhauls, hence the necessity to develop systems with a higher reliability. To increase gear contact reliability, the occurrence of gear surface distress needs to be reduced accordingly. Presented in Table 1-4 is a summary of the current trends and their impact on gear contact capability.

Table 1.4

Summary of current trends regarding Aerospace Transmissions

Objective	Programme	General Requirement	Specific Requirement
30% reduction in engine fuel consumption	Brite Euram III	Better efficiency – Higher power density	Less power loss at gear tooth level
20% reduction in systems weight	Brite Euram III	Higher power density	Higher level of gear contact stress
40% reduction in maintenance cost	Brite Euram III	Higher reliability	Reduction in gear surface distress occurrence
20% reduction in fuel consumption	Fifth Framework	Better efficiency	Less power loss at gear tooth level
25% reduction in maintenance cost	Fifth Framework	Higher reliability	Reduction in gear surface distress occurrence
Up to 50% reduction in direct operating costs	Vision 2020 (EC)	Higher reliability	Reduction in gear surface distress occurrence
Two times increase in the MTBUR	ART	Higher reliability	Reduction in gear surface distress occurrence

Table 1.4 (continued)

Objective	Programme	General Requirement	Specific Requirement
25% improvement in power-to-weight ratio	ART	Higher power density	Higher level of gear contact stress
Loss of lubrication tolerance	ART + FAA	Damage tolerance	Capability to operate at very high contact temperature with mixed lubrication regime
High temperature lubrication + lower flow rate	ART	Higher power density	Capability to operate at higher contact temperature with mixed lubrication regime
35% improvement in power-to-weight ratio	RDS-21	Higher power density	Higher level of gear contact stress
25% reduction in operating and support cost	RDS-21	Higher reliability	Reduction in gear surface distress occurrence

Considering these various programmes and regulations (which are endorsed by major governmental bodies) as representative of the current trends in Aerospace Transmissions, it appears very clear to those of us in the field of gearing tribology that we must achieve a much better understanding of gear surface behaviour and distress if we are to meet the challenges presented.

1.5 Contact and lubrication theory

In order to appreciate the interaction of the parameters influencing surface distress of gears, one has to understand the various physical phenomena, which take place at the surface and subsurface of the gear tooth during normal operation. Surface durability is directly affected by the nature and amplitude of stresses generated by the two surfaces in contact. The classic Hertz (1882) theory gives the stresses and contact dimensions for smooth, elastic bodies in contact; it does not take into account the real nature of engineering surfaces, which necessarily include some amount of surface texture like

waviness and roughness. In real gear tooth contacts it is necessary to take account of roughness effects in both dry and lubricated conditions.

1.5.1 Dry smooth surfaces in contact

Generally speaking the contact between two surfaces can be described as either conformal or non-conformal. The former deals with the case of surfaces which fit closely together i.e. the nominal area of contact is comparable to the dimensions of the surfaces. A typical example of conformal surfaces is the case of a journal bearing. The other type of contact (i.e. non-conformal contact) is encountered when the actual contact area is very small compared to the dimensions of the surfaces considered. In this instance, when non-conforming surfaces are brought into contact without deformation, contact can take place either at a point (e.g. the case of two spheres in contact) or along a line (e.g. the case of two cylinders in contact along a common generator). Gear tooth contacts fall into the category of non-conformal contact where the convex involute shape of the surfaces in contact imposes a very small area of contact.

The fundamental problem of non-conformal contact was first studied in a famous publication by Hertz (1882) and was re-assessed more recently by Johnson (1985). This study assumes that surfaces can be approximated near the contact area by a parabolic curve. Only small strains are considered implying an elastic behaviour of the materials in contact. Moreover for this particular case, only normal pressure is transmitted between the two bodies (frictionless contact). Under these assumptions, for bodies of arbitrary shape, it can be demonstrated that the relative geometry of the gap between the un-deformed bodies in contact can be reduced to that between a plane (the *xy* plane) and an elliptic paraboloid as represented in Figure 1.10 (a). With a suitable selection of *x* and *y* axis, the gap *z* can be expressed as follows:

$$z = \frac{x^2}{2R_x} + \frac{y^2}{2R_y}$$

where R_x and R_y are defined as the principal radii of curvature. The *x*-axis is selected in order to have $R_x > R_y$. Hertz showed that the shape of the elastic contact is an ellipse as shown in Figure 1.10 (b). The semi-major axis in the *x*-direction is defined as a and the semi-minor axis in the *y*-direction is defined as b. Hertz also showed

that the contact pressure distribution was semi ellipsoidal (see Figure 1.11). This distribution can be expressed as a function of the maximum contact pressure present p_0 and the semi-axes a and b:

$$p(x,y) = p_0\sqrt{(1-\frac{x^2}{a^2}-\frac{y^2}{b^2})}$$

There is unfortunately for this general case, no simple analytical expressions neither for the maximum contact pressure p_0 nor for a and b. These quantities are determined by solving elliptical integrals, which are either tabulated or are obtained using algorithms such as the one developed by Dyson, Evans and Snidle (1992). One should note that since the contact pressure is in the form of a semi-ellipsoidal distribution, the maximum contact pressure is 1.5 times the mean contact pressure.

The case of line contact, as occurs in spur gears, occurs as a/b tends to infinity. For two cylinders of radii R_1 and R_2 in contact, the contact shape tends towards that of a long rectangular strip of width $2a$ lying parallel to the cylinders' axes. The pressure distribution will be as follows:

$$p(x,y) = p_0\sqrt{1-\frac{x^2}{a^2}}$$

where $p_0 = \sqrt{\frac{PE^*}{\pi R}}$

And the half width of the contact can be analytically expressed as:

$$b = \sqrt{\frac{4w'}{\pi}(k_1+k_2)R}$$

where $k_1 = \frac{1-\nu_1^2}{E_1}$ and $k_2 = \frac{1-\nu_2^2}{E_2}$

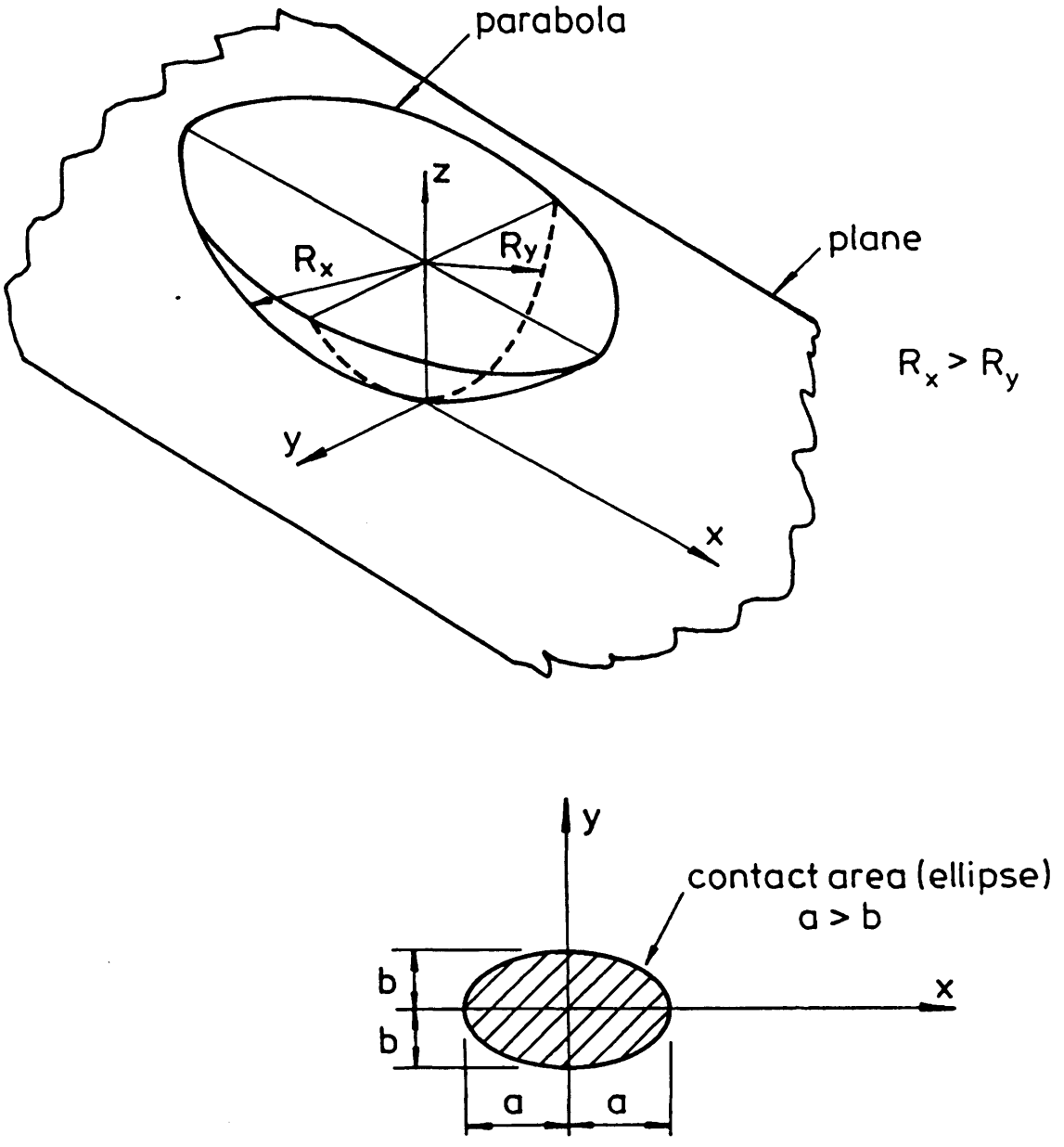

Figure 1.10: **(a)** **Contact of bodies of arbitrary shape reduced to the contact between a plane and an elliptic paraboloid**

(b) **The shape of the elastic contact area shown above**

1.5.2 Dry rough surfaces in contact

The real surfaces of contacting bodies like gears are not topographically smooth. They usually comprise a large number of peaks also called asperities and valleys. A typical gear surface which has been finished by grinding is presented in Figure 1.11. It is clear that the contact between such a surface and cannot be studied using Hertzian theory. The actual real area of contact will only be a fraction of the nominal contact area as predicted by the simple Hertz theory. In the same way, the real pressure distribution will not follow the Hertzian distribution. The local pressures as illustrated in Figure 1.12 significantly exceed the Hertzian values.

Generally speaking the texture of a surface is normally the result of the machining and finishing process. This texture can be split into three components, namely the form, the waviness and the roughness itself. These three components correspond to three different levels of wavelength ranging from larger to smaller, respectively. A large number of parameters are available to quantify the various components of the surface texture. Amplitude parameters are measures of the vertical characteristics of the surface deviations. In the same way spacing parameters are measures of the horizontal characteristics of the surface deviations. Considering roughness amplitude parameters, one can cite the most universally recognised parameter called the centre line average (CLA or Ra – ISO 4287 – 1997). It corresponds to the arithmetic mean of the absolute departures of the roughness profile from the mean line. The root mean square (rms) parameter Rq (or σ) is also a very frequently used parameter. RSm is a spacing parameter defined as the mean spacing between profile peaks at the mean line, measured within the sampling length. A very important spacing parameter as outlined by Hirst and Hollander (1974) and also by Poon and Sayles (1989) is the correlation length β^*. These authors have demonstrated a relation between sliding surface damage and the surface roughness σ and the correlation length β^*. There are also a number of interesting hybrid parameters describing both spacing and height features. One could cite the rms slope of the profile within the sampling length $R\Delta q$ where high slope values will necessarily influence the friction behaviour as indicated by Meyers (1962). Another hybrid parameter, which is of great interest to Industry, is the material ratio tp. It corresponds to the length of bearing surface, expressed as a percentage of the evaluation length L, at a depth p below the highest peak (Taylor

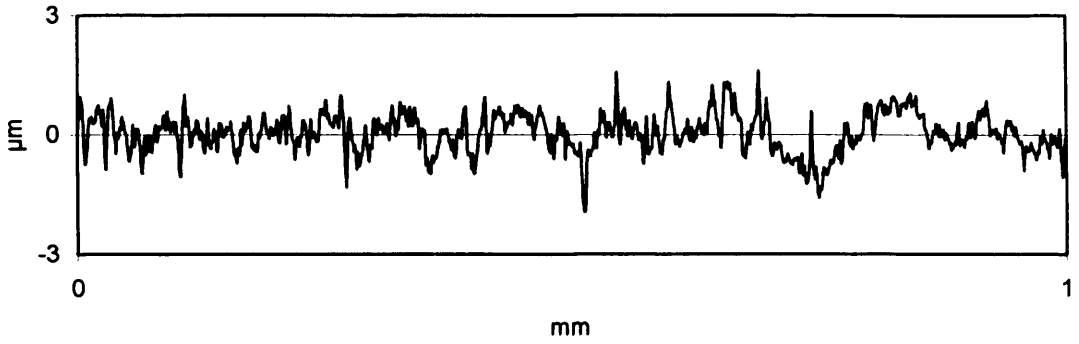

Figure 1.11: Typical surface profile of a gear ground surface

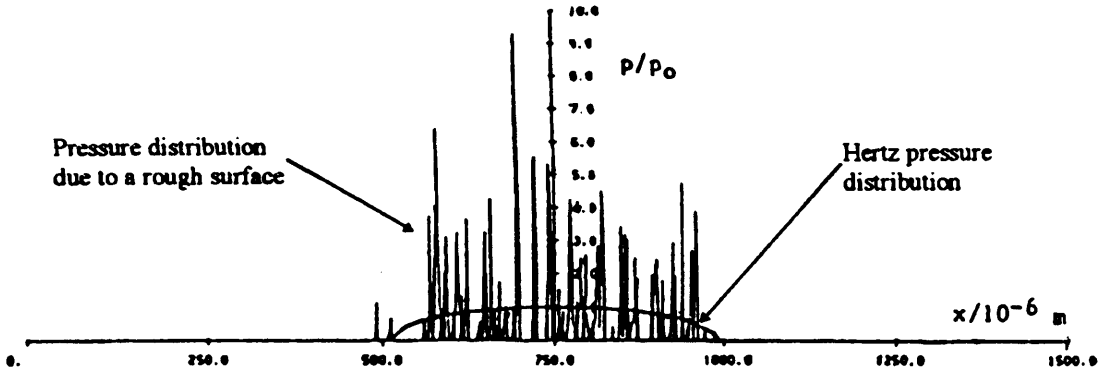

Figure 1.12: Typical contact pressure distribution in the case of dry rough surface in comparison with the Hertz pressure distribution. p_0 is the maximum Hertz pressure (from Webster and Sayles 1986)

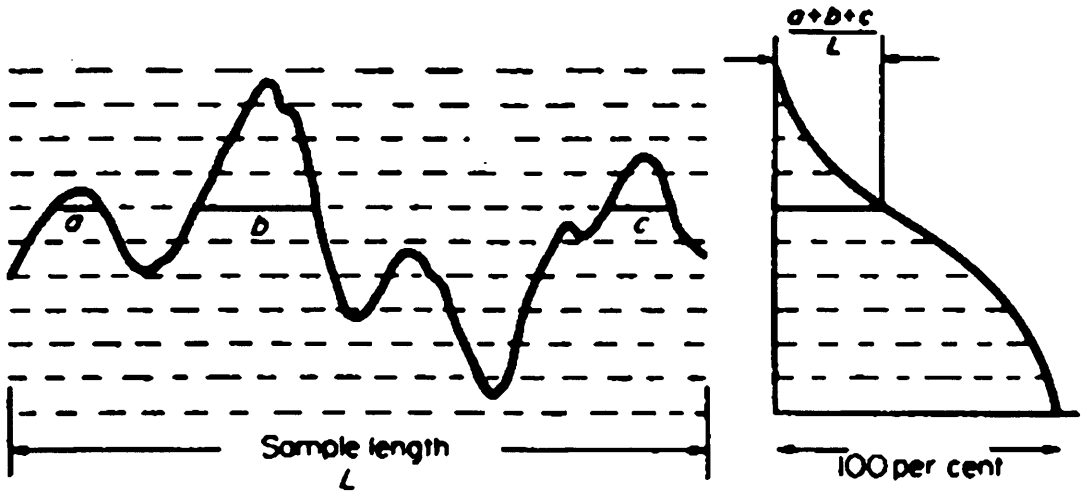

Figure 1.13: Method of deriving the Abbott-Firestone curve (from Halling 1978)

Hobson – A guide to surface texture parameters). Derived from the material ratio tp is the Abbott-Firestone curve or bearing area curve. It is constructed by measuring the fraction of sample length which lies inside the profile at various positions above the lowest point of the profile (Figure 1.13). The top portion of the curve corresponds to the portion of the surface which will quickly be worn away at the start of the operation of the machine element. The bottom portion of the curve gives an idea of the volume of the valley depth. The central portion of the curve corresponds to the long term running surface.

It is usually required to use some sort of filtering to distinguish between various components of surface finish. The filtering action is normally performed using digital filters either high-pass filters to remove the longer wavelengths or the low-pass filters to remove the shorter wavelengths.

The measurement of the surfaces is usually performed using a dedicated apparatus. In our case a Talysurf Instrument from the Taylor Hobson Company was used to perform the various surface texture measurements. The actual sensing device uses a stylus having a diamond tip of 2 μm radius. The stylus crosses the surface at a constant speed and produces an analogue voltage signal proportional to its vertical displacement. The trace obtained is then digitised at a suitable sampling interval for further digital processing. There is a filtering effect produced by the stylus tip radius with its finite dimension which removes short wavelengths. In the same way, some care has to be taken as the truncated pyramid shape of the stylus (90° apex angle) may influence the measurement of surfaces having slopes steeper than 45° angle. Fortunately most engineering surfaces exhibit much gentler slopes.

One should note also the effect of sampling interval on roughness parameters used for contact simulations which will affect results of models like the one of Webster and Sayles as presented in Figure 1.12.

The analysis of contact of rough surfaces was developed originally through the use of analytical models. More recently, numerical models have emerged capable of taking into account real roughness measured data. As far as analytical models are concerned, one can cite two important models developed by Archard (1957) and by Greenwood and Williamson (1966). The main conclusions of Archard could be summarised as follows:

- although surface asperities may flow plastically at first, they must reach a state in which the load is supported elastically;

- he developed a theory using several levels of asperity dimensions from coarser to finer asperities. This model shows that as the scale of asperities becomes smaller i.e. closer to the smooth case, the real area of contact becomes directly proportional to the applied load;
- the number of asperities in contact is proportional to the load, as the scale of asperities gets smaller.

Greenwood and Williamson's analysis used a statistical approach to model the rough surface. The roughness features themselves were modelled as asperities having a constant tip radius but having their heights varying randomly. Their main conclusions can be summarised as follows:

- the area of contact is proportional to the load
- the number of contact spots is proportional to the load
- the average contact size is independent of load

These two influential models have been of great importance in establishing some fundamental trends in the behaviour of contact between rough surfaces. Nonetheless, these models cannot take into account directly the behaviour of real surfaces.

The advent of computers and the development of numerical techniques has made possible the simulation of contact of real surface profiles. Examples of numerical models are those of Webster and Sayles (1986), Ju *et al.* (1992), and Ren *et al.* (1993). All these models use matrix of influence coefficients to relate contact pressure with surface displacement. These models can be rather time consuming particularly in the case of three-dimensional rough surfaces. New approaches have been therefore been developed including Fast Fourier Transform (FFT) as an alternative to the matrix method to establish the force-displacement relation. Ju *et al.* (1996) and Stanley *et al.* (1997) have used such an approach.

1.5.3 Smooth lubricated surfaces in contact: elastohydrodynamic theory

So far only dry surfaces in contact have been considered. In practice, a lubricant is normally used in machine elements like gears and bearings in order to reduce friction and provide a degree of separation between the surfaces. The mechanism of lubrication in gears and bearings is elastohydrodynamic lubrication (EHL). EHL theory is concerned with the two main aspects of the problem, namely hydrodynamic

lubrication and elastic deformation. Reynolds (1886) initiated one of the key developments in the field of hydrodynamic lubrication. He established the differential equation governing the generation of pressure in a film taking into account surface velocities, viscosity, and geometry. The Reynolds equation is still used as the basis for most calculations in hydrodynamic bearings, but it does not take account of the elastic deformations present in non-conforming contacts under load. In such contacts the pressures are high (of the order 1 GPa or greater) and it is also necessary to take account of the important, beneficial effect of pressure on the viscosity of the oil. One of the most widely used relationships between pressure and viscosity is the Barus law (1893) giving the viscosity η as a function of the pressure p as follows

$$\eta = \eta(p) = \eta_0 e^{\alpha p}$$

where η_0 represents the viscosity at atmospheric pressure and α is the pressure viscosity coefficient. Neglect of these effects (deformation and viscosity/pressure) leads to the prediction of unrealistically thin films. This is incompatible with practical observations where under normal operation roughness features created by the manufacturing process are still present after a large number of cycles indicating the presence of proper fluid film lubrication.

Grubin and Vinogradova (1949) were the first to propose an analytical solution for the case of non-conforming surfaces incorporating both the effect of elastic distortion and the effect of pressure upon viscosity. The contact deformation was assumed to be Hertzian, the effect of lubrication being to interpose a parallel film. Their analysis yielded a formula for the film thickness which takes account of the main operating variables. Petrusevich (1951) using a numerical solution identified another key feature of EHL lubrication. This corresponds to the local constriction and associated pressure "spike" towards the outlet of the parallel film. Dowson and Higginson (1959) used a robust numerical solution called the "inverse" method to give full solutions to the problem of hydrodynamic lubrication of loaded elastic cylinders. The principle of this inverse method corresponds to using the Reynolds equation in a different way to determine first the "hydrodynamic" oil film thickness which is then compared to the "elastic" oil film thickness due to elastic deformation. The discrepancy is then addressed by adjusting the pressure in the oil film. This differs from the "direct" method where the pressure distribution is established by first solving the Reynolds equation and then using the resulting pressures to calculate elastic deformation which

is then used to adjust the film shape, etc. The advantage of the inverse method is its better numerical stability for highly loaded cases as found in realistic engineering problems. Dowson and Higginson (1960) then used their model to study the influence of various parameters on the pressure distribution and oil film shape. It was found that load and elastic modulus have only a small effect on the film thickness and the main factors influencing the film are entraining speed, viscosity, pressure coefficient of viscosity. The formula for minimum film thickness derived by Dowson and Higginson is as follows

$$h_{\min} = 1.6\,\alpha^{0.6}\,(\eta_0 u)^{0.7}\,(E')^{0.03}\,R^{0.43}\,(w')^{-0.13}$$

It should be noted that Dowson and Higgingson's formula applies to isothermal conditions only.

An important measure of the effectiveness of an oil film under rough surface conditions is the ratio λ which is the ratio between the EHD film thickness and the composite surface roughness. Dowson (1992) emphasized its importance as an indicator of the life of highly stressed lubricated machine components. The higher the λ value, the greater the chance will be to develop a fully form EHL film thus reducing the risk of surface distress. Unfortunately for most highly loaded gearing systems as found in aerospace, the film thickness is usually of the order of the surface roughness. Hence the influence of the surface asperities (rough contact) in the EHL lubrication process has developed considerable interest in recent years.

1.5.4 Rough lubricated surfaces in contact

Although early EHL theory was a major breakthrough in our understanding of lubricated contacts its assumption of smooth surfaces limited its application to real engineering conditions, particularly those in gears. In recent years the concept of micro-elastohydrodynamic lubrication (micro-EHL) has emerged to take into account the effect of roughness features and asperity deformation. Archard first introduced the term "micro-EHL" in 1973. Cheng has been a major contributor in the field. Hence he developed a full numerical solution in the case of a single transverse asperity running against a smooth surface in an EHL contact (Lee and Cheng, 1973). He also proposed

in collaboration with Dyson (1978) a full numerical model for the inlet half of a contact between two ground rough surfaces. Cheng in collaboration with Patir (1978) proposed the so-called "average flow" model. It is based on a mean flow through a rectangular control volume that is small relative to the contact dimensions but still contains numerous asperities and possible asperity contacts. The authors introduced flow factors to assess the flow that goes through a rough bearing as a proportion of predicted flow that goes into a smooth bearing area. These flow factors are established from statistical data obtained from roughness measurements. A number of other authors have used the "average flow" model to investigate various effects of the lubrication of rough contacts. Sadeghi and Sui (1990) for example reported very large pressure fluctuations created by a single sinusoidal type asperity having an amplitude representing only a few percent of the central film thickness. Unfortunately the "average flow" model only allowed a macro evaluation of the contact behaviour. Hence only the global lubricating film shape can be predicted but no information can be gained of the behaviour of the contact at the asperity level including their individual deformation and the corresponding pressure response. First attempts to address this problem using a sinusoidal representation of the roughness were presented by Goglia *et al.* (1984), Lubrecht *et al.* (1988), Kweh *et al.* (1989), Elsharkawy and Hamrock (1991). Lubrecht used the so-called "multigrid" method. He reported that asperity deformation is much greater in the case of transverse roughness (i.e. roughness ridges orientated perpendicular to the entrainment direction) when compared to the longitudinal roughness. Average lubricating film thickness was also found to be much smaller than that found using average flow models. More recently some authors have used real surfaces as represented by profilometer traces of actual surfaces. Hence authors like Webster *et al.* (1986) have proposed steady state solutions i.e. using stationary roughness. In the same way solutions for the non-steady state problem (moving roughness) have been proposed very recently by authors like Elcoate *et al.* (2001). The results of this work have been used in the current thesis and the approach developed by Elcoate will be presented in detail in Chapter 6.

1.6 Materials used in aerospace gearing

Townsend (1983) gave a brief review of the wide variety of gear materials and processes available to gear designers. Wood, plastic, aluminium, magnesium, titanium, bronze, cast iron, low-, medium-, and high-alloy steels have all been used in gear designs. But for most high duty aerospace gears steel is the material used. Its composition, cleanliness and heat treatment are all crucial factors in determining its ability to perform reliably and resist surface distress and failure.

A gear steel has the following basic requirements: sufficient static fatigue strength to withstand instantaneous and dynamic loads; adequate toughness to withstand shock loads; adequate resistance to plastic deformation, pitting, scuffing and wear in the tooth contact area and, finally, ease of manufacture.

The most important variables that dictate the ability of an alloy to resist the applied bending and rolling contact fatigue loads are surface hardness, core strength, and case depth in a case hardened gear. An essential aspect for optimum rolling contact fatigue performance and wear resistance is a high surface hardness. The high hardness allows the surface to withstand the stresses in the contact without excessive plastic deformation. In Hertzian contacts it is important to have a high material hardness to avoid plastic deformation (the pressure at first yield in a line contact is $1.67\sigma_y$. using the Tresca yield criterion and Hardness $\approx 3\sigma_y$ (Johnson 1985)). In practice, surfaces are rough and the maximum shear stresses are shifted towards the surface and are much larger than the Hertzian value. This will be further discussed in Chapter 6.

The subsurface residual stress distribution in a gear can also play an important role. Tensile residual stresses may be detrimental, increasing the likelihood of fatigue damage, stress corrosion, and fracture; on the other hand, compressive residual stresses are usually considered beneficial.

Apart from the above-mentioned factors, careful attention to heat treatment (Jatczak 1978), grain size, cleanliness, and machining are all of prime importance in gear steel. In addition to the requirements for gear steels, aerospace transmission designs need to remain competitive in terms of weight, cost, and oil loss tolerance.

The high hardness necessary to overcome rolling contact fatigue has the drawback that it also enhances crack propagation. The progression of a surface crack or fracture through the case has a higher probability of changing direction when it reaches a more ductile core (DiRusso 1986). Therefore, the core material in the gear

must have a high fracture toughness and resistance to fatigue crack propagation to withstand the cyclic loading which is inherent in gears.

Jatczak (1978) commented on the fact that ordinarily there is no significant difference in performance between case carburised steels and homogenous high carbon components with regard to rolling contact fatigue, resistance to scuffing, and wear (if the comparison is made at equivalent hardness, microstructures, and surface carbon levels). The static and dynamic load-carrying capacities in Hertzian compression are also essentially equivalent. However, he pointed out that when bending, torsion, and impact stresses were encountered, as in gears, carburised steels always provided significantly higher fatigue strengths. This results from a combination of the higher fracture toughness and impact resistance imparted by the low carbon regions and from the compressive residual stresses produced in the case layers by carburising or nitriding.

An important aspect of case hardening is to create a case strength, which maintains a safe working margin above the induced stresses. To achieve optimum protection against case crushing it is important to ensure that the case depth exceeds the depth of the maximum Hertzian shear stress. At the same time, the surface hardness has to be as high as possible to overcome the local stresses caused by the asperities (Wilkinson, 1998).

It is now widely accepted that improved cleanliness of steels by vacuum arc remelting (VAR) and vacuum induction melting (VIM) has improved the fatigue performance of components by reducing inclusion content (Littmann *et al.* 1966). These processes are now used systematically for aerospace material production.

It has, therefore, been noted that different properties are needed for the surface and core of gear steel for aerospace use. These properties of highest possible yield stress, or hardness in the surface, and high fracture toughness in the core material cannot be achieved without surface modifications. Various methods of surface engineering are used. Surface engineering involves modifying the surface properties of a material. It can involve either surface modification or applying a new surface, i.e. a coating or both. Both can give very different surface properties from the bulk material. Implicit in the decision to engineer the properties of a surface is that some of the existing properties of the substrate material are adequate for the surface to perform satisfactorily (Bell 1993).

The aims of the process can be to improve wear, fatigue, corrosion, impact resistance, or strength at elevated temperature, for example. Aspects such as the surface hardness, bonding strength, component size, thickness of the layer, and cost of the process are all important considerations. The purpose of the presented work is to contribute to the understanding of surface distress limiting the treatments under consideration to processes that give a relatively thick, hard layer to withstand the Hertzian and high surface stresses. Consequently, thermal treatments will be discussed here, as will be some coating processes. The latter usually give a thin case, but can be very hard and can be integrated with other processes to give optimum surface characteristics. By determining the critical type of stressing and adapting the material properties to the actual type of stressing, the rolling contact fatigue strength of components, and thus life, can be improved (Schlicht *et al.* 1980).

Bell (1993) reviewed a range of surface engineering processes in relation to layer thickness (Figure 1.14). The thickness of the engineered surface can vary from several millimetres for surface welding, to a few microns for PVD and CVD coatings. The current study includes the investigation of PVD type coatings that will be detailed in Chapter 5. Likewise surface hardness spans a wide range from about 250-350 HV hardness for some spray coatings, to 1000 HV for nitrided steels, and up to 3500 HV can be achieved for PVD (TiN) coatings.

Currently the main surface engineering process available to aerospace gear designers involving surface modification is heat treatment. There are three major types of heat treatment: simple thermal treatments, where temperature variations alone are involved; thermochemical treatments, which involve processes where surface additions or losses take place by diffusion as well as thermal treatment; and thermomechanical treatments, which involve mechanical work during the heat treatment.

In thermochemical treatments metallic or non-metallic elements are added to produce a hard, wear resistant surface on components that also require toughness. The aim is to improve the fatigue performance of the component and perhaps impart better scuffing and frictional characteristics.

The treatments with non-metals mainly involve carbon and nitrogen, and these can be divided in two main categories: austenitic, where nitrogen and/or carbon are diffused into the steel in the austenite phase; and ferritic, where carbon and/or nitrogen are diffused into the ferrite phase.

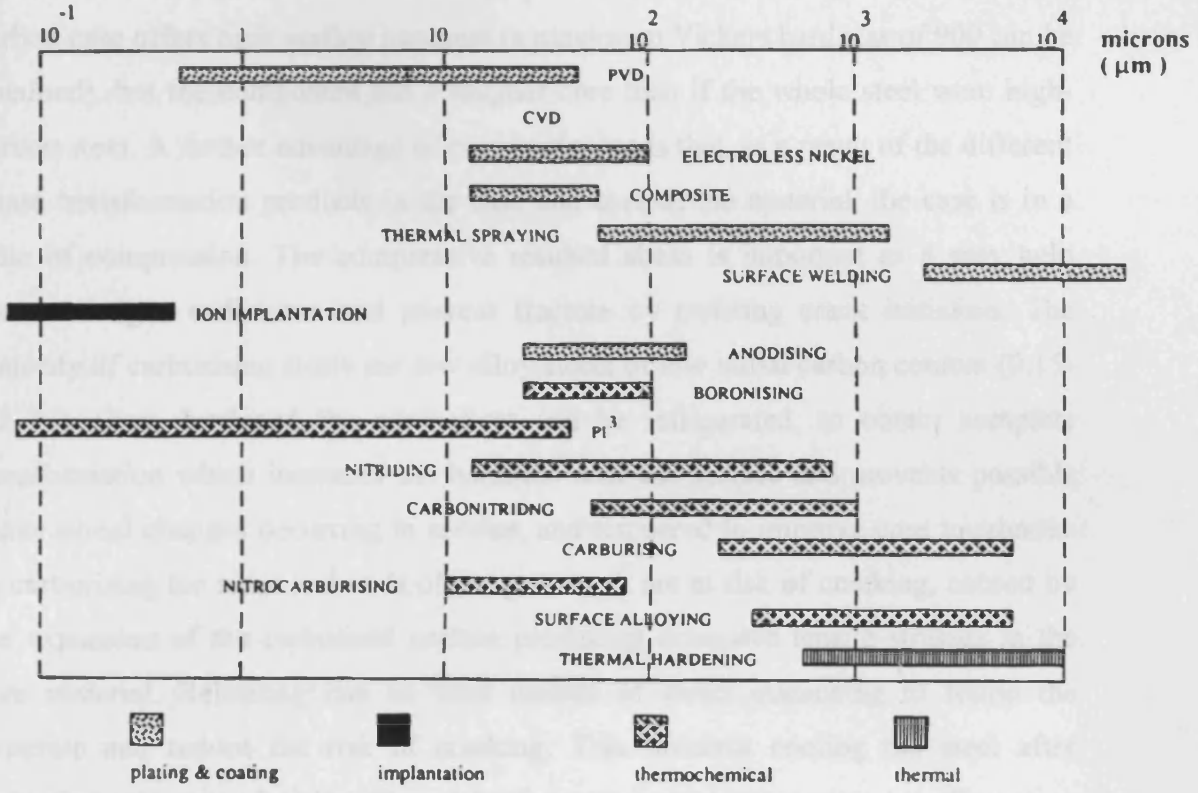

Figure 1.14: Classification of the surface engineering technologies as a function of surface modification thickness (from Bell 1993).

The main austenitic processes are carburising and carbonitriding. In carburising carbon is diffused down a concentration gradient into low carbon materials at 900 °C, or higher, for periods between 30 minutes and 16 hours, depending on the case depth required. The carbon may be supplied through a solid, liquid, or gaseous medium and the process is followed by quenching to harden the case. The increased carbon content in the case increases hardenability by creating more martensite on quenching, so that the resulting case is a mixture of martensite and retained austenite. The high carbon case offers high surface hardness (a maximum Vickers hardness of 900 can be obtained), but the component has a tougher core than if the whole steel were high-carbon steel. A further advantage of case hardening is that, as a result of the different phase transformation products in the case and core of the material, the case is in a state of compression. The compressive residual stress is important as it may help contact fatigue endurance and prevent fracture by resisting crack initiation. The majority of carburising steels are low alloy steels of low initial carbon content (0.15-0.2 %). Once hardened the component can be refrigerated, to obtain complete transformation which increases the hardness near the surface and prevents possible dimensional changes occurring in service, and tempered to improve core toughness. In carburising the sides and ends of the gear teeth are at risk of cracking, caused by the expansion of the carburised surface producing excessive tensile stresses in the core material. Reheating can be used instead of direct quenching to refine the structure and reduce the risk of cracking. This involves cooling the steel after carburising to give bainite, then reheating to just above upper transformation temperature and quenching.

The main ferritic processes are nitriding and nitrocarburising. In the nitriding process, nitrogen is added at 500-570 °C from a gaseous or liquid medium, and then the steel is air cooled. Atomic nitrogen forms at the surface and diffuses in, reacting to form nitride compounds as fine precipitates close to the surface. This produces lattice strains high enough to nucleate dislocation which, together with the precipitates, have a strong hardening effect. Compressive residual stresses are also obtained in the case. The steels used need to contain one or more of the nitriding elements aluminium, chromium, molybdenum, and vanadium. The hardness produced by nitriding (900-1100 HV) is maintained at temperatures up to 500 °C; whereas in the martensitic layers in carburised steels, hardness falls at about 200 °C. This latter feature may create some problems when considering the coating of case carburised steel when any

subsequent coating process occurs at a temperature close to 200°C. The low temperatures involved mean there is little distortion to the component, but the treatment times are longer.

The main problem with nitriding is the formation of brittle nitrogen compounds on the surface of components, these are known as the "white" layer or compound layer. It consists of a thin layer of iron nitrides, composed of an outer layer of epsilon iron nitride (typically 10 μm deep), over a layer of gamma-prime nitride (also about 10 μm deep) (Olver *et al.* 1993). Although it is very hard, it is brittle and cracks easily and can promote fatigue failure (Bell 1973, Braza 1992, and Hutchings 1992). Olver et al. (1993) analysed this white layer and deemed it necessary to remove it, as it offered little substrate protection and could be expected to fail rapidly. It is often removed by grinding or chemical means.

However, in tests described by Winter and Weiss (1981) where the white layer was removed by grinding, the surface stress endurance limit of gears made from two different nitrided materials was reduced by 10-20%. They described the epsilon iron nitride layer as being abrasion and corrosion resistant, and the gamma prime layer as being brittle, and found a tendency for the endurance limit to increase with increased epsilon to gamma prime ratio.

Distortion can be a major problem associated with heat treatment (Davies & Gittos 1989) It is caused by phase and temperature changes within the material and varies considerably from component to component. Size distortion can be predicted at the design stage and the component can be finish ground. Shape distortion, which occurs particularly in asymmetrical components, can be minimised by avoiding temperature differentials, minimising phase transformations, and avoiding rapid heating and cooling of irregular shapes. Distortion tends to be more of a problem in carburising due to the elevated temperatures involved; however, as the case is generally deeper than nitriding, finish grinding is not so much of a problem.

The last surface engineering process available to modify a component's tribological performance is coating deposition. There is, in this field a very large choice of coating materials available.

Typically, the main surface coating groups are electrochemical treatments; chemical treatments; chemical vapour deposition (CVD), physical vapour deposition (PVD), the latter being particularly suitable for gear coating and have been the subject of very important developments recently.

Electrochemical coatings are produced by electrolysis in an aqueous solution of the coating metal with the component as the cathode. Chromium is the coating mostly used for wear resistance because it combines high hardness (1000 HV) with corrosion resistance. The layer is about 0.5 mm.

In chemical treatment the component is immersed in a solution of a salt of the coating metal. After heat-treating, the component can have a hardness of 1000 HV and a good adhesive wear resistance. Hard particles can be incorporated in both processes (e.g. silicon carbide).

CVD compounds are reacted in the gas phase to form a dense layer on a heated substrate. Titanium nitride and carbide are the most widely used deposits (1-10 μm depths). The temperatures are high (800-1000 °C), which limits the choice of substrate.

PVD is performed at sub-atmospheric pressures. Thermal evaporation or electrical sputtering of the chosen material generates the coating. Titanium nitride is the most popular (1-10 μm depths). Substrate temperatures can be kept below 500 °C but have to be maintained typically above 200°C which can develop potential problems as will be discussed in Chapter 5.

Materials, which have been under consideration in this study, include both case carburised steel (EN36) as well as nitrided steel (EN40) with and without the "white layer". Coatings will also be under consideration which in our case are PVD type coatings.

1.7 Investigations into the different types of gear surface failure: scuffing failure

Scuffing is a very complex phenomenon requiring a detailed understanding of the contact mechanics involved, the modes of heat transfer together with knowledge of the physical and chemical state of the surfaces and lubricants. When scuffing takes place as described by Dyson (1975), it usually induces fusion of a superficial layer of the case of the contacting materials. This fusion (or welding) is associated with a large amount of smoke and noise. Its occurrence is very sudden and usually requires the test machine to be stopped more or less immediately. Scuffing is encountered in all types of mechanical devices whether lubricated or not when the combination of load and

sliding velocity exceeds a certain level. This value is currently not particularly well established. It is a common type of surface distress in gears, bearings or cam and follower devices. The appearance of an industrial scuffed gear is shown in Figure 1.15 showing the extent of the surface distress.

Historically, two main theories have been developed to explain the occurrence and the mechanism of scuffing. The thermal approach was developed first followed by the chemical approach and the elastohydrodynamic approach. Blok (1939) proposed the traditional thermal approach which is still very much used in design offices. This theory is based on the so-called "flash temperature". According to Blok, scuffing occurs when the surface temperature exceeds a critical value. Blok developed a model (Blok, 1937) to assess the surface temperature of the contacting bodies by superimposing the bulk temperature and a localised temperature called the flash temperature. Although this is a popular model it is controversial; many gear experts and gear designers are not convinced that it can reliably predict scuffing. In this model the flash temperature is obtained analytically by considering an infinite heat source along the Oy direction (see Figure 1.16) and of width $2a$ along the x direction. This source is placed on the surface of a semi-infinite body. The heat source moves relative to the body with a constant velocity U. The heat source dissipates a heat flux $q(\xi)$ in the z direction (into the semi-infinite body). The surface (z = 0) is supposed to be adiabatic outside the heat source area and the semi-infinite body is at an initial constant temperature. The increase in surface temperature in the area of contact between the heat source and the semi-infinite body $-a \le x \le a$ is given by the following formula:

$$\Delta T(x) = \frac{1}{\sqrt{\pi \rho C k U}} \int_{-a}^{x} \frac{q(\xi)}{\sqrt{x-\xi}} d\xi$$

Where:

ρ denotes the density of the solid surface

C denotes the specific heat of the solid surface

k denotes the thermal conductivity of the surface

Under EHL conditions the contact pressure is expected to be distributed in a form close to the Hertzian which is a semi-elliptic distribution.

In this case, the heat source can be expressed as follows:

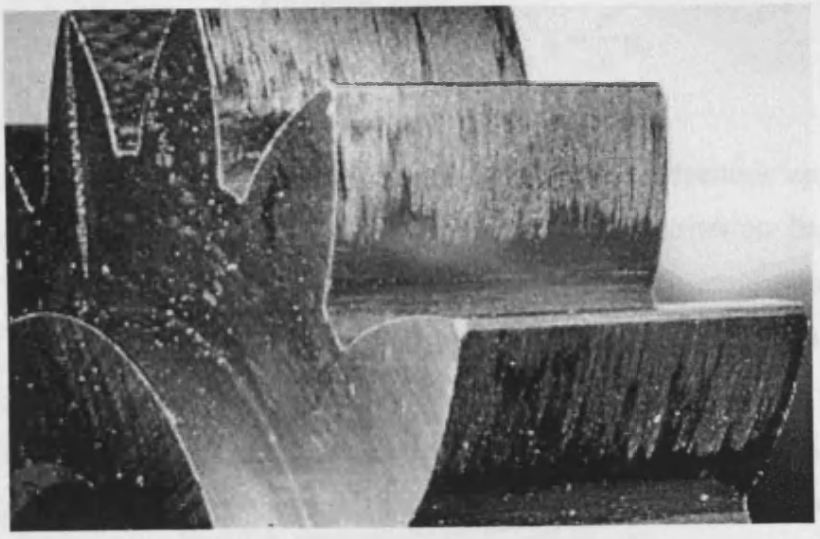

Figure 1.15: **Photograph showing the aspect of the scuffing surface distress as encountered with gears.**

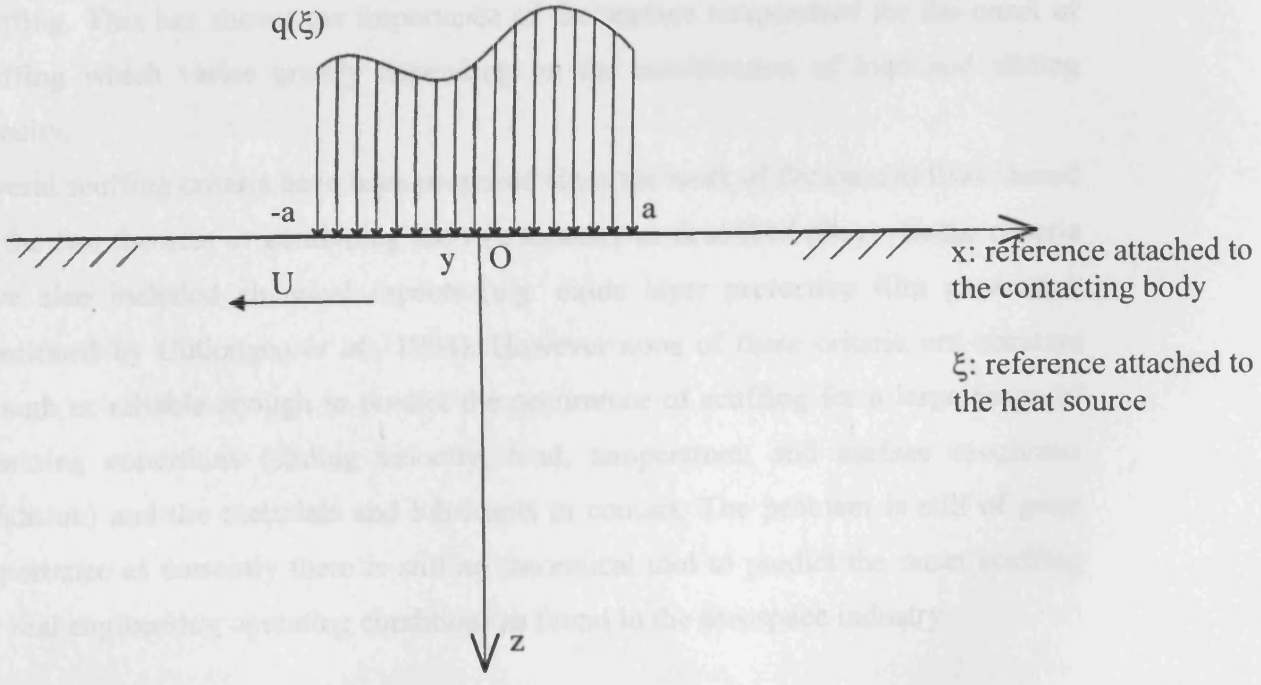

Figure 1.16: **Mobile heat source on a semi-infinite body illustrating the assumptions considered by Blok (1937) for the flash temperature theory.**

$$q = q_0\sqrt{1-\frac{x^2}{a^2}} \qquad \text{and} \qquad \bar{q} = \frac{\pi}{4}q_0$$

The second main theory which can be described as the hydrodynamic approach was first presented by Dyson (1976). He proposed a scuffing criterion based on the collapse of the lubricating film present in an elastohydrodynamic contact in the presence of sliding. He established that scuffing cannot occur if the lubricant viscosity is sufficiently high at the inlet of the contact. This can be understood by considering the state of the lubricant subjected to extreme pressure in an elastohydrodynamic type contact. Hence, the lubricant behaves like a solid body. Under these conditions, the lubricating film has a stiffness well above that of the contacting surfaces and will behave like a protective layer between the two surfaces allowing them to avoid metal to metal contact between asperities.

More recently, Enthoven *et al.*(1993) have used a ball and disc machine and an infrared temperature measurement technique for measuring the temperature of the surface of the contact. This measurement was performed before and after the onset of scuffing. This has shown the importance of the surface temperature for the onset of scuffing which varies greatly depending on the combination of load and sliding velocity.

Several scuffing criteria have been proposed since the work of Dyson and Blok, based on the two theories or combining the two theories as described above. Some criteria have also included chemical aspects (e.g. oxide layer protective film generation mentioned by Cutiongco *et al.*, 1994). However none of these criteria are accurate enough or reliable enough to predict the occurrence of scuffing for a large range of operating conditions (sliding velocity, load, temperature, and surface roughness condition) and the materials and lubricants in contact. The problem is still of great importance as currently there is still no theoretical tool to predict the onset scuffing for real engineering operating conditions as found in the aerospace industry.

1.8 Investigations into the different types of gear surface failure: micropitting failure

Micropitting is considered to be pitting on the scale of the roughness as opposed to conventional pitting which occurs on the scale of the nominal Hertzian, or macro, contact. Both phenomena may be considered as a form of surface fatigue failure. With the increased use of hardened gears micropitting has become of serious concern particularly to the aerospace industry. The types of gears which are mostly affected by this type of damage are the heavily loaded ones with hardened teeth. The problem has been extensively studied by a number of authors (Berthe *et al.* 1980, Shotter 1981, Olver *et al.* 1986, Webster *et al.* 1995). Micropitting is characterised by the presence of fine surface pits (typically 20 μm deep and about the same diameter) and the occurrence of local plastic deformation and shallow surface cracks (the appearance of a micropitted gear is shown in Figure 1.17). This can give rise to severe wear (Olver *et al.* 1986) or progress into destructive pitting (Berthe *et al.* 1978). This can in turn induce loss of the tooth profile leading to noise. Serious cases can precipitate scuffing and even the complete fracture of the tooth. Berthe *et al.* (1980) have indicated that the rate of micropit formation depends on running-in. Hence, when running in takes place i.e. when the pressure at asperity tips decreases to a value within the elastic limit of the material, the rate of formation of micropits with time tends to zero and the fatigue life is consequently increased. This trend has also been demonstrated with superfinished gears (Krantz *et al.* 2001) where effectively the surface is pre- run in using a polishing process prior to testing. In this particular case, the lives of the gears with superfinished teeth were found to be about four times greater than those of ground gears made of the same case carburised material. The phenomenon of micropitting appears with both synthetic and mineral oils and with both through-hardened and case-hardened steels of either carburised or nitrided forms (Shotter 1981). The wear associated with micropitting as mentioned earlier was related by Olver *et al.* (1986) to plastic deformation, fatigue cracking, ductile extrusion, and fracture on a scale associated with the asperity contact. The stress raising feature was the roughness producing local plastic deformation, despite the low Hertzian applied stress. This underlines the necessity to consider the micro-EHL effects of the oil film since these influence the contact pressures and, through non-Newtonian and time-dependant behaviour, determine the traction forces at the micro contacts. Olver *et al.* (1986) also suggested methods to prevent the occurrence of severe micropitting.

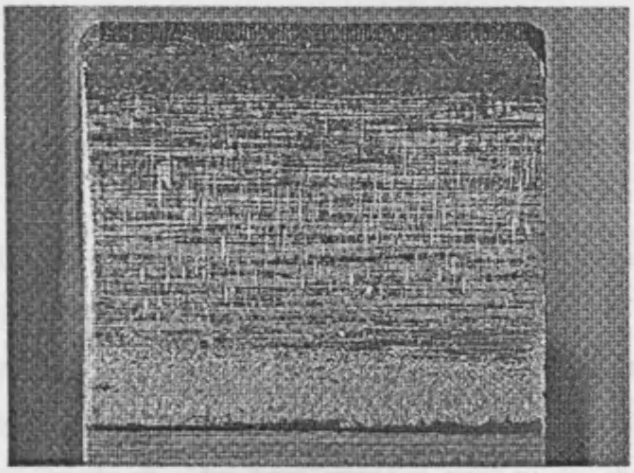

Figure 1.17: Gear tooth showing micropitting damage in the root region. (Design Unit, Newcastle University)

Hence, both surfaces in contact should be made as hard as possible. This conclusion suggests case hardening treatments like nitriding or ultra hard coatings that are both considered in the present work. It is suggested also that the surface experiencing more cycles should be harder and that the harder surface should be made as smooth as possible. This requirement can be met using superfinishing type treatments as used in the experimental programme of work presented here. Lastly, it is recommended that the lubricant film thickness should exceed the combined roughness height. This in turns emphasizes the importance of characterising the contacting rough surfaces and of assessing the lubricant film thickness of the real rough contact using time dependent solvers as developed for example by Elcoate *et al.* (2001) and used also in the current work.

1.9 Objectives of the thesis

The overall objective is to obtain a better understanding of the parameters influencing surface distress for surfaces typically found in aerospace gears. To achieve this, a substantial experimental programme will be carried out to quantify the effect of different parameters such as different substrate materials, different kinds of surface finish and different kinds of ultra hard coatings applied on the substrates being considered. The experimental program will be conducted using an existing disc machine which was developed originally to simulate aerospace gearing. It will extend the work already carried out by Patching *et al.* (1994) on scuffing performance of aerospace gear tooth contacts. This experimental work will necessitate a major modification of the rig as used by Patching and will necessitate the complete design and manufacture of a new test rig dedicated to experiments on micro-pitting.

Following the experimental work acquired profiles from a digital profilometer will be used to carry out EHL computer modelling of the various real rough surfaces experimentally tested in various configurations. The EHL model selected for this work is the one developed by Elcoate *et al.* (2001). Analysis of the results acquired from the computer model will be used to help understand the behaviour of the various tested configurations and to isolate the key features influencing the surface distress as experienced during the tests. Finally, a number of objective parameters as developed

by Tao *et al.* (2003) will be used to discriminate between the various configurations in terms of pressure behaviour, pressure cycling behaviour and film thickness behaviour.

CHAPTER 2.

A test rig for the investigation of scuffing of high speed, high temperature gear contacts

2.1 Introduction

This chapter describes the machine which has been used to perform the scuffing tests. All scuffing experiments described in this thesis were performed using the equipment first devised by Patching *et al* (1994). The original engineering background to this work was the need to understand the behaviour and failure of gear tooth contacts used in demanding aerospace applications such as aircraft engine and helicopter gearboxes. Scuffing tests, designed to measure the performance of a particular combination of lubricant and gear steel are usually impracticable on full-scale machinery, while tests using smaller gears are expensive. Furthermore, it is difficult to measure quantities of interest for research purposes, such as friction and bulk temperature. Fundamental research investigations of scuffing under controlled conditions are therefore more conveniently carried out through the use of disc machines. The adoption of disc machines in gear contact research is well established (see, for example, Bell and Dyson, 1972; Bell, Dyson and Hadley, 1975). The main advantage of the disc machine is the relatively low cost of test specimens and the ability to closely control operating conditions. The main disadvantage with disc machines is their inability to reproduce the complicated kinematical and dynamical conditions of the gear mesh. However, in fundamental studies of the little understood problem of scuffing it is first necessary to be able to understand the relatively simple, well-defined conditions of constant load and steady sliding and entrainment before the more complicated aspects of gearing can be addressed.

2.2 Representation of gear tooth contacts by equivalent cylinders

The representation of spur gear contacts using discs can be justified by considering some of the fundamental properties of involute gears. Merritt (1962) demonstrated

that in the case of spur gears the tooth surface can be considered as part of the surface of a cylinder. In the same way, two cylinders in contact with appropriate equivalent rolling and sliding between them may represent the conditions of the tooth engagement. This situation is illustrated in Figure 2.1 which shows a pair of spur gear teeth in contact at an arbitrary point C. This point of contact is at a distance s from the pitch point P. Two equivalent cylinders having the following radii can then represent the contact at point C:

$$R_1 = R_a \sin\theta - s$$

$$R_1 = R_b \sin\theta - s$$

R_a and R_b represent the pitch radii of the respective gears and θ is the pressure angle.

In a disc rig using discs of a fixed diameter and driven together with a fixed gear ratio only one geometric and kinematic condition can be modelled. In disc machine scuffing experiments, therefore, the attempt is usually made to represent the worst case of sliding between gear teeth which occurs at tips of the teeth.

2.3 Description of the rig

The machine was first designed and built for an earlier EPSRC/Rolls-Royce project with the aim of reproducing the conditions found in present and future designs of gearing used in gas turbine engines.

Apart from the high speed/high temperature capability other special features are the use of crowned discs to give a self-aligning contact, and axial finish of the disc surfaces, which reproduces the orientation of finish found on gears. These aspects will be further developed in sections 2.4 and 2.6. The machine was first commissioned and used in a series of scuffing tests described by Patching *et al (1994).*

The original design of the machine was carried out in close collaboration with Rolls-Royce in the UK with the aim of reproducing the rolling/sliding speeds and contact pressures found in typical gear meshes. The outline of the original specification is as follows:

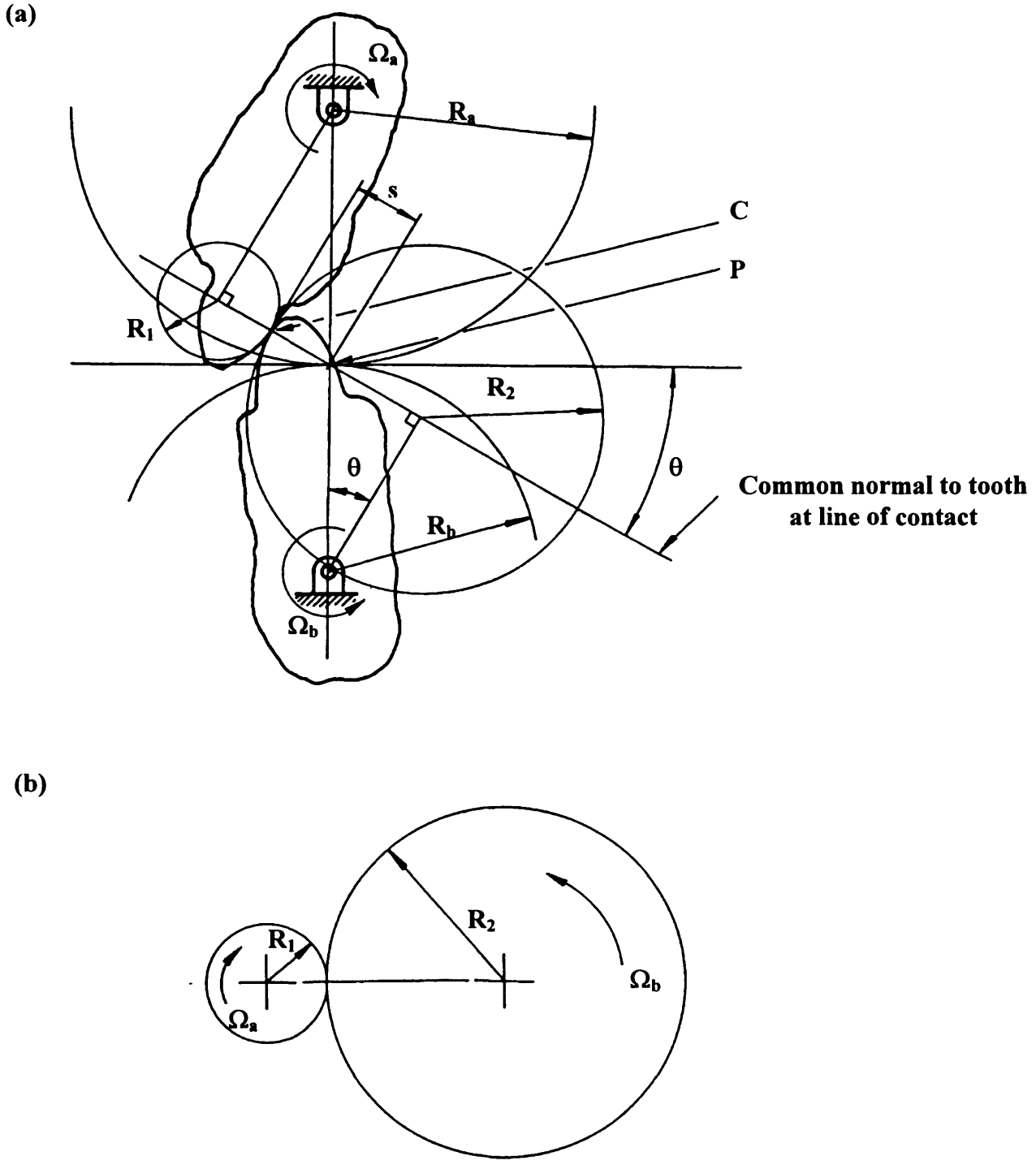

Figure 2.1: Representation of the contact of involute spur gears using equivalent cylinders.
(a) Meshing of a pair of spur gears in contact at an arbitrary point C (point P is the pitch point)
(b) Representation of the gear mesh by two equivalent cylinders of radii R_1 and R_2

- Sliding speed up to 25 m/s
- Maximum Hertzian contact pressure up to 1.7 GPa
- Oil feed temperature up to 200 deg C
- Lubricant: synthetic (di-ester) meeting MIL-L-23699 C requirement

The machine was intended to operate at relatively high speed, and in order to minimise the power required to drive the discs it was decided to use rolling element bearings to support the test shafts. The layout of the test head and its drive arrangement is shown in Figure 2.2. Each test shaft is supported on a two-row spherical roller bearing at one end, and a cylindrical roller bearing at the other end. The spherical roller bearing provides high radial load capacity together with axial location, and the cylindrical roller bearing provides radial support without axial restraint. The shafts are of EN36 steel (equivalent to AMS 9310), case carburised and hardened to 680 Vickers Hardness Number (30 kg). The shafts were carefully finish-ground on dead centres. An interference fit was provided between the discs and shafts (minimum 0.015 mm, maximum 0.025 mm on diameter) and the discs are pressed on to the shafts using a hydraulic press. After testing, the discs are pressed off the shafts and the shafts are re-fitted with new discs. The shafts are provided with central and radial feed holes for thermocouple leads to allow measurement of the bulk temperature of the discs. A general view of the machine is shown in Figure 2.3.

Toothed belts and pulleys drive the two test shafts from the two outputs from a splitter gearbox. A toothed belt drives the input shaft of the gearbox and pulleys from a 18.5 kW "*TASC*" variable speed drive motor. The maximum speed of the *TASC* unit is 2800 rpm so speed-increasing pulley ratios are used to achieve the highest speeds required. The drive was designed to operate the machine with a maximum test shaft speed of 12,000 rpm which gives a disc surface speed of 47.88 m/s. By using different combinations of pulleys on the output shafts of the splitter gearbox and drive shafts of the test head it was possible to obtain test shaft speed ratios from 1 (pure rolling) to almost 5. The surfaces of both discs moved in the same direction relative to their contact, but at different speeds, depending on the gear ratio selected. As mentioned earlier, the rig was designed to operate at sliding speeds up to 25 m/s. This is representative of the extreme conditions which can be encountered in aerospace gears

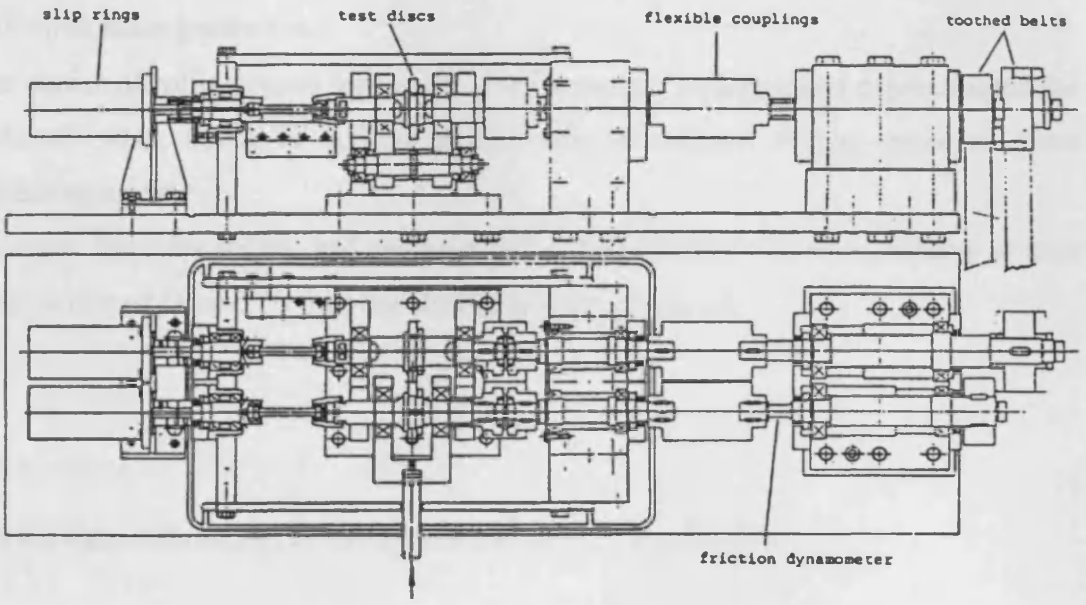

Figure 2.2: **Section and plan drawing of the test head and drive arrangement of the high speed scuffing rig.**

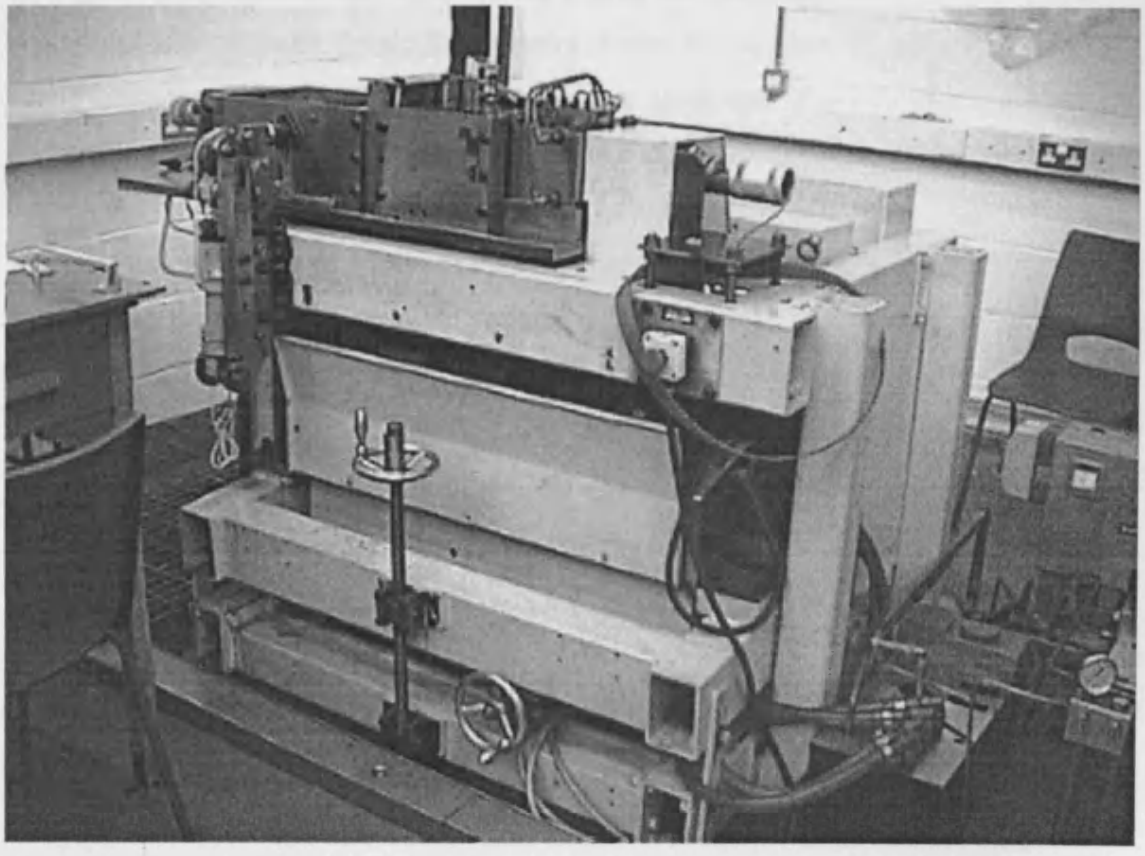

Figure 2.3: **Overall view of the scuffing rig.**

as already illustrated in section 1.2 in relation to the high speed input stages of helicopter main gearboxes.

The choice of rolling speed for the rig given a desired sliding speed depends upon the slide/roll ratio, which is defined as the ratio of relative sliding speed to mean entraining speed.

If two surfaces are rolling and sliding together with surface velocities relative to their conjunction of U_1 and U_2 then the sliding speed is defined as:

$$U_s = U_1 - U_2$$

and the mean entraining, or rolling velocity is: $U_r = \frac{U_1 + U_2}{2}$

The slide/roll ratio is therefore given as: $\frac{U_s}{U_r} = 2\frac{(U_1 - U_2)}{(U_1 + U_2)}$

In a gear tooth contact this ratio varies during the meshing cycle. When contact occurs at the pitch point the sliding velocity is zero so the slide/roll ratio is also zero. The maximum slide/roll ratio occurs at the gear tooth tips. The maximum values of slide/roll ratio calculated for typical gas turbine engine gears range from about 0.4 to 0.8.

In a two disc machine with discs of equal diameter, and in which both surfaces move in the same direction relative to the contact, as they would if connected by a single pair of gears, the slide/roll ratio may be expressed in terms of the ratio, G of the shaft speeds as:

$$\frac{U_s}{U_r} = 2\frac{(G-1)}{(G+1)}$$

where G is the "gear ratio" = $U_1/U_2 \geq 1$.

The highest gear ratio currently attainable in the two-disc machine used in this work is 4.24, which gives a slide/roll ratio of 1.24

The choice of slide/roll ratio to be used in a disc machine in order to provide an exact simulation of gear tooth action is not straightforward because the "entraining" action of the inlet region of an elastohydrodynamic contact depends upon the geometrical conformity of the surfaces as well as their mean speed. For line contacts the geometrical conformity is described in terms of the radius of relative curvature of the two surfaces. In the disc machine used in this work, in which the discs are 76.2 mm diameter, the radius of relative curvature in the entraining direction is 19.05 mm. In spur gears the radius of relative curvature between tooth contacts depends, in general, on the position considered in the meshing cycle. An approximate indication of the radius of relative curvature, which applies when contact occurs at the pitch point, is given by:

$$R = \frac{r_1 \cdot r_2}{(r_1 + r_2)} \sin \Phi$$

where ϕ is the pressure angle of the gear teeth and r_1 and r_2 are the pitch radii of the two gears in mesh. If we take the special case of equal gears so $r_1 = r_2 = r$ and a typical pressure angle of 20 degrees, we see that for R = 19.05 mm we obtain r = 111.4 mm. The disc machine contact is therefore geometrically equivalent (in the entraining direction) to the contact (at the pitch point) between a pair of equal, 20 degrees pressure angle gears, each of pitch diameter 222.8 mm.

It is suggested that as regards the film forming aspect of the *inlet* region geometry a mismatch of geometrical conformity between the discs and gears may be compensated for by an adjustment of the entraining speed in the disc machine simulation. Thus in cases where a disc machine gives a *higher* inlet region geometrical conformity than that occurring in the gears to be simulated, a *lower* entrainment speed could be used. In such a case a target sliding speed and film forming effect could be matched in the disc machine by operating at a rather higher slide/roll ratio than that occurring in the gears to be simulated.

The machine was designed to impose a maximum load of 4 kN at the contact which, for the geometry chosen (i.e. 76.2 mm diameter discs, each with 304.8 mm crown radius) gives a maximum Hertzian contact pressure of about 1.7 GPa. The load is applied by means of a hydraulic ram through a bell-crank and push rod mechanism.

The slower speed disc was mounted in a swinging arm bearing housing as shown and the end of the push rod in contact with this arm made contact through a crossed knife edge so that the load was applied at an accurately pre-determined point. In this way any tendency to twist the loading arm (which would have moved the contact band between the two discs) was minimised. The line of action of the loading was designed to pass through the contact between the discs. A proprietary electrical resistance load cell mounted on the bell crank provides a direct measurement of the load. A rapid reduction of the load was required when scuffing failure between the discs is detected so as to leave some of the "run-in" surface of the discs for profile measurements. This was achieved by providing a manually operated quick-release valve in the hydraulic supply to the ram, which dumped the system pressure back to the tank.

The test oil was circulated to the test discs and support bearings from an electrically heated tank which is designed for heating oil at temperatures up to 300 deg C. The maximum power input to the tank was 4.6 kW. The contents of the tank are stirred rapidly to prevent the development of hot spots. A hydraulic pressure filter with a steel mesh element rated at 1 μm is used in the test oil supply line. The filter body is fitted with special high temperature seals, and all supply and drainage pipes to and from the test head are in stainless steel.

2.4 Description of the test samples

Samples used for the various tests were carefully designed, as the original aim was to simulate actual contacts as found in aerospace gearing. Key points that had to be considered were: geometry (physical dimensions); material; heat treatment; finishing; and inspection. The geometry chosen (Figure 2.4) is based on an external diameter of 76.2 mm (3.00 inches). This selection is based on past experience and past experimental programs that used a similar dimension thus allowing direct comparisons. The choice in favour of this particular dimension was made originally as desired operating sliding and rolling speeds as well as power requirements were compatible with a rig operated in a university laboratory. The inner (bore) diameter of the discs was made to a close tolerance to give an interference fit on the test shafts. The discs were further secured by a key and locknut. A 2.2 mm diameter hole was

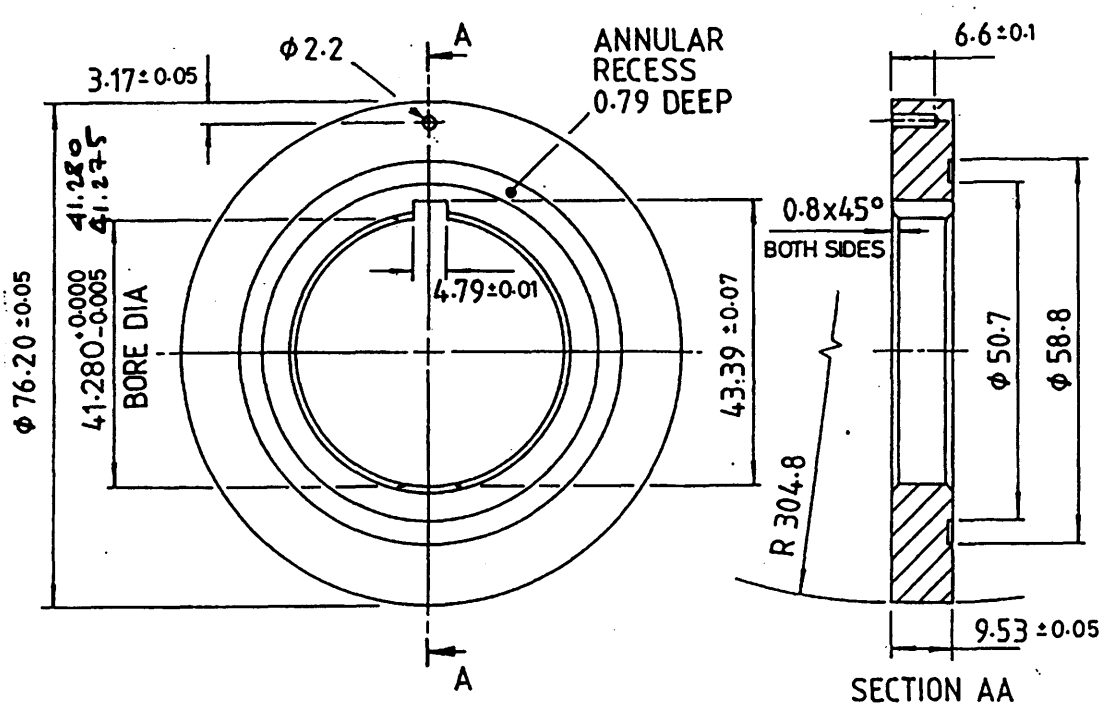

Figure 2.4: Drawing of test discs

provided 3 mm below the working surface of the discs for location of a thermocouple (J-type). This enabled the measurement of the bulk temperature of the disc.

A key feature of the discs is the direction of surface finish. Since the testing work was designed to be relevant to gears it was considered vital to reproduce the direction of finish as found on gear teeth. Gear tooth flanks finished by conventional grinding have a finish direction perpendicular to the rolling/sliding direction. In the disc machine this requires that the discs have an axial finish i.e. grinding marks perpendicular to the circumferential direction. A special method was developed to achieve axial finish as described in section 2.6.

2.5 Metallurgical properties of baseline samples

As outlined in section 1.6, the most commonly adopted material for aerospace gearing is case carburised and hardened steel and the most commonly used alloy is that meeting the US specification AMS 6260 (AISI 9310). Previous work carried out by Patching (1994) used such a material supplied by Rolls Royce under a Rolls-Royce material specification 6010. Hence to allow for direct comparison with the work carried out by Patching (1994) a bar of this steel was acquired from Rolls-Royce. This steel served as the material for baseline samples as well as a substrate for tests performed on coated samples as presented in Chapter 5. The chemical composition as a percentage of weight of the steel is presented in Table 2.1. The heat treatment was performed using a typical aerospace treatment specification, details of which are presented in Table 2.2, and was supplied by the Boeing Company. The Colledge & Morley Gears Company, an approved subcontractor of the UK aerospace industry, performed all machining (except the final axial grinding) and heat treatment for the baseline test samples.

Table 2.1

Composition of the steel used for baseline samples (% wt)

Element	C	Si	Mn	P	S	Ni	Cr	Mo
max	0.18	0.35	0.55	0.015	0.012	4.30	1.4	0.30
min	0.14	0.10	0.25	0.0	0.0	3.80	1.0	0.20

Table 2.2

Heat treatment specification as used for the baseline samples

Normalize @ 930°c ± 10°C	3 Hours ±15 minutes
Harden @ 850°c ±10°C	3 Hours ± 15 minutes
Temper @ 530°c ± 5°C	3 Hours ± 30 minutes
Carburize @ 927° ± 10°C to yield a carburized case depth (RC 50) of 0.036 to 0.042 inch, with a surface carbon (second 0.002" cut) of 0.65 to 0.95% Carbon.	
Cool to room temperature after carburizing and then	
Stress Relieve @ 566 to 621°C 4 hours ± 15 minutes	air cool
Copper plate all over, for protection during hardening.	
Harden @ 788 to 829 °C	for 30 minutes at temperature
Quench in oil 24 to 60°C	
Subzero treat, within 60 minutes of quenching, for 3 hours minimum @ –79°C or lower.	
Temper @ 160°C ± 5°C	for 3 hours ± 15 minutes
Final hardness values to be:	
Carburized surface hardness HRC 60 to 63	
RC 60 depth to be 45% of 0.036" (0.016" of as carburized case)	
Core hardness to be HRC 36 to 41	
As carburized case depth (HRC 50) 0.036 to 0.042"	

2.6 Surface finish of the test samples: axial grinding

Following heat treatment all test samples used in the experimental programme presented in this thesis were ground using the same process and apparatus. The process for achieving axial finish was initially developed at Cardiff University using a special set-up, which combines a surface-grinding machine and the headstock/tailstock of a cylindrical grinder. In all cases (apart from nitrided samples with the compound layer on – see Chapter 4) discs were first cylindrically (and

circumferentially) ground. Final grinding of the test surfaces was then performed with the discs mounted on a mandrel in the special grinding rig. After the final, axial grinding, the disc was removed from the mandrel and press-fitted on the test rig shafts. A very close fit of the discs on the mandrel for the whole grinding process ensured a good concentricity of the disc on its test shaft.

The principle of the grinding rig used is illustrated in Figure 2.5(a). The abrasive wheel was in the form of an internal cone. The radius of the crown generated on the test disc depends upon the angle of this cone and the displacement between the axes of the abrasive wheel and the test disc as shown. The surface of the test disc is generated by line contact between the abrasive wheel and the test disc. If R is the required crown radius, r is the radius of the test disc and α is the angle of the cone as shown then the required distance d between the axis of the abrasive wheel and that of the test disc is given by

$$d = (R - r)\sin\alpha$$

In order to obtain finishing marks which are close to axial in direction it is desirable to have the generating radius large compared with the thickness of the disc; but there are usually practical limits on the size of abrasive wheel which can be used in a particular grinding machine. In the grinding machine available at Cardiff the abrasive wheel diameter was approximately 180 mm, and in order to achieve the crowning radius of 304.8 mm (12 inches) referred to above, the angle α was chosen to be 15 degrees and the setting distance d was therefore 69.1 mm. A scale drawing of the arrangement used is shown in Figure 2.5(b). The abrasive wheels were supplied in a pre-formed state as shown with a recess to allow for dressing of the wheel as wear occurred. Diamond dressing was performed using a special angle-dressing tool which accurately maintained the 15 degree cutting face of the abrasive wheel. The wheel was discarded when the recess was removed as a result of repeated dressing.

The grinding rig itself was based on a Jones and Shipman (J & S) model 1400 surface grinding machine with the headstock, bedplate and tailstock of a Myford MG 12 cylindrical grinding machine mounted on the bed of the J & S machine. The normal axial movement of the J & S bed was locked to prevent movement and fixing the vertical position of the wheel spindle also set the setting height. The work

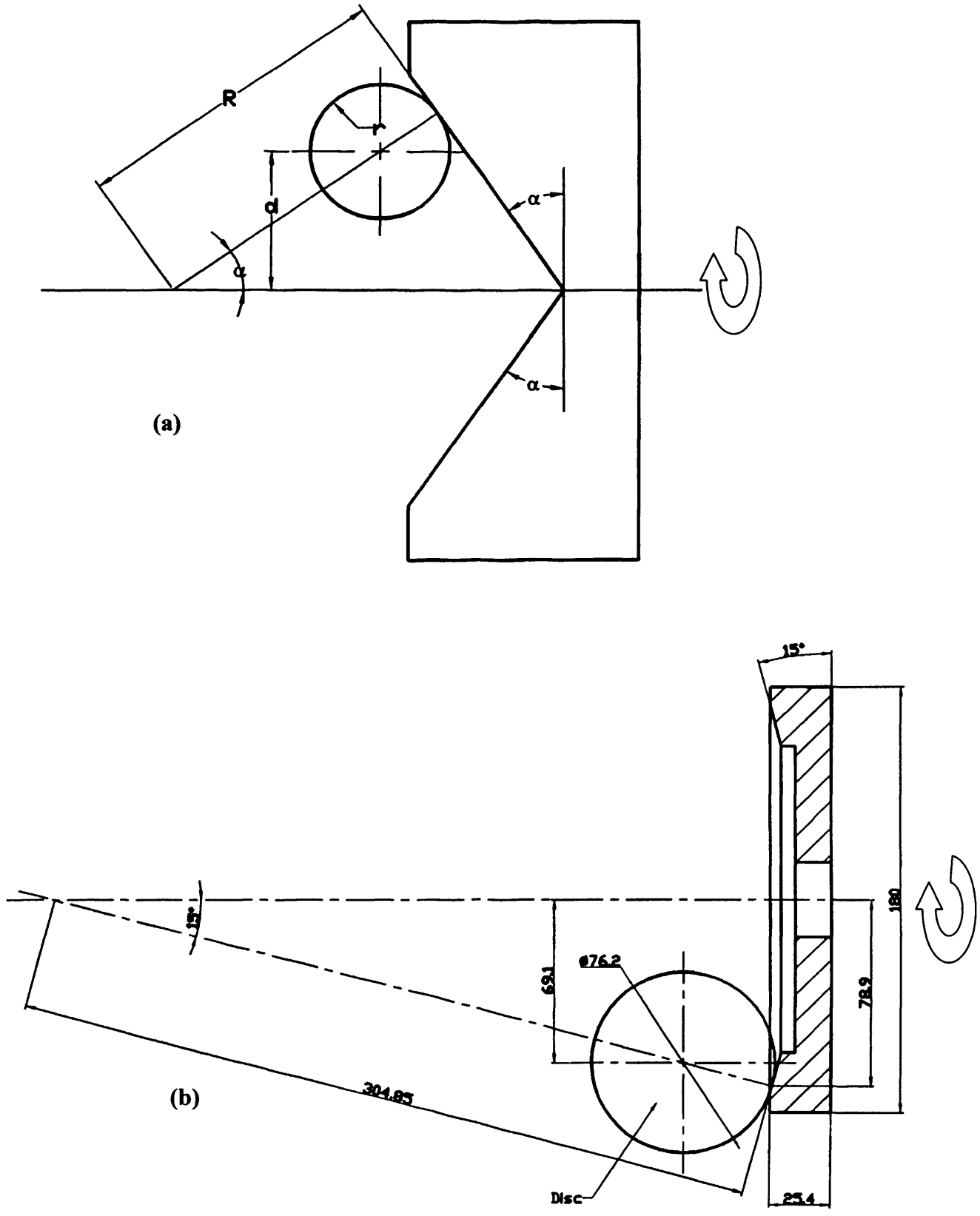

Figure 2.5: Generation of crowned geometry and axial finish
(a) principle of the generating process
(b) scale drawing of the grinding arrangement (from Patching – 1994)

was fed to the abrasive wheel by adjustment of the J & S bed in the direction parallel to the J & S grinding spindle.

Care was also taken in order to align the test disc relative to the abrasive wheel so that the crown was "centred" on the test disc. The axial position of the bed of the J & S machine was adjusted so that when a cut was taken the grinding tracks on both edges of the test disc were of equal width. In practice it was found that once the initial setting-up had been made there was no further need for adjustments to the grinding rig, other than feeding in the cut and periodic dressing of the abrasive wheel to maintain the correct generating geometry. The arrangement was easy to use and was an extremely effective solution to the problem of producing accurate, crowned, axially finished test discs. Figure 2.6 shows the approximately axial grinding marks generated using this technique.

The crowning radius of the discs was checked by taking a profile, in the axial direction, using the Taylor Hobson Form Talysurf 2. The vertical dynamic range of this apparatus is 1 mm allowing relatively large displacements of the pickup stylus. The form radius feature of the device was used to check the crown radius of the test samples as well as their surface finish (measured in the circumferential direction). A maximum deviation of ± 1mm from the specified crown radius of 304.8 mm was achieved. The maximum deviation from the specified outer diameter of the discs (76.2 mm) was ± 0.1 mm.

The normal direction in which surface finish of the test discs was measured was the circumferential direction (perpendicular to the axial direction i.e. to the grinding marks). Because of the large dynamic range capability of the apparatus as outlined earlier, a measurement along the circumferential direction of the discs of length 10 mm was possible. Figure 2.7 shows the setup used to acquire circumferential profiles using the Form Talysurf. After the raw profiles were acquired they were filtered to remove the longer wavelength components of finish (waviness) using a digital filter (Gaussian type) with a cutoff wavelength of 0.25 mm. The roughness average (Ra) was then computed. For all tests performed within this experimental programme, discs with a ground finish have been finished to a Ra measurement of 0.4μm ± 0.05μm Ra. A typical surface profile is shown on Figure 2.8 (only the first millimetre of the measured surface is shown). Raw profiles (i.e. unfiltered) were also exported as separate files using the profilometer software. These exported files were then used for the contact simulations described in Chapter 6.

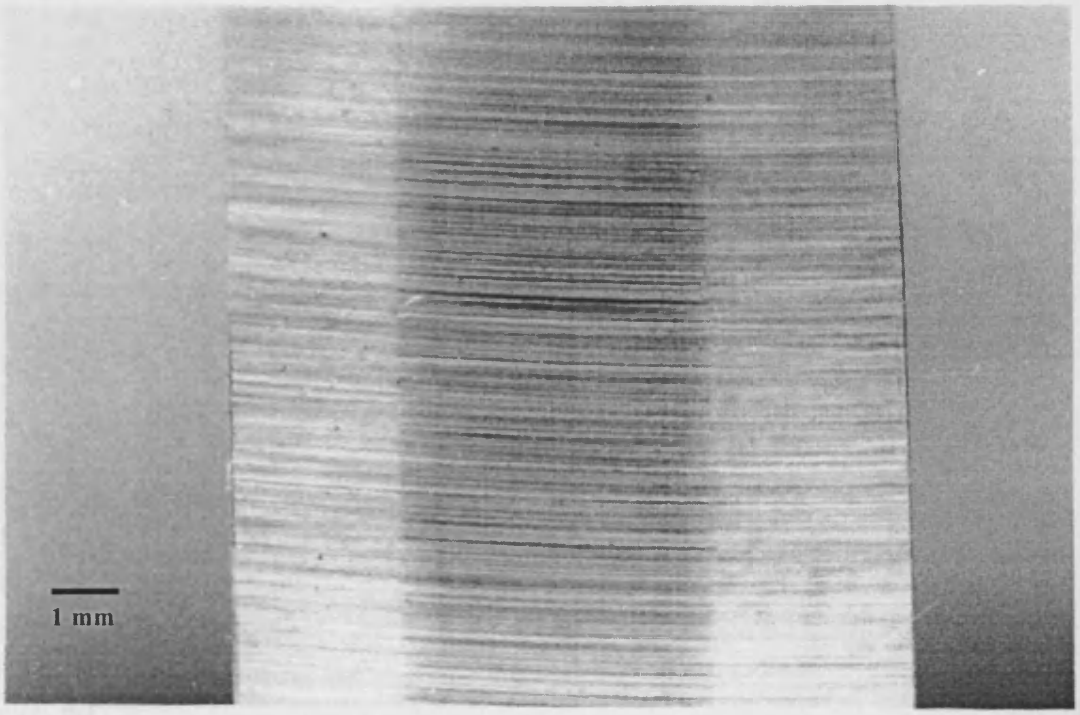

Figure 2.6: **Photograph of the test disc showing axial finish. The central darker band corresponds to oil staining; the disc having been run in the rig at load.**

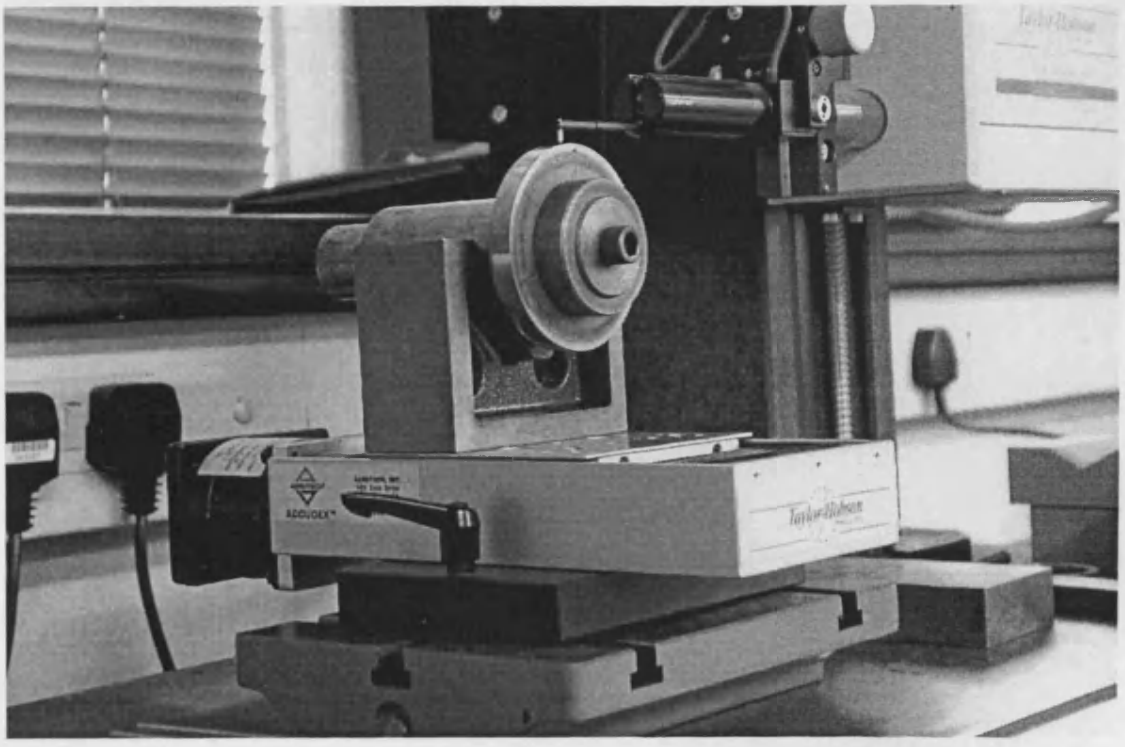

Figure 2.7: **Photograph showing measurement of a surface profile in the circumferential direction using the Form Talysurf. Also shown is the motor-driven cross-traverse allowing three-dimensional profilometry.**

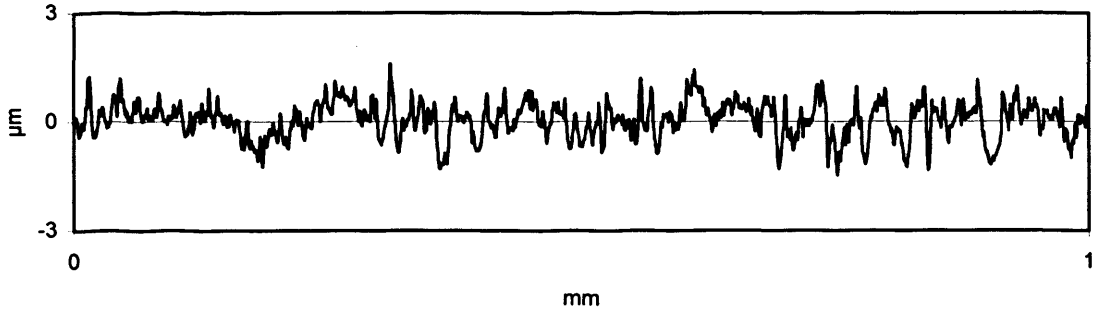

Figure 2.8: **Typical circumferential profile taken from test discs. In this particular case, the type of surface finish corresponds to a ground disc.**

2.7 Surface finish of the test samples: superfinishing

The advantage of using a polishing or "superfinishing" treatment on gear type surfaces after grinding has been demonstrated by a number of authors. Hence, Patching *et al.* (1995) have demonstrated the clear advantage of using a superfinishing treatment in order to improve scuffing resistance. Britton *et al.* (2000), have shown the clear benefit in terms of reduced sliding friction (particularly in the case of high lubricant temperature). And, finally, Krantz *et al.* (2001) have demonstrated a significant gain in terms of surface (micropitting) fatigue life of gears as a result of superfinishing.

2.8 Description of contact conditions

As mentioned in paragraphs 2.4 and 2.5, crowned discs are used in the experimental test rig. The Hertzian dry contact area is therefore in the form of an ellipse. Contact dimensions and pressure for elliptical Hertzian contacts may be found using the simple iterative algorithm described by Dyson et al (1992). The radii of relative curvature at the contact are 19.05 mm in the circumferential direction and 152.4 mm in the axial direction giving a ratio of principal radii of 8.0. The axis ratio of the Hertzian contact ellipse calculated using the above method is 3.91. For an assumed load between the test discs of 5000 N and using typical elastic properties of steel (E = 200 GPa; ν = 0.3) the semi-major and semi-minor dimension of the contact ellipse are calculated to be 2.29 mm and 0.59 mm, respectively, and the maximum contact pressure is 1.77 GPa.

2.9 Data acquired during a typical scuffing test

The bulk temperature of the surfaces in the inlet to the lubricated contact that is of key importance in elastohydrodynamic lubrication is measured by embedding thermocouples just beneath the surfaces of both discs. The leads from these thermocouples are connected through silver/graphite slip rings to a continuous chart

recorder. The slip rings are of a special type for use with thermocouples. The thermocouples were of the iron/constantan type (J type) insulated with PTFE. The thermocouple junction is made in a small copper ferrule of 2.0 mm diameter which is a close fit in a hole provided in the test discs. The location of this hole has been described in section 2.4 and is illustrated in Figure 2.4. The ferrule was pressed and expanded into the hole with a hollow punch. This provides a reliable mechanical anchorage of the junction and also ensures good thermal contact between the junction and the steel disc. The thermocouple leads are routed through the hollow test shafts and short drive shafts, which have flexible couplings at both ends, to the slip rings which are mounted outside the test head as shown in Figure 2.3.

The tangential friction force between the discs is measured by monitoring the torque in the shaft driving (or, strictly, braking) the slower speed test shaft. A reduced section of the shaft was fitted with electrical resistance strain gauges, which are connected to a suitable electronic unit through a third silver/graphite slip ring unit. The strain gauge units were bonded to the dynamometer shaft and temperature sensitive compensating elements were incorporated to eliminate thermal drift of the unit. A specialist supplier carried out this work. The output from the electronic unit was also continuously recorded on the chart recorder.

2.10 Progress of a typical scuffing test (prior to modification of the existing facility)

The load applied to the contact between the discs is carefully controlled and known as the "standard" loading sequence. A standard loading regime was adopted in which the load is increased at intervals of 3 minutes until either scuffing failure is detected or the load limit of the machine is reached before a scuff occurs. The increment by which the load is increased at each stage was chosen to give a constant increase of 0.1 GPa in the corresponding dry contact (Hertzian) pressure for a nominally smooth surface. The load stages and the corresponding loads and maximum Hertzian pressures are given in Table 2.1 below.

Table 2.1

Standard loading sequence used in scuffing tests

Load Stage	Time/min	Load/N	Max Hertz Pressure/GPa
1	0	180	0.6
2	3	290	0.7
3	6	430	0.8
4	9	620	0.9
5	12	850	1.0
6	15	1120	1.1
7	18	1460	1.2
8	21	1850	1.3
9	24	2320	1.4
10	27	2850	1.5
11	30	3450	1.6
12	33	4150	1.7

To conduct a test the machine is assembled with the discs and shafts in place. The test oil is first heated to the desired oil feed temperature by switching on the test oil heaters. During this heating period the test oil is circulated through the test head so that static thermal equilibrium of the machine is attained. The test oil is heated to 100 deg C and the gearbox oil to 45 deg C. A light load is then applied through the hydraulic ram to bring the discs into light static contact. This load is typically 100 N.

Prior to the modification of the test rig, the chart recorder was turned on to provide the continuous monitoring of disc temperatures and friction force and the zero temperature and friction readings of the recorder are checked. The main drive motor for the machine was then started and the speed gradually increased manually up to the pre-determined speed for the test. The speed was checked by the digital read out of the rpm counters attached to the two shafts. When the required speed was set the machine was allowed to run for a short period of time, typically three minutes, to allow the bulk temperatures of the two discs to stabilise. The first load of the standard loading sequence as described earlier was then applied with a manually operated pressure relief valve.

The progress of the test in terms of temperature and friction measurements was continuously recorded on a chart recorder. A typical chart is shown in Figure 2.9. There are two important points to note here about the chart record. Firstly, the zero level for the friction recording was set at line 10 on the chart. This allowed the indication of a negative as well as the positive friction reading. At the start of all the tests with low loads applied the friction force between the two discs is very small and the driving belt is turning the slow shaft against the frictional losses in the slow shaft bearings. This was recorded as a negative friction. The friction instrumentation was calibrated to give a reading of the frictional force at the contact and the scale is 40 N per division. The two temperature traces are zeroed at the zero line on the chart and calibrated for a full-scale deflection of 400 deg C.

Secondly, the pens on the chart recorder are offset to allow for the crossing over of the traces. This means that the slow disc trace lags by approximately 2 mm behind the fast disc trace which in its turn lags behind the friction trace by the same amount. The friction trace was used as the benchmark for the test, and load changes were applied as this trace passed the appropriate line on the chart. In all the tests the chart recorder was set to move at 10 mm/min.

We now examine Figure 2.9 in more detail. The behaviour of both friction and bulk temperatures is typical of this type of scuffing test. At chart position 1 the machine is nearing the end of the static warm up period. The temperatures of the two discs are approximately 70 and 75 deg C and have stabilised. The actual difference in temperature is mainly a function of the static position of the discs and the position of the embedded thermocouple with respect to the jet of heated oil at 100 deg C being supplied from the test oil tank. Just before chart position 1.5 the light load of approximately 100 N is applied, the main drive motor is started and the discs are bought up to the test speed. This is indicated by the oscillations in the friction line followed by a small negative friction reading as the full test speed is reached. The two discs were then run at the required speed with a light load until the running temperatures were stabilised. A feature of all the tests is that at the lighter loads the temperature of the slow disc is higher than that of the fast disc. At chart position 3.5 the first load of 180 N was applied and this produced an increase in both the disc bulk temperatures and the frictional force at the contact. At this stage the friction in the contact was sufficient to overcome the bearing friction and our convention of positive

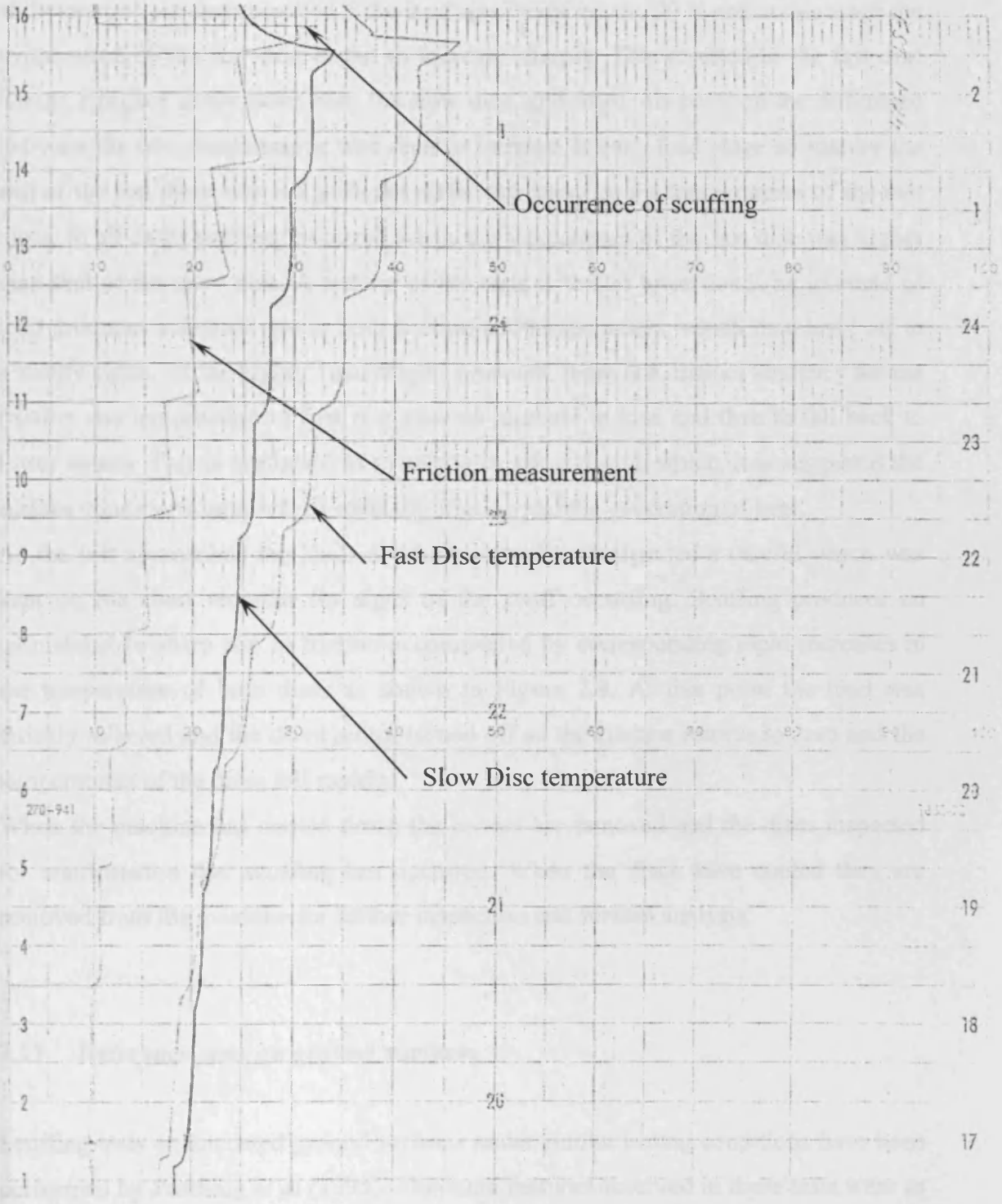

Figure 2.9: **A typical test trace from the chart recorder from a test on case carburised steel with a ground finish performed at a sliding speed of 7 m/s.**

friction shows that the fast disc was trying to drive the slow disc through the oil film at the contact. At chart position 5 the load was increased to 290 N and at this stage the temperature of the fast disc began to increase sharply. This resulted in the fast disc having a higher temperature than the slow disc, and from this point on the difference between the two temperatures was seen to increase at each load stage so that by the end of the test there was a significant difference between the temperatures of the two discs. In all cases scuffing occurred when the temperature of the fast disc was higher than that of the slow disc. A feature of the tests is that at lower loads an increase of load produces a sudden rise in both friction and temperatures, which then level off to a steady value. At the higher load stages, however, there is a distinct tendency for the friction and temperature to first rise after an increase in load and then to fall back to lower values. This is attributed to a running in effect during which, it is suggested the surface conditions improve, so reducing friction and the generation of heat.

As the test approached the loads at which a scuff was expected a careful watch was kept on the chart recorder for signs of the scuff occurring. Scuffing produces an unmistakable sharp rise in friction accompanied by corresponding rapid increases in the temperature of both discs as shown in Figure 2.9. At this point the load was quickly relieved and the drive motor turned off so the friction returns to zero and the temperatures of the discs fall rapidly.

When the machine has cooled down the covers are removed and the discs inspected for confirmation that scuffing has occurred. When the discs have cooled they are removed from the machine for further inspection and surface analysis.

2.11 Reference tests on ground surfaces

Scuffing tests on uncoated ground surfaces under similar testing conditions have been performed by Patching *et al* (1995). The main features observed in these tests were as follows. The scuffing load as a function of the sliding speed for ground samples is illustrated in Figure 2.10. The scuffing load decreases significantly as sliding speed increases over the range of sliding speeds considered. In all cases of scuffing with the ground surfaces there was strong evidence of "running in" of the surfaces before scuffing took place. Surface profiles taken before running and from the un-scuffed parts of the run track as shown in Figure 2.11 *(a)* and *(b)* demonstrate significant

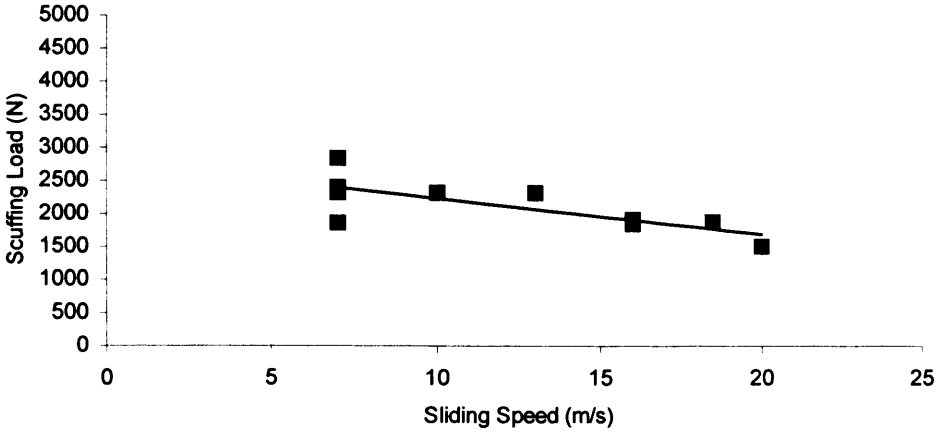

Figure 2.10: **Experimentally determined scuffing loads as a function of sliding velocity for ground surface tests (least squares fit also shown) – from Patching *et al* (1994)**

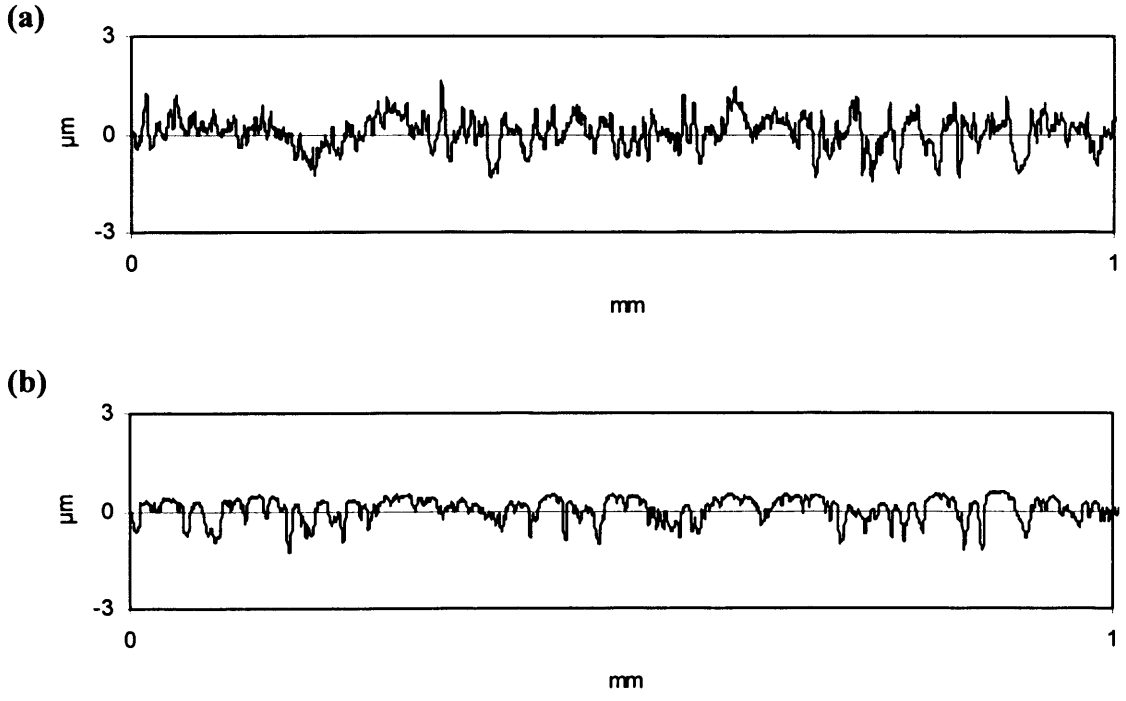

Figure 2.11: **Circumferential profiles of a case carburised ground disk. (a) *before* scuffing test; (b) run-in but un-scuffed part of surface profile *after* scuffing test**

modification of the peaks of the surface asperities but with little or no effect on the valley features. In all cases of scuffing between ground surfaces, the scuffing scar occurred at the transverse edge of the contact. This suggested that for these relatively rough surfaces the scuffing was due to severe side leakage of the lubricant from valley features at the edge of the contact where transverse pressure gradients are high. This view of scuffing failure of rough surfaces is reinforced by theoretical modelling (Evans *et al.*, 1996).

2.12 Problems associated with the use of the existing test facility

Although the rig in its original configuration operated satisfactorily, and has enabled a detailed investigation of the effect of superfinishing on surface distress of gears (Patching *et al.*, 1994), several shortcomings were identified at the start of the current project:

- The speed was controlled only in an open loop manner, manually by the operator (giving a fairly high sensitivity to the load).
- The applied load on the discs was also controlled manually.
- There was no automatic data acquisition as such apart from data plotted on the chart recorder.
- The standard load regime had to be implemented manually every 3 minutes.
- From the safety point of view, there were no thresholds that would stop the test if one of the monitored parameters exceeded set limits

All these considerations, plus the fact that it was desirable to acquire some experience for the implementation of the control system for the planned pitting rig, prompted the design and commissioning of a control system for the existing scuffing rig.

2.13 Development of a digital control system for the rig

The philosophy behind the planned control system was that it could revert back at any time to the "manual operation" of the rig. Hence it was decided to "piggy back" the new system onto the existing one. Figure 2.12 shows the general arrangement of the two systems together with (in bold) the added components.
The control system is of digital type and uses a classic configuration i.e. a PC, a Data Acquisition Card, a multiplexer and links to analogue or digital output/inputs of the various instruments and drives. The control software used is the Windows-based "Labview" system from the National Instruments Company. Hardware was obtained from the same company facilitating integration of the whole system. The hydraulic circuitry had to be heavily modified in order to put into service a solenoid controlled proportional valve for the automatic operation of the rig. The control card for the valve was integrated and interfaced with the control system for a 0-10V input signal, and a 2.5A power supply was connected to power the solenoid. The "piggy back" policy had to be slightly compromised at this stage as the return to the manually operated valve was found to be rather impractical. Instead, it was decided to implement a manual control of the proportional valve using a manually operated potentiometer.

The speed control for the main drive motor was also incorporated into the overall control system. This required the installation of an optically-coupled connection in order to overcome earthing problems. Analogue or digital output signals from the load cell, speed counters, torque dynamometer, and thermocouple electronic units were connected to the multiplexer in the data acquisition system. New PC software using "Labview" was developed. This enabled:

- Reading of all analogue or digital output signals from the various instruments.
- Conversion of these signals into relevant physical quantities.
- Generation of files for storing these quantities (typical rate: 1 datum/sec).
- Control of the load and speed through a virtual PID type control loop by generating the appropriate 0-10V signal in accordance with the order signal.
- The operator to impose various thresholds for a safe operation of the rig.

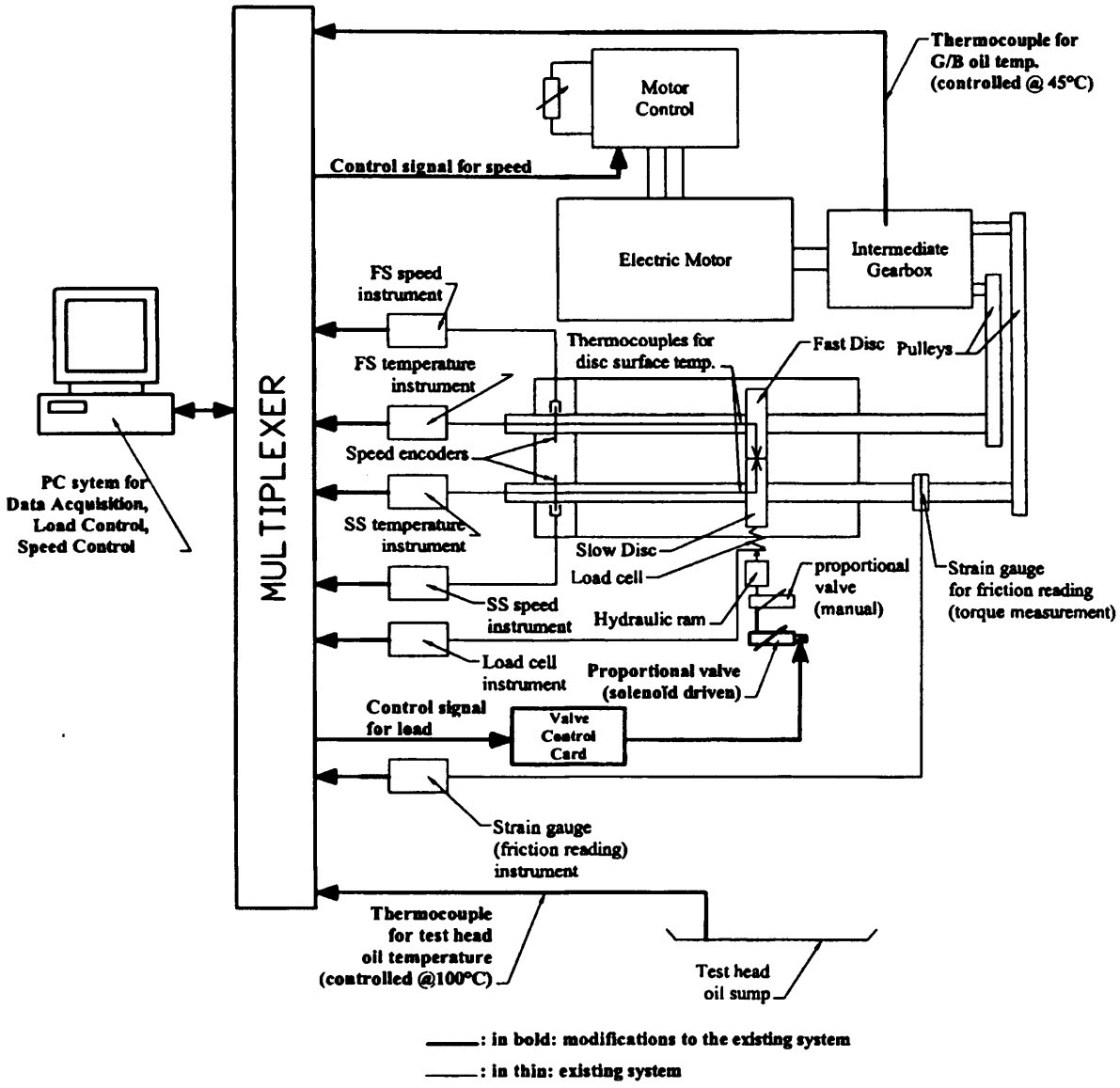

Figure 2.12: Schematic layout of the modifications of the existing scuffing rig.

- The operator to decide on a particular load regime different from the "standard" one (including a steadily increasing load ramp).
- The creation of the appropriate virtual control panel for the operation of the whole rig from the PC.

Two control cabinets were situated side by side as shown in Figure 2.13. One includes all the instruments and commands for the manual operation (old configuration) and one includes the PC, Data Acquisition Card and Mutiplexer. A screened cable links the two cabinets.

Figure 2.14 shows screen dumps of the PC control panel. The top panel gives temperature trends. The bold (yellow and green curves) are slow and fast shaft temperatures, respectively. Thin lines correspond to ancillary temperatures. The purple curve shows the tangential friction force acting at the surface of the discs, and the blue curve indicates the applied load. In this case the standard load regime was chosen.

On the top right hand side of the control panel are the real time values of the different parameters. Green and red square blocks indicate whether parameters fell within acceptable limits determined by the various thresholds introduced by the operator. The block on the control panel (just beneath the parameter real time values) allows for the selection of the automatic or manual operation of the speed and the load. Orders in terms of load and speed are also introduced at that level. It is also possible to hold the load at a certain level overriding the pre-established load regime. A smooth load ramp instead of a step-wise increase can also be selected at this level. Just beneath this part of the control panel is a push button to start/stop logging data, and there is also an emergency push button, which executes a computer controlled stopping sequence.

This sequence is used when scuffing is detected. Other parts of the control panel are not shown here. They include the definition of the various thresholds, the definition of the desired load regime (the "standard" one being loaded by default) and the file name where data will be stored.

Although this computer-controlled system operated satisfactorily, a number of challenges had to be overcome and/or are still to be addressed. Analogue signals from the various instruments were of great variety. The friction measurement exhibits a very low level, noisy signal that requires very careful treatment. The electro-hydraulic

Figure 2.13: Photograph of the two control cabinets.

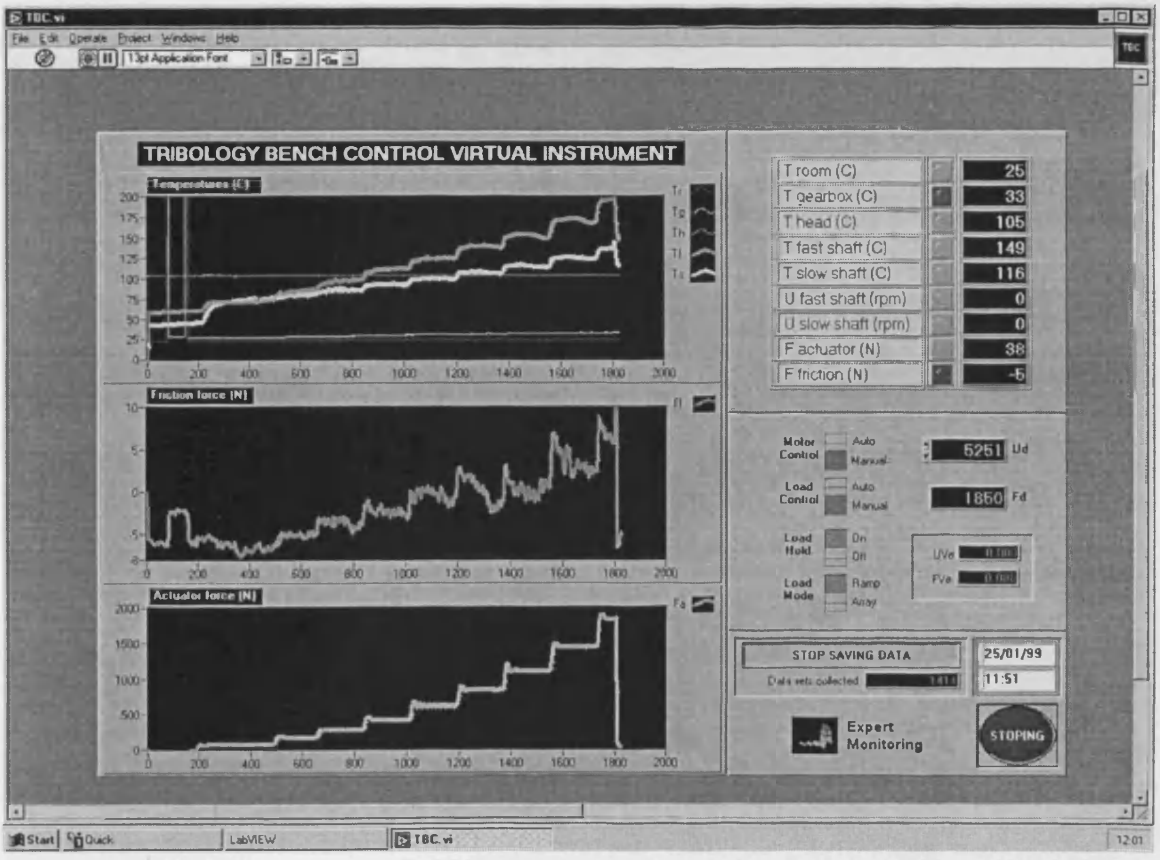

Figure 2.14: The scuffing rig PC control panel (developed in "Labview").

valve was designed to operate for a much higher pressure range than that applied to the loading ram, and because its operation was restricted to the lower part of its operating range some non-linearity was observed at light loads. This problem will be addressed in future work. Electromagnetic perturbation was also present particularly when starting the main drive motor. Re-routing of some signal cables alleviated this problem.

In conclusion, the implementation of a computerised control system was judged to be successful. Testing productivity was improved as a result of automatic operation along with the precision for speed and load orders as a result of the PID control loop. The speed is now virtually insensitive to the load, being adjusted instantly when the load varies. The operation is also safer due to the various thresholds in force. Real time data logging allows also for much more flexible processing and presentation of results from the scuffing tests. This project also aided the design of the control system for the pitting rig described in section 3.4.

CHAPTER 3.

A test rig for the investigation of micropitting of high speed, high temperature gear contacts

3.1 Introduction

As described in Chapter 1, the other very important category of surface distress encountered in surface hardened gearing for aerospace type applications is micro-pitting. It is a surface fatigue phenomenon on the scale of surface roughness that can degenerate into macro-pitting or serious cracking leading to tooth rupture in the extreme case. The need to better understand how this phenomenon develops over time has prompted the design and manufacture of a specific experimental facility dedicated to the monitoring of micro-pitting. NASA Glenn Research Center in the USA sponsored this activity as this type of surface distress is of primary concern in the helicopter transmission industry. The original aim was to develop a rig capable of evaluating the surface endurance limit (micro-pitting being as already mentioned a fatigue phenomenon) of a particular type of material, surface treatment or novel type of coating. This requires a rig capable of running at relatively high rotation speed compatible with sliding velocities as encountered in aerospace but also the capability to run for a large number of cycles. For example, based on the author's own industrial experience, micro-pitting tests can, depending on the configuration, result in tests running for up to 60 millions cycles before any surface distress is recorded.

3.2 Design philosophy

On the basis of experience gained at Cardiff University on the simulation of gear contacts using discs, it was decided to develop the new test rig based on the same technology employed for scuffing tests, namely a two-disc rig using equal discs of 76.2 mm (3 inches) diameter. An overall view of the rig as finally manufactured can be seen in Figure 3.1. The idea of using discs to simulate gear contact micro-pitting surface distress was suggested by a number of authors such as Onions *et al.* (1974),

Figure 3.1: **Overall view of the pitting rig.**

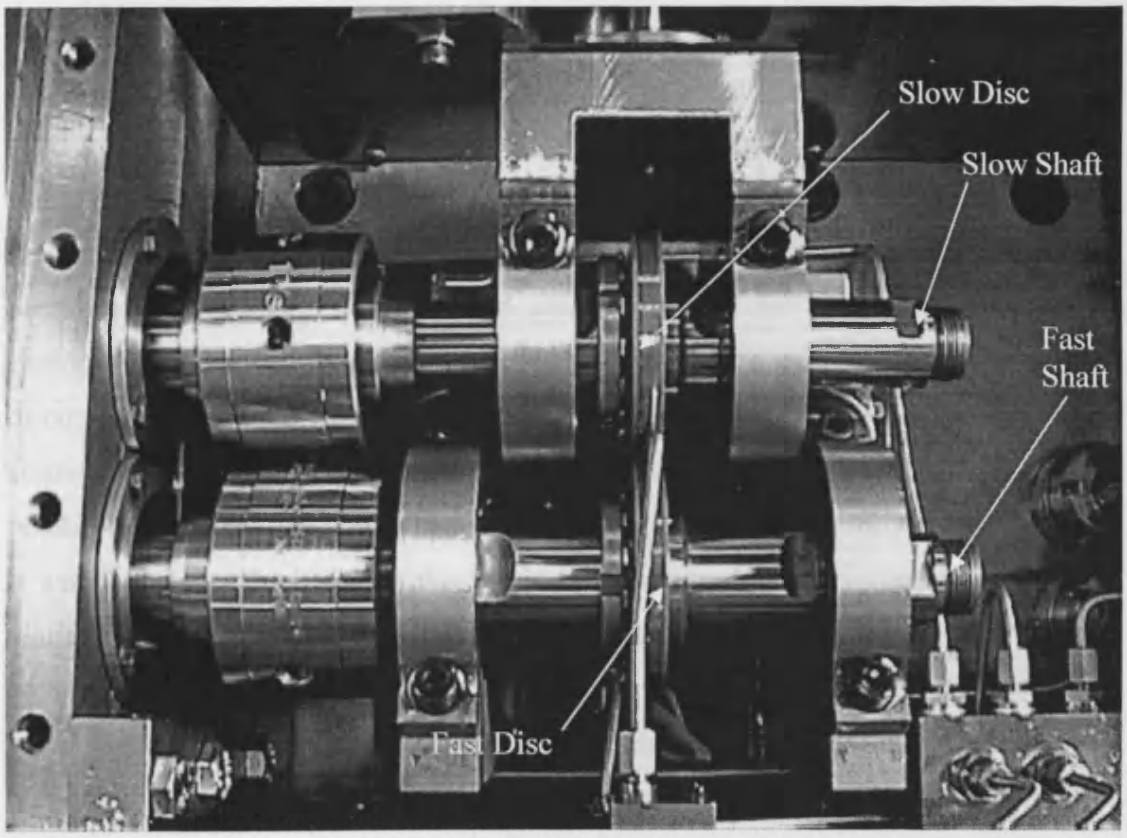

Figure 3.2: **The disc assembly in the test head of the pitting rig.**

Webster *et al.* (1995). As in the case of scuffing experiments, disc tests allow the fundamental study of the contact conditions without including dynamic effects as encountered with real gears. Hence, the test head as presented in Chapter 2 that comprises the two shafts supporting the test discs, the geared couplings and the loading mechanism was reproduced in the new micropitting rig.

The general specification that was adopted for the rig is as follows:

- Maximum Hertzian contact pressure for the discs: 2 GPa
- Fixed sliding speed of 16 m/s
- Minimum safety factor: 3
- Life of 5 years.

The choice of the maximum contact pressure was based upon industrial practice for micro-pitting tests, this load corresponding to a good compromise in terms of test duration without deviating too much from load levels as used on industrial gears. This maximum Hertzian pressure corresponds to a maximum normal force between the discs of 6.8 kN. The choice of a fixed sliding speed was based on the fact that it corresponds to a typical maximum common tip sliding speed as found in transmission gears particularly in the aerospace sector. It is also a sliding speed for which Cardiff University has accumulated a large number of experimental data particularly in the scuffing tests. However, the design, as will be discussed later, allows through the use of change gears the variation of the slide-roll ratio between the two surfaces of the discs. The rig was designed to have a life of 5 years of operation.

Precautions were taken to assess the capacity of this configuration and the associated components to sustain the load and cycles required for micro-pitting tests. For example, all pipes were modified from the original design using stainless steel instead of copper. This allows for long uninterrupted operations at high temperatures without contamination of the lubricating oil. All components were assessed to determine their reliability level and hence confirm or otherwise their suitability for micropitting tests. It was found that the bearings that could be accommodated for supporting the shafts could not meet the total expected life of the rig. Hence, their life will theoretically cover about 67 tests corresponding to 2.7 years of continuous operation. It should be noted though that bearing life depends greatly on the gear configuration used during testing i.e. the selection of slide roll ratio. In the same way, the stresses experienced by the rig are greatly affected by the coefficient of friction at the contact of the test

discs. All calculations made during the evaluation of the design were performed assuming a traction coefficient of 0.05, which is a conservative value with respect to the typical value of 0.01 found during scuffing tests. It is expected that the thermocouple slip rings will require replacement fairly frequently if they remain in contact throughout fatigue testing. For this reason it is proposed that the carbon brushes be "lifted" when temperature readings are not required.

3.3 Description of the rig

The rig includes five main sub-assemblies: the drive system, the step-up gearbox, the loading mechanism, the ancillary system and the test head. The latter includes the discs, shafting, bearing support and lubrication circuitry and was kept identical to the earlier scuffing rig as can be seen in Figure 3.2.

The drive system is simpler than that used in the existing bench. The drive is direct from a high-speed electric motor to the actual test shafts. There is a step-up stage using helical gears (ratio of 2.029) from the input shaft to the fast shaft of the test head (see Figure 3.3). The characteristics of this gear stage are outlined in Table 3.1.

Table 3.1

Helical gear data

Gear	PCD / mm	OD / mm	Module / mm	Number of teeth	Helix Angle	Pressure Angle
1	186.38	191.38	2.5	71	17°45'	20°
2	91.88	96.88	2.5	35	17°45'	20°

This configuration was chosen to limit the maximum speed requirement for the drive motor. The selected high speed motor was manufactured in Germany by the Perske Company. It is of heavy-duty type capable of continuous operation delivering a constant power of 10 kW through the whole speed range (2000 – 6000 rpm).

The two shafts supporting the disc samples are gear connected through a set of spur gears allowing for a discrete selection of slide slide-roll ratios (see also Figure 3.3). The sliding speed chosen for the operation of the rig as discussed earlier was fixed at

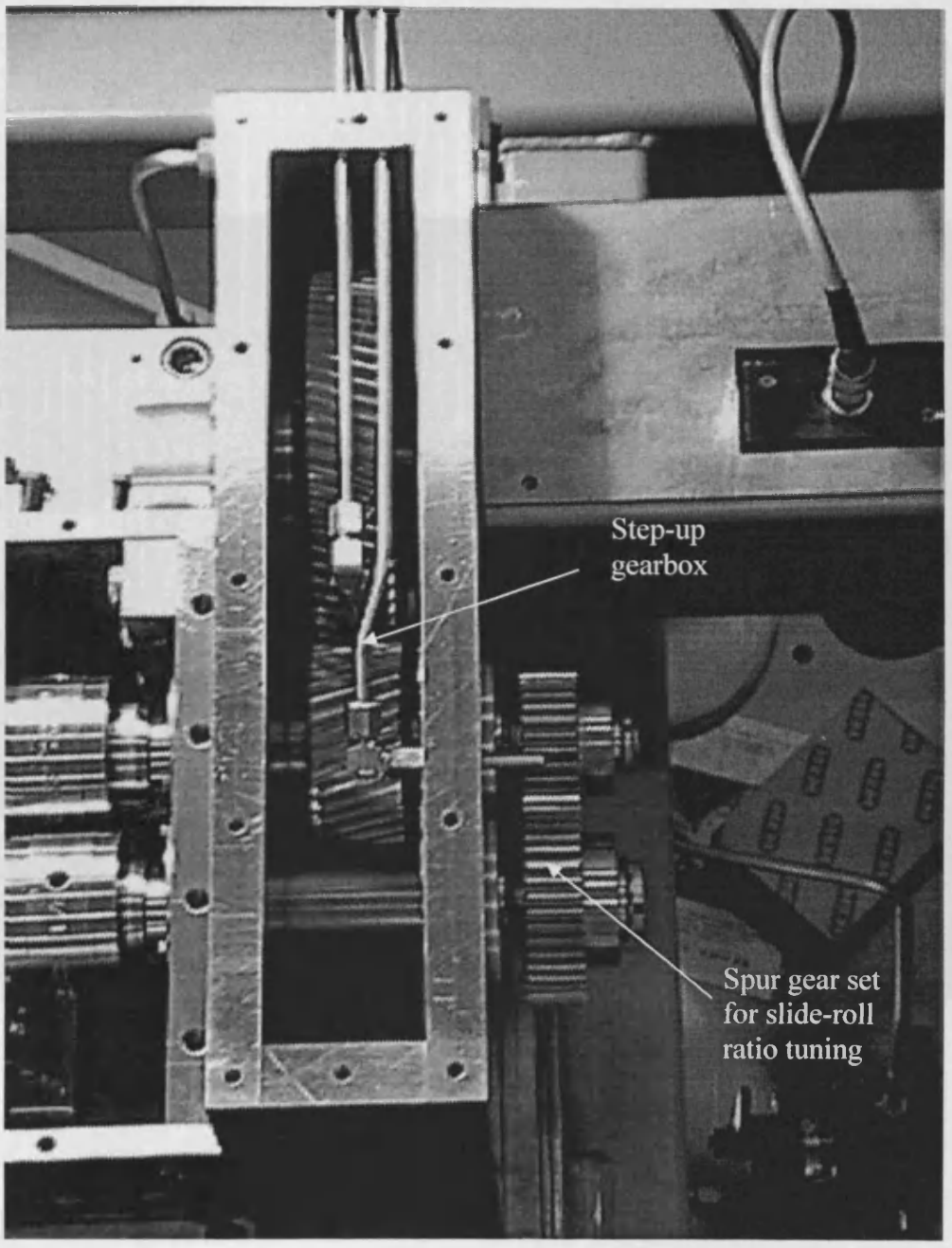

Figure 3.3: **The step-up gearbox and the spur gear set connecting the shafts.**

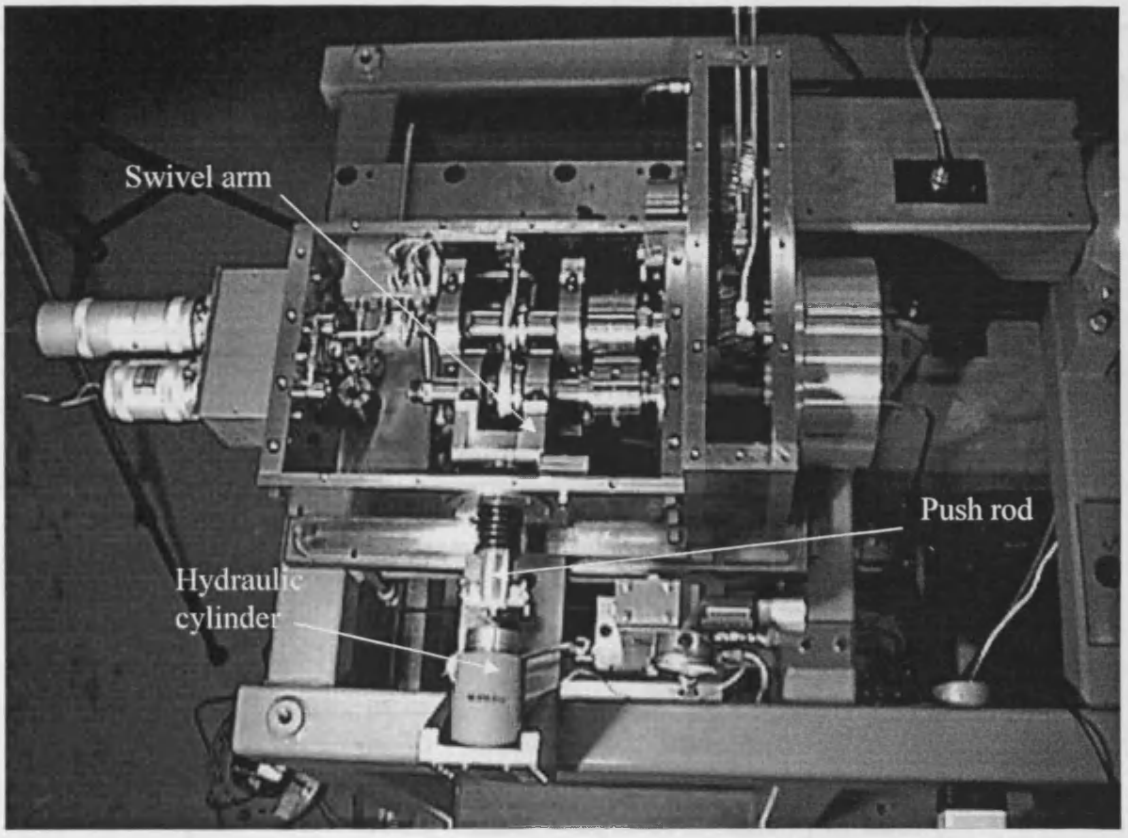

Figure 3.4: **Overall view of the pitting rig showing the loading mechanism.**

16 m/s considered as being the standard sliding speed for medium to high speed applications. This gives a number of possible slide-roll ratios as illustrated in Table 3.1 depending on the gear set selected. For a typical engineering application, the slide-roll ratio is about 0.4. The set currently mounted on the rig have 29/43 teeth giving a slide-roll ratio of 0.39.

Table 3.2

Possible slide-roll ratios available on the pitting rig

Spur gear set number of teeth		Slide-roll ratio	Spur gear ratio	Fast disc rotation speed / rpm	Slow disc rotation speed / rpm
21	51	0.833333	2.428571	6817	2807
22	50	0.777778	2.272727	7161	3150
23	49	0.722222	2.130435	7557	3547
24	48	0.666667	2	8020	4010
25	47	0.611111	1.88	8567	4557
26	46	0.555556	1.769231	9223	5213
27	45	0.5	1.666667	10025	6015
28	44	0.444444	1.571429	11028	7017
29	43	0.388889	1.482759	12317	8306

The characteristics of the spur gears are detailed as follows in Table 3.3.

Table 3.3

Spur gear data

	Spur Gear 1		Spur Gear 2	
Slide/roll ratio	PCD / mm	Number of teeth	PCD / mm	Number of teeth
0.833333	44.45	21	107.95	51
0.777778	46.57	22	105.83	50
0.722222	48.68	23	103.72	49
0.666667	50.80	24	101.60	48
0.611111	52.92	25	99.48	47
0.555556	55.03	26	97.37	46
0.5	57.15	27	95.25	45

Table 3.3 (continued)

	Spur Gear 1		Spur Gear 2	
Slide/roll ratio	PCD / mm	Number of teeth	PCD / mm	Number of teeth
0.444444	59.27	28	93.13	44
0.388889	61.38	29	91.02	43

The loading mechanism is also a simplified version of that used in the existing scuffing rig. It consists, as illustrated in Figure 3.4, of a hydraulic cylinder actuating a push rod. In order to ensure a near perfect radial loading, the inner conical end of the push rod contacts a steel ball mounted in the swivel arm where the slow shaft is installed. The capacity of the hydraulic cylinder allows a constant load corresponding to a 2 GPa Hertzian contact pressure between the test discs (6.8 kN). Mounted on the cylinder is a strain gauge type load cell to monitor the applied load. The ancillary system consists of two hydraulic pumps. One pump is used for the lubrication of the rig itself including the discs. The other pump is used to power the hydraulic cylinder. The two pumps share the oil from a single sump. This sump is temperature controlled (typical temperature: 90°C). A steel mesh filter rated at 1μm is included in the feed to the test head. The general layout of the oil circuitry of the micropitting rig is presented in Figure 3.5.

3.4 Rig digital control system

In order to monitor conditions during micropitting tests instrumentation was implemented on the rig. The general layout of the instrumentation as well as the control system is presented in Figure 3.6.
The instrumentation of the pitting rig includes:

- A force display connected to the load cell mounted on the hydraulic cylinder to monitor the radial load applied to the disc samples

- Two thermocouples displays linked with J type thermocouples to monitor near surface temperatures of the samples (thermocouples being embedded into the samples)
- One thermocouple display to monitor the oil sump temperature
- Speed and torque displays linked to an integrated speed and torque measurement device. This device is capable of rotational speeds up to 12,000 rpm.

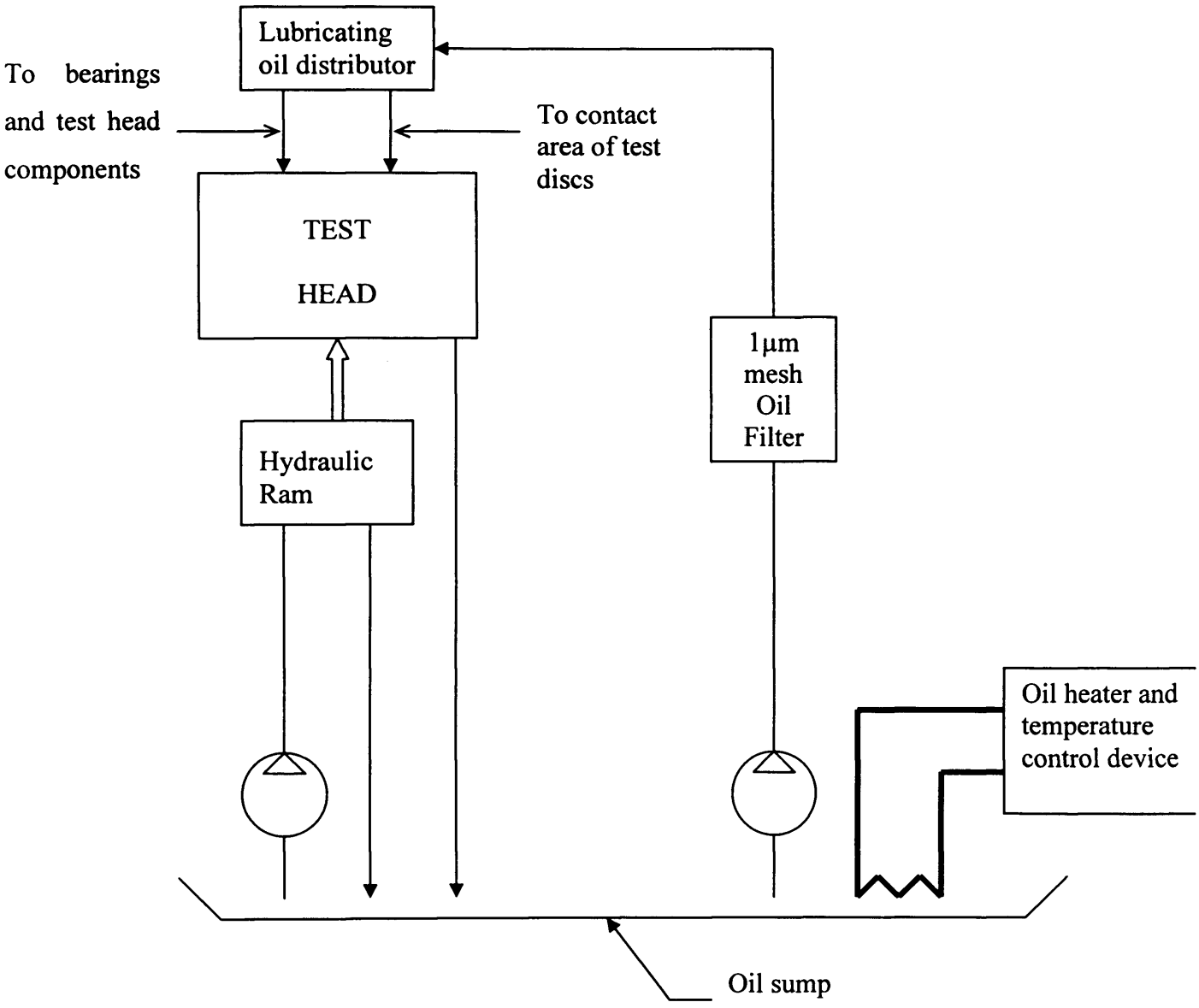

Figure 3.5: Block diagram of the oil circuitry of the micropitting rig.

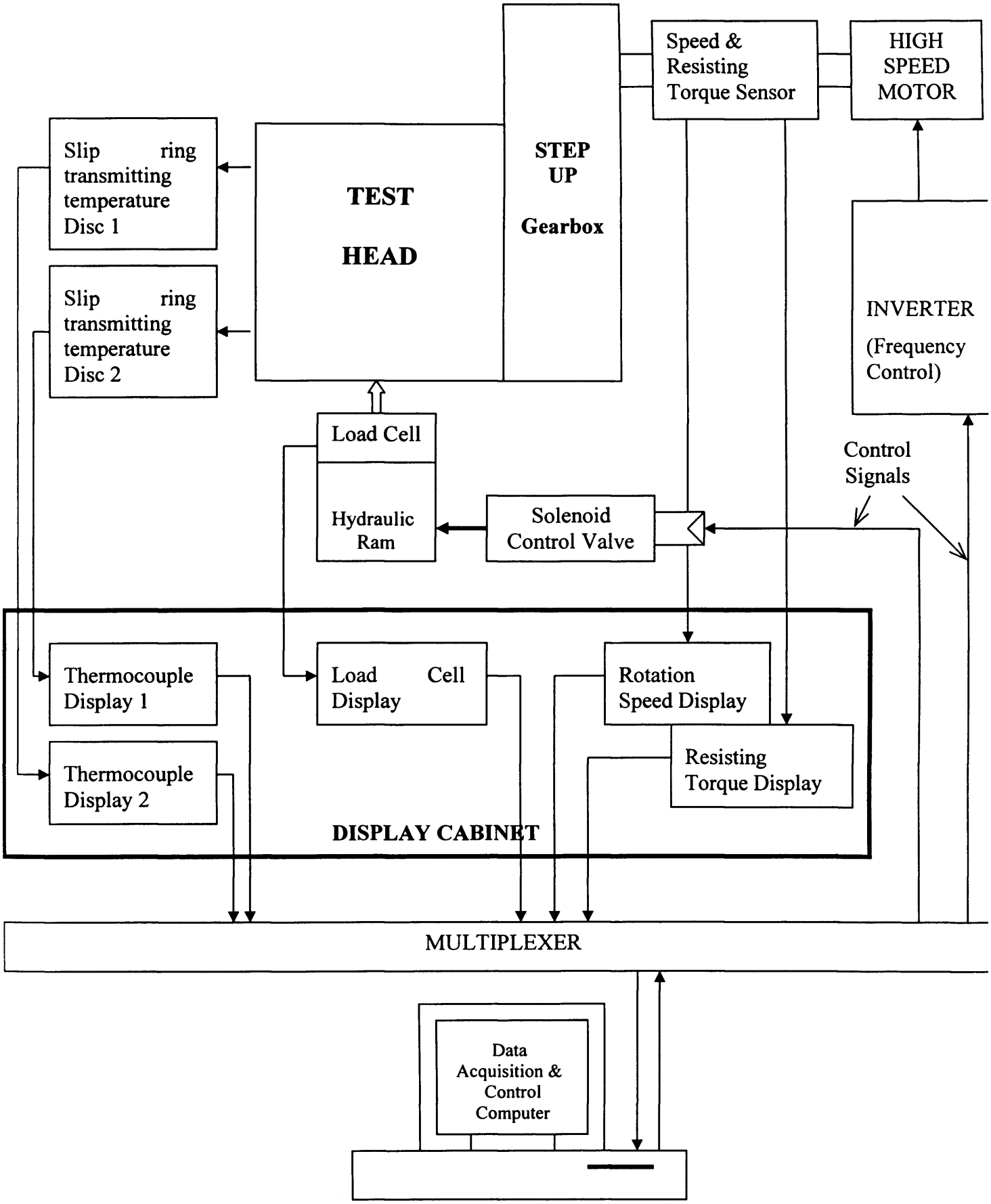

Figure 3.6: Block diagram of the instruments and the control system of the micropitting rig.

As with the scuffing rig, the general philosophy was to implement the data acquisition system *onto* existing instruments. This approach was found to give a satisfactory backup of the operation of the rig which could be operated "manually" if required. The data acquisition system is based (as for the scuffing rig) on a "virtual instrument" developed using the PC based software "Labview" from the National Instruments Company. Data acquisition hardware was also from the same company. The whole system has in fact developed as a shared facility for both the scuffing and the pitting rig allowing for significant cost savings.

A PID type control system is also part of the application developed in "Labview". It is possible to control both the load and the speed, the latter being operated by orders sent to the inverter controlling the motor speed. The control panel developed in "Labview" is shown in Figure 3.7 and includes parameter monitoring similar to that used in the scuffing rig. Shaft temperature evolution is shown in the top screen, friction through the measurement of the input torque is displayed in the middle screen. The load evolution over time appears on the lower screen. Real time data are also repeated in the top right of the panel. Auto or manual operation can be selected directly on the screen. Data acquisition and emergency stop are activated through push buttons also present on the panel.

Another part of the control panel as shown in Figure 3.8 includes the monitoring of the number of cycles logged by the fastest rotating element. The load regime can then be decided in terms of load for a certain number of cycles directly on the control panel. This regime can then include a run-in period followed by a progressive increase of load up to the required Hertzian contact pressure for the pitting test.

To ensure safe operation, various thresholds can be selected in terms of temperature, speed or load range to ensure a safe operation of the rig.

A suitable sensor that will allow the detection of pitting and hence trigger the end of the test still needs to be developed. A development programme was intiated in parallel with the development of the rig itself. The idea is to use a sensor based on the use of a monochromatic light source aimed at the disc surface. The "reflected" signal is collected electronically and the signal is then processed. So far, results obtained from the collected signal correlate very well with the actual surface roughness of the discs. The advantage of the device is that it allows real time measurement of a surface profile that includes the whole circumference of the discs. Development tests were run at different rotation speeds (up to 4000 rpm) with no noticeable shift in the

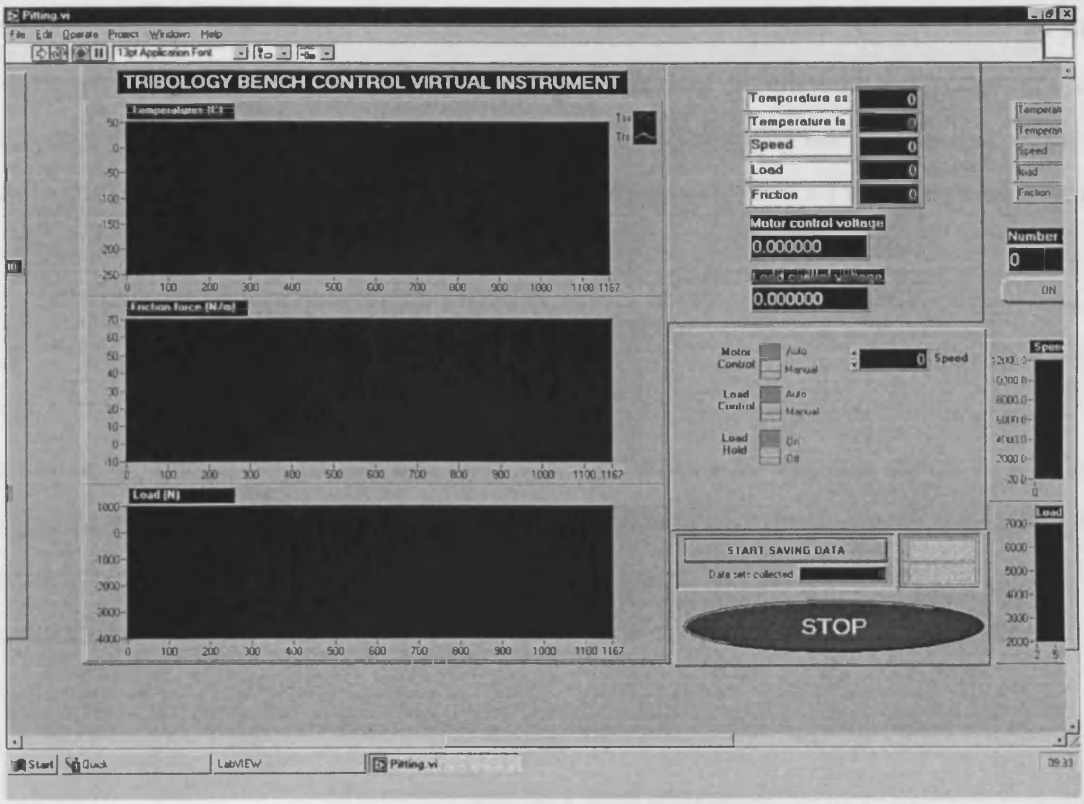

Figure 3.7: Control panel (left hand side) of the pitting rig.

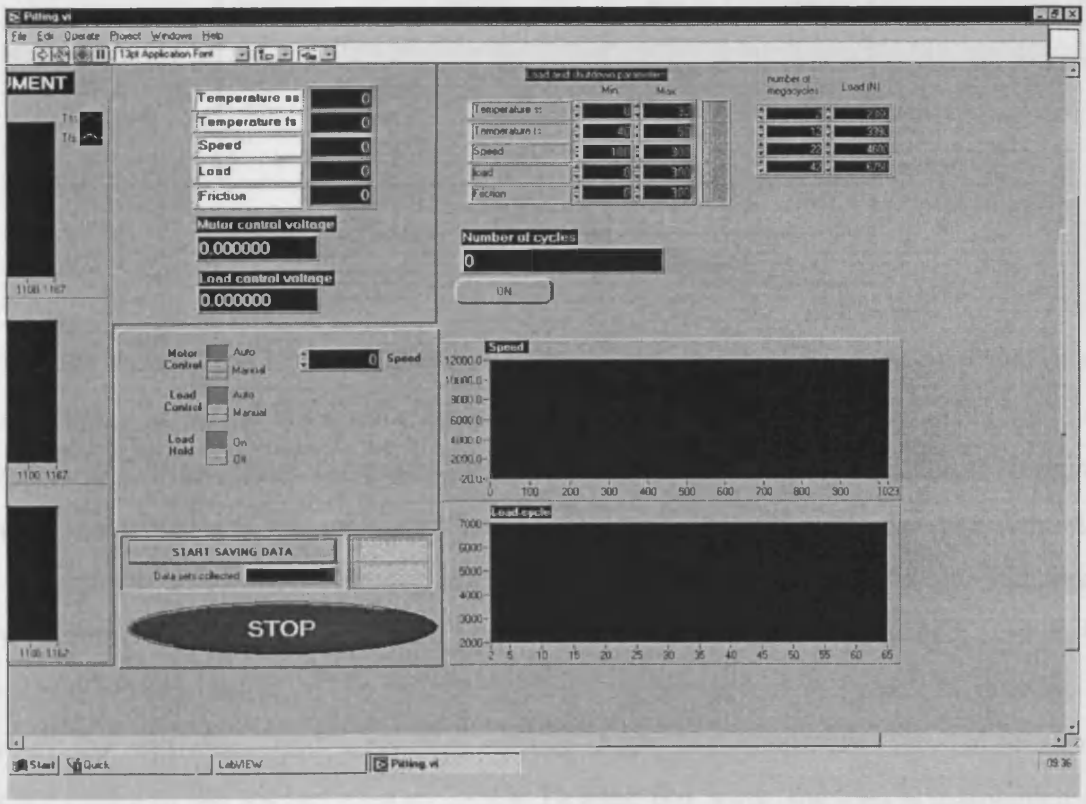

Figure 3.8: Control panel (right hand side) of the pitting rig.

recorded signal. This device could potentially be used to monitor the evolution of the running-in period and once the surface profile has stabilised, the recording as currently performed by the sensor could allow triggering the end of the test when a micro-pit is detected. Presently the time lag to trigger the end of the test is estimated to be of the order of one second.

3.5 Typical test sequence

In order to assess the endurance limit of the surface of the test discs, a loading sequence has to be determined. Based on the industrial experience of the author in terms of micro-pitting tests performed on real gears, the proposed load sequence is summarised in Table 3.4.

Table 3.4

Micro-pitting test load sequence

Cycles / 10^6	Load / kN	Max Hertzian Pressure / GPa
2	3.2	1.7
10	4.0	1.8
10	5.0	1.9
38	6.8	2.0
above	6.8	2.0

The load sequence is divided into four different stages. The first stage corresponds to the running-in period which is estimated to be about 2 millions cycles. This value is typical to the one found for helicopter gears. The corresponding Maximum Hertzian pressure is relatively low as again this corresponds to typical industrial requirements. Two plateaus follow this running-in period where the load is progressively increased by increments of 0.1 GPa over a period of 10 million cycles. The last plateau is reached after a period of 38 million cycles – again typical in industrial practice – where the maximum load is reached corresponding to a maximum Hertzian pressure at the centre of the contact area of 2 GPa. Beyond this point, the load is maintained at a corresponding level of 2 GPa until micro-pitting occurs. This onset being detected by the sensor as discussed earlier. Detection of micropitting would trigger the end of

the test. Using the control/data-acquisition system, the number of cycles is logged automatically and load can be increased precisely to the level identified by the prescribed load sequence. As mentioned earlier, metal temperatures close to the surface of the discs are recorded at a frequency compatible with the data logging system. In the same way, load and rotation speeds are logged through the whole duration of the test.

3.6 Work planned

The rig has now been commissioned (both hardware and control/data acquisition system). It has been tested up to the maximum design speed (12,000 rpm for the fast shaft) and is now ready for micropitting testing in terms of assessing the surface endurance limit of a particular alloy/surface treatment and/or coating. Nonetheless, the assessment of an endurance limit requires a large number of tests, which would also require a large number of test rigs. Useful information on the development of micropitting can be obtained by concentrating on the evolution of the surface texture during a micro-pitting type test as well as the evolution of the mixed lubrication regime as typically encountered on ground discs. This requires in-situ facilities to assess precisely the surface texture modification occurring during the tests. The rig has therefore been modified in order to install an in-situ surface texture measurement device. The general layout of the modified rig is shown in Figure 3.9. This modification includes the following elements:

- A portable profilometer;
- One of the sidewalls of the rig test head has been modified with a significant cutout to allow for the traverse motion of the roughness measurement device. Another plate has to be mounted when tests are being run to "block" the cutout;
- A stand supporting a two-axis table supporting the profilometer allowing displacement along the longitudinal and the transverse axis of the rig.

These major modifications allow direct in-situ measurements of the disc surface texture without having to dismantle any other components of the rig. Obviously this

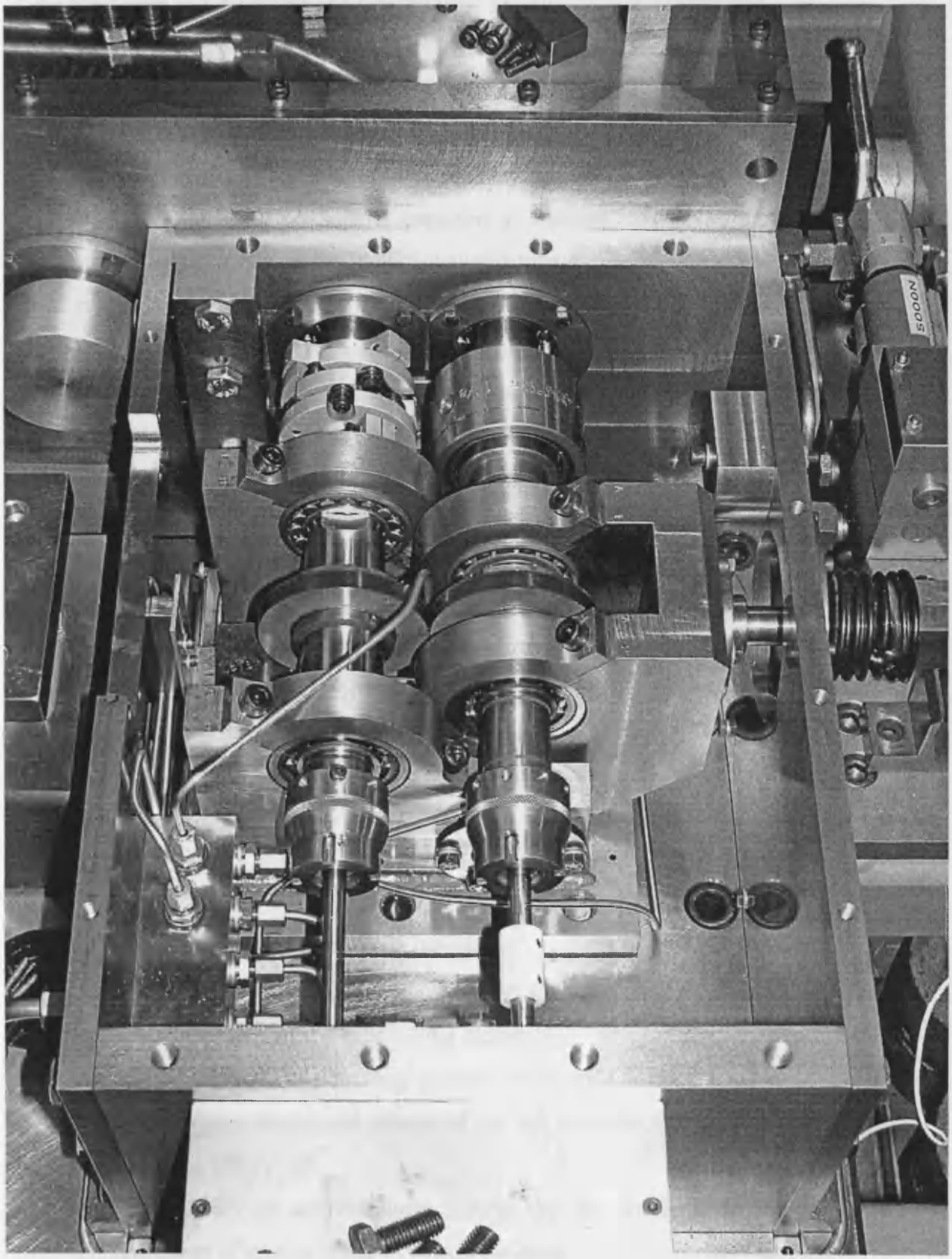

Figure 3.9: **Photograph showing an overview of the modified rig for in-situ surface texture measurements.**

can only be carried out once the rig has been stopped. The modifications mentioned above have been validated and can now be used directly.

The second aspect of the development of rig that has been envisioned is the investigation of the lubrication regime. The mixed lubrication regime that prevails with ground discs generates a number of metal-to-metal contacts at surface asperity level. This regime tends to change over time due to the running-in process. The number of metal-to metal contacts is expected to decrease over time if running in results in an improved surface finish. The way this transformation takes place, and the rate at which it occurs needs to be investigated. The way in which the whole running-in process takes place may have a considerable influence on the development of surface distress as a large degree of metal-to-metal contact may result in a large amount of asperity deformation capable of having a harmful effect on surface durability (Errichello, 2000). It is proposed to use measurements of the electrical contact resistance between the discs as an indicator of the lubrication regime. This technique is not new in principle and it has been presented by a number of authors such as Czichos (1977). The technique is based on the measurement of a voltage between the test discs which are part of an electrical bridge circuit. This requires the complete electrical insulation of one of the test discs from its surrounding. A specific modification of the rig has been carried in order to achieve the above-mentioned requirement. This modification includes the following elements:

- Modification of the couplings linking one of the test shafts (the slow shaft) to the driving system: mounting of driving keys made of PEEK plastic material allowing for electric insulation
- Mounting of bearings in place of the existing ones fitted with silicon carbide (SiC) ceramic type rolling elements
- Modification of the loading pushrod to include a spacer made of non-conductive material and change of the ball used for the loading arm to an SiC type ball
- Modification of the couplings linking the test shafts to the slip rings: inclusion of spacers made of plastic material.

All these mechanical modifications have been implemented. The electronic treatment of the voltage signal from the discs still needs to be implemented in order to perform the investigation. Once all the modifications are implemented notably on the signal treatment side, the facility will allow comprehensive investigations that will be included in future experimental programmes:

- Assessment of the surface endurance limit in terms of micropitting resistance
- In-situ surface texture measurement using a portable profilometer fully integrated with the rig
- Real time investigation of the surface texture using a novel sensor allowing the monitoring of the surface texture modifications including modifications during the very important running-in period
- Real time investigation of the lubrication regime to assess the occurrence of metal-to-metal contacts allowing the evaluation of the severity of the lubricated contact conditions.

CHAPTER 4.

Scuffing performance of nitriding steel

4.1 Introduction

As indicated in Chapter 1, nitrided steel has the potential to serve as a very effective surface treatment for gears. Nitriding can achieve very high case hardness (typically from 850 to 1200 HV) and this has obvious attractions from the tribological point of view. The treatment also has the advantage of allowing significantly higher operating temperatures in comparison with case-carburised surfaces, which are usually tempered at a temperature of about 150-200 °C. The nitriding process also has the advantage that it is carried out at a temperature which avoids distortion of the part so subsequent machining to achieve dimensional form is usually unnecessary. This feature is particularly advantageous in the case of gears of thin section such as crown gears. There is however a "growing" effect due to the treatment. For example, in the case of the nitriding of a low-alloy steel to a nitriding depth of 0.4 to 0.6 mm, the growth in the diameter of a shaft is typically 15 to 20 μm. The increase in diameter depends on the amount of nitrogen embedded, but this can be calculated and allowed for. This effect needs to be taken into account particularly when gears are due to be ground after nitriding.

Historically, the treatment has been used in industry from the early sixties. It has been applied to gears but also on components such as cam followers and even on bearing races though with a modified version of the treatment in order to ensure a sufficient case depth.

This treatment may be carried out on a metal already hardened and tempered such as on parts which require a high core mechanical strength. It can also be performed on finished parts in which case it is not followed with any secondary treatment. The parts to be treated are placed in a medium which releases nitrogen at a temperature ranging between 500 and 600°C. The latter element combines with the various atoms forming the structure of the steel to form nitrides. In the case of gas nitriding which is the process used for the samples used in the work described here, parts are put in a

furnace filled with gas causing an enrichment of nitrogen on the surface of the parts. The temperatures of treatment lies between 490 and 550 °C and this is maintained for 20 to 40 hours. The depth of the nitrided layer obtained varies typically from 0.2 to 0.4mm. Gas nitriding proceeds in three steps as follows:

1. Thermal dissociation of ammonia (NH_3) into nitrogen (N) and hydrogen (H):

$$2NH_3 \longrightarrow 2N + 3H_2$$

2. Absorption of nitrogen (N) by iron in a solid solution at the surface.

3. Diffusion of nitrogen towards the core of the part.

Alloys used for this process are the low carbon alloy type steels alloyed typically with chromium, molybdenum, aluminium or vanadium. Typical examples of content are 30 Cr Al Mo 6 – 12, 30 Cr Al V 6 – 3, 40 Cr Al Mo 6 - 12, etc...

The treatment itself takes place in a furnace which is usually of cylindrical form. After loading, the furnace is purged with nitrogen, which is then heated by forced convection up to the temperature of treatment. The mixture of active gas NH_3 is then injected, and maintained at the required temperature for the required length of time depending on the depth of the desired layer. The nature and depth of the layer depend, according to the grade of steel used, on the time, the temperature, and the composition of the atmosphere of treatment. These parameters are usually fully computer controlled.

The resulting layer comprises:

1. A layer of combination from 5 to 25 microns in thickness where nitrogen is combined in the form of iron nitrides. Under the light microscope, this outermost layer appears white when etched in 2% nital and is therefore referred to as the "white layer". The recognition that the white layer is a mixture of compounds of iron and nitrogen has led to its more appropriate designation as the "compound layer"
2. A layer of diffusion between 0.1 and 1mm in depth according to the steel grade and the processing time. This layer usually comprises finely dispersed nitrides which are responsible for the good mechanical properties of the case.

4.2 Metallurgical investigation

The base material for the test samples used in this experimental programme correspond to 722M24 (BS970 : part 2) also known by the old designation as EN40B. The chemical composition of the base material is given in Table 4.1.

Table 4.1

Chemical composition of the nitriding steel (% by weight.).

C	Mn	Cr	Mo	Si	Ni
0.33	0.59	2.98	0.53	0.23	0.16

The core strength of this alloy is found to be approximately 680 MPa.

All nitrided samples were gas nitrided by Allen Gears for 60 hours. First investigation revealed a case hardness measured on the compound layer between 742 and 752 HV and a case hardness without the compound layer between 726 and 732 HV.

A metallurgical investigation was carried out using two test samples referred to as EN40BA1 and EN40BA3. Figure 4.1 describes the areas which were analysed.

The samples were sectioned according to the diagram: the upper vertical section designated 1, and moving clockwise on the diagram, the second section designated 2 and the third section designated 3. The six sections are therefore designated: EN40BA1 1,1 1,2 1,3 and EN40BA3 3,1 3,2 3,3.

The first requirement was to measure the effective Nitrided Depth. In order to determine this quantity, the samples were sectioned using an abrasive cut-off wheel, then electroplated with nickel to protect the edge; mounted in thermosetting plastic; ground on SiC papers and polished first using 6 μm then 1 μm diamond paste. The samples were then chemically etched using a 2 % solution of nitric acid in ethanol (Nital). A calibrated Leitz Miniload II microhardness tester, using a pyramidal Vickers indenter and a 200 gf load, was used to produce the microhardness profiles. Figure 4.2 shows the microhardness profile of EN40BA3 3,1 obtained in this way.

If we take the substrate hardness as 260 $HV_{0.2}$, the case depths, e, (defined as core hardness + 100 HV) are given below in Table 4.1.

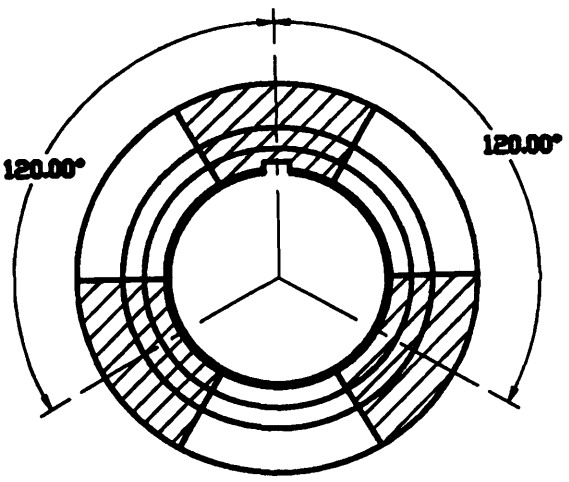

Figure 4.1: **Diagram showing the hatched areas of disc samples located 120° apart and used for metallurgical investigations.**

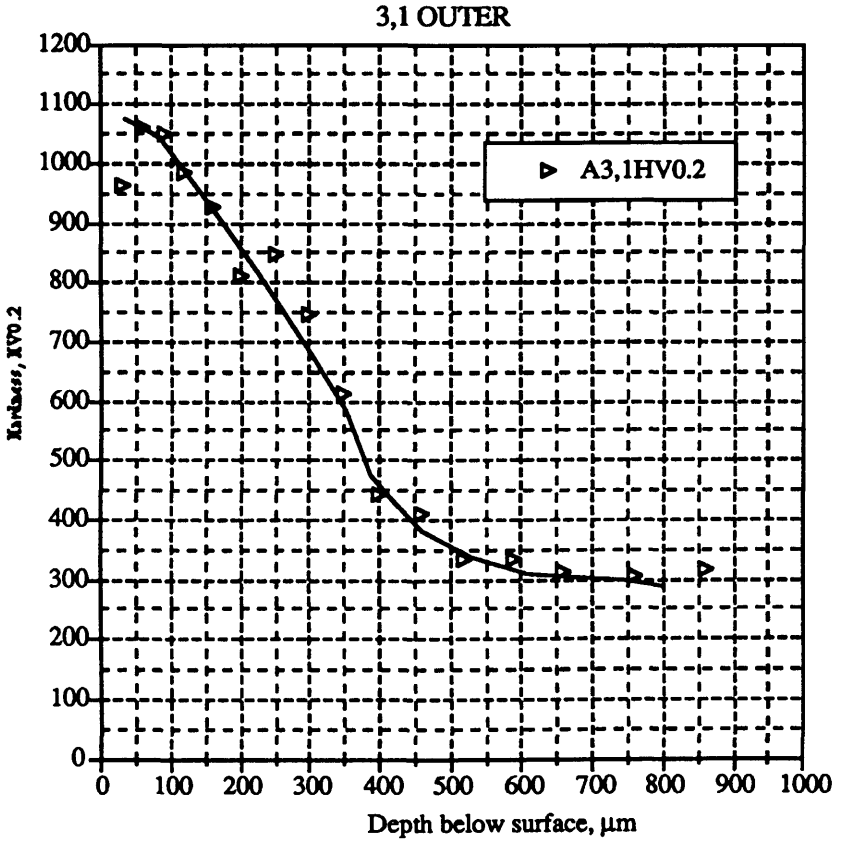

Figure 4.2: **Microhardness profile from section 3,1.**

Table 4.2

Case depth assessment of samples EN40BA1 and EN40BA3

sample	case depth (e) /μm
1,1	480
1,2	560
1,3	570
3,1	500
3,2	580
3,3	480

These results correspond to an average case depth of $\bar{e} = 528.33\mu m$ with a standard deviation of $\sigma = 42.59\mu m$. The minimum case depth corresponds to $e_{min} = 480\mu m$ and a maximum case depth of about $e_{max} = 580\mu m$. The values found are in good agreement with those found by Mridha *et al.* (1982).

Optical and scanning electron micrographs were taken of cross sections through the nitrided surfaces. The optical micrographs, an example of which is given in Figure 4.3, show a protective Ni electroplated layer at the surface, beneath which is the compound layer, and the diffusion zone. The micrographs have been printed at two different exposures to show the detail of both the compound layer and the diffusion zone.

The compound layer is of a similar thickness (15-20 μm) for all the samples. It can be seen that it comprises an upper, porous zone, beneath which is a dense region. This can be seen more clearly in Figure 4.4, which shows a back-scattered electron, scanning electron micrograph.

The diffusion zone contains:

- some iron-nitride growing into its surface from the compound layer,
- a dark band about 200 - 250 μm from the surface,
- large grain boundary precipitates on prior austenite grain boundaries running parallel to the surface, which can be seen more clearly in Figure 4.4.

These features are found in gas nitrided steels as outlined by Mridha *et al.*, 1982.

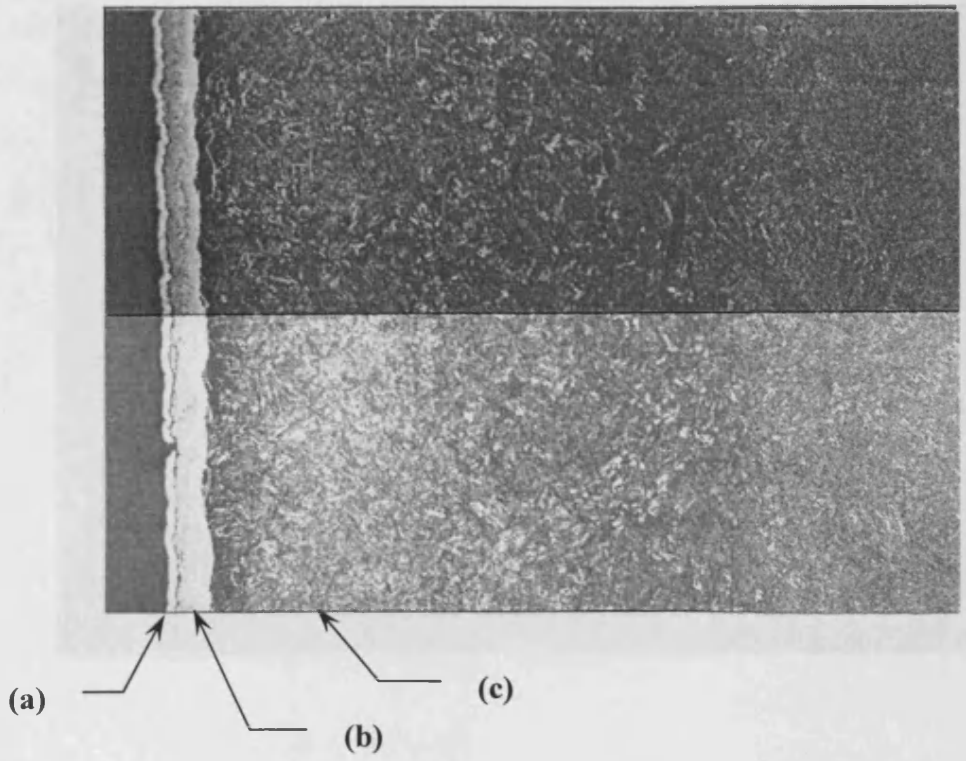

Figure 4.3: **Optical micrograph taken from section 3,1 showing the cross-section of the nitrided layer:**

(a) electroplated protective Ni layer
(b) compound layer
(c) diffusion zone

Micrograph shown at two different exposures to increase contrast in the diffusion zone (bottom part), compound zone (top part)

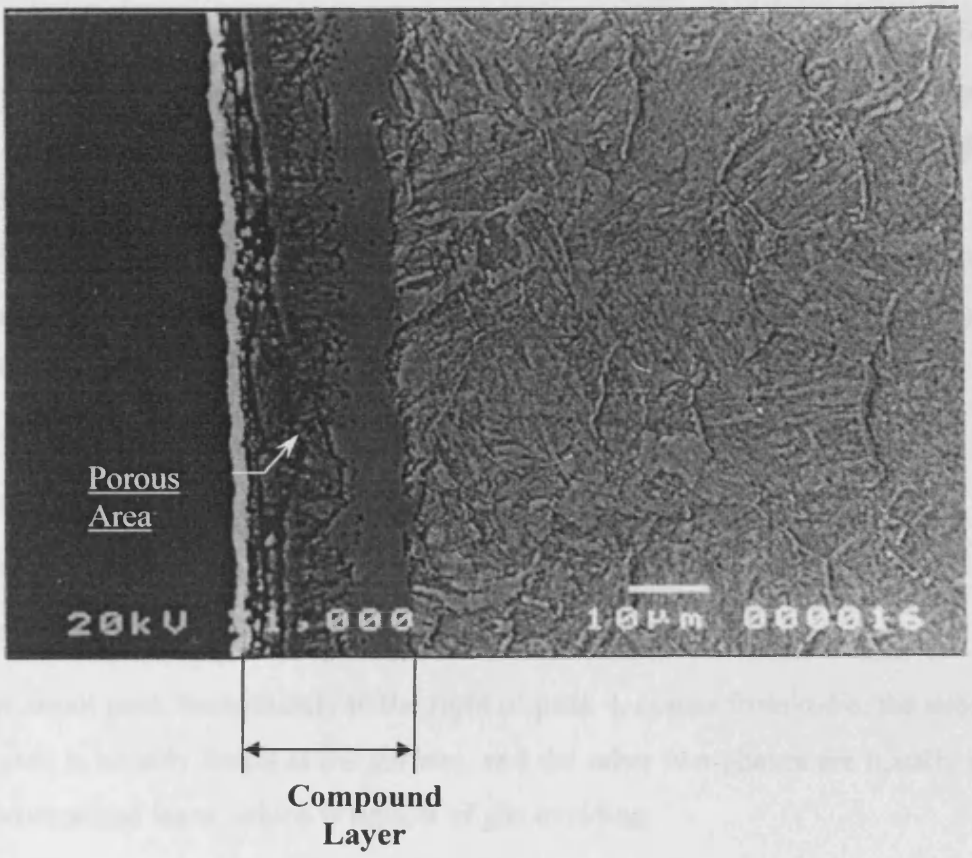

Figure 4.4: **Back-scattered electron scanning electron micrograph showing in more details the structure of the compound layer including a porous area near the surface. Shown on this micrograph as well are large grain boundaries.**

The dark band is a result of precipitation of fine carbides. The carbon is displaced from $(Fe,Cr)C_3$ by the advancing nitrogen which forms CrN. The large grain boundary precipitates are also a result of displaced carbon, which recombines with iron to form essentially cementite, Fe_3C on grain boundaries. These precipitates, it is thought, only tend to form parallel to the surface because of a compressive residual stress system resulting from the nitriding preventing their growth normal to the surface.

As for the compound layer, in addition to the microscopy techniques described above, X-ray diffraction was carried out using a standard diffractometer and Cr k_α radiation, which has a penetration depth in iron- based materials of approximately 15 μm. The scans were taken from a flat surface of each of the samples, and are shown below in Figure 4.5.

The results for the two samples are essentially identical, showing the presence of both ε-$Fe_{2-3}(N,C)$, γ-Fe_4N and Fe_3O_4. The peaks, numbered from left to right represent:

1. Fe_3O_4.
2. ε-$Fe_{2-3}(N,C)$
3. ε-$Fe_{2-3}(N,C)$, γ-Fe_4N
4. ε-$Fe_{2-3}(N,C)$
5. γ-Fe_4N

and the small peak immediately to the right of peak 4, comes from α-Fe, the substrate. The oxide is usually found at the surface, and the other two phases are usually mixed in the compound layer, which is typical of gas nitriding.

4.3 Scuffing tests with compound layer present

A number of tests were carried out with samples where the compound layer was left on after the nitriding treatment. This is an unusual practice as the metallurgical structure of the compound layer (porosity, heterogeneity, presence of cracks at the surface) would suggest that removal is mandatory. For example it is regarded as a compulsory practice in the aerospace industry. Nonetheless, other industries, like those manufacturing gears for naval applications, recommend retention of the

(a)

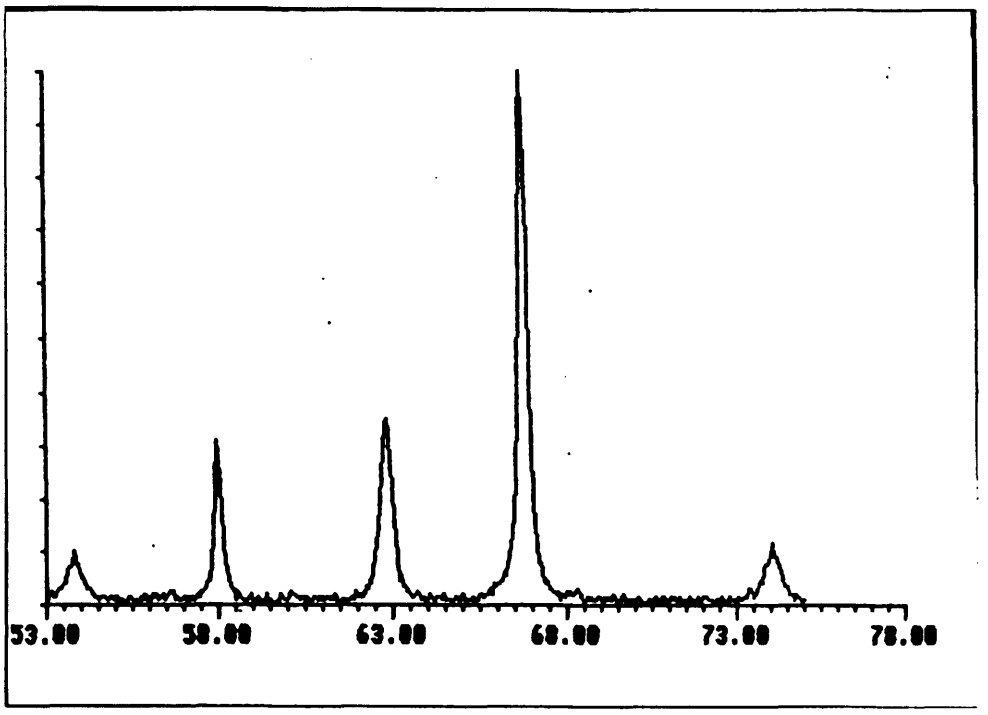

(b)

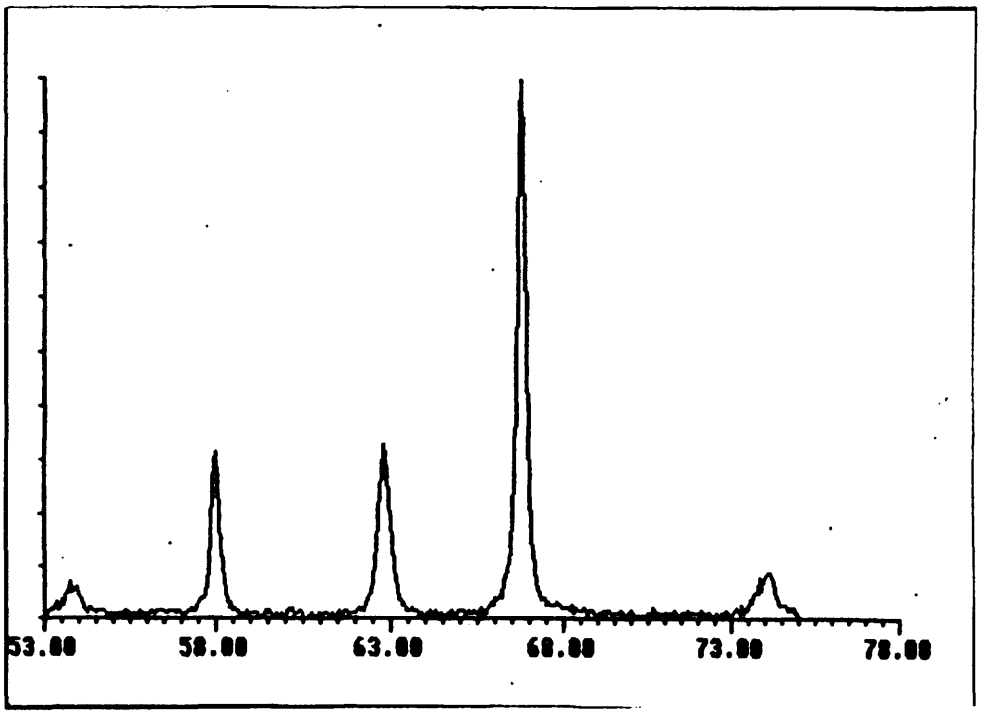

Figure 4.5: **X-ray diffraction diagrams revealing the presence of various oxides, carbides and nitrides present in the compound layer function of the intensity and the position of the diffraction peak.**

compound layer which they justify as a benefit in terms of friction behaviour, scuffing resitance and overall reliability. This is common practice, for example, in the "Allen Gear Company" which is part of the Rolls-Royce group. Clearly there are advantages of using such an approach in terms of process schedule. With this configuration, all machining operations take place *prior* to the heat treatment (typically rough turning and grinding) and then the nitriding treatment. No further operations are required after treatment. This simplifies the schedule and has, no doubt, direct cost benefits. Two manufacturing problems are to be borne in mind, however. The first aspect is the fact that grinding, if used, takes place on material in a relatively soft state (i.e. prior to heat treatment) which requires special grades of grinding wheels. The second drawback is that grinding in a soft state results necessarily in coarser roughness state. The resulting surface roughness level is typically R_a = 1μm which may be compared with a typical value of R_a = 0.4 μm for a pre-hardened material. A higher level of roughness may have an adverse effect when compared to the level of oil film thickness that can be generated in engineering contacts.

In all a total of ten tests were performed on the nitrided samples with the compound layer on. Tests were performed at three different levels of sliding speed: 7, 16 and 20 m/s, with three tests at each sliding speed. The summary of the results obtained is presented in Table 4.3. These results exhibit a large degree of scatter, particularly in the case of the scuffing load at the two higher sliding speeds i.e. 16 and 20 m/s. This trend will be further discussed in more detail when we describe the condition of the samples after tests, but it appears that scuffing failure corresponded in these cases to a sudden delamination of the unstable compound layer. On the other hand, Table 4.3 indicates excellent behaviour of this configuration (i.e. "white layer on") at the lower sliding speed. For example, in two instances of sliding at 7 m/s the maximum load capacity of the rig was reached without any indication of scuffing. The measured friction values are particularly low. This trend tends to confirm the belief that the compound layer improves the friction behaviour.

Table 4.3

Summary of results from ground nitrided samples with "compound layer on"

Test number	5	6	7	8	2	3	4	9	10	11
Peripheral Velocity of Fast Shaft/ms^{-1}	9.15	9.15	9.15	9.15	20.95	20.95	20.95	26.18	26.18	26.18
Peripheral Velocity of Slow Shaft/ms^{-1}	2.15	2.15	2.15	2.15	4.94	4.94	4.94	6.17	6.17	6.17
Mean Entraining Velocity/ms^{-1}	5.65	5.65	5.65	5.65	12.95	12.95	12.95	16.18	16.18	16.18
Sliding Velocity/ms^{-1}	7.00	7.00	7.00	7.00	16.00	16.00	16.00	20.00	20.00	20.00
Scuffing Load/N	4250 no scuff	4125 no scuff	4170	4453	1876	1135	1472	1145	1130	1480
Maximum Bulk Temperature of Fast Disc/°C	172	196	190	mal func.	204	146	164	176	148	156
Maximum Bulk Temperature of Slow Disc/°C	134	152	152	162	mal func.	116	120	128	108	112
Mean Bulk Temperature of Discs/°C	153	174	171	n/a	n/a	131	142	152	128	134
Maximum Peak Hertzian Contact Pressure/GPa	1.71	1.70	1.70	1.74	1.31	1.10	1.20	1.11	1.10	1.21
Traction Coefficient at Scuffing Load	0.018	0.024	0.024	0.027	0.025	0.021	0.022	0.030	0.018	0.016

Results showing the scuffing load as a function of sliding speed are given in Figure 4.6. These results for nitrided samples with the compound layer on are subject to

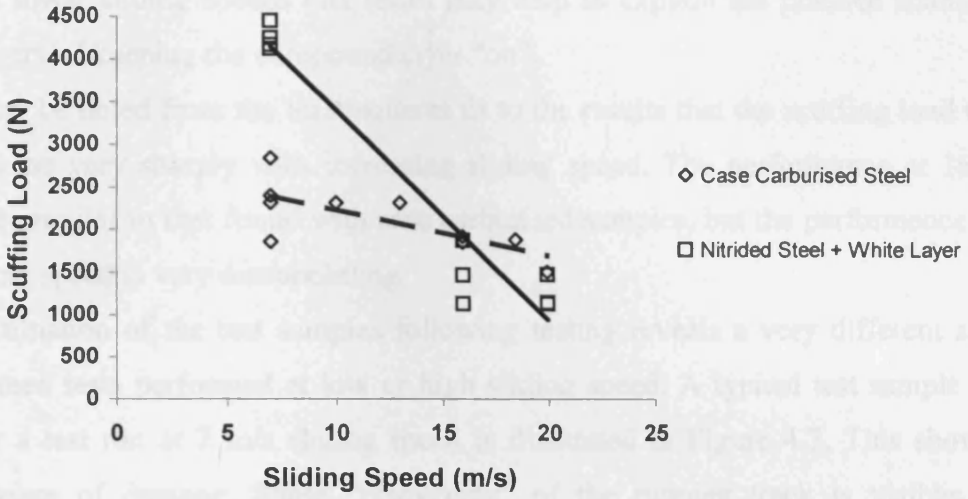

Figure 4.6: **Experimentally determined scuffing loads as a function of sliding velocity for the ground nitrided with compound layer ("white layer") surface compared to reference Case Carburised surface tests. Least square fit also shown: continuous line: nitrided samples; dotted line: case carburised samples.**

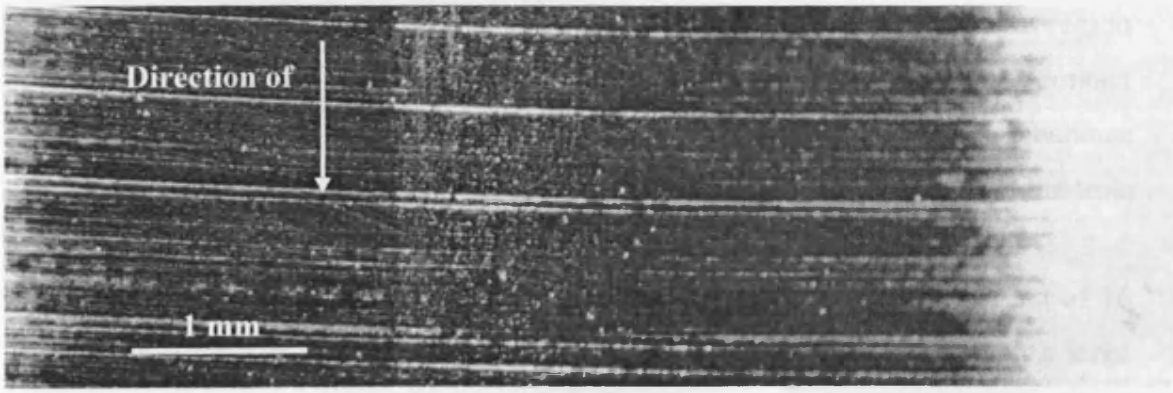

Figure 4.7: **Photograph of a ground nitrided sample with the compound layer "on" following a scuffing test performed at 7 m/s sliding speed.**

significant scatter particularly at high sliding speeds as already noted. The performance at the low sliding speed is significantly better than the results obtained with the baseline samples, however. Since industrial and naval gears tend to operate with lower sliding speeds this result may help to explain the practice found in this industry of keeping the compound layer "on".

It may be noted from the least-squares fit to the results that the scuffing load tends to decrease very sharply with increasing sliding speed. The performance at 16 m/s is rather similar to that found with case carburised samples, but the performance at high sliding speed is very disappointing.

Examination of the test samples following testing reveals a very different situation between tests performed at low or high sliding speed. A typical test sample surface after a test run at 7 m/s sliding speed is illustrated in Figure 4.7. This shows little evidence of damage. Some "blackening" of the running track is visible; this is probably no more than staining due to the presence of the lubricating oil at the high surface flash temperature reached during the test. The shallow white trace at the centre of the contact appears to correspond to the compound layer starting to delaminate as experienced at higher sliding speeds.

For tests performed at 16 m/s the appearance of the test samples after testing is rather different. A typical case is illustrated in Figure 4.8. In this sample the compound layer has delaminated completely in the area of maximum contact pressure. As such the position and appearance of the scuffing damage is quite different to that described by Patching *et al.* (1995). Whereas in Patching's results scuffing occurred at the edge of the running track and was associated with lubrication failure in the thin film region at this position, the present results suggest that failure was due to the effects of contact pressure which is at its maximum at the middle of the running track. The appearance of samples from the scuffing tests performed at 20 m/s is similar to that from the tests performed at 16 m/s.

Typical profiles from the fresh and run in surfaces tested at the sliding speed of 16 m/s are illustrated in Figure 5.9. These profiles, as discussed earlier, exhibit a large degree of running-in in which the peaks of surface roughness have been reduced leaving valleys relatively intact. The initial surface roughness before the test was R_a = 1.0 μm.

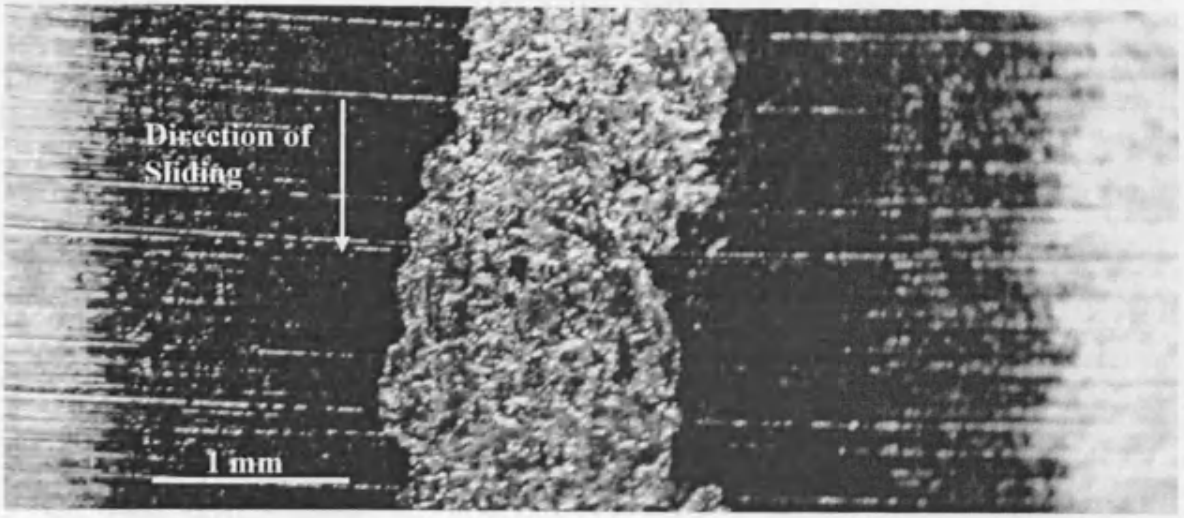

Figure 4.8: **Photograph of a ground nitrided sample with the compound layer "on" following a scuffing test performed at 16 m/s sliding speed.**

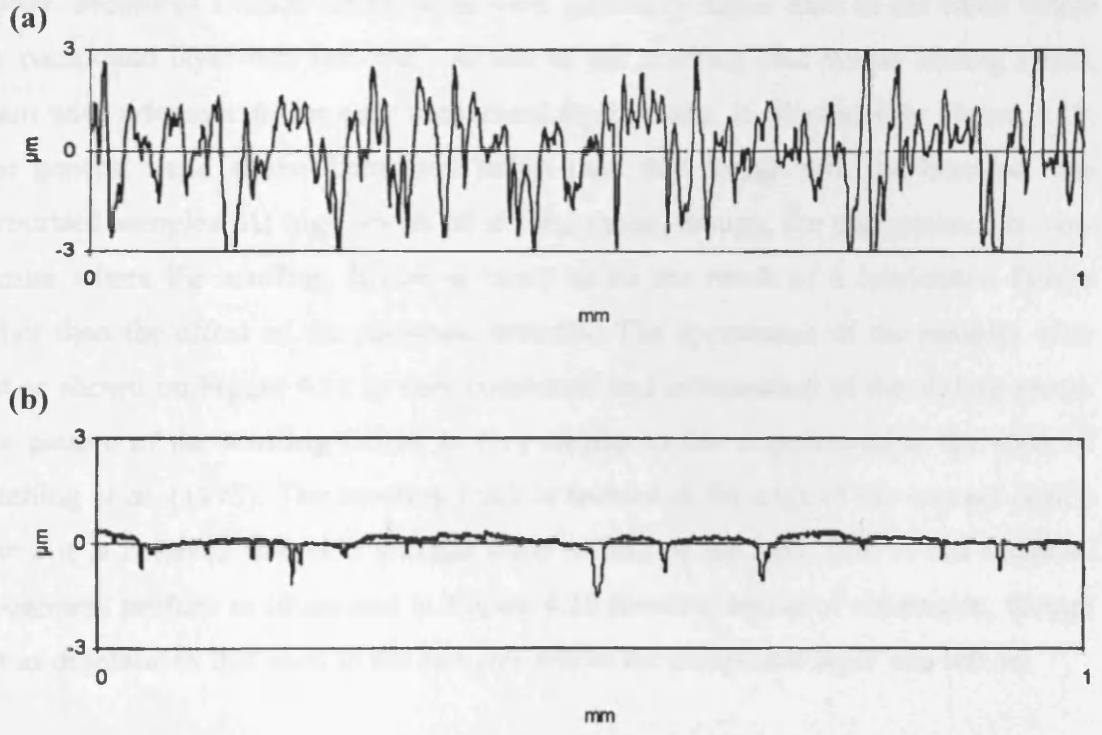

Figure 4.9: **Surface profile of a ground nitrided sample with compound layer "on". (a) *before* scuffing test. (b) *after* a scuffing test performed at 16 m/s.**

4.4 Scuffing tests on ground nitrided samples

Ten tests were performed with nitrided samples where the compound layer was removed by grinding. The range of conditions was the same as that used in testing the samples where the compound layer was left on. The manufacturing process for these samples can be summarised as follows:

- Rough turning
- Cylindrical grinding
- Nitriding treatment
- Final axial grinding

This replicates the process used in aerospace practice where the compound layer is judged to be undesirable. The summary of the results obtained is presented in Table 4.4.

It can be seen that the results obtained were generally more consistent with less scatter. Measured friction coefficients were generally higher than in the cases where the compound layer was left "on". A plot of the scuffing load versus sliding speed, again with reference to the case carburised steel results, is illustrated in Figure 4.10. The general trend shows behaviour better than that found with the baseline case carburised samples. At high levels of sliding speed, though, the performance is very similar where the scuffing failure is likely to be the result of a lubrication failure rather than the effect of the substrate material. The appearance of the samples after test as shown on Figure 4.11 is very consistent and independent of the sliding speed. The pattern of the scuffing failure is very similar to that experienced in the work of Patching *et al.* (1995). The scuffing track is located at the edge of the contact region where it is believed that side leakage leads to loss of the EHL film at this location. Roughness profiles as illustrated in Figure 4.12 reveal a degree of running-in, though not as dramatic as that seen in the samples where the compound layer was left on.

Table 4.4

Summary of results from ground nitrided samples with compound layer "Off"

Test n°	16	30	31	32	1	12	13	33	34	35
Peripheral Velocity of Fast Shaft/ms^{-1}	9.15	9.15	9.15	9.15	20.95	20.95	20.95	26.18	26.18	26.18
Peripheral Velocity of Slow Shaft/ms^{-1}	2.15	2.15	2.15	2.15	4.94	4.94	4.94	6.17	6.17	6.17
Mean Entraining Velocity/ms^{-1}	5.65	5.65	5.65	5.65	12.95	12.95	12.95	16.18	16.18	16.18
Sliding Velocity/ms^{-1}	7.00	7.00	7.00	7.00	16.00	16.00	16.00	20.00	20.00	20.00
Scuffing Load/N	3520	3517	3529	4113	2337	2910	1915	1867	1880	1871
Maximum Bulk Temperature of Fast Disc/°C	196	199	195	199	246	268	252	244	220	226
Maximum Bulk Temperature of Slow Disc/°C	155	157	158	165	190	204	180	192	183	182
Mean Bulk Temperature of Discs/°C	175.5	178.0	176.5	182.0	218.0	236.0	216.0	218.0	201.5	204.0
Maximum Peak Hertzian Contact Pressure/GPa	1.61	1.61	1.61	1.70	1.40	1.51	1.31	1.30	1.31	1.30
Traction Coefficient at Scuffing Load	0.034	0.036	0.036	0.033	0.029	0.026	0.038	0.028	0.026	0.024

4.5 Scuffing tests on superfinished nitrided samples

Six tests where performed on samples that were superfinished after being nitrided and ground. All the superfinishing work was carried out using the zinc chips process described earlier. The surface finish of the samples was R_a = 0.05 μm. Tests were

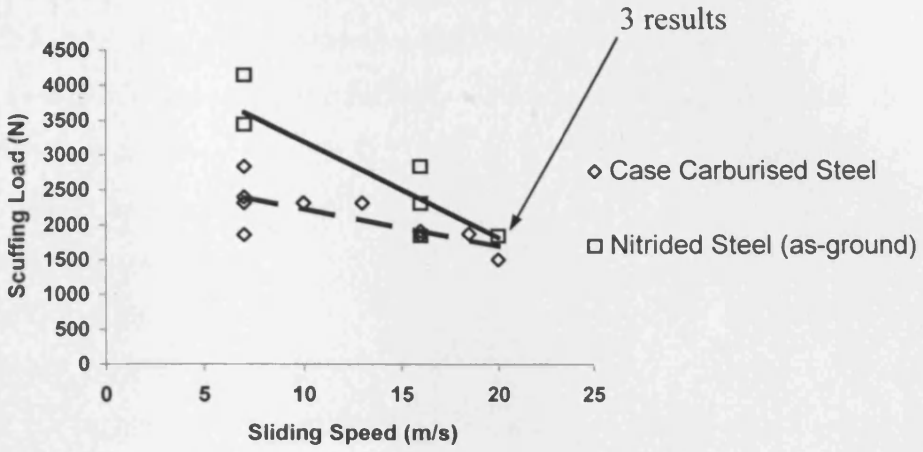

Figure 4.10: **Experimentally determined scuffing loads as a function of sliding velocity for the ground nitrided without the compound layer ("as-ground") surface compared to reference Case Carburised surface tests. Least square fit also shown: continuous line: nitrided samples; dotted line: case carburised samples.**

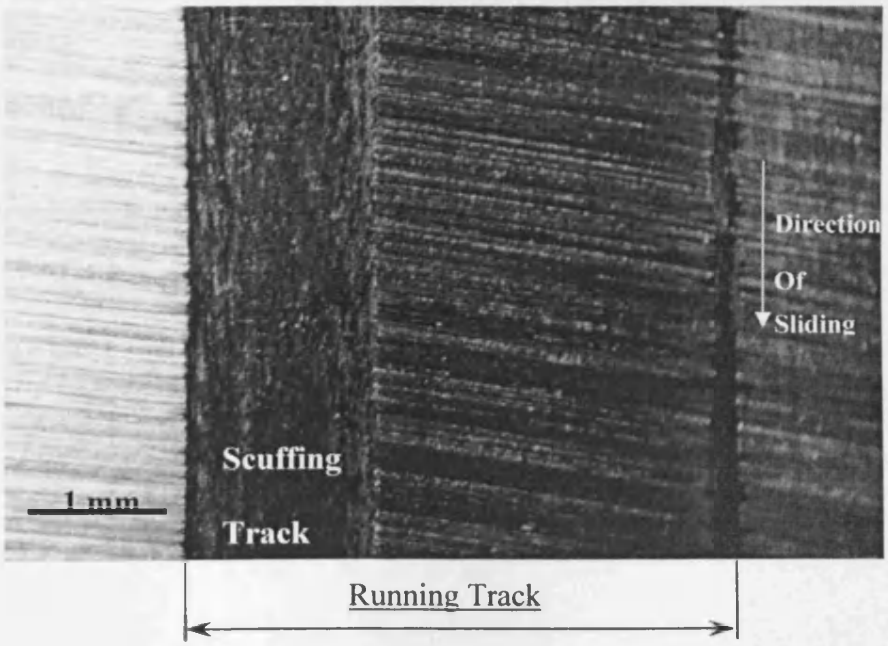

Figure 4.11: **Photograph of a ground nitrided sample without the compound layer following a scuffing test performed at 16 m/s sliding speed. Scuffing track located on the side of the running track.**

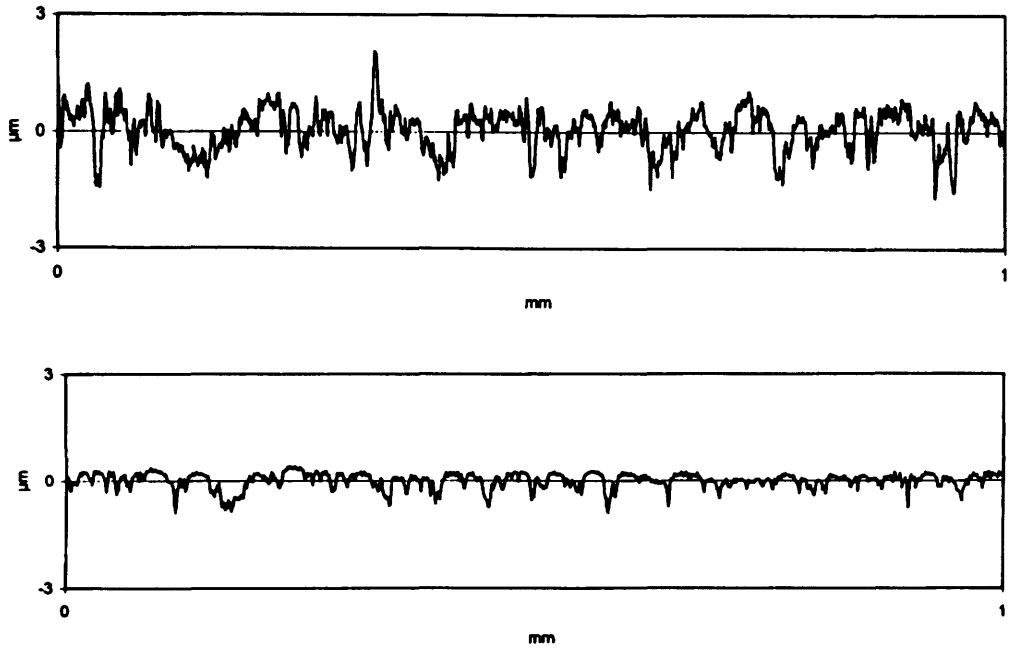

Figure 4.12: **Surface profile of a ground nitrided sample without the compound layer. (a) *before* scuffing test. (b) *after* a scuffing test performed at 16 m/s.**

carried out at the highest sliding speeds i.e. 16 and 20 m/s as it is believed that superfinishing is a possible treatment for gears running at high levels of sliding velocity as found in the aerospace industry. The manufacturing process consisted of:

- Rough turning
- Cylindrical grinding
- Nitriding treatment
- Axial grinding
- Superfinishing treatment

The total process therefore consisted in five separate phases compared to the three phases for the samples where the compound layer was left on. If used in engineering practice such a process would undoubtedly have an impact from the cost point of view.

The summary of results obtained with the superfinished samples is presented in Table 4.5. These results show high levels of scuffing resistance even at very high sliding speeds where the maximum load capability of the rig was reached in two instances (tests 39 and 44). In all cases though, scuffing failure occurred.

The very low traction coefficients obtained in all the tests may be noted.

The appearance of the samples after testing was the same in all tests as illustrated in Figure 4.13. Scuffing failure took place invariably in the middle of the running track in the area of maximum contact pressure. Such behaviour is again very consistent with that found by Patching *et al.* (1995). Numerical simulations carried out by Patching showed that superfinished surfaces produce an almost pure Hertzian pressure distribution in cases where the roughness features are extremely small when compared to the level of oil film thickness (very high λ values). Examination of surface profiles taken before and after testing showed no change in the surface finish.

Table 4.5

Summary of results from ground nitrided and superfinished samples

Test n°	15	36	37	38	39	44
Peripheral Velocity of Fast Shaft/ms^{-1}	20.95	20.95	20.95	26.18	26.18	26.18
Peripheral Velocity of Slow Shaft/ms^{-1}	4.94	4.94	4.94	6.17	6.17	6.17
Mean Entraining Velocity/ms^{-1}	12.95	12.95	12.95	16.18	16.18	16.18
Sliding Velocity/ms^{-1}	16.00	16.00	16.00	20.00	20.00	20.00
Scuffing Load/N	2890	4159	4189	3461	4190	4207
Maximum Bulk Temperature of Fast Disc/°C	160	187	187	175	196	190
Maximum Bulk Temperature of Slow Disc/°C	124	145	149	138	156	156
Mean Bulk Temperature of Discs/°C	142	166	168	156	176	173
Maximum Peak Hertzian Contact Pressure/GPa	1.51	1.70	1.71	1.60	1.71	1.71
Traction Coefficient at Scuffing Load	0.012	0.008	0.009	0.007	0.008	0.007

4.6 General comparison of scuffing performance between nitrided and case carburised surfaces

Tests performed on samples made of nitrided steel and heat-treated using a gas nitriding process exhibited mixed results. The process in which the compound layer was left on the samples produced particularly variable scuffing performance. At low sliding speed, the performance is very good and far exceeds the level of performance found with the baseline material (case carburised). Traction coefficients were also lower than those encountered with the baseline material as shown in Table 4.6. These coefficients were found to be almost constant over the whole speed range. Typically the traction with nitrided (compound layer on) samples was about 25 % less than that obtained with the baseline samples. The lower traction was reflected in the lower bulk

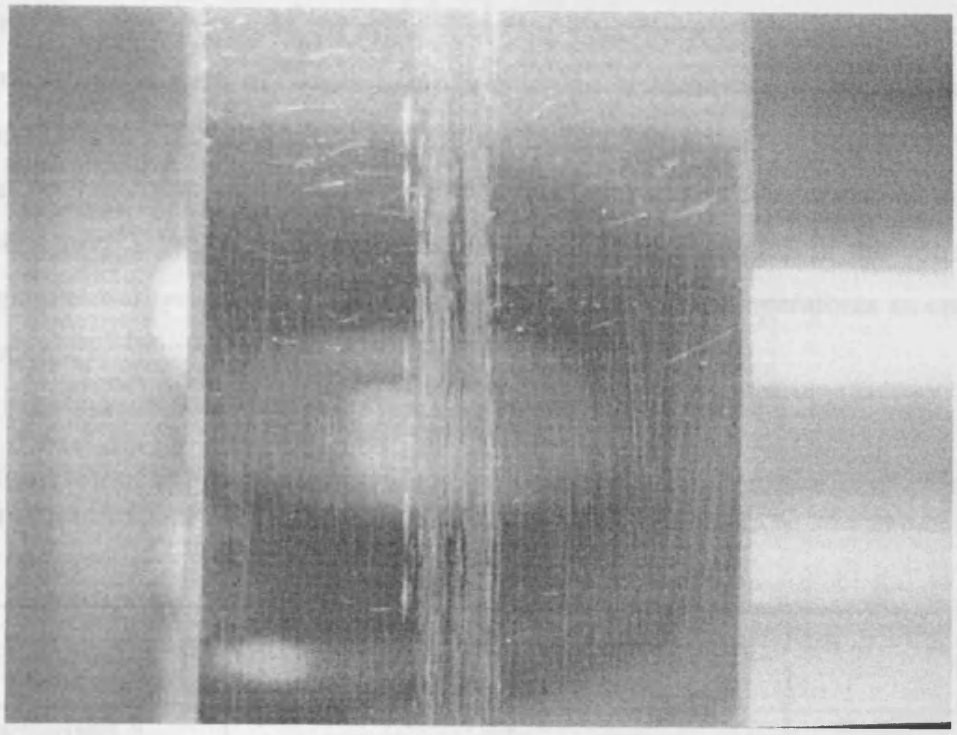

Figure 4.13: **Photograph of a ground nitrided and superfinished sample following a scuffing test performed at 16 m/s sliding speed. Scuffing track located in the middle of the running track.**

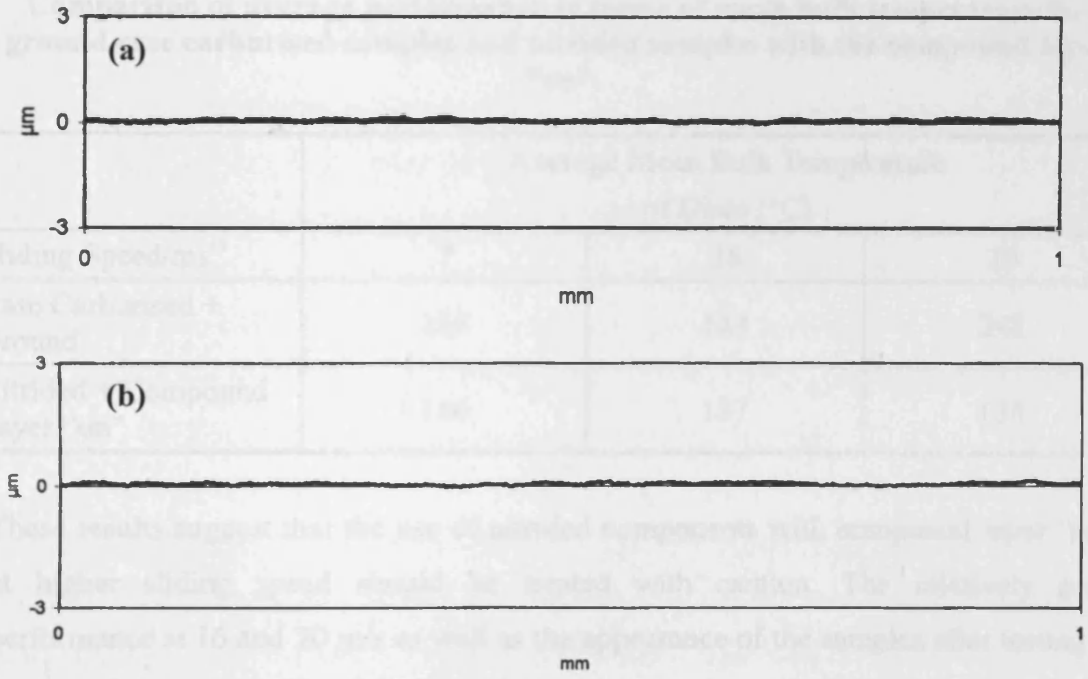

Figure 4.14: **Surface profile of a ground nitrided superfinished sample. (a) before scuffing test. (b) after a scuffing test performed at 16 m/s.**

temperatures obtained under the same operating conditions of load and speed as shown in Table 4.7. The case of 7 m/s exhibits a higher temperature in the case of nitrided samples. This could be explained by the very high level of run-in encountered with these samples, resulting in a "superfinished" like surface finish. This situation would have induced a very high level of plastic deformation. The dissipation of the corresponding deformation energy could possibly explain the higher disc temperatures as encountered experimentally.

Table 4.6

Comparison of average performances in terms of mean traction coefficient for ground case carburised samples and nitrided samples with the compound layer "on".

	Average Traction Coefficient		
Sliding Speed/ms^{-1}	7	16	20
Case Carburised + Ground	0.035	0.029	0.023
Nitrided + Compound Layer "on"	0.023	0.023	0.021

Table 4.7

Comparison of average performance in terms of mean bulk temperature for ground case carburised samples and nitrided samples with the compound layer "on".

	Average Mean Bulk Temperature of Discs (°C)		
Sliding Speed/ms^{-1}	7	16	20
Case Carburised + Ground	156	184	242
Nitrided + Compound Layer "on"	166	137	138

These results suggest that the use of nitrided components with compound layer "on" at higher sliding speed should be treated with caution. The relatively poor performance at 16 and 20 m/s as well as the appearance of the samples after testing is a cause for concern. The fact that what appears to be serious delamination of the surface takes place under these severe conditions reinforces the view that removal of

the compound layer should take place in practice if high sliding speeds are contemplated.

Results obtained with samples where the compound layer was removed after nitriding treatment are much more consistent. The behaviour in this case is very similar to that observed by Patching *et al.* (1995). The overall scuffing performance of the nitrided/ground samples is superior to that seen with the baseline samples as illustrated in Figure 4.10, although the gain is marginal at high sliding speed. The mean traction coefficients as illustrated in Table 4.8 are generally slightly higher than the baseline disks. It may be noted that traction and temperature rise are related as might be expected.

Table 4.8

Comparison of average performance in terms of mean traction coefficient for ground case carburised samples and nitrided samples with the compound layer removed.

	Average Traction Coefficient		
Sliding Speed/ms^{-1}	7	16	20
Case Carburised + Ground	0.035	0.029	0.023
Nitrided + Ground	0.035	0.031	0.026

Mean bulk temperatures at the scuffing load encountered with these samples are slightly higher than those encountered with the baseline samples as illustrated in Table 4.9. This is consistent with traction coefficients as outlined above. The superior scuffing performance of nitrided samples may be related to their higher temperature capability due to their relatively high tempering temperature (typically 600°C).

The performance of nitrided and superfinished samples is similar to that observed by Patching (1995) using case carburised superfinished samples. Scuffing load as a function of the sliding speed, as presented in Figure 4.15, reveals a scuffing performance at high sliding speed which is relatively insensitive to the speed (within the experimental scatter). These results appear to be slightly in favour of the nitrided configuration. The average traction coefficient and the average mean bulk temperature are presented in Table 4.10.

Table 4.9

Comparison of average performance in terms of mean bulk temperature for ground case carburised samples and ground nitrided samples with the compound layer removed.

	Average Mean Bulk Temperature of Discs (°C)		
Sliding Speed/ms^{-1}	7	16	20
Case Carburised + Ground	156	184	242
Nitrided + Ground	178	223	208

Table 4.10

Comparison of average performance in terms of mean bulk temperature for ground case carburised samples and ground nitrided samples with the compound layer removed (superfinished).

	Average Traction Coefficient		Average Mean Bulk Temperature of Discs (°C)	
Sliding Speed/ms^{-1}	16	20	16	20
Case Carburised + Superfinished	0.011	0.010	174	186
Nitrided + Superfinished	0.010	0.007	159	168

Both traction coefficient and mean bulk temperatures are lower in the case of nitrided samples compared to the baseline material. This difference may be due to the slightly different finish obtained on the nitrided samples. Patching's samples were finished by the Westland Co whereas the samples used in the present work were finished in the Cardiff University Abral plant.

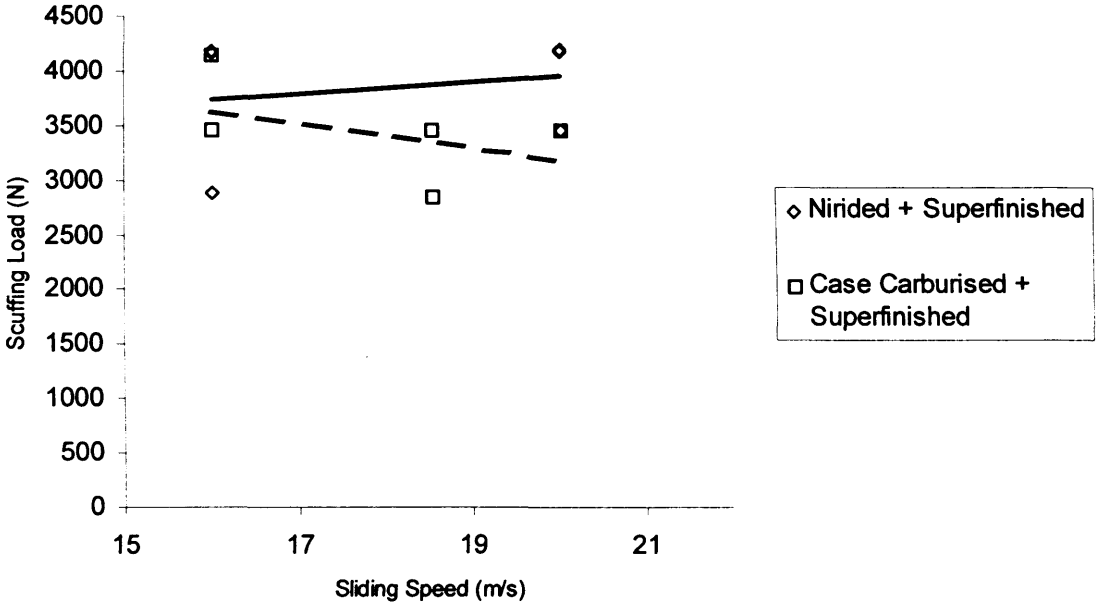

Figure 4.15: **Experimentally determined scuffing loads as a function of sliding velocity for the nitrided superfinished surface compared to reference superfinished Case Carburised surface tests. Least square fit also shown: continuous line: nitrided samples; dotted line: case carburised samples.**

CHAPTER 5.

Experimental study of the scuffing performance of ultra hard coatings

5.1 Introduction

The use of thin, super-hard coatings such as diamond-like carbon (DLC) or boron carbide has been proposed, and in a number of cases adopted, as an anti-wear treatment for various machine elements. This chapter describes an experimental program with the aim of investigating the possible benefits of using thin hard coatings to enhance the scuffing resistance of case hardened steel in gearing applications with steel, surface finish and lubricant type as currently found in aerospace practice. The baseline for this experimental test program was the scuffing performance of conventionally ground uncoated surfaces with a typical roughness of 0.4 μm Ra.

Thin hard coatings have been used in industry for various applications since the late 70s and early 80s and have been found to offer benefits in terms of wear resistance, chemical inertness and low sliding coefficient of friction. They are typically deposited using different variations of the physical vapour deposition (PVD) technique (Sproul, 1996). Amongst thin hard coatings the diamond like carbon (DLC) types have been selected for a number of industrial applications both for tooling and machine elements. Part of this same family are the metal doped DLC coatings (Me-DLC), which are investigated in this study and which appear to offer a better adherence and greater toughness than bare DLC coatings. The other type of coating considered in this study was boron carbide (B_4C). As outlined by Eckardt *et al.* (2000), boron carbide is a promising alternative to Me-DLC coatings, giving enhanced chemical and thermal stability combined with extreme hardness. Moreover, the coating process requires a lower quantity of reactive gas, which is advantageous.

The tests described here were carried out using discs, but care was taken to reproduce the finish found on real gears both in terms of the amplitude of roughness and the orientation of the roughness relative to the direction of rolling and sliding of the

surfaces as described in Chapter 2. Rolling and sliding speeds were in the range of 7 to 20 m/s corresponding to operating conditions at the upper limits of current aero gas turbine engine and helicopter gearing practice and beyond. The utility of disks as a means of simulating gear tooth contacts has already been described in chapter 2. The emphasis in the disc tests described here was upon a fundamental study of the behaviour of friction, temperature and surface changes during the stages preceding scuffing and the effects and possible benefits of using ultra hard coatings.

5.2 Description of Me-DLC coatings

Metal-doped diamond like carbon coatings are part of the large family of DLC coatings. These coatings are deposited using reactive dc magnetron sputtering (Teeter *et al.*, 1996). Typically, the process uses a proprietary sputtering system as shown in Figure 5.1. The process is fully described by Hans *et al.* (2000). It is divided into four main stages. First, samples are heated and cleaned using Argon ion etching. A metallic interlayer is then deposited on the samples, the usefulness of which will be further explained. The samples then receive their functional coating (Me-DLC) before being unloaded from the coating machine. The whole process takes place under very high vacuum (typically 10^{-3} Pa). Regarding the chemical structure of the resulting coating, it should be noted that carbon has an outer electron structure of $1s^2\ 2s^2\ 2p^2$ where s and p refer to electron orbitals. The subscript is the number of electrons in the orbital. $2s^2$ and $2p^2$ are the only orbitals used to form bonding. When carbon chemically links to other atoms, say carbon, the s and p orbitals mix together to give new hybrid orbitals. This yields stronger bonds. In diamond, each carbon is joined to four others at the corners of a tetrahedron. The orbitals used for this strong bonding are a mixture of the s + p orbitals are mentioned above. These orbitals are called sp^3 hybrids. The shape of the sp^3 hybrids is tetrahedral as illustrated in Figure 5.2. The overlap of the four lobes that this structure exhibits is responsible for chemical bonding. If the long distance order becomes disorganized, the resulting material is amorphous. It exhibits, in the case of amorphous diamond, the same bonds as in diamond i.e. a hard but amorphous structure. There are other hybrid orbitals that occur in carbon e.g. sp^2. This structure has the shape of a planar triangle as illustrated in

Figure 5.1: **Photograph of the type of magnetron sputtering system used for Me-DLC coating tested in the experimental programme (from Balzers).**

(a)

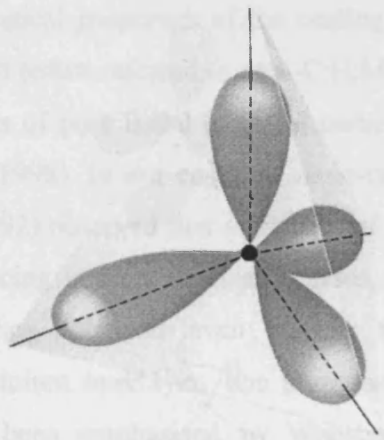

(b)

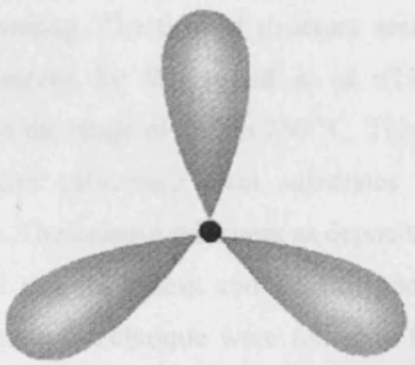

ure 5.2: **Representation of the carbon chemical orbital structure contained in a DLC coating, (a): sp^3 tetrahedral bonding giving "diamond like" properties. (b) sp^2 trigonal planar bonding giving "graphite like" properties.**

Figure 5.2. This typical structure occurs in graphite. In the case when the graphite layers made of these planar triangles do not stack "correctly", the resulting material is amorphous. In the case of Diamond Like Carbon Coatings, the base structure is essentially amorphous containing a mixture of sp^3, sp^2 hybridised carbon. Schematically, as outlined above, the sp^3 atomic orbital corresponds to a "diamond like" structure whereas the sp^2 atomic orbital corresponds to a "graphite" like structure. The ratio sp^3/sp^2 ("diamond/graphite") in the coating is difficult to control but it plays a significant role in the behaviour of the coating as emphasized by Zaidi *et al.* (2000). The structure also includes a fairly large proportion of hydrogen since hydrogen is present in the vacuum chamber as a result of the decomposition of hydrocarbons (usually acetylene) used to generate the carbon phase (Wang *et al.*, 1992). In the coating considered here the hydrogen content is stated to be from about 12 to 16 % atomic percent (Bloyce, 2001). This element plays a crucial role in explaining some of the tribological properties of the coating (Liu *et al.*, 1998). The metal doped DLC coating itself (often referred to as a–C:H:M), includes metals in the form of small nano-crystallites of pure metal or metal carbide dispersed throughout the carbon network (Donnet, 1998). In our case, the nano-crystallites correspond to metal carbide. Wang *et al.* (1992) observed that a gradient of metal content is present from interface to surface reducing internal residual stresses, hence promoting better adhesion. In order to enhance adhesion even further, the commercial coater systematically deposits a chromium interlayer. The importance of this interlayer in heavily loaded contacts has been emphasised by Wanstrand *et al.* (1999) who suggests that the thinner the interface of chromium, the better the mechanical and tribological properties of the coating. The type of structure seen in these coatings is usually columnar as also observed by Wanstrand *et al.* (1999). The deposition temperature for the coating is in the range of 200 to 250 °C. This parameter may be of concern when considering case carburised steel substrates with low tempering temperatures of the same order. The coating thickness as deposited on the test samples described here was about 3.2 μm. Hardness and elastic modulus for the coating assessed using the nano-indentation technique were found to be respectively 11.37 GPa and 121.0 GPa (Bloyce, 2001). The hardness value is consistent with measurements made by (Harris *et al.*, 1997). The ratio E/H was therefore about 11. The ratio $E_{coating}$ / $E_{substrate}$ is also significantly smaller than 1, assuming an elastic modulus for the steel substrate of between 200 and 210 GPa.

5.3 Description of Boron Carbide coatings

Due to their very high hardness and low surface friction, boron carbide coatings have also been used in a variety of engineering applications as a means of enhancing wear performance (Hu *et al.*, 1998). They can be deposited at relatively low substrate temperatures e.g. below 120°C (Cermignani *et al.*, 1998). The coating is applied in the same way as DLC coatings by physical vapour deposition using magnetron sputtering. The process can be divided into three in-line operations as illustrated in Figure 5.3. The first operation consists of cleaning the samples using ion etching. The actual coating of samples using boron carbide targets follows the first operation. These targets contain typically 80% (wt) of Boron and 20% (wt) of Carbon. The last operation is the unloading of samples. The whole process takes place under very high vacuum (typically $1.33 \cdot 10^{-5}$ Pa). The chemical structure of the coating is amorphous with a majority of B_4C carbides. Some boron oxides as well as boron oxy-carbides are also normally present with about 15-18 % oxygen located mostly at the surface (Hu *et al.*, 1998). The physical structure of the coating used in our experiments was columnar similar to the DLC coating and illustrated in Figure 5.4. The process requires a bias voltage applied to the steel substrate and was 60V dc in our case. Hu *et al.* (1998), have emphasized the particular importance of the bias voltage which affects both the hardness and elastic modulus of the coating. With the 60Vdc bias used here, a coating hardness of about 17 GPa and an elastic modulus of about 180 GPa was obtained. This gives a ratio E/H of about 10.5, which is comparable to the DLC coating but with a higher intrinsic hardness and elastic modulus. The coating thickness was 2.7 μm. It may be noted that the elastic modulus of both coatings investigated is lower than the elastic modulus of the steel substrate of the test discs.

5.4 The problem of elastic mismatch

In order to help understand the behaviour of the various coatings it is useful to consider some aspects of the mechanics of contact of coated systems and in particular the issue of elastic mismatch between the coating and its substrate. A number of authors (Olver, 1997; Oliveira *et al.*, 1996) have studied the effects of a coated system

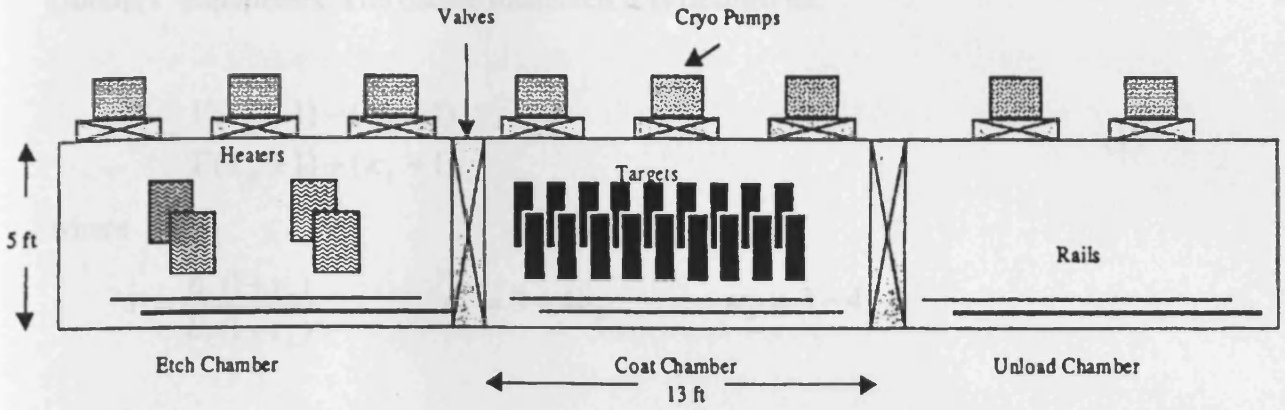

Figure 5.3: **Schematic representation of the coating facility for B_4C coatings (from Cermignani *et al.*, 1998).**

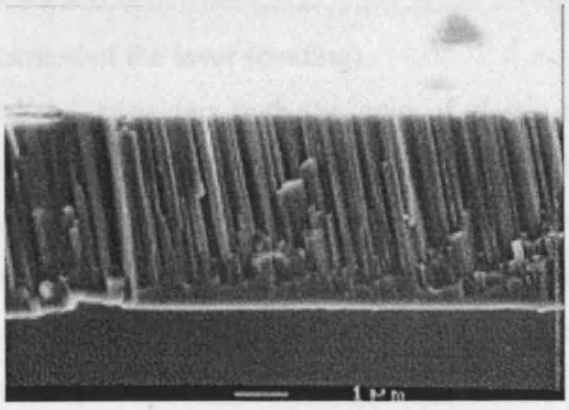

Figure 5.4: **Photograph of cross-section of a B_4C coating performed with a 60Vdc bias voltage showing the typical columnar structure (from Hu *et al.*, 1998).**

on the contact pressure distribution, and the real area of contact as well as the influence of physical property mismatch in relation to coating failures (Oliveira *et al.*, 1996; Plumet, *et al.*, 1998; Sainsot, *et al.*, 1990). Oliviera considered the mismatch between elastic properties of the layer (subscript L) and substrate (subscript S) using Dundurs' parameters. The elastic mismatch α is defined as:

$$\alpha = \frac{\Gamma(\kappa_S + 1) - (\kappa_L + 1)}{\Gamma(\kappa_S + 1) + (\kappa_L + 1)} \tag{1}$$

where

$$\Gamma = \frac{E_L(1+\nu_s)}{E_S(1+\nu_L)} \qquad \kappa_L = 3 - 4\nu_L \qquad \kappa_S = 3 - 4\nu_S$$

According to Oliviera α must be between –1 and +1, and in the case of a layer less stiff than the substrate (the case considered in this experimental programme), α has to be negative.

Oliviera plots the contours of a dimensionless delamination pressure $p_0^{delam}\sqrt{a}/K_{IC}^{L}$ as a function of the elastic mismatch and the dimensionless coating thickness h/a. p_0^{delam} represents the contact pressure required to cause the coating to delaminate from the substrate; a is the contact half width; K_{IC}^{L} is the stress intensity factor of the layer (coating); h is the thickness of the layer (coating).

Plumet, on the other hand, considers both the ratio of elastic modulii and the ratio between the coating thickness and the square root of the contact area size as important in assessing coatings. The last parameter requires knowledge of the load involved. In the case of the experiments to be described the appropriate load is that at which scuffing occurred. The above parameters known before testing are given in Table 5.1.

Table 5.1

Coating parameters as proposed by Oliviera *et al.* [1] and Plumet *et al.* [2] for the coatings tested in the current work

Coating	E1/E2 from [2]	α from [1]
Me-DLC	0.6	–0.3
Boron Carbide	0.9	–0.1

E_1: coating elastic modulus E_2: substrate elastic modulus

α: elastic mismatch

These figures would suggest minimum perturbation of subsurface stresses as indicated by both Plumet, *et al.*, (1998) and Sainsot, *et al.*, (1990). The elastic mismatch parameter as presented by Oliviera *et al.* taken from Dundurs does, however, indicate a significant difference between the two coatings that will be further commented upon in the conclusions.

5.5 Scuffing tests with ground case carburised samples coated with Me-DLC

In all nine tests were carried out with substrates having a ground finish. Three sliding speeds of 7, 16 and 20 m/s were used. Three tests were performed at each sliding speed. The results of these tests are presented in Table 5.2. Results showing the scuffing load as a function of sliding speed are given in Figure 5.5.

The results obtained using Me-DLC coatings are subject to significant scatter, but in general the performance is slightly inferior to that of the uncoated discs. It may be noted from the least-squares fit to the results that the scuffing load tends to decrease only slightly with increasing sliding speed. This suggests that failure is determined by load *per se*, and in this case the critical value of the load is about 2000 N which corresponds to a maximum Hertzian contact pressure of 1.3 GPa. The concept of a critical load is supported by visual examination of the failed surfaces as shown in Figure 5.6. The surface distress suggests a mechanism of coating delamination that then degenerates into scuffing. Areas in those locations where the coating had maintained its integrity indicate that scuffing did not occur. Coating adhesion seems to play a crucial role in the behaviour of these case carburised samples coated with Me-DLC type material. The large scatter in the results illustrated in Figure 5.5 is also characteristic of these tests where delamination tends to occur fairly randomly. Once some of the coating has been displaced it has a radical detrimental effect on the scuffing resistance. The relatively poor performance of this coating (compared to the

Table 5.2

Summary of results using Me-DLC coated samples

Test n°	19	20	21	24	25	26	27	28	29
Type of Substrate	CC	CC	CC	CC	CC	CC	CC	CC	CC
Type of Finish	GR	GR	GR	GR	GR	GR	GR	GR	GR
Peripheral Velocity of Fast Shaft/ms^{-1}	20.95	20.95	20.95	26.18	26.18	26.18	9.15	9.15	9.15
Peripheral Velocity of Slow Shaft/ms^{-1}	4.94	4.94	4.94	6.17	6.17	6.17	2.15	2.15	2.15
Mean Entraining Velocity/ms^{-1}	12.95	12.95	12.95	16.18	16.18	16.18	5.65	5.65	5.65
Sliding Velocity/ms^{-1}	16.00	16.00	16.00	20.00	20.00	20.00	7.00	7.00	7.00
Scuffing Load/N	1917	1203	1824	2407	1167	1211	1495	2399	1493
Maximum Bulk Temperature Of Fast Disc/°C	152	126	272	184	120	122	103	134	104
Maximum Bulk Temperature Of Slow Disc/°C	120	99	192	mal func.	103	102	91	113	mal func.
Mean Bulk Temperature Of Discs/°C	136	113	232	n/a	112	112	97	125	n/a
Maximum Peak Hertzian Contact Pressure /GPa	1.31	1.13	1.29	1.42	1.11	1.13	1.21	1.42	1.21
Traction Coefficient at Scuffing Load	0.010	0.025	mal func.	0.012	0.005	0.007	0.021	0.023	0.020

CC: case carburised substrate GR: ground substrate surface finish

uncoated samples) may suggest that the treatment, which involves temperatures of the order of the tempering temperature of the steel, reduces the hardness of the underlying material. A further feature of these Me-DLC coated samples is the significant degree of run-in or surface finish improvement during the tests. This phenomenon occurred for all three sliding speeds. Typical profiles from the fresh and run in surfaces at the sliding speed of 16 m/s are illustrated in Figure 5.7. Apart from the situation when the

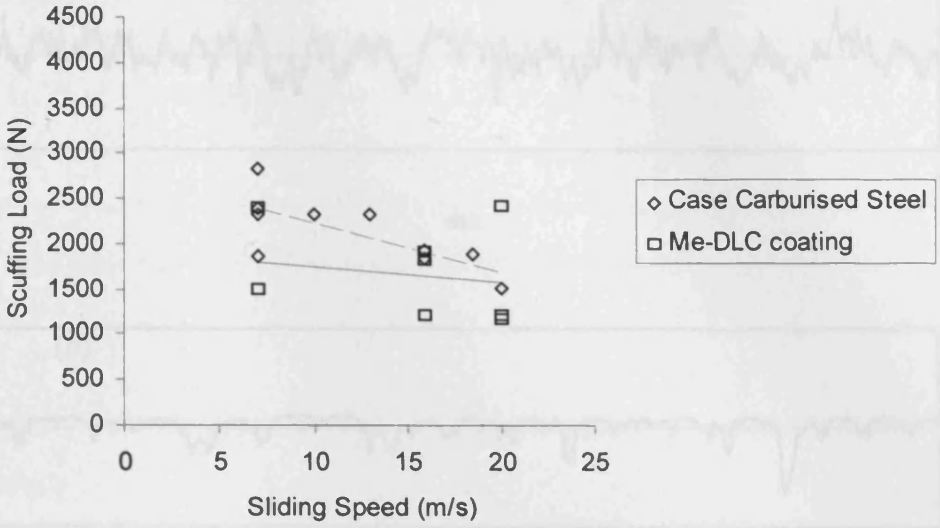

Figure 5.5: **Experimentally determined scuffing loads as a function of sliding velocity for the ground case carburised with Me-DLC coated surface compared to reference case carburised surface tests. Least square fit also shown: continuous line: Me-DLC coating; dotted line: case carburised samples.**

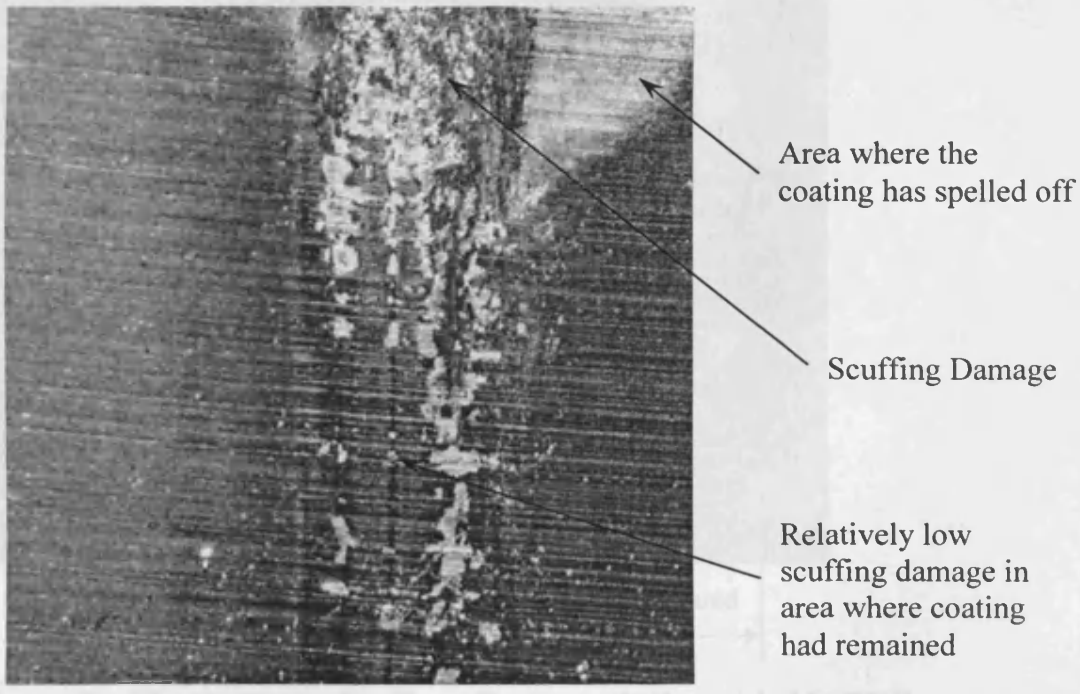

Figure 5.6: **Photograph of a case carburised sample with Me-DLC coating following scuffing.**

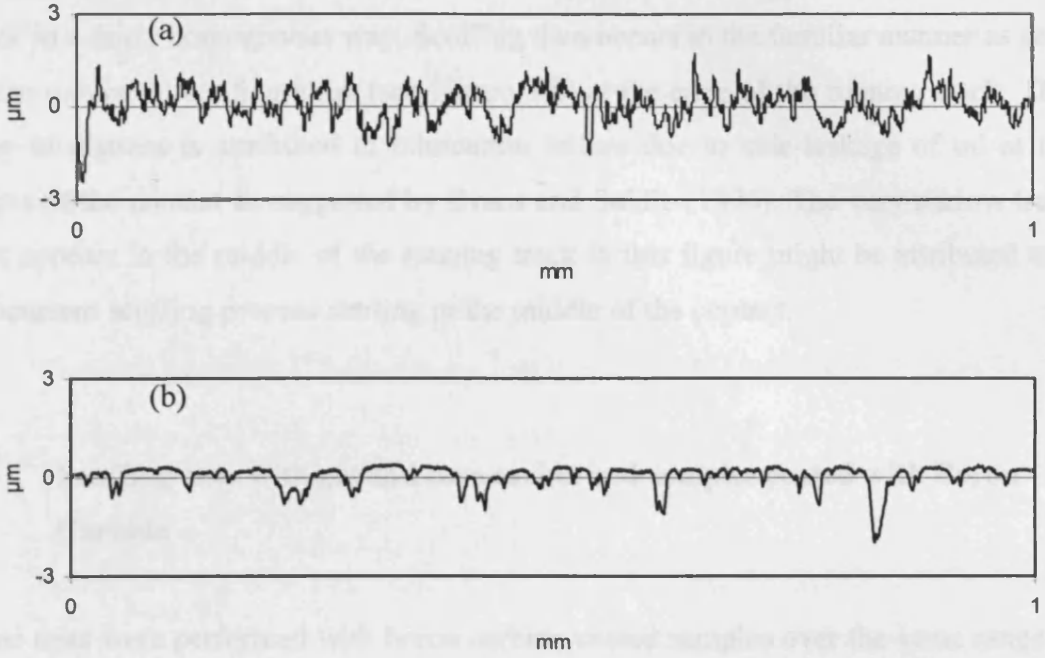

Figure 5.7: **Surface profile of a case carburised steel disc with Me-DLC coating. (a) *before* scuffing test. (b) *after* scuffing test performed at 16 m/s. (profiles taken in the circumferential direction).**

Figure 5.8: **Scuffing pattern of a Case Carburised disc with Me-DLC coating sample where scuffing occurred at the edge of the track. Most of the coating has disappeared from the running track; a concurrent scuffing degradation appears to be starting in the middle of the track where the surface was in a near "superfinished" condition.**

coating delaminates, it is noted that the coating tends to disappear from the running track in a fairly homogenous way. Scuffing then occurs in the familiar manner as seen in the un-coated configuration (see Figure 5.8) at the edge of the running track. This type of distress is attributed to lubrication failure due to side-leakage of oil at the edges of the contact as suggested by Evans and Snidle (1996). The very narrow trace that appears in the middle of the running track in this figure might be attributed to a concurrent scuffing process starting in the middle of the contact.

5.6 Scuffing tests with ground case carburised samples coated with Boron Carbide

Nine tests were performed with boron carbide coated samples over the same range of conditions as used in the Me-DLC tests. Some additional tests were performed at 16 m/s sliding speed. Test results are presented in Table 5.3 and show a significant improvement when compared to the Me-DLC coating tested under identical conditions with the same substrate. This configuration also shows an improvement in scuffing capacity over the simple case carburised baseline as illustrated in Figure 5.9. However, it may be noted that the scuffing load decreases significantly with sliding speed. As in the case of Me-DLC there is evidence of run-in during the tests as illustrated in Figure 5.10. The delamination that occurred with the Me-DLC coating was not experienced under the same conditions with the boron nitride material. The coating tends to disappear from the running track in a fairly uniform way. Scuffing, when it finally happens, occurs in the familiar manner as seen in the un-coated samples at the edge of the running track as illustrated in Figure 5.11. The unscuffed surface near the centre of the contact becomes polished in a similar manner to the Me-DLC coated samples as also shown in Figure 5.11. The boron carbide coated samples exhibit a performance almost as impressive as the nitrided sample coated with Me-DLC coating as it will be presented in 5.7. The maximum possible load was reached in two tests at 16 m/s, although scuffing occurred soon after application of this load.

Another interesting aspect of these tests is the mean bulk temperature of the discs as a function of the sliding speed as illustrated in Figure 5.12. This figure shows a comparison with the mean bulk temperatures reached with the benchmark case

carburised samples. Temperatures attained in the case of the boron carbide samples are significantly lower than those reached with case carburised samples in spite of the fact that the scuffing loads were higher. The mean bulk temperature is also less sensitive to the degree of sliding. This supports the general claim that these coatings give lower friction.

Table 5.3

Summary of results from case carburised + Boron Carbide coating tests

Test n°	40	41	42	43	44	45	46	47	48
Type of Substrate	CC	CC	CC	CC	CC	CC	CC	CC	CC
Type of Finish	GR	GR	GR	GR	GR	GR	GR	GR	GR
Peripheral Velocity of Fast Shaft/ms^{-1}	20.95	20.95	20.95	20.95	9.15	26.18	26.18	26.18	9.15
Peripheral Velocity of Slow Shaft/ms^{-1}	4.94	4.94	4.94	4.94	2.15	6.17	6.17	6.17	2.15
Mean Entraining Velocity/ms^{-1}	12.95	12.95	12.95	12.95	5.65	16.18	16.18	16.18	5.65
Sliding Velocity/ms^{-1}	16.00	16.00	16.00	16.00	7.00	20.00	20.00	20.00	7.00
Scuffing Load/N	4182	4181	2834	2868	3723	1859	2827	1873	4144
Maximum Bulk Temperature of Fast Disc/°C	227	215	163	136	134	163	mal func.	124	150
Maximum Bulk Temperature of Slow Disc/°C	168	mal func.	134	115	120	130	139	109	133
Mean Bulk Temperature of Discs/°C	198	n/a	149	126	127	146	n/a	116	142
Maximum Peak Hertzian Contact Pressure/GPa	1.71	1.70	1.50	1.50	1.64	1.30	1.50	1.30	1.70
Traction Coefficient at Scuffing Load	0.016	0.012	0.013	0.007	0.006	0.013	0.011	0.009	0.015

CC: case carburised substrate GR: ground substrate surface finish

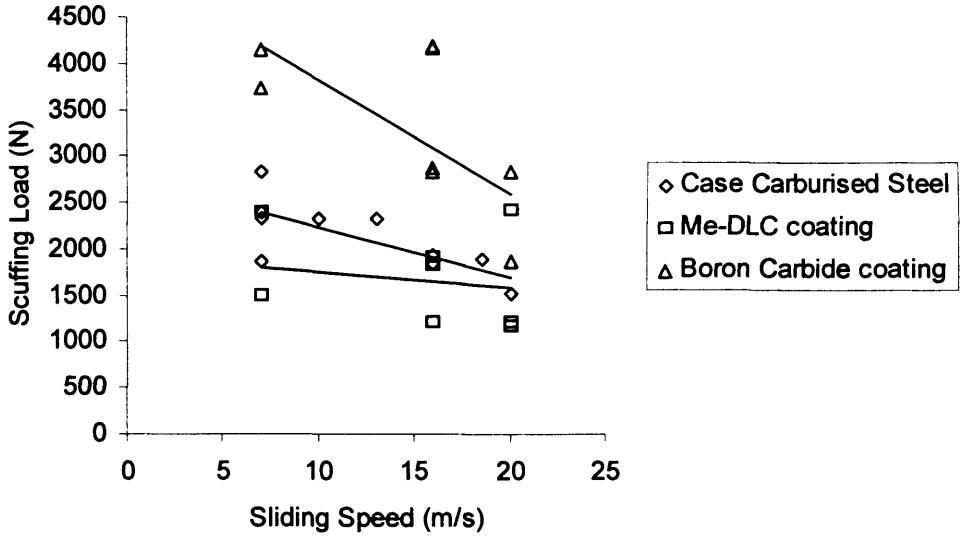

Figure 5.9: **Experimentally determined scuffing loads as a function of sliding velocity for the ground case carburised discs with boron carbide coated surface compared to Me-DLC coated surface and reference case carburised surface tests (least square fits also shown).**

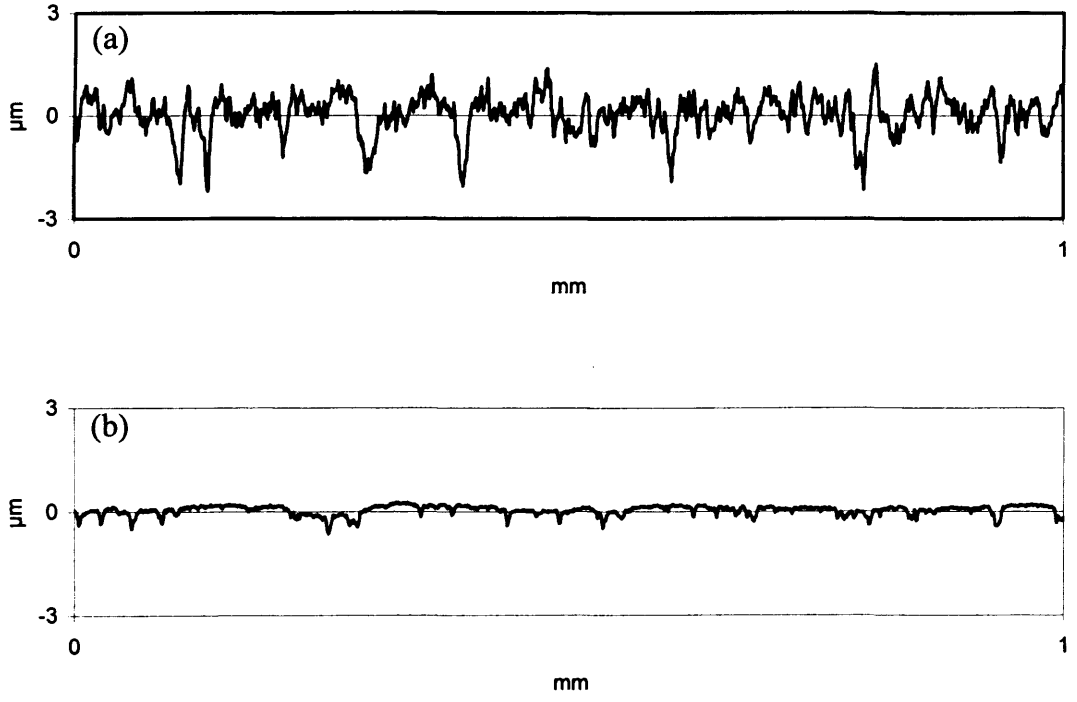

Figure 5.10: **Surface profile of a case carburised disc with boron carbide coating. (a) *before* scuffing test; (b) *after* scuffing test performed at 16 m/s.**

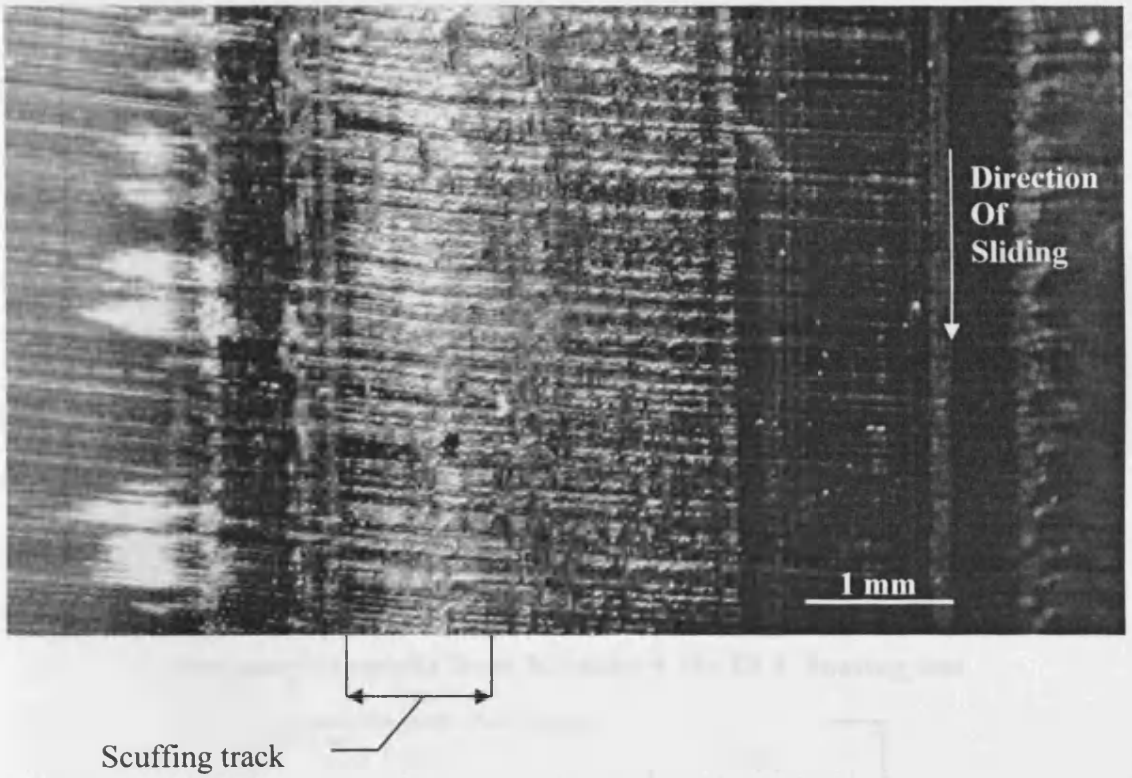

Figure 5.11: **Photograph of the ground case carburised disc coated with boron carbide sample after a 16 m/s sliding speed scuffing test.**

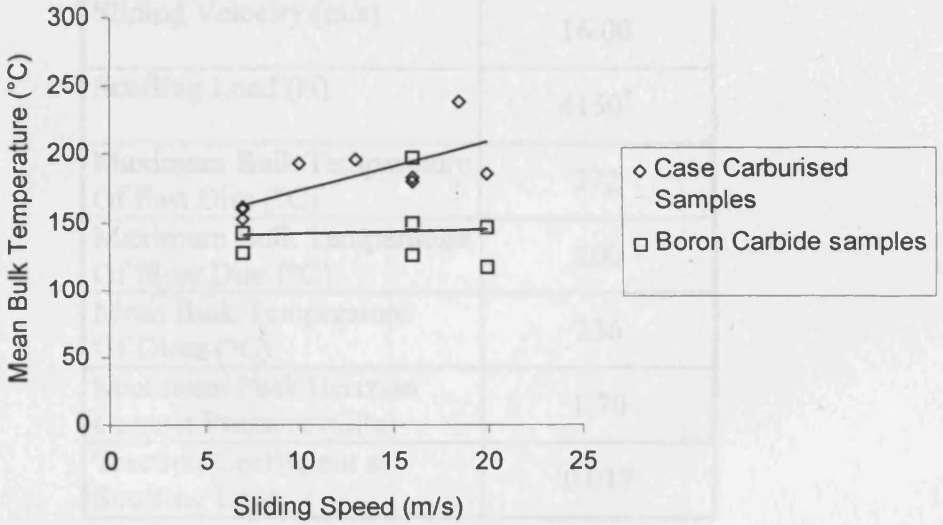

Figure 5.12: **Comparison of mean bulk temperatures between un-coated case carburised and boron carbide coated samples.**

5.7 Scuffing tests with superfinished nitrided samples coated with Me-DLC

In addition to the tests with case carburised and ground substrates a single test was carried out using a nitrided and ground disk coated with Me-DLC and run at a sliding speed of 16 m/s. The results of this test are presented in Table 5.4 (test number 14). In this test no scuffing was experienced even at the load limit of the rig (the load being maintained for about 30 mins). The appearance of the nitrided sample after the test is shown in Figure 5.13. Significant run-in occurred as illustrated in Figure 5.14. An interesting feature of this test is the maximum mean bulk temperature reached (236°C), which is the highest encountered in the project. This confirms the very good high temperature behaviour of the nitrided substrate.

Table 5.4

Summary of results from Nitrided + Me-DLC coating test

Test n°	14
Type of Substrate	Nit
Type of Finish	GR
Peripheral Velocity of Fast Shaft (m/s)	20.95
Peripheral Velocity of Slow Shaft (m/s)	4.94
Mean Entraining Velocity (m/s)	12.95
Sliding Velocity (m/s)	16.00
Scuffing Load (N)	4150†
Maximum Bulk Temperature Of Fast Disc (°C)	272
Maximum Bulk Temperature Of Slow Disc (°C)	200
Mean Bulk Temperature Of Discs (°C)	236
Maximum Peak Hertzian Contact Pressure (GPa)	1.70
Traction Coefficient at Scuffing Load	0.017

†: no scuffing occurred; the load corresponds to the maximum testing load used.

A limited number of tests were also performed on nitrided/superfinished substrates coated with Me-DLC (see Table 5.5). All the superfinishing work was carried out using the zinc chips process described earlier. Tests were carried out at only one sliding speed of 16 m/s due to a limited availability of test samples. The results obtained are remarkable as no scuffing was experienced in any of the three tests even at the highest possible load (the maximum load being maintained for about 30 mins). With the superfinished samples there was no indication of running in of the already smooth surfaces.

Table 5.5

Summary of results from Nitrided + Superfinished + Me-DLC coating test

Test n°	45	46	47
Type of Substrate	Nit	Nit	Nit
Type of Finish	SF	SF	SF
Peripheral Velocity of Fast Shaft (m/s)	20.95	20.95	20.95
Peripheral Velocity of Slow Shaft (m/s)	4.94	4.94	4.94
Mean Entraining Velocity (m/s)	12.95	12.95	12.95
Sliding Velocity (m/s)	16.00	16.00	16.00
Scuffing Load (N)	4246†	4231†	4276†
Maximum Bulk Temperature Of Fast Disc (°C)	138	143	146
Maximum Bulk Temperature Of Slow Disc (°C)	122	126	126
Mean Bulk Temperature Of Discs (°C)	130	134	136
Maximum Peak Hertzian Contact Pressure (GPa)	1.71	1.71	1.72
Traction Coefficient at Scuffing Load	0.003	0.003	0.003

†: no scuffing occurred; the load corresponds to the maximum testing load used.

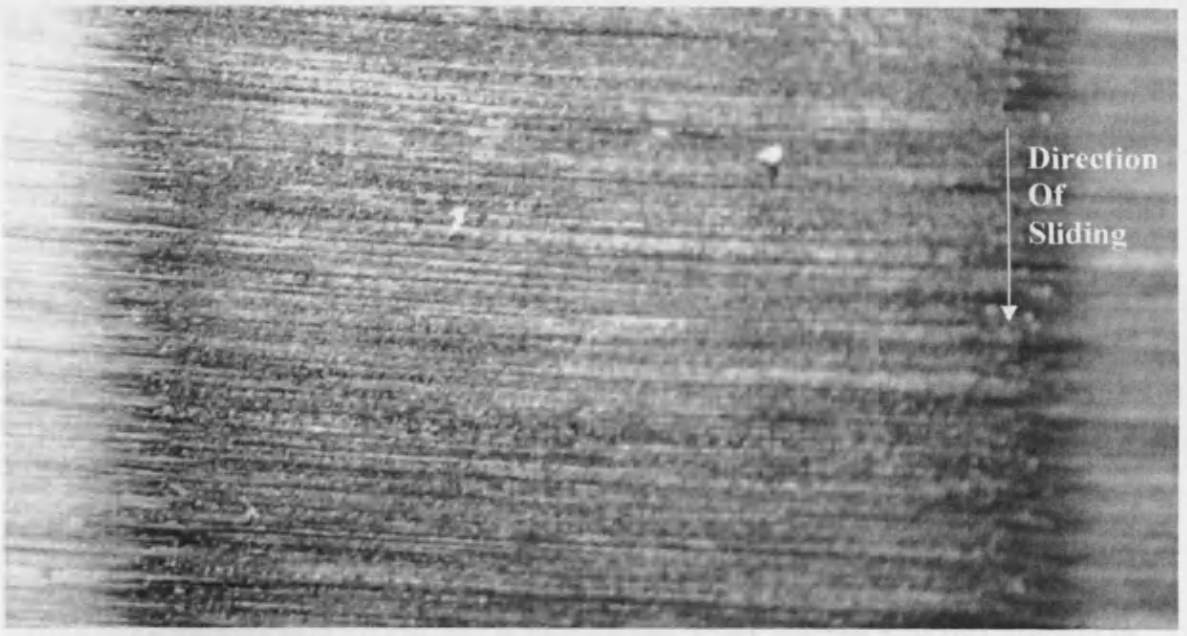

Figure 5.13: **Photograph of the nitrided + ground sample coated with Me-DLC coating after a 16 m/s sliding speed scuffing test (no scuffing occurred).**

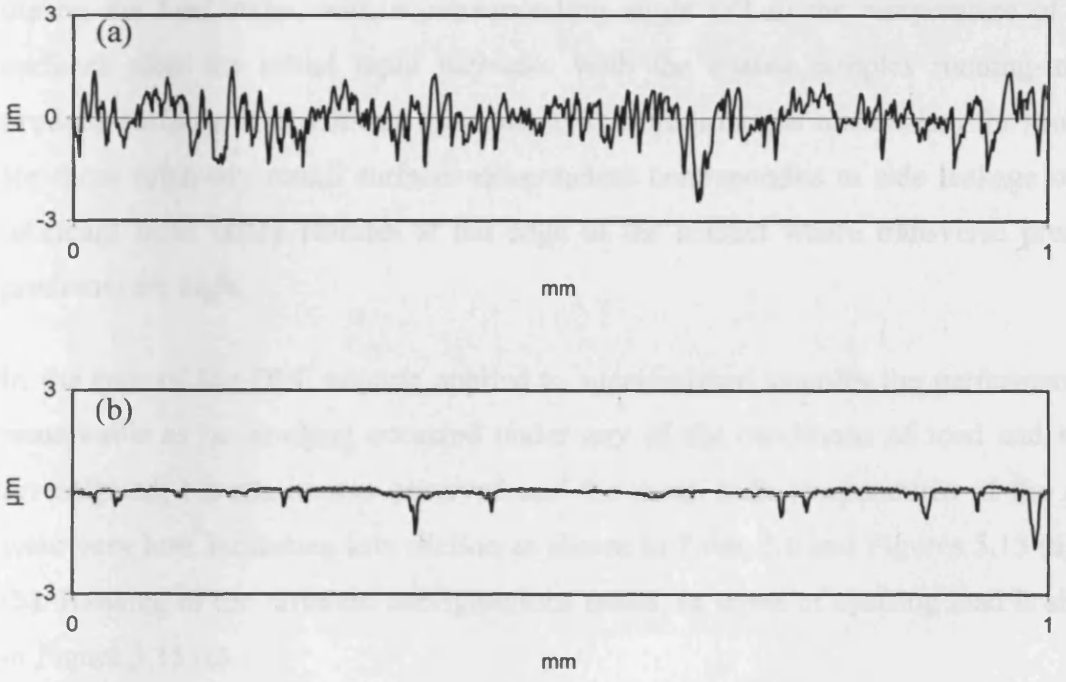

Figure 5.14: **Surface profile of a nitrided disc with Me-DLC coating. (a) *before* scuffing test; (b) *after* scuffing test performed at 16 m/s).**

5.8 General comparison between un-coated and coated configurations

As in earlier work (Patching *et al.* 1995) with uncoated case-carburised samples, it was found that in all cases of scuffing with the coated, ground surfaces there was strong evidence of running in of the surfaces before scuffing took place. This effect was particularly evident in the case of the Me-DLC coated samples as outlined earlier. The surface profiles taken before running and from the un-scuffed parts of the run track show significant modification of the peaks of the surface asperities but with little or no effect on the valley features. In the case of the Me-DLC coated samples the effect produced a near "superfinished" surface and scuffing occurred near the centre of the running track, a characteristic of all tests carried out by Patching (1995) in which superfinished (but un-coated) samples were tested. Evidence of this running in effect is seen during the progress of the test in the behaviour of friction and temperature when running at constant load, particularly at the higher load stages. In the early stages the friction force remains almost constant during the period of constant load, but at heavier loads there is a tendency for the friction force to decline during the load stage, with a corresponding slight fall in the temperature of both surfaces after the initial rapid increase. With the coated samples running-in can produce surfaces of a polished appearance, but the principal mechanism for scuffing for these relatively rough surfaces nevertheless corresponded to side leakage of the lubricant from valley features at the edge of the contact where transverse pressure gradients are high.

In the case of Me-DLC coating applied to superfinished samples the performance is remarkable as no scuffing occurred under any of the conditions of load and speed investigated. No run-in was observed and the mean bulk temperatures of the disks were very low, indicating low friction as shown in Table 5.6 and Figures 5.15 (a) and (b). Ranking of the different configurations tested, in terms of scuffing load is shown in Figure 5.15 (c).

The general behaviour of these coated systems has been explained in terms of both chemical composition and structure, and from the contact mechanics point of view. It has been reported by a number of authors (Wang *et al.* (1992), Zaidi *et al.* (2000) that hydrogen plays a key role in the physical properties of DLC coatings. Wänstrand *et*

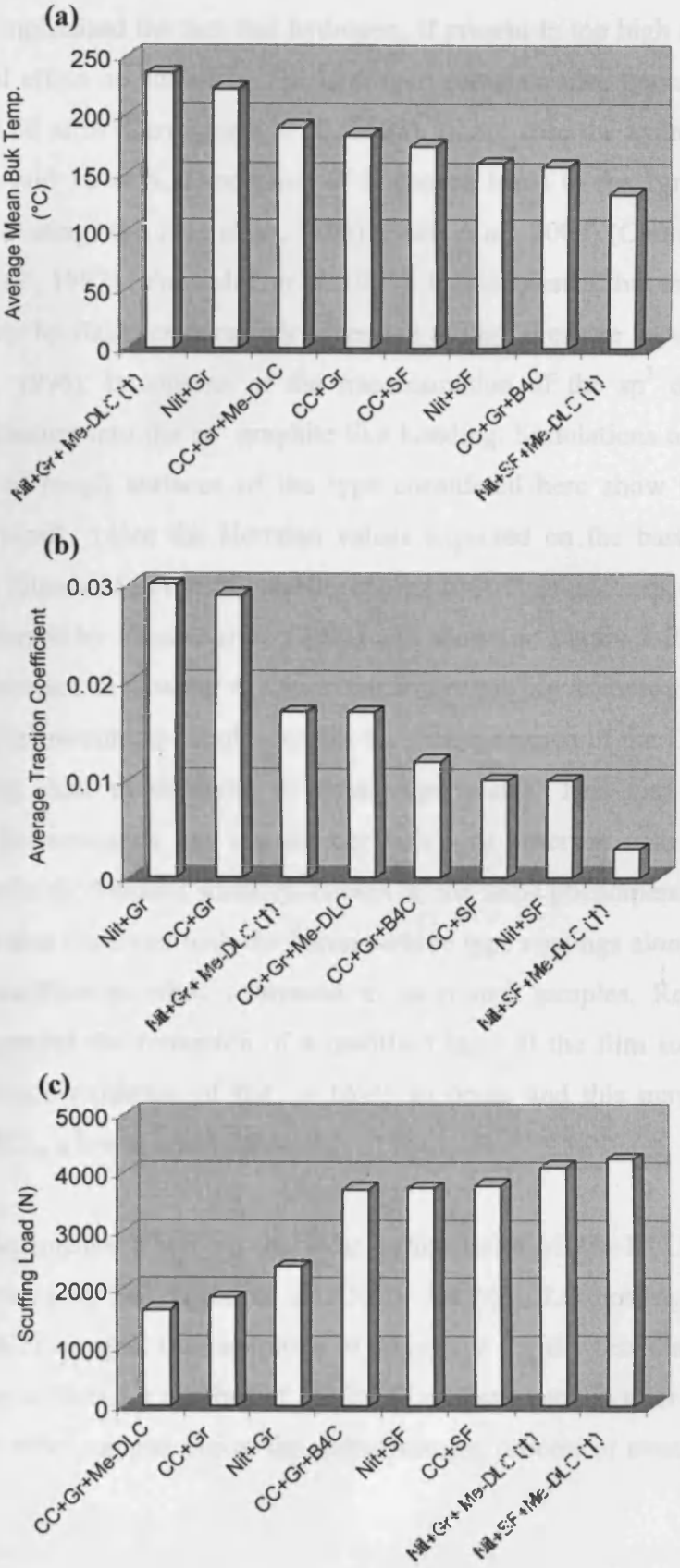

Figure 5.15: **Comparison of performance between the different configurations for tests performed at 16 m/s sliding speed. Uncoated configurations added for comparison. (a) average mean bulk temperature at scuffing load; (b) average traction coefficient at scuffing load; (c) scuffing load.**

al. (1999) also emphasised the fact that hydrogen, if present in too high a proportion, has a detrimental effect on adhesion. The hydrogen content varies typically between 10 at.% to about 50 at.% (Cermignani *et al.*, 1998). In our case the hydrogen content was between 12 and 16 at.%. Desorption of hydrogen leads to the "graphitisation" process of DLC coatings (Le Huu *et al.*, 1996) (Zaidi *et al.*, 2000) (Cermignani *et al.*, 1998) (Harris *et al.*, 1997) (Voevodin, *et al.* 1999). It is suggested that this is induced in sliding contacts by flash temperatures generated at high pressure asperity contacts (Le Huu *et al.*, 1996). It consists of the transformation of the sp^3 diamond like bonding of the coating into the sp^2 graphite like bonding. Simulations of the contact and lubrication of rough surfaces of the type considered here show that asperity pressures are typically twice the Hertzian values expected on the basis of smooth surfaces. This is illustrated in recent time-dependent contact simulations of real rough surfaces as developed by Elcoate *et al.* (2001) and shown in Figure 5.16; this aspect being further discussed in Chapter 6. Graphitisation occurring at these high-pressure peaks of sliding micro-contacts could explain the disappearance of the DLC coatings from the running track as observed in these experiments. This may also be the explanation for the extremely low traction coefficient as observed with both ground coated and superfinished coated surfaces. However, the same phenomenon of coating disappearance is also observed with the boron carbide type coatings along with much lower traction coefficients when compared to as-ground samples. Reigada *et al.* (2000) have suggested the formation of a modified layer at the film surface due to local heating. Hence oxidation of B_4C is likely to occur and this may induce the formation of H_3BO_3, a low friction material.

Oxygen has a detrimental effect on the wear performance of Me-DLC coatings as clearly demonstrated by Bewilogua *et al.* (2000) for Me-DLC coatings containing more than 5 at.% of oxygen. Concentration of oxygen is usually less than this figure but Bewilogua *et al.* found a number of Me-DLC coatings used in their experiments incorporating far more oxygen due to the manufacturing process or even exposure to air.

(a)

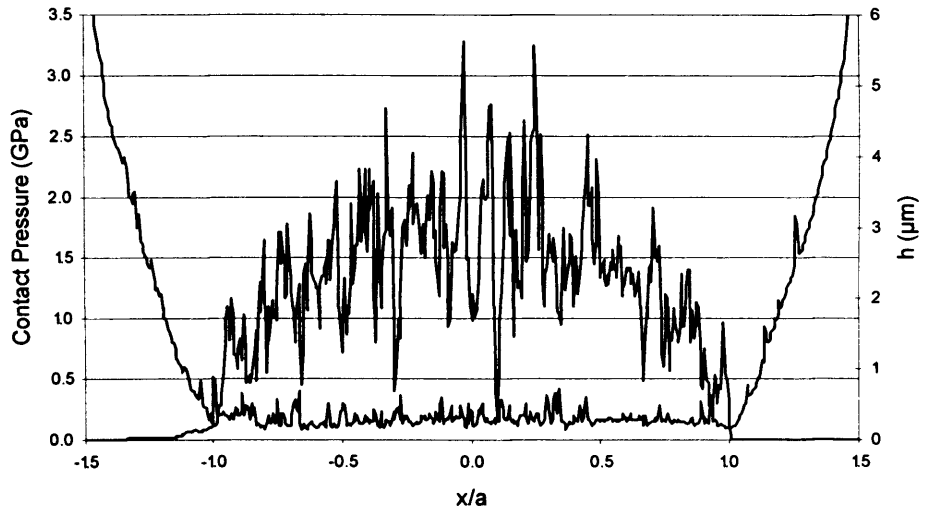

(b)

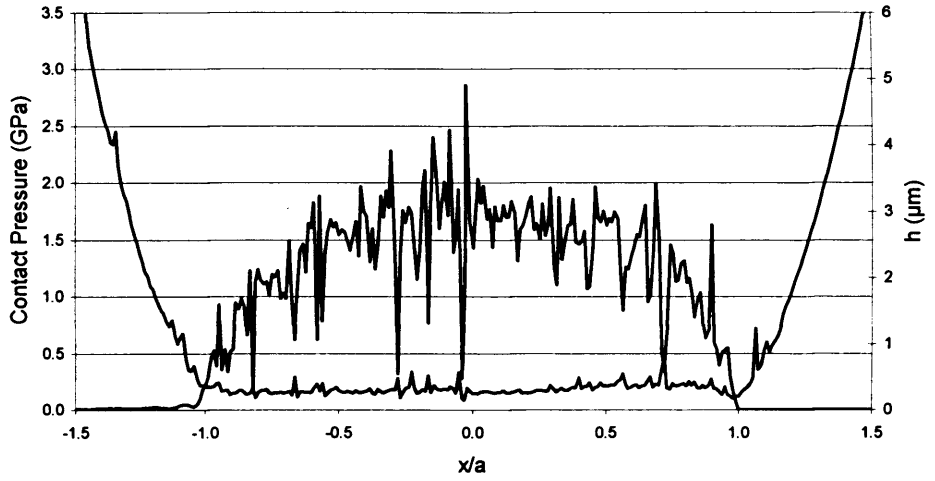

(c)

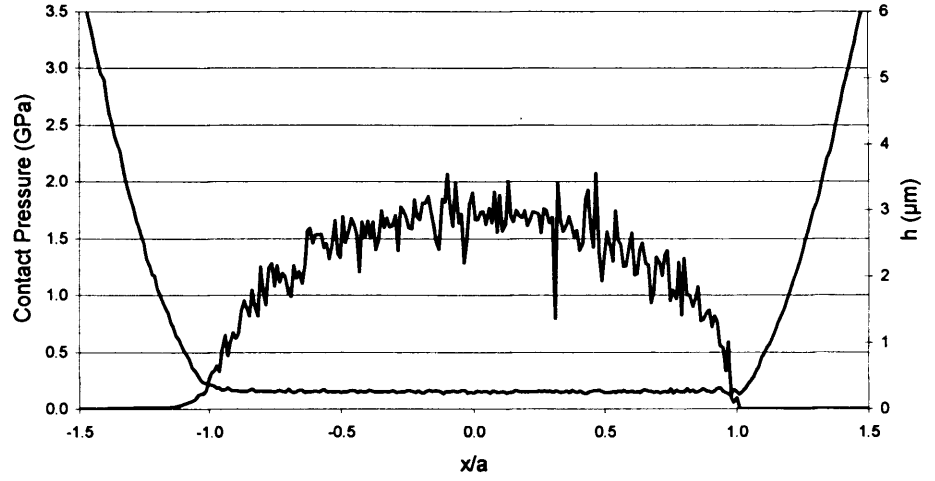

Figure 5.16: **Time dependent elastohydrodynamic lubrication simulation of real rough surfaces as tested at 16 m/s sliding speed with a Me-DLC coating (only one time step is shown). The nominal Hertzian contact pressure at scuffing was 1.7 GPa for each configuration. (a) case carburised ground; (b) nitrided ground; (c) nitrided superfinished. For all configurations, roughness profiles as used in the solver were taken after tests from an un-scuffed part of the running track very close to the scuffing trace.**

Table 5.6

Comparison of average scuffing performance of different coating/substrate combinations.

Configuration	Average Mean Bulk Temperature of Discs (°C)	Average Traction Coefficient	Average Scuffing Load (N)
Case Carburised + Ground	184	0.029	1850
Case Carburised + Superfinished	174	0.010	3801
Nitrided + Ground	223	0.031	2387
Nitrided + Ground + Me-DLC	236†	0.017†	4100†
Case Carburised + Ground + Me-DLC	190	0.017	1648
Case Carburised + Ground + Boron Carbide	157	0.012	3732
Nitrided + Superfinished	159	0.010	3746
Nitrided + Superfinished + Me-DLC	133†	0.003†	4251†

Mean bulk temperature, traction coefficient and scuffing loads for various test configurations run at 16 m/s sliding speed. Temperatures and traction coefficients were measured to prior to scuffing. Results from un-coated superfinished case carburised and nitrided samples, from another experimental programme, are included for comparison purposes.

†: no scuffing occurred; the loads correspond to the average maximum testing load. Temperatures and traction coefficient measured at maximum testing load

From the contact mechanics point of view, taking into account the elements presented in 5.4, one may consider as presented by Oliviera, the critical load to initiate fracture *in* the coating and the critical load to initiate delamination *at* the interface. With the very small *h/a* ratios as found in the present tests and the elastic mismatch parameters as illustrated in Table 5.7 (which recalls elements from Table 5.1), it can be concluded from the Oliviera study that the Me-DLC coated system requires very low energy to both initiate fracture in the coating or delamination at the interface.

This could in part explain the poor behaviour observed during the tests showing clear signs of coating flaking and/or delamination. On the other hand, the Boron Carbide coating system, which has a much lower elastic mismatch, would perform more effectively on this basis.

Table 5.7

Coating parameters as indicated in Oliviera *et al.* [1] and Plumet *et al.* [2] for the coatings being tested in this work

Coating	E_1/E_2 from [2]	$e_1/\sqrt{A_0}$ from [2]	h/a from [1]	α from [1]
Me-DLC	0.6	0.0172	0.006	−0.3
Boron Carbide	0.9	0.0155	0.005	−0.1

E_1: coating elastic modulus E_2: substrate elastic modulus
$e_1 = h$: coating thickness
A_0: uncoated contact area size at scuffing (average of all tests)
a: point contact half width at scuffing (average of all tests)
α: elastic mismatch

With the coating configurations as used in this experimental programme and the contact conditions (typically Hertz contact semi-dimensions calculated for the maximum testing load) assessed using the approach presented by Sharif *et al.*, (2000), the ratio between coating thickness and semi contact width (or square root of the contact area size as used by Plumet *et al.*) is very small. This would suggest that the coating has a negligible influence on the maximum contact pressure and the contact area compared to the uncoated configuration ($e_1/\sqrt{A_0} < 0.05$).

Overall the problem of mismatch of elastic properties would indicate a significant functional difference between the two coatings considered here and may explain the superior adherence of the boron carbide coating compared to the Me-DLC type.

The most outstanding scuffing performance obtained was with the nitrided sample coated with Me-DLC. The adherence of the coating was good, and scuffing could not be provoked even at the highest loading available. The elastic properties of the substrate are assumed to be close to those of the case-carburised samples so the elastic mismatch would be expected to be similar. The hardness mismatch between substrate and coating was less, however, due to the higher hardness achieved in the nitriding process. Holmberg *et al.* (1998) emphasise the advantage of having a substrate as hard as possible to avoid fracture of the brittle coating due to plastic deformation of the substrate.

As was seen in earlier work on uncoated discs surface roughness is of great importance in relation to scuffing. Jiang and Arnell (2000) have studied the effect of substrate roughness on DLC coatings and consider a critical maximum contact pressure that triggers the onset of a wear mode characterised by crack formation and

flaking. The suggested critical contact pressure is about 3.7 GPa for the DLC coatings studied. In the case carburised DLC coated samples as considered in this study levels of contact pressure as found in the contact simulations were very similar to this threshold value when scuffing occurred as shown on Figure 5.16(a). This critical pressure (and corresponding load) could indeed explain the scuffing limit for this configuration as shown in Figure 5.5 where the scuffing load was almost constant over a range of sliding speeds.

CHAPTER 6.

Micro-Elastohydrodynamic analysis of the test samples

6.1 Introduction

In order to complete the experimental programme and obtain some further insight into the behaviour of the contacts under investigation it was decided to carry out a micro-elastohydrodynamic numerical analysis of the different cases that were tested. The two important parameters obtained from this numerical analysis which give a key insight into the "quality" of the contact are as follows. On the one hand there is the time dependent lubricant film thickness separating the two surfaces in contact. The propensity for these profiles to exhibit or not a fully developed elastohydrodynamic film should allow the correlation of the behaviour of these profiles with their elastohydrodynamic response as investigated with this numerical analysis programme and as suggested for example by Martin *et al.* (2001). The second parameter is the time dependent contact pressure generated by the real roughness profiles being tested and used in the solver. This latter information can be considered as crucial when considering the behaviour of coated configurations as suggested by Jiang *et al.* (2000). In the same way the tendency to micropitting can be advantageously investigated using detailed contact pressure analysis at asperity the level by taking into account asperity pressure cycling as suggested by Tao *et al.* (2003).

6.2 The EHL numerical solver for line contacts of real rough surfaces

6.2.1 Introduction

Real gear surfaces operating under industrial conditions of load, speed and oil viscosity are considered as operating under mixed lubrication conditions. This condition can be summarised as occurring when the roughness features are far greater in height than the predicted EHL film thickness, the magnitude of which may be calculated using the classical formula of Dowson and Higginson. As a result, it can be

anticipated that a large degree of interaction between asperities of the two surfaces, and in some instances some solid contacting, is likely to occur. Due to the fact that the problem concerns basically two rough surfaces moving relative to their instantaneous contact, there is a need to treat the problem as a time dependent one. In addition the high shear rate imposed on the lubricant separating micro-asperities results in a largely non-Newtonian behaviour as observed for example by Evans *et al.* (1986).

The solver used for this work includes both the time-dependent treatment as well as the non-Newtonian behaviour. This model was developed by Elcoate *et al.* (2001) in the first instance and has been refined since by others, and is based on a theoretical model for line contacts as found in spur gears. The key feature of this solver is that it allows solving the elastic and hydrodynamic film thickness simultaneously making use of a consistent mass-conserving fully coupled method. It allows analysis of conditions with extremely low lambda ratio values as well as solid contact situations. The solver has also predicted micro-cavitation taking place under severe conditions of thin films and high roughness.

6.2.2 Problem formulation

The EHL solver takes into account two fundamental relationships. The first one corresponds to the Reynolds equation for the lubricant relating its pressure to the film thickness. The second relationship deals with the elastic deflection of the rough surfaces caused by the action of the pressurised lubricant. The Reynolds equation can be expressed as follows:

$$\frac{\partial(\rho h)}{\partial t}+\frac{U_1+U_2}{2}\frac{\partial(\rho h)}{\partial x}-\frac{\partial}{\partial x}\left(\frac{\rho h^3}{12\eta}S\frac{\partial p}{\partial x}\right)=0 \qquad (6.1)$$

The S is the non-Newtonian factor which depends on pressure, film thickness, sliding speed and pressure gradient. Considering shear thinning using the Eyring model, the S factor is available in closed form taken from Conry et al. (1986) as follows:

$$S=\frac{3(\Sigma\cosh\Sigma-\sinh\Sigma)}{\Sigma^3}\sqrt{1+\frac{\eta^2(U_2-U_1)^2}{\tau_0^2h^2}\frac{\Sigma^2}{\sinh^2\Sigma}} \qquad (6.2)$$

Where $$\Sigma=\frac{h}{2\tau_0}\frac{dp}{dx}$$

The dependence of the viscosity of the lubricant on pressure is taken into account using the well–known Roelands formula:

$$\eta = \eta_0 e^{(\log \eta_0 + 9.67)(1+5.1\times10^{-9}p)^Z - 1)} \tag{6.3}$$

In the same way the dependence of the lubricant density on pressure is given using the Dowson and Higginson formula:

$$\rho = \rho(p) = \rho_0 \left(\frac{1+\gamma p}{1+\lambda p} \right) \tag{6.4}$$

There is no account in the model of variation of viscosity with temperature and the viscosity is taken at conditions that prevail at the inlet and outlet of the contact i.e. 100 °C. This assumption can be questioned when considering the temperatures reached close to the contact when scuffing occurred. This simplification could lead in terms to an overestimation of the lubricant film thickness. Nonetheless, viscosity does not depend much on temperature at high temperature.

Considering the elastic equation, it can be expressed in its discretised form as follows:

$$\frac{\partial^2 h(x_j)}{\partial x^2} = \sum_{all\ k} f_{k-j} p_k + \frac{1}{R} + \frac{\partial^2 \Phi}{\partial x^2} \tag{6.5}$$

Using this differential form for the elastic deflection, it is possible to solve Eqs. (6.1) and (6.5) simultaneously as described by Elcoate *et al.* (2001). Such an approach is possible due to the rapid decay of the influence coefficients f_i as the index i increases from zero as described by Evans *et al.* (2000) in comparison with the more conventional approach using influence coefficients derived from the conventional integral equation. Numerically, the discretisation process itself is done differently for Eq. (6.1) and for Eq. (6.5). Hence Eq. (6.1), is discretised using second order finite elements and Eq. (6.5) is discretised using a central finite difference scheme. In their discretised forms, the equations are then expressed as an overall matrix problem with h and p being the unknown quantities at each node of the computing mesh. The whole problem, thanks to the rapid decay of the f_i coefficients, becomes of narrow banded form allowing the variables to be solved simultaneously.

As described earlier, the typical lubrication regime may induce solid contacting. In this case the scheme chosen to deal with this particular issue can be summarised as follows. For example, if in a particular timestep a converged result is obtained with a negative calculated film thickness, then the most negative film thickness is set to zero. The hydrodynamic equation corresponding to this nodal point is deleted from the problem matrix, but the elastic deflection equation is retained. In this way the film

thickness value of zero is a boundary condition for the elastic deflection equation which ensures that the pressure distribution obtained remains entirely consistent with the film shape. The pressure developed in the coupled solution at the contacting node is then an automatic boundary condition for the hydrodynamic equation on both sides of the contacting node. The timestep is then recalculated. This procedure is repeated for the timestep, adding no more than one contact point per timestep recalculation, until a converged result with no negative calculated film thicknesses is obtained.

Another feature which results from the numerical analysis, and mentioned earlier, is the phenomena of micro-cavitation which corresponds to cavitation at the asperity level. This situation occurs when a full film solution is not obtained at each node point and is described as "in-contact cavitation". It is well known that in elastohydrodynamic lubrication cavitation takes place at the exit of a contact, where the calculated pressure falls to sub-ambient values. Situations occur in rough-surface EHL contacts where composite valley features are increasing in volume with time. If flow into such a feature from the micro contacts at either side is insufficient, then the pressure in the composite valley feature will fall. If this effect is sufficiently strong then the oil "trapped" in the composite valley can become entirely decompressed, returning progressively to ambient pressure. If the calculated pressure becomes negative then the lubricant is regarded as cavitated. A post-processing marker indicates that such a situation has occurred during the solution procedure.

6.2.3 Description and structure of the solver

In this section we describe the key stages included into the solver to achieve a converged solution in terms film thickness and pressure. The whole process is presented using a flow chart as illustrated in Figure 6.1. The analysis begins by reading the input data in terms of geometry of the surfaces in contact, load and lubricant characteristics. The roughness profile itself is entered in the form of a data file generated directly from a filtered profile obtained from the profilometer. This file includes a series of "z-altitudes" spaced at a regular interval (usually 0.25 μm). The initiation of the problem also consists of producing an interpolation through these z-points using second order splines. This is to obtain continuity of the second derivative which is necessary in the numerical treatment. Part of the initiation process is also to solve the smooth steady state problem using a Hertzian pressure distribution serving as an initial boundary condition for the solver. The second stage is the transient stage

of the process that consists of updating ("moving") the roughness profile as a function of time. In the third stage the solver computes the transient right hand side of the Reynolds equation i.e. the term $\frac{\partial(\rho h)}{\partial t}$ (the "squeeze term"). In the fourth stage the solver establishes the contribution to the elastic equation of pressure far away from the discretisation node of interest. Next (step 5) comes the introduction of the boundary conditions. Following these preliminary stages the calculation matrix can be set (step 6). Stage 7 consists of solving the matrix to give pressure and film thickness. If convergence is achieved then pressure and film thickness values are updated. If not then further iterations are performed.

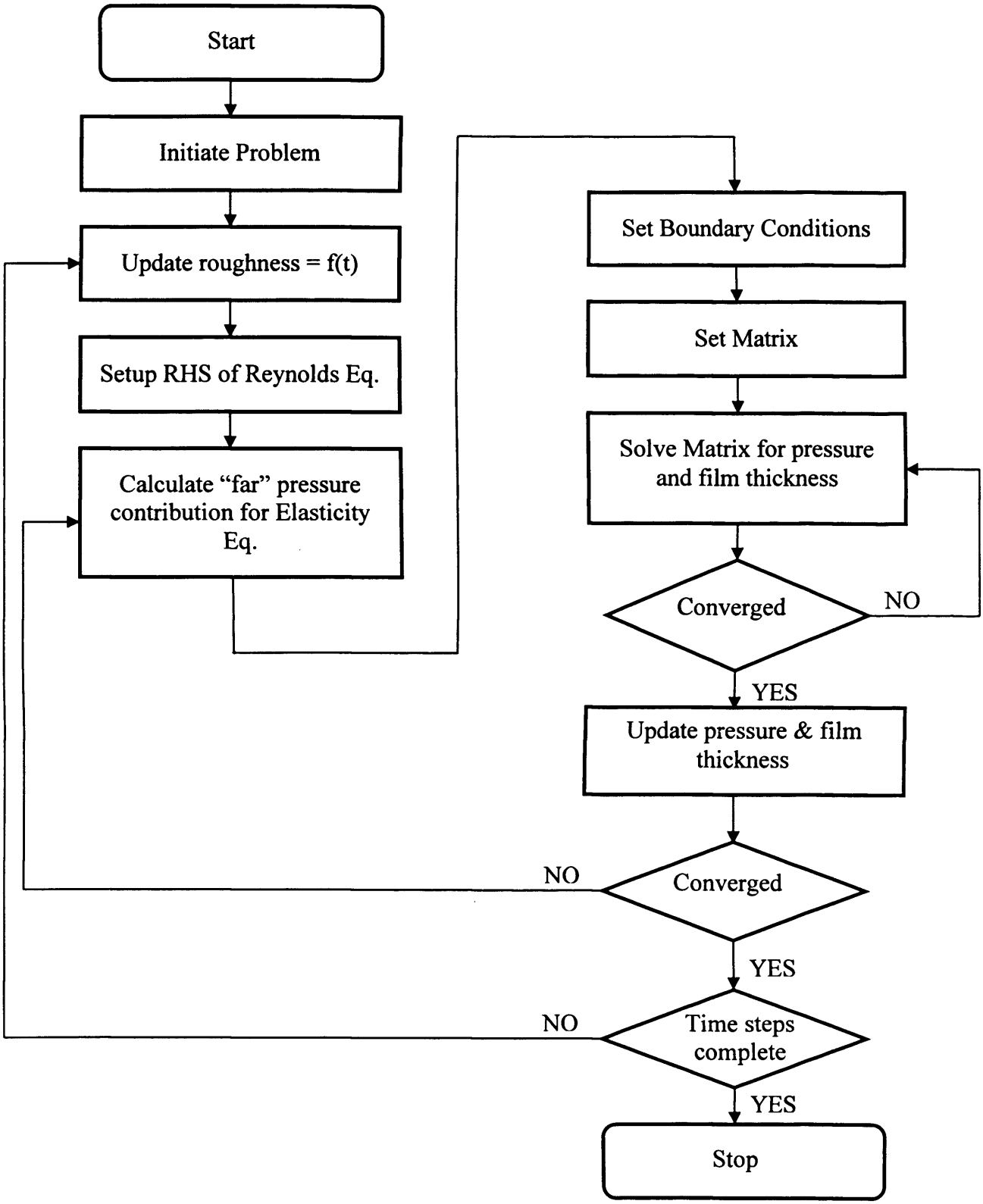

Figure 6.1: **Flow chart diagram detailing the key stages of the micro-EHL solver as used for this work**

6.2 Point contact treated as equivalent line contact

As detailed in Chapter 2, the geometry of the test samples is such that the contact is a point contact which becomes an elliptical shape under load. The dimensions of the corresponding Hertzian contact ellipse give an axis ratio of 3.91. It was noted by Holmes *et al.* (2003) that for an axis ratio of about 4 under different loading conditions, different slide-roll ratios, etc, the centre line of a point contact can be effectively treated as a line contact. The difference in terms of contact pressure and film thickness as outlined by Holmes is minimal except for extreme slide-roll ratios. The line contact assumption was therefore made in this programme of work. The line contact that was equivalent to the centre line of the elliptical contact occurring in the scuffing tests was determined as follows. The elliptical contact semi-dimension in the rolling direction (a) for the scuffing test was established and this dimension was also used in the line contact. The corresponding line loading was then calculated from the Hertzian relation:

$$w' = \frac{\pi E' a^2}{2R_x}$$

Where:

E' is the reduced elastic modulus

R_x is the principal radius of relative curvature in the entrainment direction.

The scuffing tests were performed with discs made of steel, the E' value was taken as 200 GPa and their radius in the rolling direction was 38.1 mm. Table 6.1 summarises the results of these calculations. Analyses were confined to tests carried out at 16 m/s since this was the most widely used test condition.

6.3 Roughness data conditioning for processing by the solver

The profilometer as described in Chapter 2 creates output files containing the spacing in the x-direction as well as all the z-coordinates describing the profile. The heading

Table 6.1

Calculation of linear load for the equivalent line contact for the various scuffing test results considered in the numerical analysis

Test n°	Scuffing Load / N	Calculated contact dimension "a" / mm	Equivalent linear load / N/m
2	1876	0.4188	0.82184E+06
12	2910	0.4848	0.11013E+07
14	4100	0.5435	0.13841E+07
17	1921	0.4221	0.83493E+06
19	1917	0.4218	0.83377E+06
37	4189	0.5474	0.14040E+07
41	4181	0.5470	0.14022E+07
46	4231	0.5492	0.14134E+07
48	4231	0.5457	0.13953E+07

of this file is presented in Figure 6.2(a). The corresponding profile obtained is a raw profile as illustrated in Figure 6.2(b) that includes features such as curvature and waviness. This surface profile needs to be filtered as discussed in Chapter 2 and needs to be formatted to be compatible with the input format that the solver uses. A small "Visual Fortran" routine was developed in order to perform the above-mentioned operations i.e. the filtering and the formatting. A copy of the Fortran source file is presented in Appendix A and consists of three basic parts: reading of the data, filtering, formatting and creation of the appropriate output file with data in the correct order. The formatting process consists of organising the data into a file with ".dat" extension with z-coordinates placed at a particular position in the file corresponding to a position already used in previous work and from where input files for the solver were developed. The filtering process itself requires specification of a cut-off value. Based on the recommendations of standards like BS EN ISO 4288:1998 Geometrical product specifications - Surface texture: profile method - Rules and procedures for assessment of surface texture, the cut-off used for the filtering of these profiles was 0.25 mm. This corresponds to the typical recommendation for ground surfaces. The routine establishes the mean line which is then deducted from the profile. Presented in Figure 6.3, are the filtered profiles as used for the simulation work after being

"filtered" using the software routine as developed for this work. For clarity reasons, filtered profiles are presented over a profile length of 1mm allowing the clear discrimination of the valley features. All profiles were acquired from test samples after test in a run-in area i.e. subjected to experimental conditions slightly offset from the scuffing scar. This is taken to represent the surface texture condition at the time of scuffing.

6.4 Results of simulation

6.4.1 Introduction

All the key configurations which were tested during the course of the experimental programme were included in the simulation work. The configurations considered for the simulation work are summarised in Table 6.2. As mentioned earlier, attention was given in selecting configurations that were all tested at 16 m/s sliding speed in order to allow for direct comparison.

Table 6.2

List of configurations considered for the numerical analysis (all tests performed at 16 m/s sliding speed)

Test n°	Configuration
2	Nitrided steel + Ground + Compound Layer
12	Ground + Nitrided steel
14	Nitrided steel + Ground + Me-DLC coating
17	Case Carburised steel + Ground (baseline)
19	Case Carburised steel + Ground + Me-DLC coating
37	Ground + Nitrided steel + Superfinishing
41	Case Carburised steel + Ground + B_4C coating
46	Ground + Nitrided steel + Superfinishing + Me-DLC coating
48	Ground + Nitrided steel + Superfinishing (alternative)

(a)

```
1 2
EN40BA 0.000000e+000 PRF
CX M 4.039300e+004 MM 1.000000e+000 D
CZ M 4.039300e+004 MM 1.600000e-005 L
EOR
STYLUS_RADIUS 0.000000e+000
MM
SPACING CX 2.500000e-004
MAP 1.000000e+000 CZ CZ 1.000000e+000 1.000000e+000
MAP 2.000000e+000 CZ CX 1.000000e+000 0.000000e+000
EOR
869
871
871
872
```

Roughness profile spacing along the x-direction (0.25 µm)

z-ordinate in µm

(b)

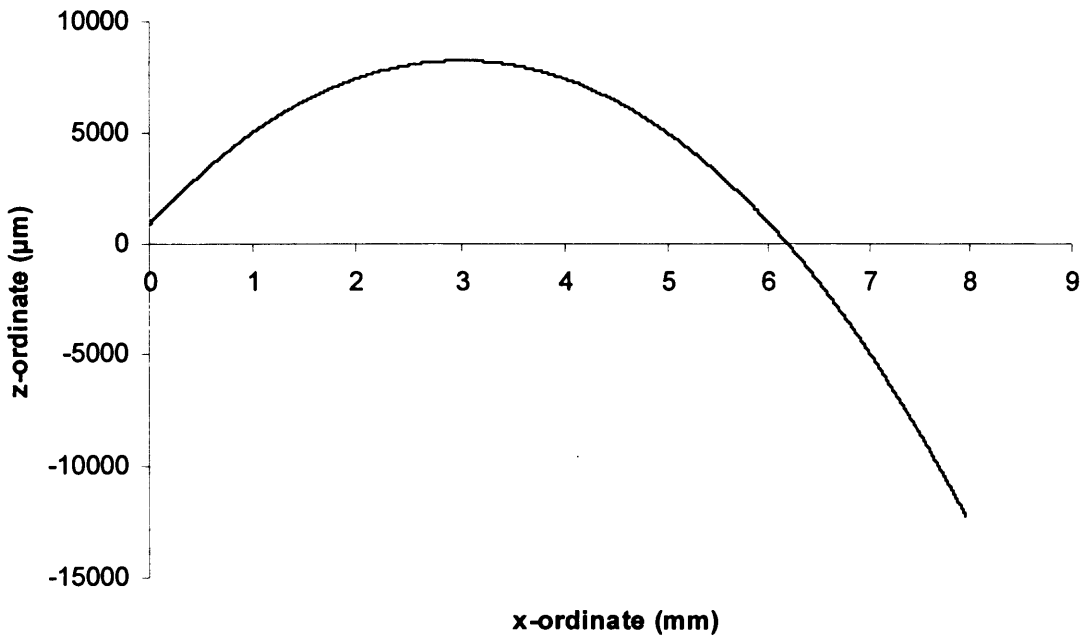

Figure 6.2: **(a) Heading of the raw profile exported file (*.prf) as obtained from the profilometer**
(b) Raw surface as imported from the profilometer software including form and waviness

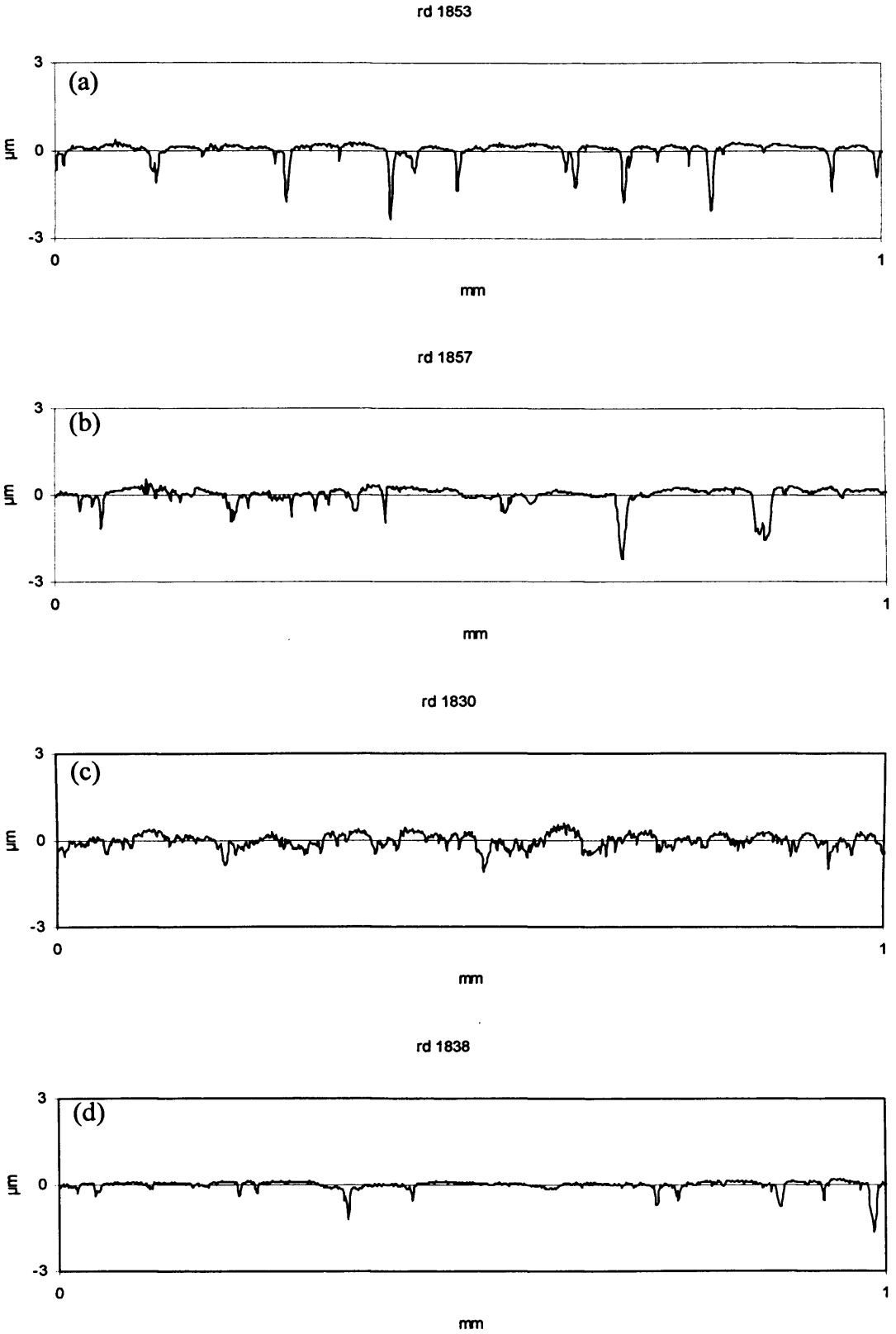

Figure 6.3 (a): Surface profiles as used for the simulation work

(a) Nitrided steel + Ground + Compound Layer on fast shaft

(b) Nitrided steel + Ground + Compound Layer on slow shaft

(c) Ground + Nitrided steel (both shafts)

(d) Nitrided steel + Ground + Me-DLC coating on fast shaft

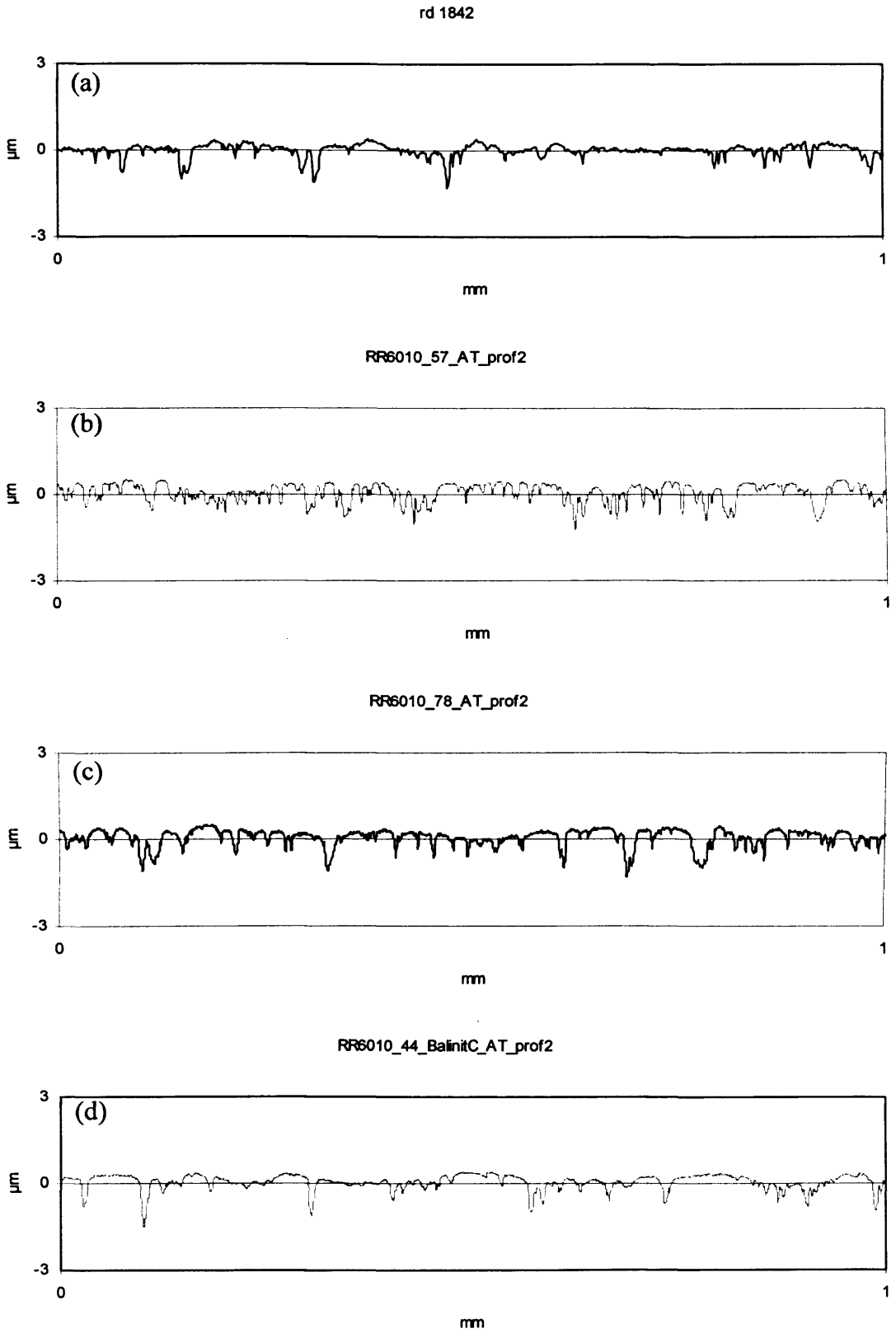

Figure 6.3 (b): Surface profiles as used for the simulation work

(a) Nitrided steel + Ground + Me-DLC coating on slow shaft
(b) Case Carburised steel + Ground (baseline) on fast shaft
(c) Case Carburised steel + Ground (baseline) on slow shaft
(d) Case Carburised steel + Ground + Me-DLC on fast shaft

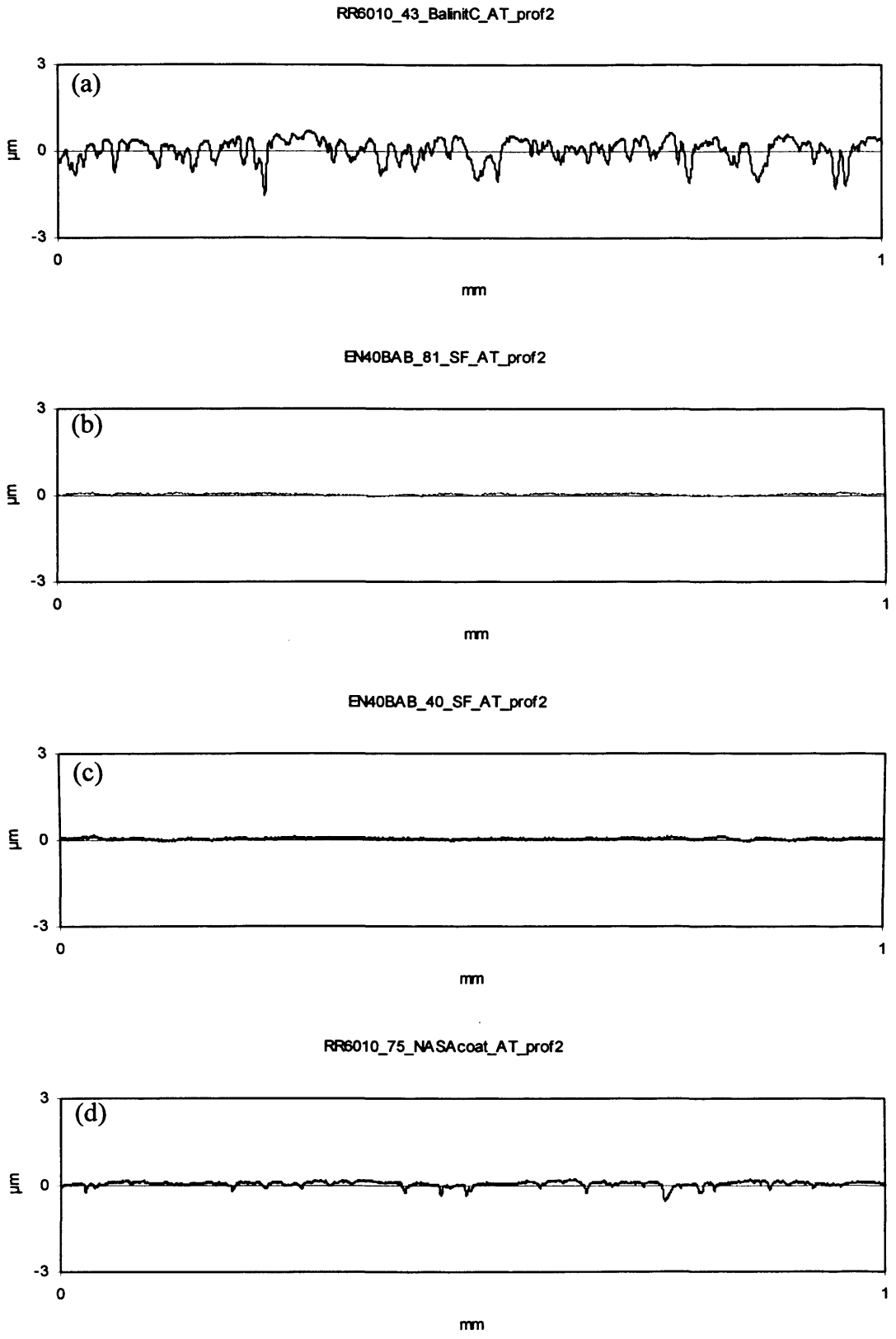

Figure 6.3 (c): Surface profiles as used for the simulation work

(a) Case Carburised steel + Ground + Me-DLC on slow shaft

(b) Ground + Nitrided steel + Superfinishing on fast shaft

(c) Ground + Nitrided steel + Superfinishing on slow shaft

(d) Case Carburised steel + Ground + B_4C coating on fast shaft

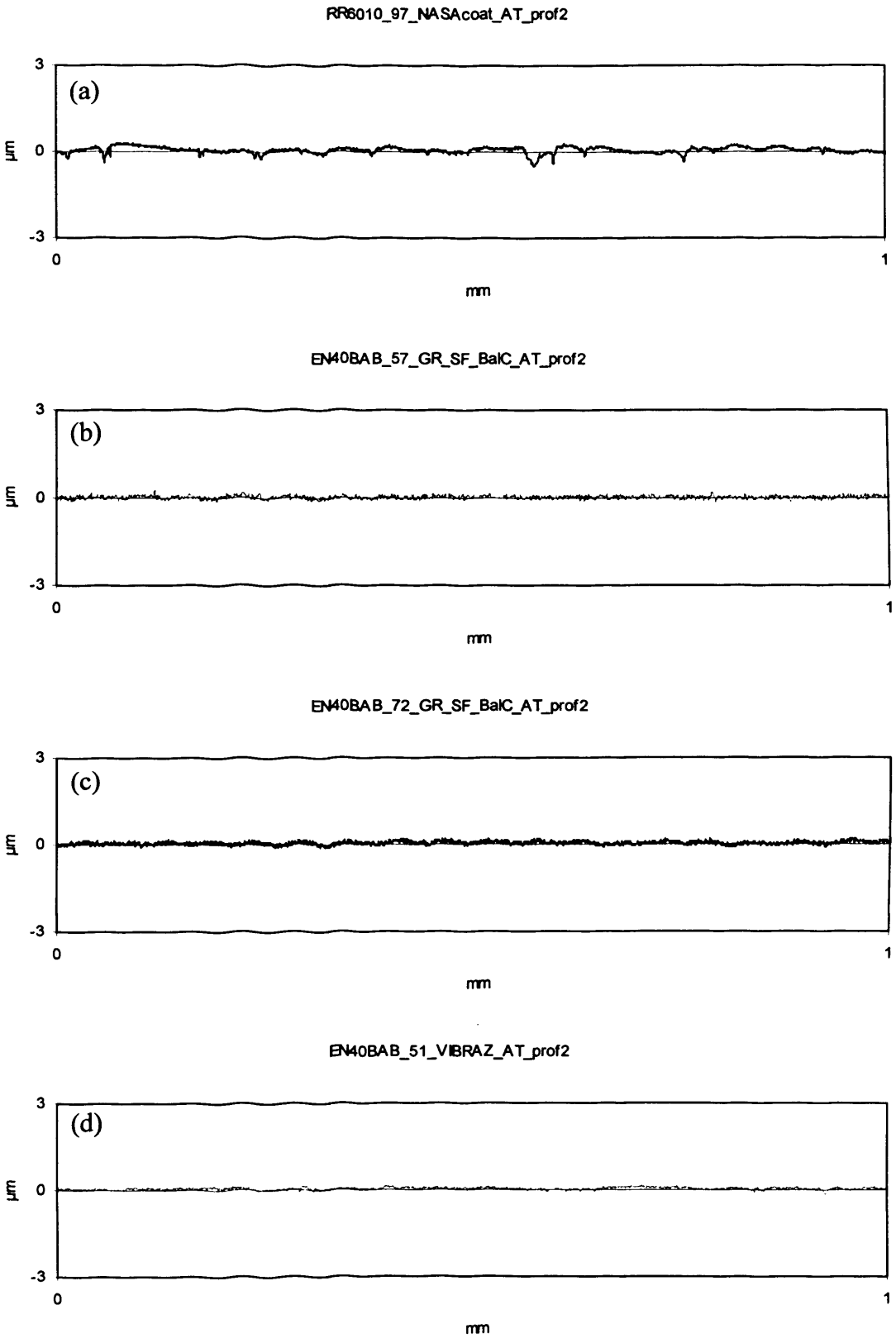

Figure 6.3 (d): Surface profiles as used for the simulation work

(a) Case Carburised steel + Ground + B_4C on slow shaft

(b) Ground + Nitrided steel + SF + Me-DLC on fast shaft

(c) Ground + Nitrided steel + SF + Me-DLC on slow shaft

(d) Ground + Nitrided steel + SF (alternative) on fast shaft

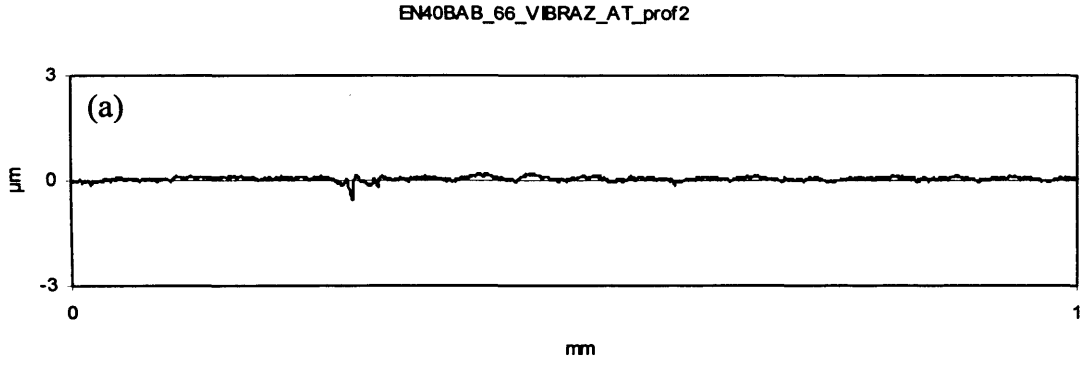

Figure 6.3 (e): Surface profiles as used for the simulation work
(a) Ground + Nitrided steel + SF (alternative) on slow shaft

The profiles that were used in the simulation work are listed in Table 6.3 and their graphical representation is shown as already mentioned, in Figure 6.3. Usually three surface profiles were acquired after test for each of the test samples, and by convention the second one was the one chosen for investigation. As tests were run using two contacting discs running at different speeds, surface profiles were taken from what described as the "fast shaft" (surface velocity = 20 m/s) and from the "slow shaft" (surface velocity = 4 m/s). This corresponds to a slide-roll ratio, as defined in Chapter 2, of 1.23. For the first profiles, "rd" denotes roughness data. For the rest acquired under the "Windows" based environment, RR6010 denotes the type of case carburised steel as used by the Rolls Royce Company. EN40BAB denotes the type of nitrided steel used from the first nitriding batch and the second machining batch. GR denotes a ground surface. SF stands for superfinished. "Balinit C" corresponds to the commercial name of the Me-DLC coating. "NASA coat" corresponds to the B_4C coating as supplied by NASA for this work. VIBRAZ corresponds to the alternative superfinishing treatment tested in this work. PROF2 denotes in all cases the second profile acquired from the samples.

Table 6.3

Test sample surface profile reference used for the simulation work

Test n°	Fast Shaft	Slow shaft
2	rd1853	rd1857
12	rd1830	rd1830*
14	rd1838	rd1842
17	RR6010_57_PROF2	RR6010_78_PROF2
19	RR6010_44_BalinitC_PROF2	RR6010_43_BalinitC_PROF2
37	EN40BAB_81_SF_PROF2	EN40BAB_40_SF_PROF2
41	RR6010_75_NASAcoat_prof2	RR6010_97_NASAcoat_prof2
46	EN40BAB_57_GR_SF_BalC_PROF2	EN40BAB_72_GR_SF_BalC_PROF2
48	EN40BAB_51_VIBRAZ_PROF2	EN40BAB_66_VIBRAZ_PROF2

* same as fast shaft as no other profile was acquired

Results from the simulation work give the time dependent pressure and film thickness over the whole contact length but extend well before and after it. Hence, in terms of the Hertzian contact dimension "a", results extend from $-3\,a$ to $1.5\,a$. In the results shown here, for example in Figure 6.4, results are restricted to the range

$-1.5\,a$ to $1.5\,a$. The inlet area of the contact is to the left hand side of the graph and the outlet of the contact corresponds to the right hand side of the graph. Included in figures of this type are the two "real" surfaces in their relative positions at a particular time step. Unfortunately, only a small number of key time steps can be represented. This corresponds to a very partial representation as the behaviour of the rough surfaces. The real behaviour can most easily be appreciated by constructing an animated sequence of film and pressure distributions as the time steps progress. Key time steps are shown in Figures 6.4 to 6.12 covering all tested configurations. Each figure shows the smooth case result. This is an essential step as it verifies that the solution is basically consistent with the given operating conditions. The second part of the figure shows the rough surfaces in contact at a particular time step. For clarity reasons the surfaces have been shown offset by 3μm in the vertical direction. Note that the scales of the graphs (horizontal and vertical) have been chosen to be identical for all representations to allow for direct comparisons. This carries the disadvantage though of stretching the curves particularly along the horizontal direction while minimising certain effects (like typical EHL outlet effects). The pressure scale is located to the left hand side of the graph and film and surface deflection scale is located to the right hand side of the graph. h represents the film thickness through the contact area and h_1 and h_2 represent the deformed "fast" and "slow" surfaces, respectively.

6.4.2 Simulation results for ground case carburised samples

Simulation results obtained for the ground case-carburised samples are presented in Figure 6.4(1). This configuration may be regarded as the baseline reference for comparison with other cases. The smooth case in Figure 6.4(1) (a) includes all the key features of an EHL contact as described by Dowson and Higgingson (1966). The overall shape of the bounding solids is similar to that produced by a dry contact. The lubricating film separating the two surfaces within the contact area is very close to parallel with a local constriction towards the outlet region. The pressure distribution is close to the Hertzian modified by a gradual build up of pressure in the inlet region and a pronounced pressure spike at the end of the Hertzian contact zone (outlet). Both constriction and pressure spike are close to the exit of the contact ($x/a \approx 1$) but are hardly noticeable on the graph due to the scale used. In the case of the ground case

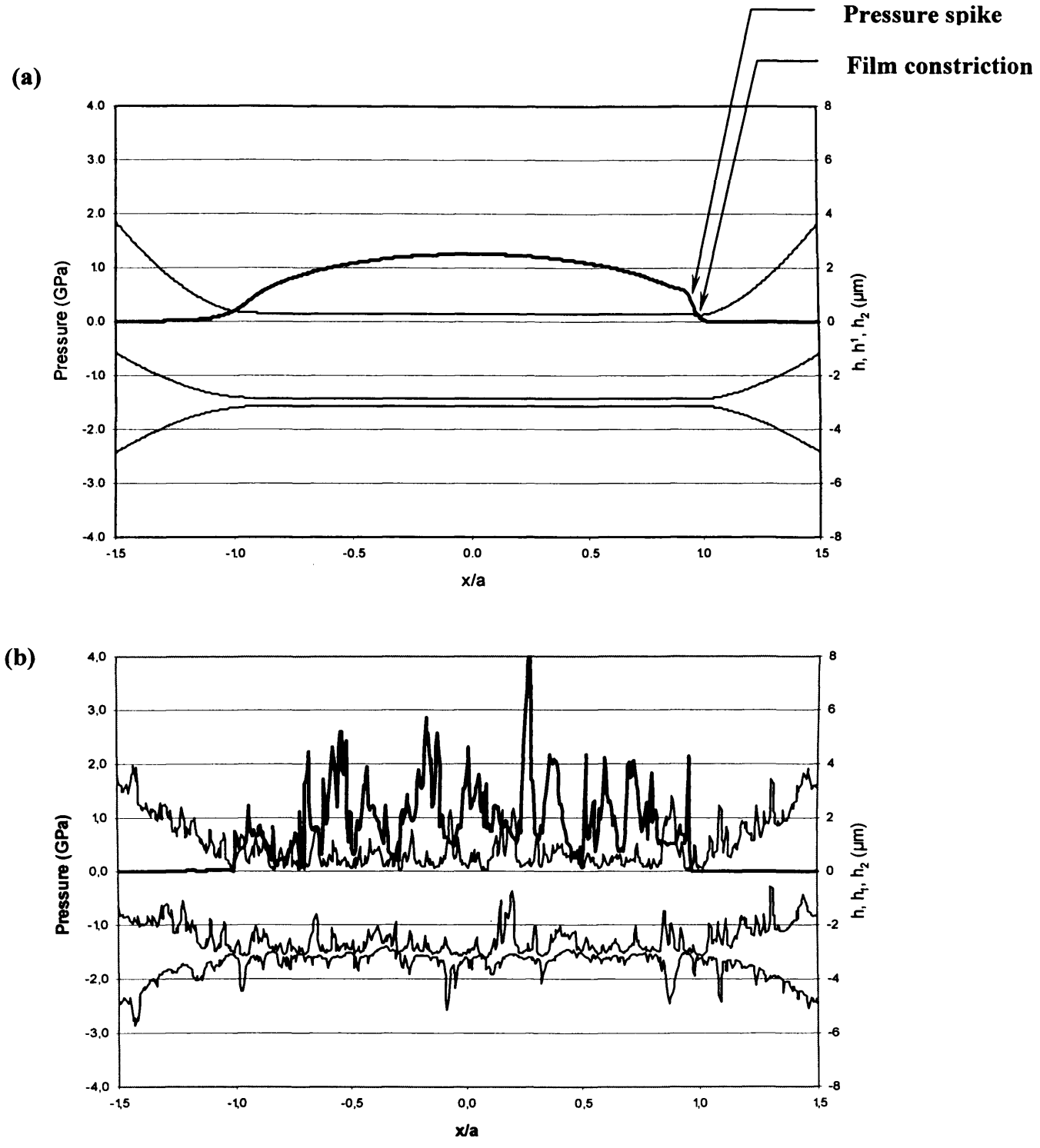

Figure 6.4(1): Simulation results of the baseline ground case carburised samples run at a sliding speed of 16 m/s
(a) The smooth case
(b) The two rough surfaces in contact
Pressure shown in bold

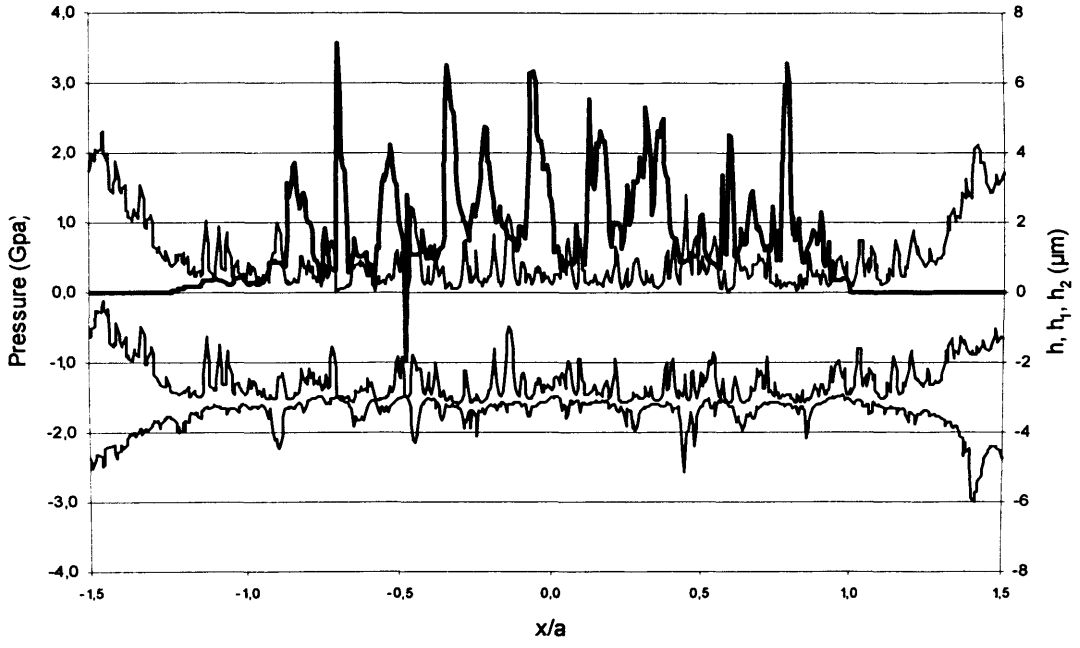

Figure 6.4(2): Simulation results of the baseline ground case carburised samples run at a sliding speed of 16 m/s showing the occurrence of micro-cavitation in the conjunction located at x/a = -0.475
Pressure shown in bold

carburised steel, the maximum pressure is found to be 1.25 GPa which is consistent with the imposed load. The minimum film thickness is h_{min} = 0.249 μm and the central film thickness is h_{cen} = 0.285 μm. Both values are consistent with classical EHL theory. One noticeable feature in this instance, is the central film thickness being about a third smaller than the actual roughness level (Ra = 0.4μm). This confirms that surface roughness effects will be of importance.

The simulation results of the two rough surfaces in contact are shown in Figure 6.4(1) (b). The time step shown is that at which the maximum pressure peak occurred during the whole simulation. The pressure distribution departs very significantly from the "smooth" case with a number of pressure peaks well above the maximum Hertzian pressure. The maximum pressure encountered (for the tested surface) was of the order of 4.2 GPa i.e. nearly 3.5 times higher than the maximum Hertzian pressure. The area of maximum pressure located near the centre of the contact corresponds to an instant where the facing surfaces produce a very small effective bearing area ($x/a \approx 0.05$). This is the case for most of the pressure peaks illustrated in Figure 6.4(1) (b). The surrounding areas where pressure peaks are found include a number of roughness valleys which are noticeably pressurised. This is the case for example in the two facing valleys located between $x/a = 0.3$ and $x/a = 0.4$. This effect has already been reported by Elcoate *et al.* (2001) who indicated the way in which valley pressures can contribute to load bearing. The ground case carburised configuration includes occurrences of metal to metal contact. These are found where the h value is down to zero. Such "dry" contacts are particularly detrimental to the surfaces in contact as the level of friction encountered locally will be intense. As a result of the high local temperatures generated tempering may occur even if actual scuffing is avoided. A count over the time steps considered for the analysis indicates 23 occurrence of metal to metal contact. This very crude measure of surface interaction cannot be considered as an absolute criterion but is seen as useful when making comparisons with other configurations. In addition to the effect of high local friction on temperature there is also the detrimental effect on local subsurface shear stresses.

Figure 6.4(2) shows results for a time step at which micro-cavitation occurs as explained in 6.2.2. At the chosen time step the pressure becomes negative at x/a =0.475 as the roughness feature conjunction tends to create at that particular instant a cavity which becomes depressurised. This effect could possibly also be detrimental to

the surfaces when considering the well-known effects of cavitation in other engineering applications such as high pressure pumps.

6.4.3 Simulation results for ground nitrided samples

The simulation results shown in Figure 6.5 (a) and (b) correspond to the nitrided samples which were finish-ground before heat treatment resulting in the compound layer being left on. The smooth case is almost identical to that of the ground case carburised configuration as the scuffing load was the same. The maximum Hertzian pressure obtained is 1.25 GPa, the minimum film thickness is 0.249 μm and the central film thickness is 0.285 μm. In this case the ratio between the smooth-surface film thickness and the typical roughness dimension is even more severe as the average roughness (Ra) of these soft-ground samples was of the order of 1μm.

The results of the simulation of the two rough surfaces in contact are shown in Figure 6.5 (b). As before the time step shown corresponds to the highest pressure peak encountered during the simulation. In this case the peak pressure was 3.1 GPa compared to 1.25 GPa in the reference case. This pressure peak also occurs in a similar area of the contact. Of note are the large numbers of narrow valleys creating a similar number of pressure ripples. Unfortunately with this configuration there are a number of features due to numerical effects. The results show a large number of negative film thicknesses that do not have physical significance. It is suggested that the model reached its limits in terms of its ability to deal with severe thin film conditions. In this case we can anticipate a large number of metal to metal contacts. The fact that this configuration equalled the scuffing performance of the baseline samples in spite of the higher roughness may possibly be attributed to a better friction behaviour as discussed in Chapter 4.

In the second configuration involving nitrided surfaces the samples were finish-ground after nitriding which is the usual aerospace practice. In this case the roughness was similar to that of the baseline samples (Ra = 0.4 μm). Simulation results for this configuration are presented in Figure 6.6. The smooth-surface case differs slightly from the two previous cases as scuffing was experienced at a higher load. The maximum pressure is 1.4 GPa with a minimum film thickness of 0.239 μm and a central film thickness of 0.273 μm.

Simulation results for the two rough surfaces in contact are shown in Figure 6.6 (b). Again, the time step shown corresponds to the highest pressure peak encountered

(a)

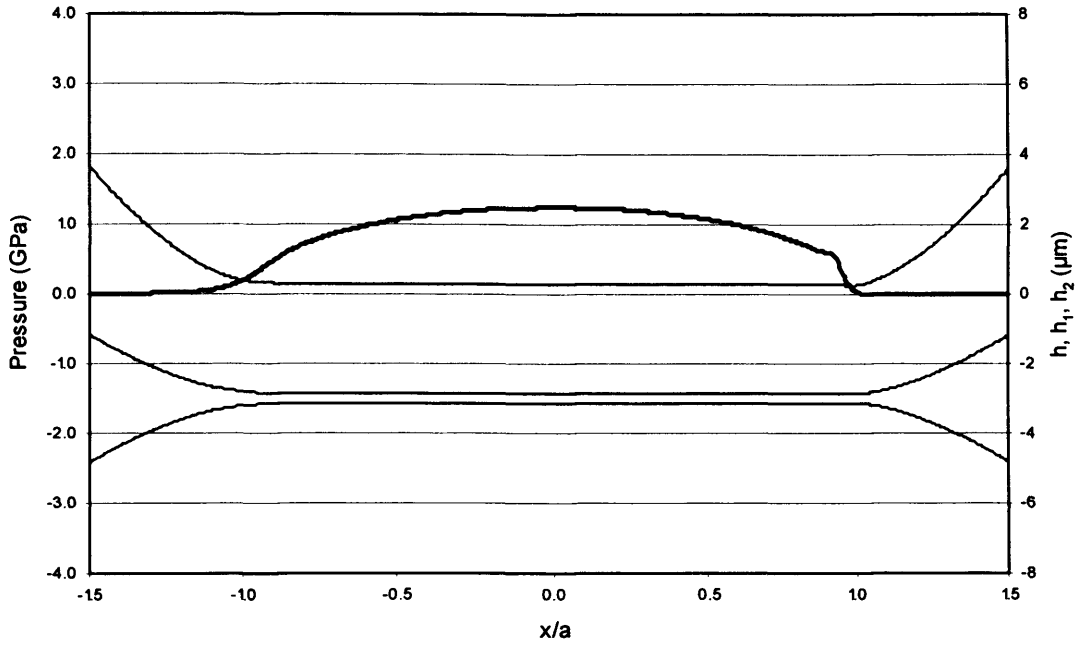

(b)

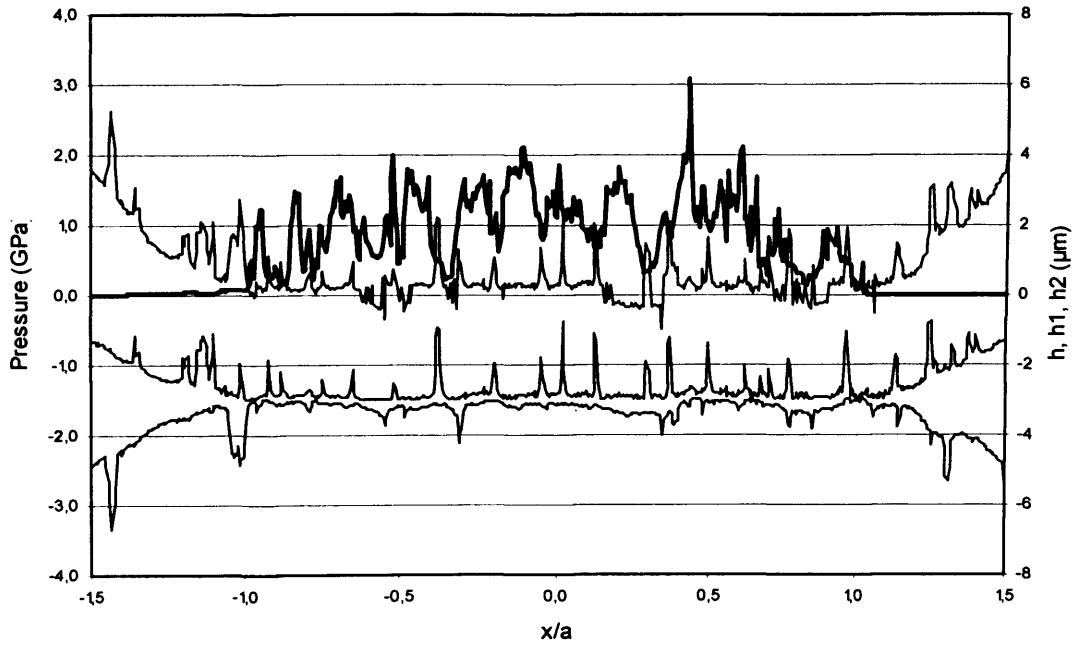

Figure 6.5: **Simulation results of the ground compound layer on and nitrided configuration with samples run at a sliding speed of 16 m/s**
(a) The smooth case
(b) The two rough surfaces in contact
Pressure shown in bold

(a)

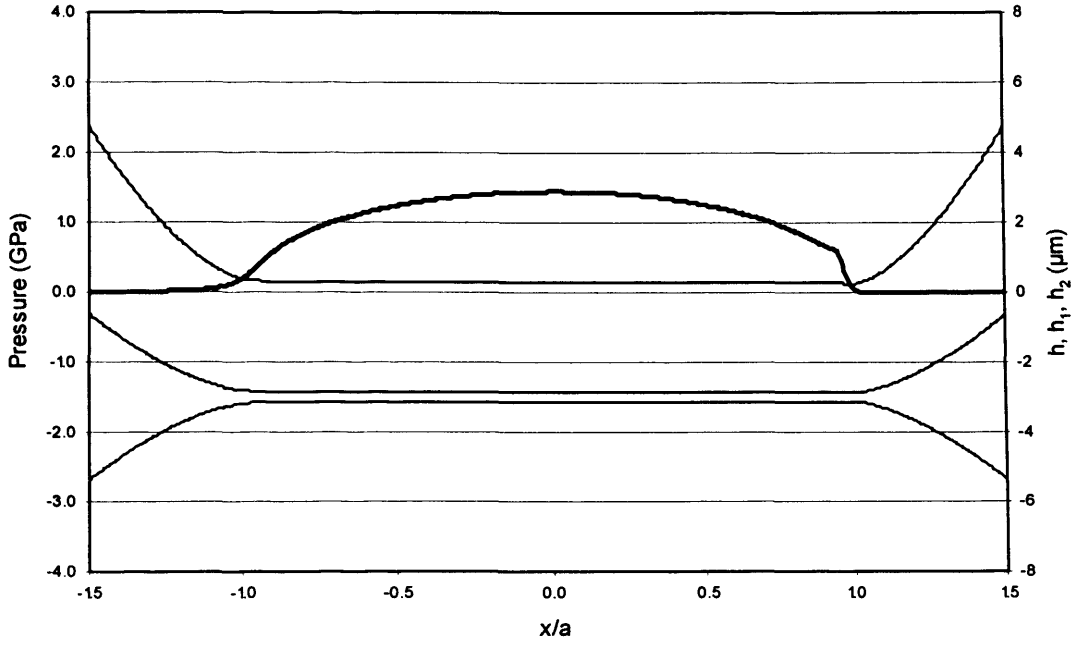

(b)

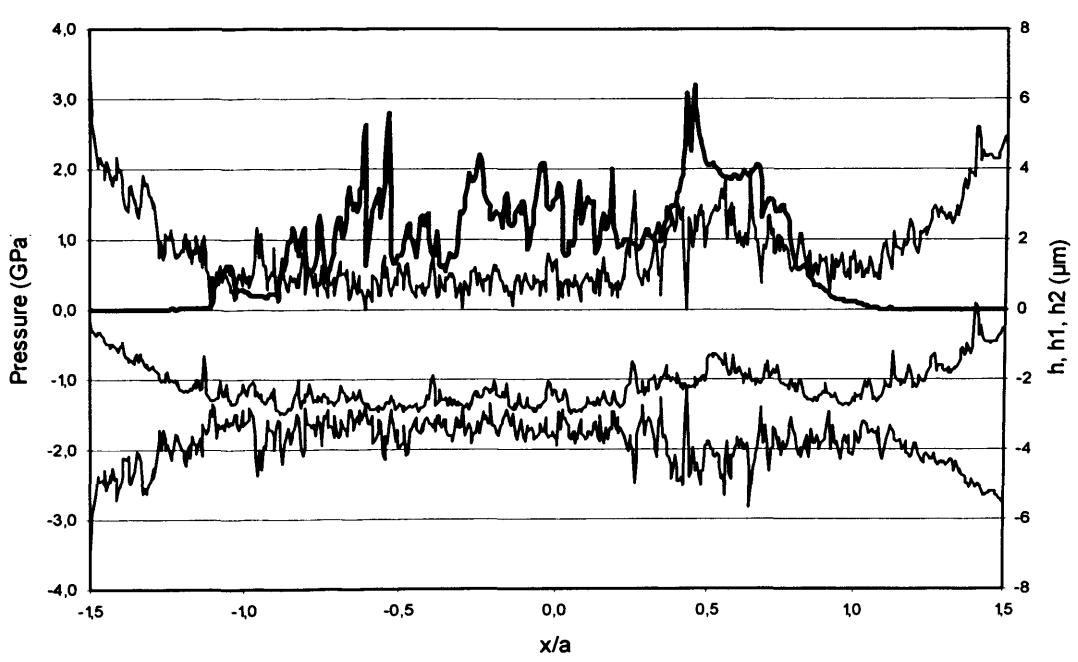

Figure 6.6: **Simulation results of the ground and nitrided configuration for samples run at a sliding speed of 16 m/s**
(a) The smooth case
(b) The two rough surfaces in contact
Pressure shown in bold

which was 3.20 GPa. This is lower than the baseline ground case carburised samples (4.2 GPa). An interesting feature of this result is the area near the exit of the contact where film thickness is maintained at a very high level (typically 1.5 μm). This might be explained by the roughness quality of the upper surface which exhibits particularly rounded features. As with the baseline configuration, a number of solid contacts are experienced though with a lower occurrence. Only seven solid contacts are experienced compared to twenty three in the case of the ground case carburised configuration. This difference may also explain the better overall performance of the ground nitrided configuration. Also experienced with this configuration is the micro-cavitation phenomenon as found with the baseline configuration. Again, for the time interval considered for the simulation, the level of negative pressure encountered is very small (-0.001 GPa) when compared to nearly -1 GPa for the baseline configuration. This confirms that the rougher surface produces more severe lubrication conditions.

6.4.4 Simulation results for samples coated with Me-DLC

Two configurations are considered in this case. First we consider the case of the baseline case carburised and ground material coated with the Me-DLC material. Second we examine behaviour with the same coating applied to the nitrided/ground samples. Figure 6.7 presents the results obtained with the coated case carburised steel. Results for the smooth case shown in Figure 6.7 (a) exhibit a maximum pressure at the centre of the contact of 1.25 GPa matching exactly the one encountered with the uncoated configuration (same scuffing load). The minimum film thickness is h_{min} = 0.249 μm and the central film thickness is h_{cen} = 0.285 μm.

The corresponding rough surface behaviour is illustrated in Figure 6.7 (b) which again corresponds to the time step at which the maximum pressure occured. The actual level of maximum pressure is very considerable as it reaches a value of nearly 4.0 GPa. This is consistent with the level found with the uncoated configuration (4.2 GPa) and this is expected because the presence of the coating does not affect the underlying roughness. The numerical results exhibit a number of solid contacts between the two surfaces, but the occurrence is significantly lower than for the baseline configuration (three compared to twenty three). This could possibly be explained by the appearance of the run-in surface as illustrated in Figure 6.3 (b) – case (h) where the roughness pattern essentially consists of flat bearing surfaces with a number of deep valleys.

(a)

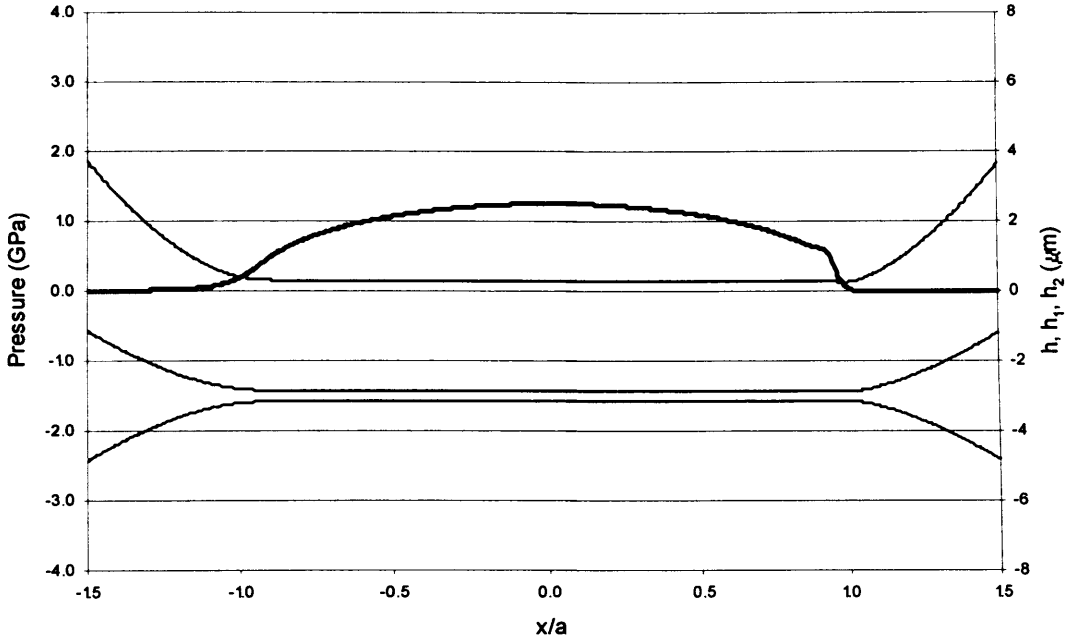

(b)

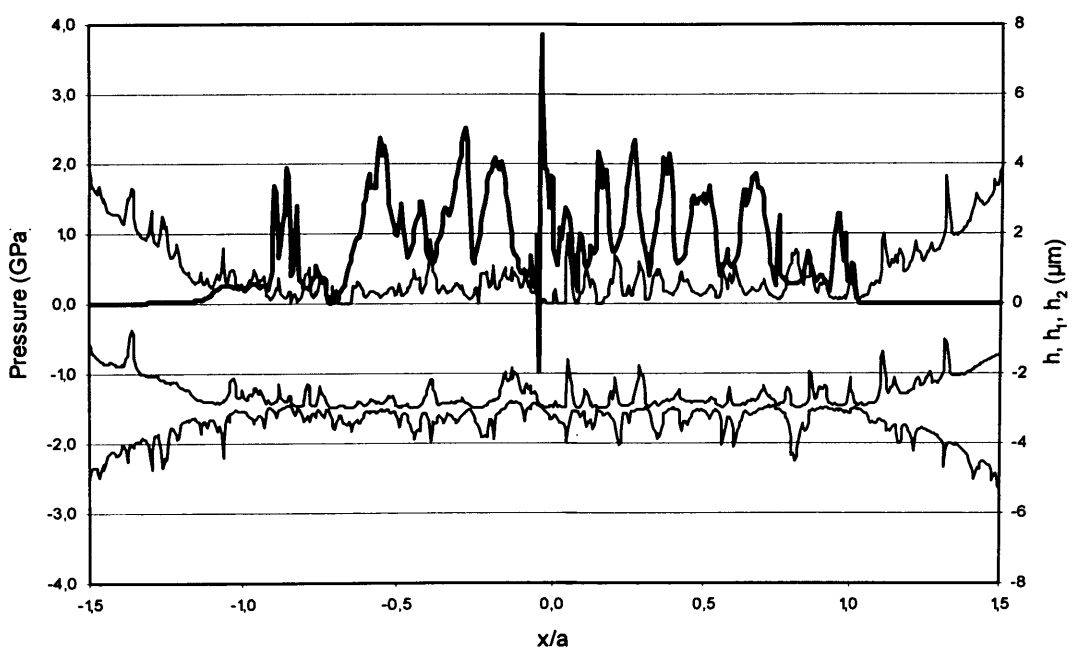

Figure 6.7: **Simulation results of the ground case carburised and coated with Me-DLC coating for samples run at a sliding speed of 16 m/s**
(a) The smooth case
(b) The two rough surfaces in contact
Pressure shown in bold

Also encountered in this case is micro-cavitation as illustrated in Figure 6.7 (b) where this phenomenon occurs immediately before the maximum peak of pressure. The level of negative pressure is very consistent with the baseline configuration where in both instances this level is of the order of -1GPa.

Turning to the ground nitrided coated configuration, the smooth case reveals a maximum pressure of 1.62 GPa as illustrated in Figure 6.8 (a). This corresponds to a much higher scuffing load when compared both to the baseline uncoated configuration and the coated case carburised steel. The minimum film thickness is h_{min} = 0.232 μm and the central film thickness is h_{cen} = 0.263 μm. This level is again well below the average roughness level of 0.4 μm.

The simulation results obtained for the two rough surfaces in contact at the time step corresponding to the maximum peak pressure (3.58 GPa in this case) are illustrated in Figure 6.8 (b). For this configuration no solid contact was encountered and the minimum film thickness registered was of the order of 0.011 μm (about 36 times lower than the average roughness level of the fresh surface). The pressure response as illustrated in Figure 6.8 (b) exhibits less pressure amplitude variation about the Hertzian pressure line than the coated baseline as illustrated in Figure 6.7 (b). This comparison is further illustrated in Figure 6.9 where the pressure response for both coated configurations (case carburised and nitrided) are shown on the same graph normalised to the maximum Hertzian pressure. The pressure ripple amplitude about the Hertzian line in this case appears higher than in the case of the case carburised coated configuration. Some micro-cavitation is also present for this configuration (see Figure 6.8) but to a much smaller extent when compared to the coated baseline configuration. All these factors tend to explain the better scuffing behaviour of the coated nitrided configuration.

6.4.5 Simulation results for ground case carburised samples coated with Boron Carbide

The results for this alternative coating are shown in Figure 6.10. The smooth case as illustrated in Figure 6.10 (a) exhibits a maximum Hertzian pressure similar to the coated nitrided configuration (in this case 1.63 GPa). Contact conditions in terms of minimum film thickness and central film thickness are as a result identical i.e. h_{min} = 0.232 μm and h_{cen} = 0.263 μm. This is obviously consistent with what was discussed in Chapter 5 where the scuffing behaviour for this alternative coating was found to be

(a)

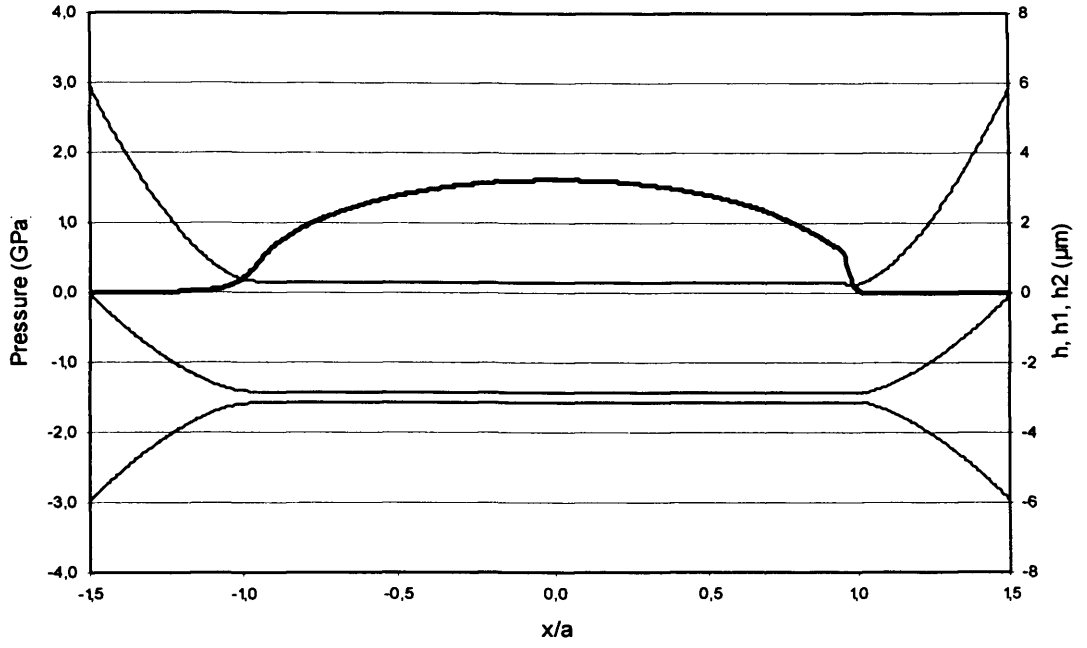

(b)

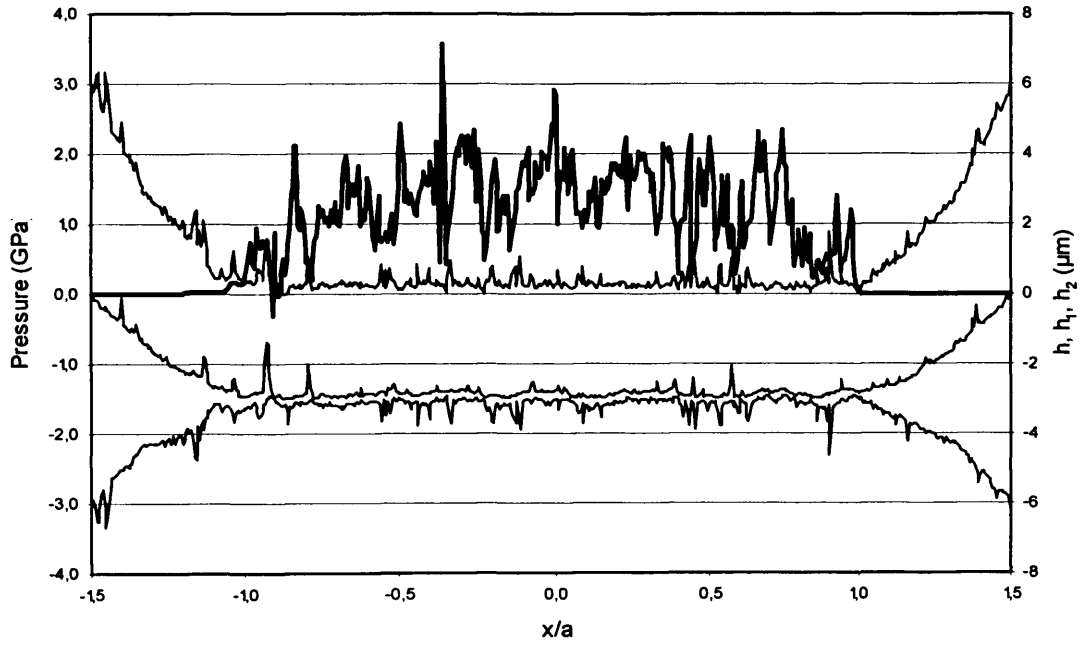

Figure 6.8: **Simulation results of the ground + nitrided steel + Me-DLC coating configuration for samples run at a sliding speed of 16 m/s**
(a) The smooth case
(b) The two rough surfaces in contact
Pressure shown in bold

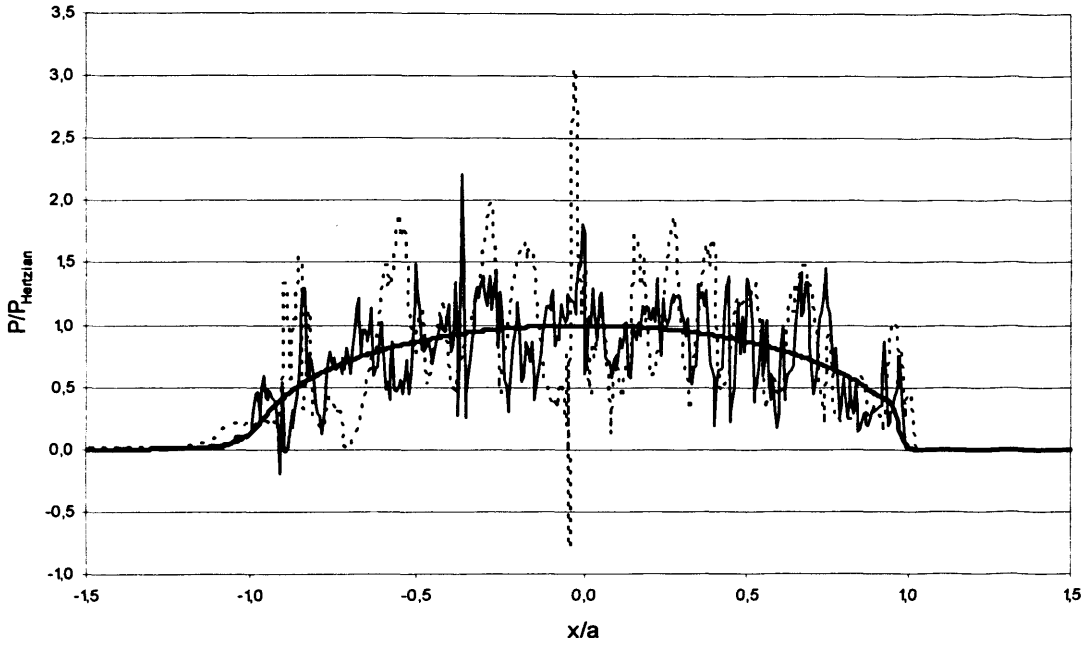

Figure 6.9: **Simulation results of the ground + nitrided steel (simple line) and the case carburised (dotted line) + Me-DLC coating configuration for samples run at a sliding speed of 16 m/s <u>normalised</u> with the maximum Hertzian pressure Smooth Hertzian pressure case shown in bold**

superior to both the baseline un-coated configuration and the Me-DLC coated case carburised steel.

The rough surface case at the time step corresponding to the peak pressure (3.40 GPa) is illustrated in Figure 6.10 (b). No solid contacts (minimum film thickness was 0.016 μm) or micro-cavitation were encountered. Again the normalised results in comparison with the coated baseline case carburised steel (see Figure 6.11) show less pressure ripple than the baseline configuration.

6.4.6 Simulation results for superfinished samples

Three configurations were considered all of which were based on nitrided samples. The first superfinished configuration used the proprietary process "Abral" performed after the grinding process. The second configuration was very similar to the first but a Me-DLC type coating was applied to the surface after the superfinishing treatment. In the third configuration an alternative superfinishing treatment was used in which ceramic pellets immersed in water were used in place of zinc as used in the "Abral" process. The advantage of this process is supposedly its harmless effluents.

The smooth case for the three configurations corresponded to a maximum Hertzian pressure, respectively, of 1.63 GPa (simple superfinishing); 1.64 GPa for the coated superfinished configuration and 1.63 GPa for the alternative superfinishing. This shows very little difference between the performance of the various configurations and it should be noted that for all these configurations, no scuffing was experienced. The corresponding predicted central film thickness was 0.263 μm for all configurations and the minimum film thickness was 0.232 μm for all configurations.

Considering the rough surfaces in contact results as illustrated in Figures 6.12, 6.13, 6.14, there is very little pressure ripple about the Hertzian line. The pressure reached a peak value of 2.42 GPa in the case of the simply superfinished configuration. It reached a maximum value of 2.10 GPa in the case of the coated configuration and a value 2.38 for the alternative process. This slight difference in favour of the coated configuration may be due to the roughness feature pattern induced by the Me-DLC coating being subjected to heavy loading as discussed in Chapter 5. In all three cases using superfinished surfaces no solid contact is experienced and a minimum film thickness is maintained: 0.138μm for the simple superfinishing, 0.142 μm for the coated configuration and 0.124μm for the alternative process. In all cases, the

minimum film thickness is above the average roughness level (typically 0.1μm) which no doubt helps to explain the excellent performance of these configurations.

(a)

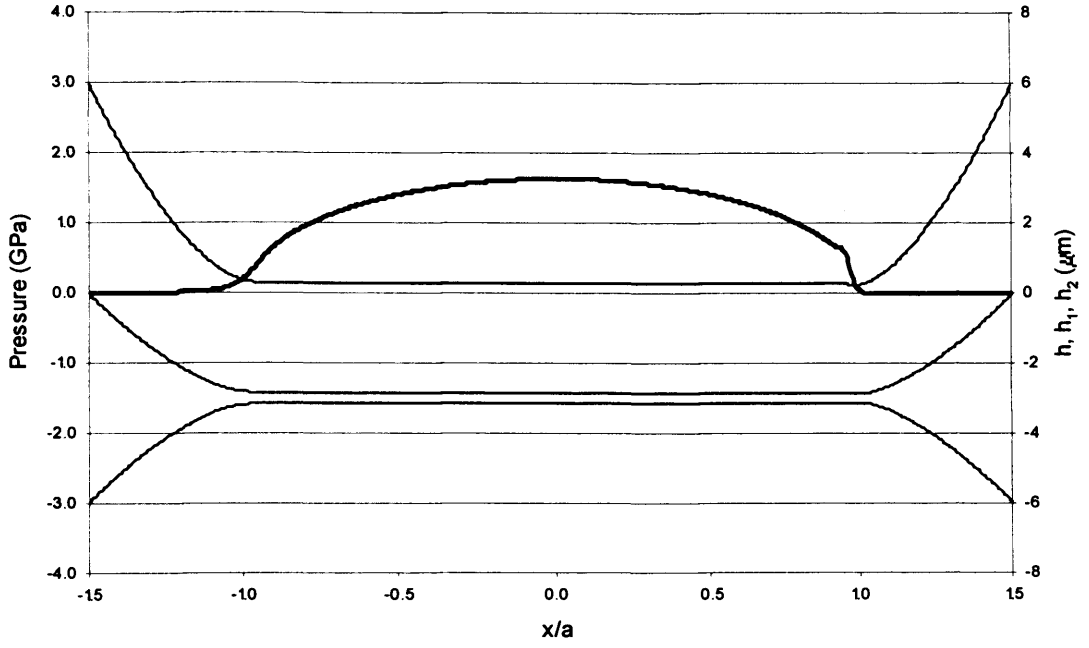

(b)

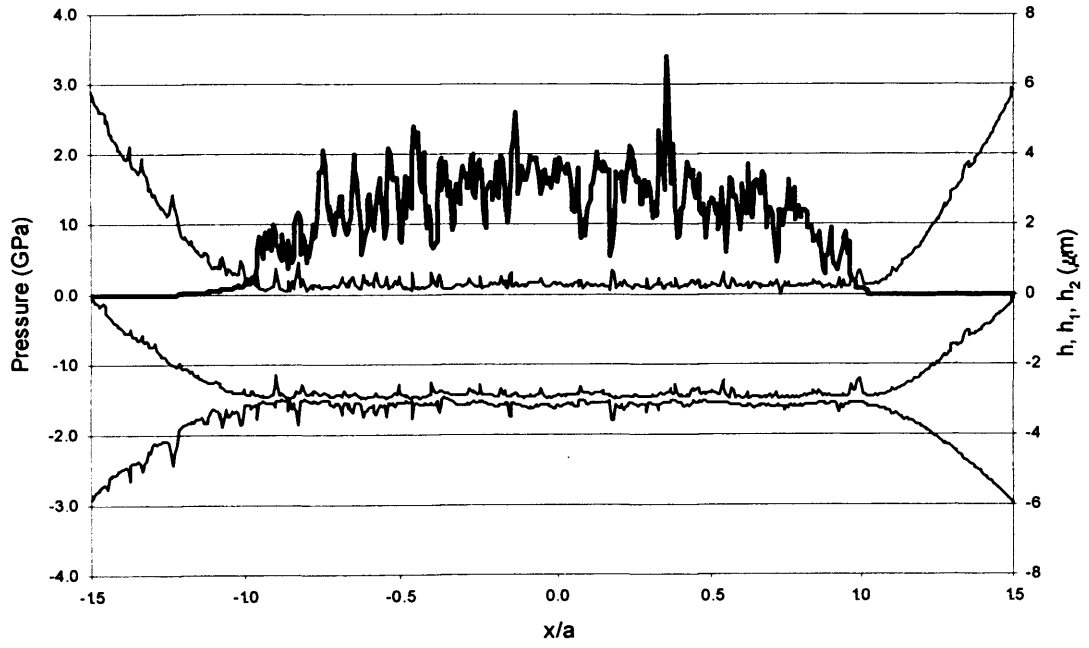

Figure 6.10: **Simulation results of the ground case carburised and coated with B_4C Boron Carbide coating for samples run at a sliding speed of 16 m/s**
(a) The smooth case
(b) The two rough surfaces in contact
Pressure shown in bold

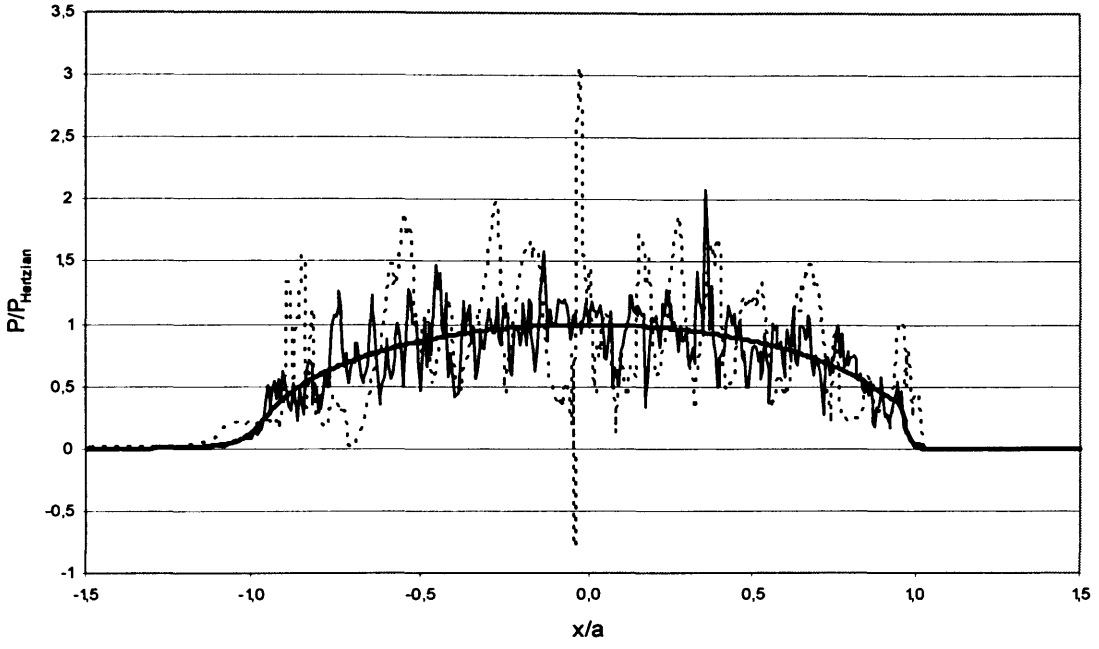

Figure 6.11: **Simulation results of the case carburised (dotted line) + Me-DLC coating configuration compared with case carburised (continiuous line) + B_4C coating for samples run at a sliding speed of 16 m/s <u>normalised</u> with the maximum Hertzian pressure**
Smooth Hertzian pressure case shown in bold

(a)

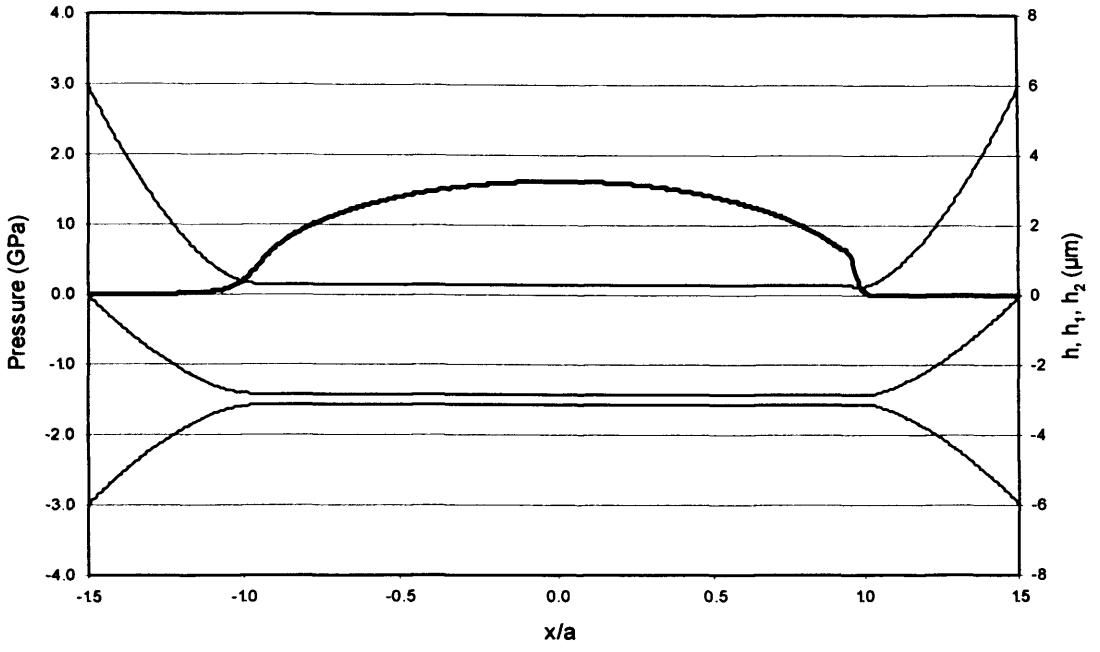

(b)

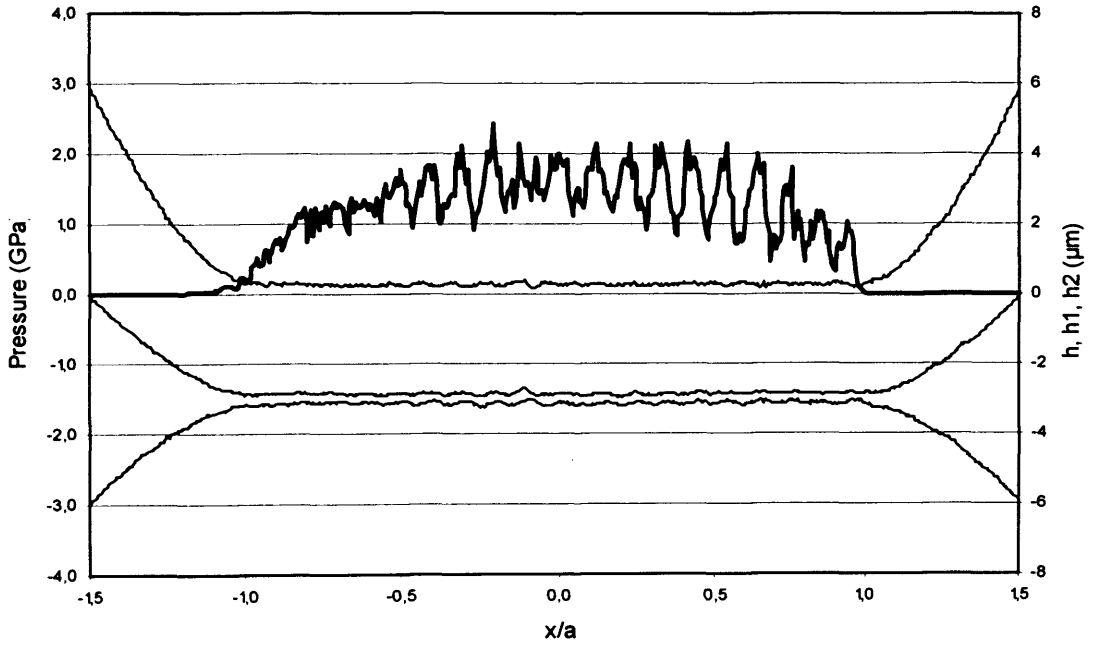

Figure 6.12: **Simulation results of the nitrided, ground and superfinished configuration for samples run at a sliding speed of 16 m/s**
(a) The smooth case
(b) The two rough surfaces in contact
Pressure shown in bold

(a)

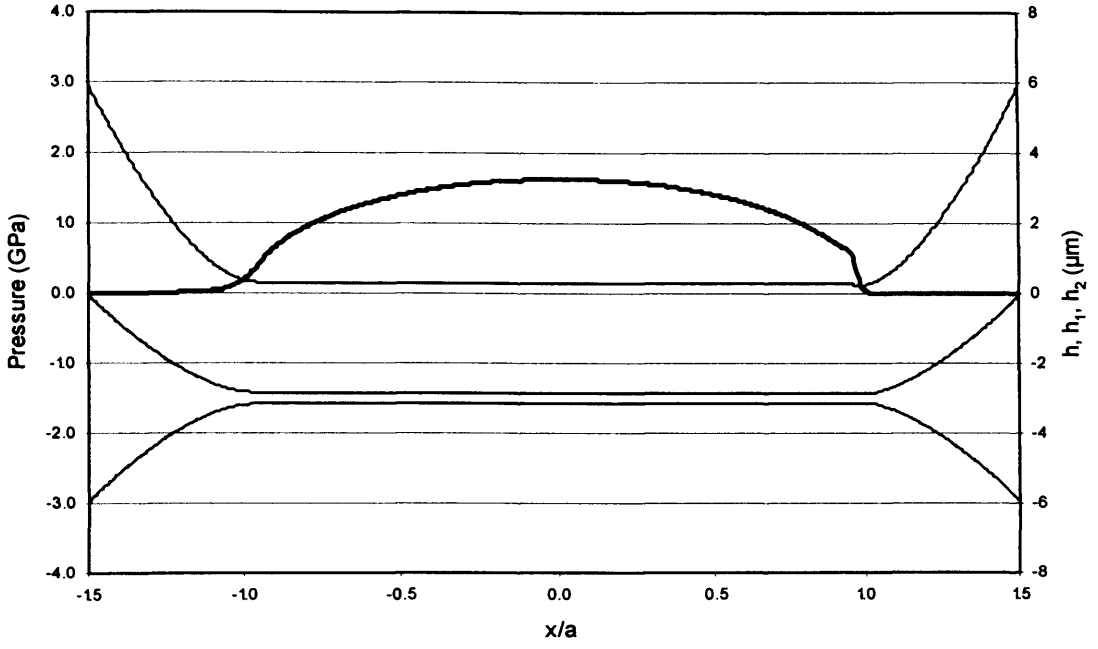

(b)

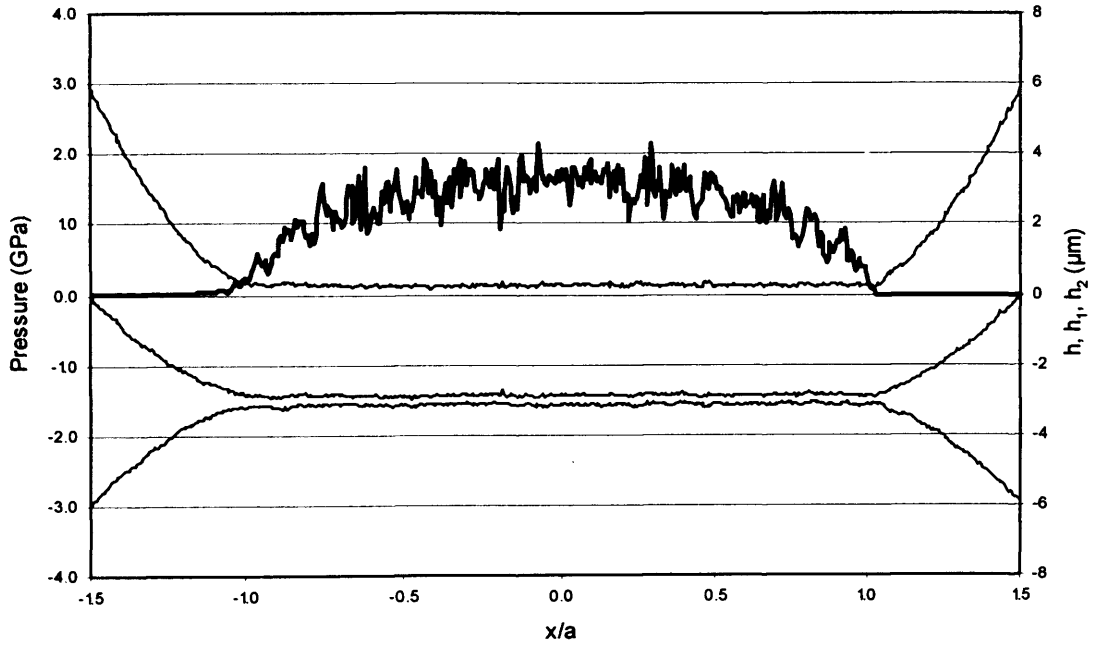

Figure 6.13: **Simulation results of the ground + nitrided steel + superfinishing + Me-DLC coating configuration for samples run at a sliding speed of 16 m/s**
(a) The smooth case
(b) The two rough surfaces in contact
Pressure shown in bold

(a)

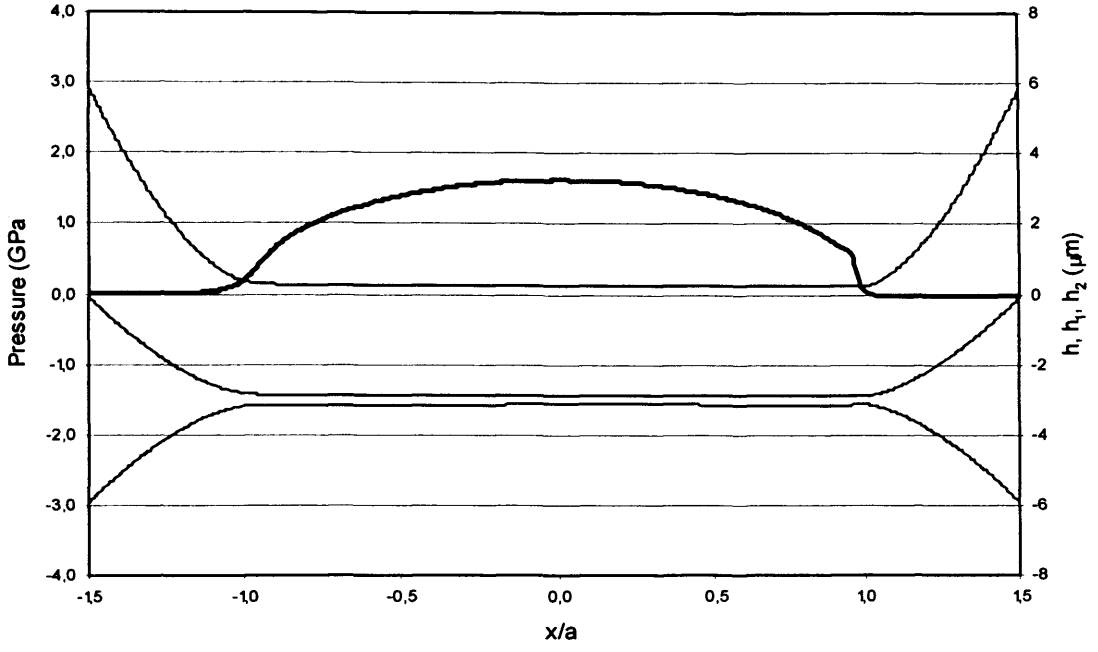

(b)

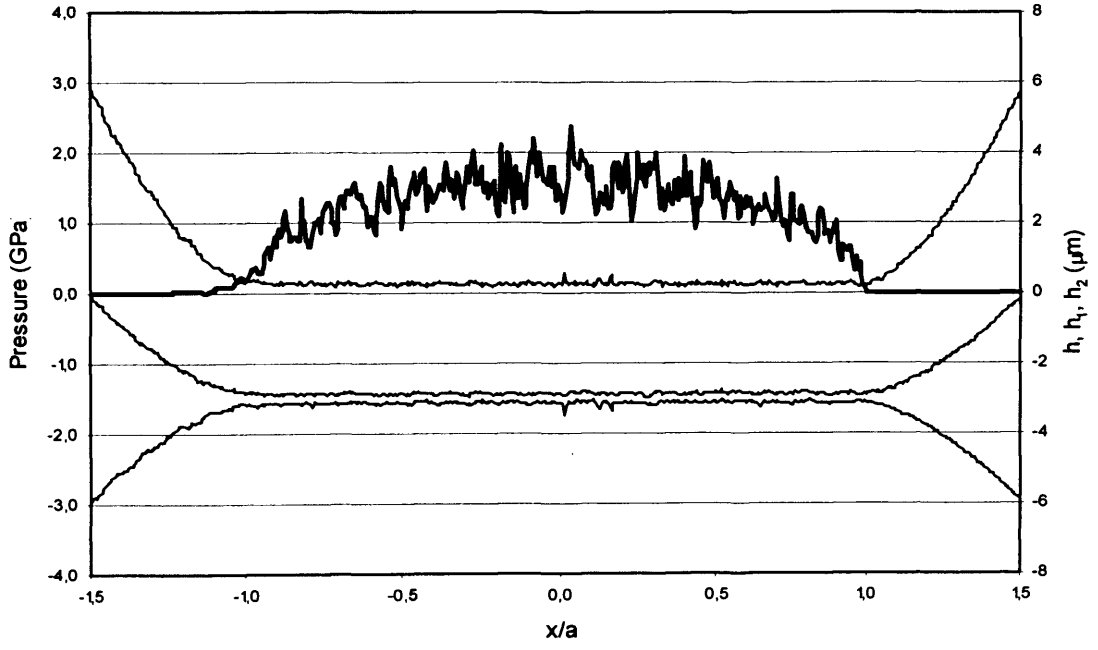

Figure 6.14: **Simulation results of the ground + nitrided steel + superfinishing (alternative process) configuration for samples run at a sliding speed of 16 m/s**
(a) The smooth case
(b) The two rough surfaces in contact
Pressure shown in bold

6.5 General comparison of results of simulation

6.5.1 Introduction

In order to allow for a direct comparison of results between the different configurations, a number of objective performance parameters have been used as proposed by Tao *et al.* (2003). The parameter $\Phi(p)$ is defined as the fraction of the Hertzian contact area that has a pressure that exceeds p. The parameter $\Phi(h)$ is the fraction of the Hertzian contact that has a film thickness that is less than h. A further aspect considered is that of pressure cycling. A routine was added to the solver to count the number of pressure cycles occurring, within the equivalent Hertzian region, between specified upper and lower limits. Pressure cycling is considered to be relevant to the micropitting contact fatigue phenomenon. In the following and for all configurations under study, a lower pressure limit of 0.5 GPa was set.

6.5.2 Comparison of the nitrided configurations

The comparison was carried with reference to the case carburised ground configuration. Figure 6.15 shows the variation of the $\Phi(p)$ parameter. This suggests that the configuration in which the compound layer is left on tends to give lower pressures within the contact. This is explained by the high degree of running in experienced by the surfaces as shown in Figure 6.3. Considering the second parameter $\Phi(h)$ as illustrated in Figure 6.16, the difference in behaviour appears rather clearly. Both the nitrided with compound layer on and the baseline configuration show overall a film formation for the majority (50%) of the contact area above 0.4 μm which is of the same order as the average roughness. This result would tend to indicate a rather favourable lubrication regime for the overall contact area. On the other hand, the nitrided ground configuration exhibits much thinner films across the majority of the contact area. Figure 6.16(b) shows the thin film part of the graph. When assessing the area of the low film thickness, there is a similar behaviour for the nitrided with compound layer on and the baseline configuration with a clear advantage for the former. Indeed there is only 1.5% of the contact area with an oil film lower than 0.1μm, against 3.5% of the contact area with an oil film lower than 0.1μm. The behaviour on the other hand is very different for the nitrided ground configuration whereby there is a non negligible proportion of the contact area with virtually no

(a)

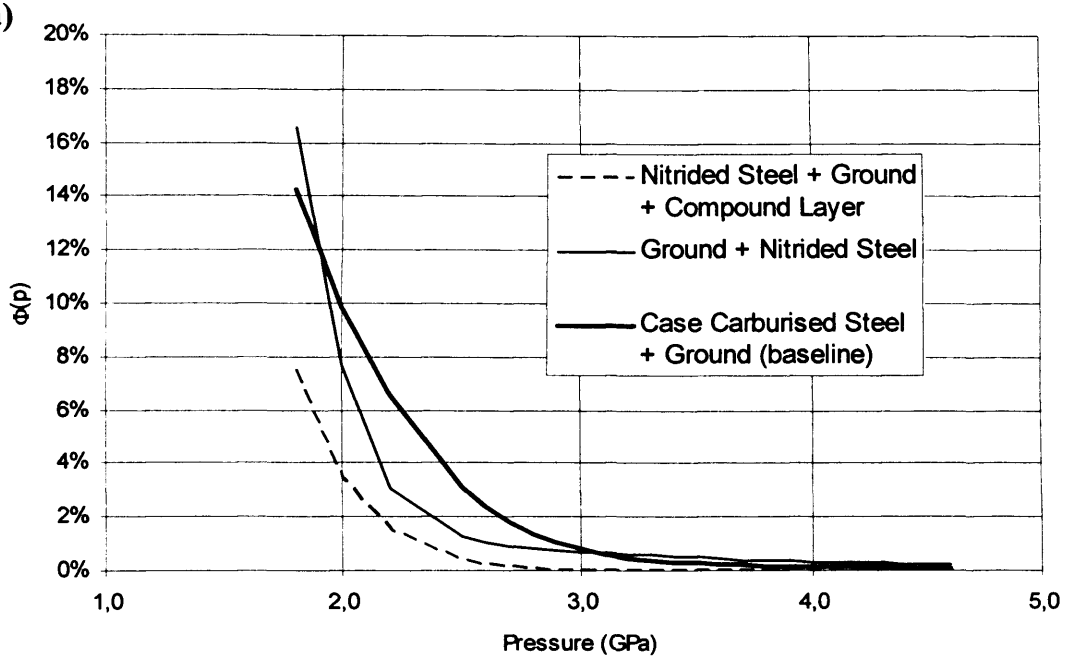

(b)

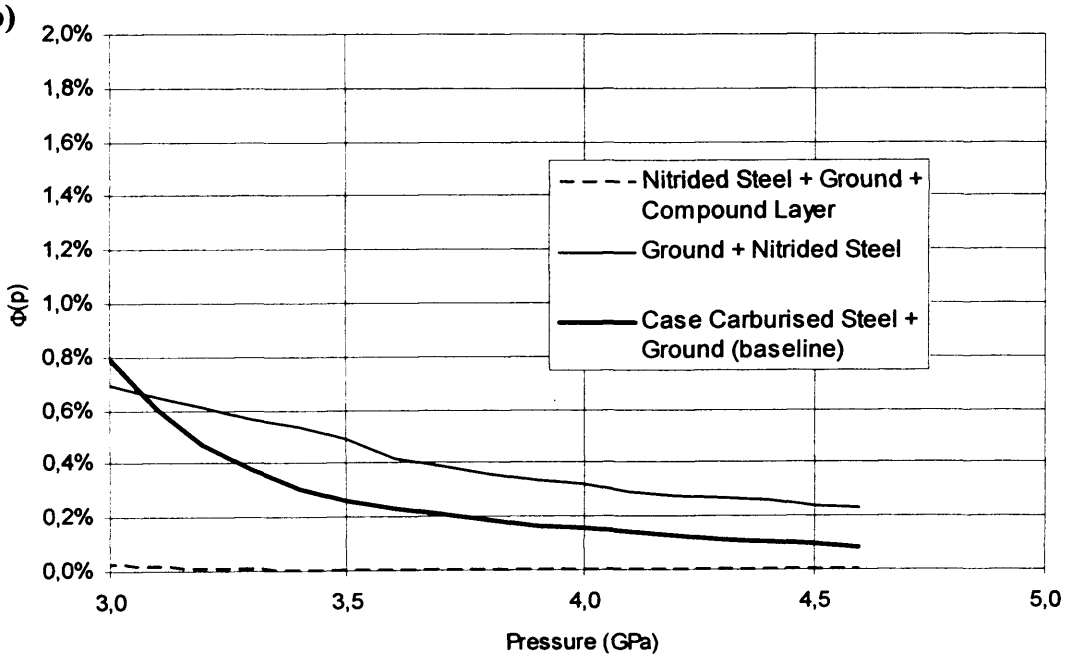

Figure 6.15: **High pressure behaviour for the nitrided configurations with reference to the baseline configuration**
(a) The full spectrum
(b) A close-up of the highest pressure area

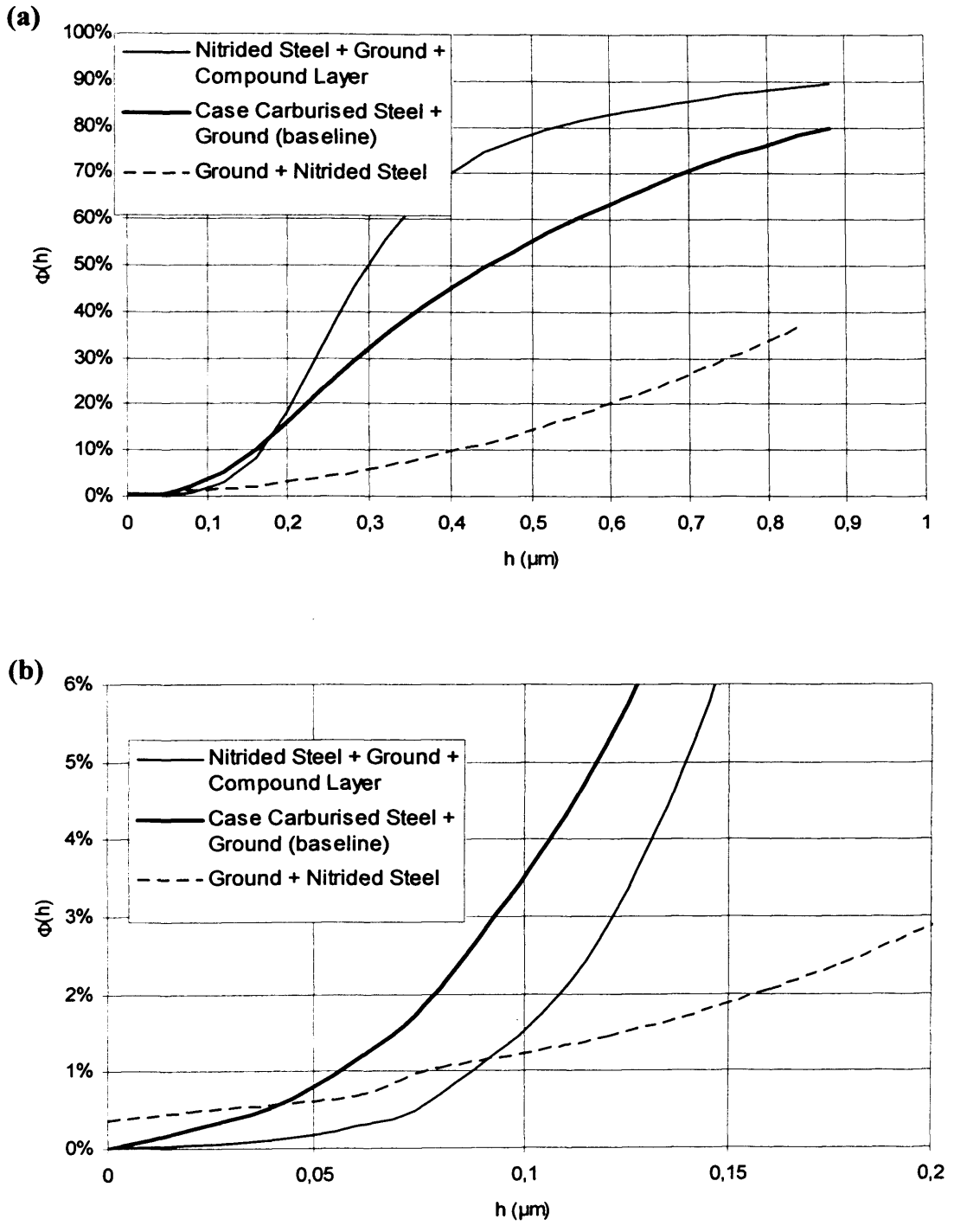

Figure 6.16: **Low film thickness behaviour of the nitrided configurations with reference to the baseline configuration**
(a) The full spectrum
(b) A close-up of the lowest film thickness area

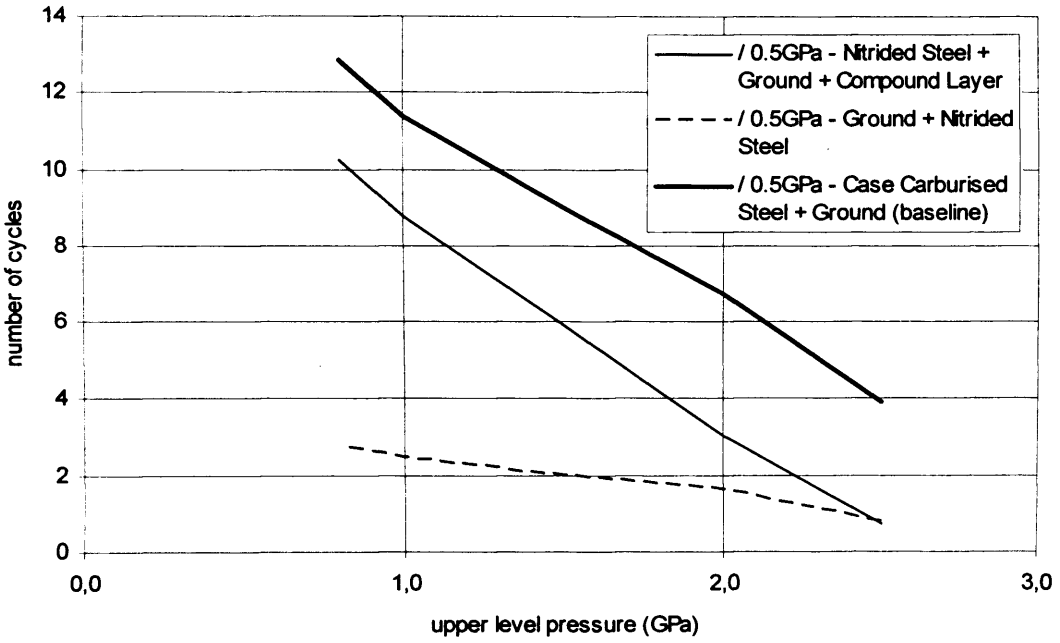

Figure 6.17: Pressure cycle counts obtained for the nitrided configurations with reference to the baseline configuration for a lower pressure cycle limit of 0.5 GPa

lubricating film. There is also a somehow surprising line crossover with the trend lines of the other configurations. Hence, this corresponds to a lower proportion of the contact with a very thin film (say <0.1 μm) when compared with the two other configuration. Remarkably, this trend is maintained whereby the curve demonstrates that there is no clear bearing area i.e. with a large proportion of the contact with a significant lubricating film. The scuffing behaviour of this configuration (better than the baseline) remains from the film formation point of view rather unclear. From the pressure cycle count point of view as illustrated in Figure 6.17, the ranking becomes fairly obvious in favour of the nitrided ground configuration which exhibits the lowest cycle counts. This could in part explain the known (by the author) better performance in terms of micro-pitting resistance of the nitrided ground steel for aerospace applications.

6.5.3 Comparison of the Me-DLC coated configurations

The same analysis has been carried out for the coated configurations and the high pressure behaviour which is illustrated in Figure 6.18 exhibits a clear ranking in favour of the nitrided and ground substrate. This was confirmed also by the test results whereby this configuration experienced virtually no scuffing. There is hardly any area subjected to a pressure greater than 4 GPa. The baseline configuration from the high pressure behaviour point of view is the least favourable despite a scuffing performance of the same order as the uncoated configuration. From the low film thickness behaviour point of view as illustrated in Figure 6.19, there is also a clear ranking in favour of the coated nitrided configuration confirmed by test results. The least favourable configuration appears to be the baseline uncoated one despite again a performance similar to the coated configuration. From the pressure cycle counts point of view as illustrated in Figure 6.20, the clear ranking is maintained with the exception of the nitrided ground configuration which exhibits in relative terms a higher number of counts towards the high end of the spectrum (around 2.5 GPa).

6.5.4 Comparison of the case carburised coated configurations

Two types of coating were considered as applied to the case carburised substrate, namely the Me-DLC coating and the Boron Carbide coating. From the high pressure behaviour point of view as illustrated in Figure 6.21, a clear ranking emerges in favour of the Boron Carbide coating which gives much lower pressures throughout

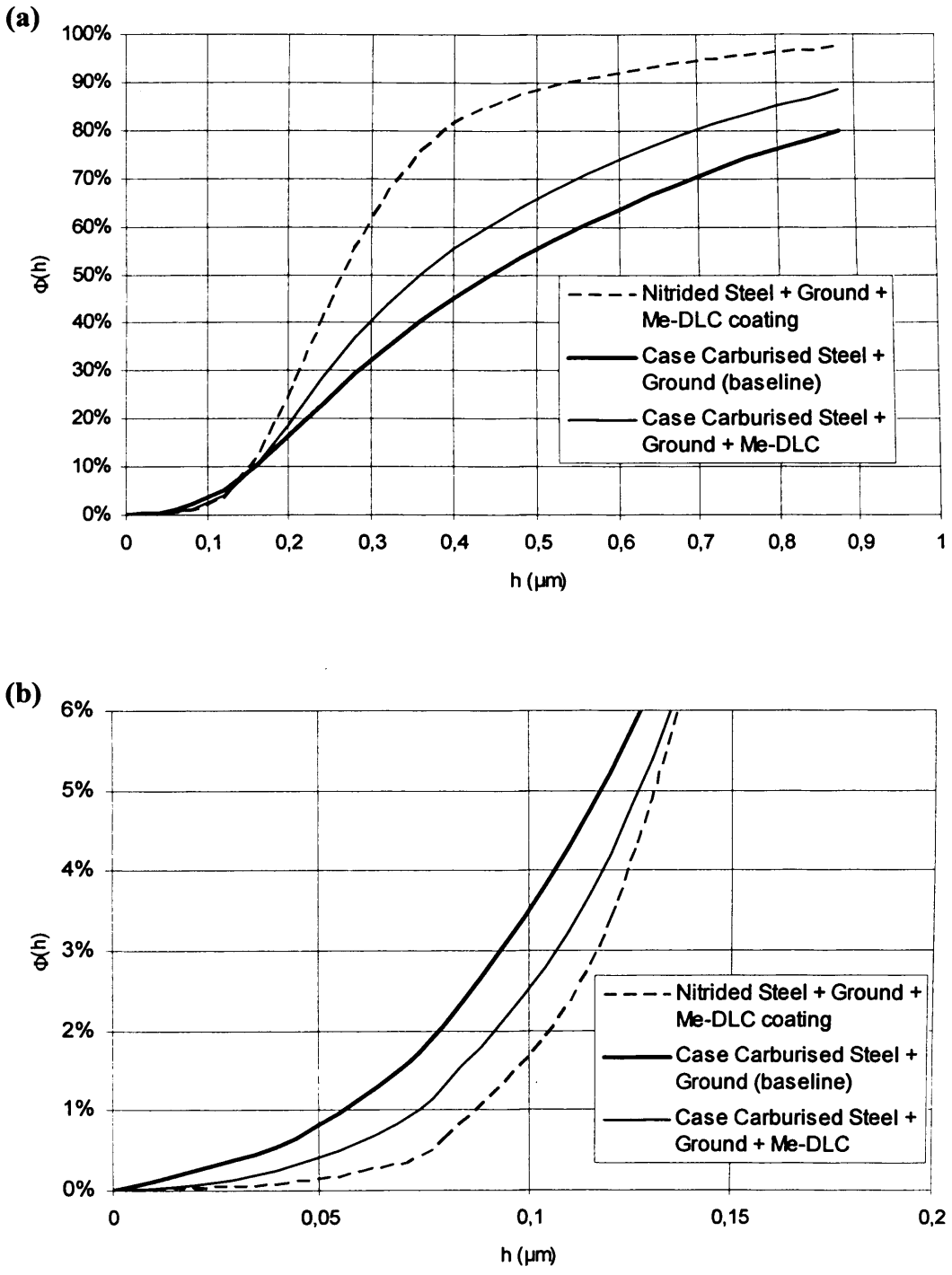

Figure 6.19: **Low film thickness behaviour of the Me-DLC coated configurations with reference to the baseline configuration**
(a) The full spectrum
(b) A close-up of the lowest film thickness area

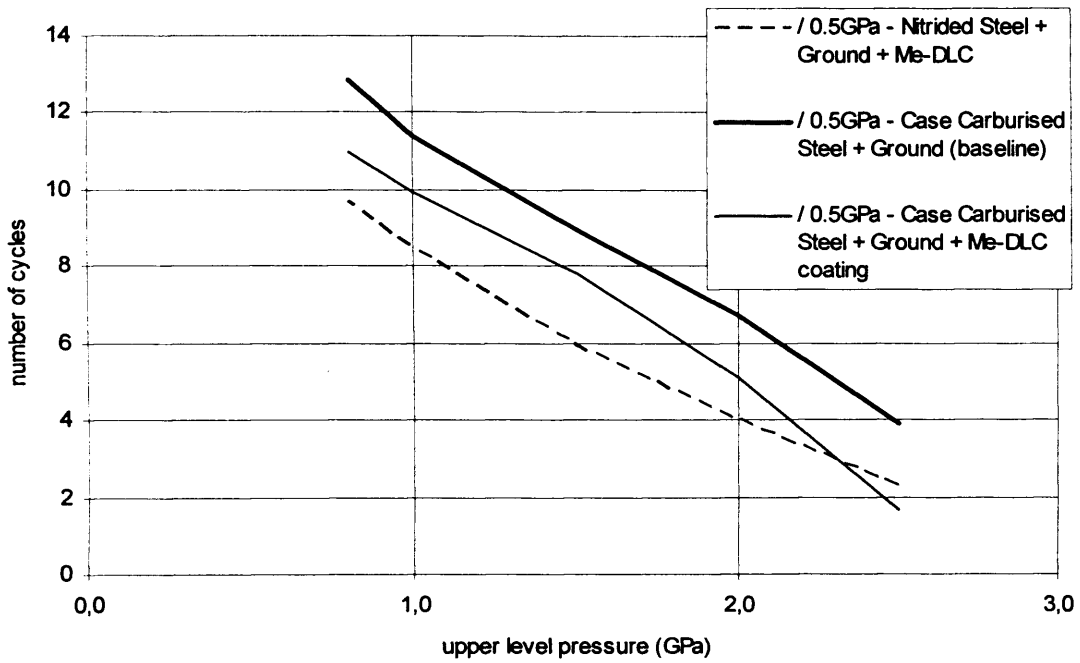

Figure 6.20: Pressure cycle counts obtained for the coated configurations with reference to the baseline configuration for a lower pressure cycle limit of 0.5 GPa

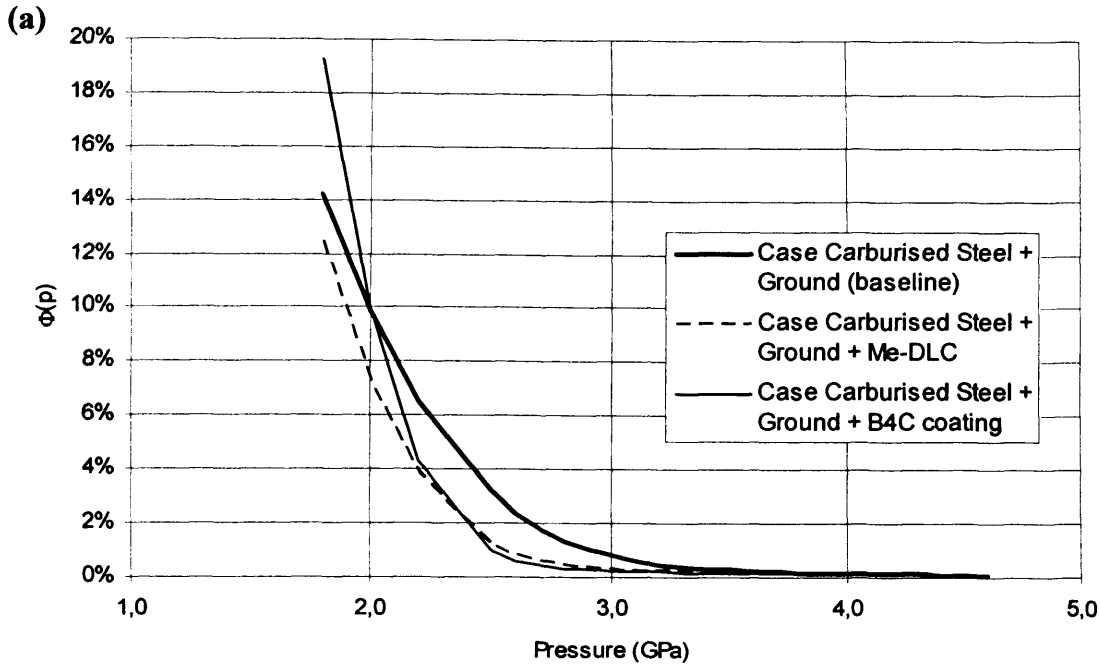

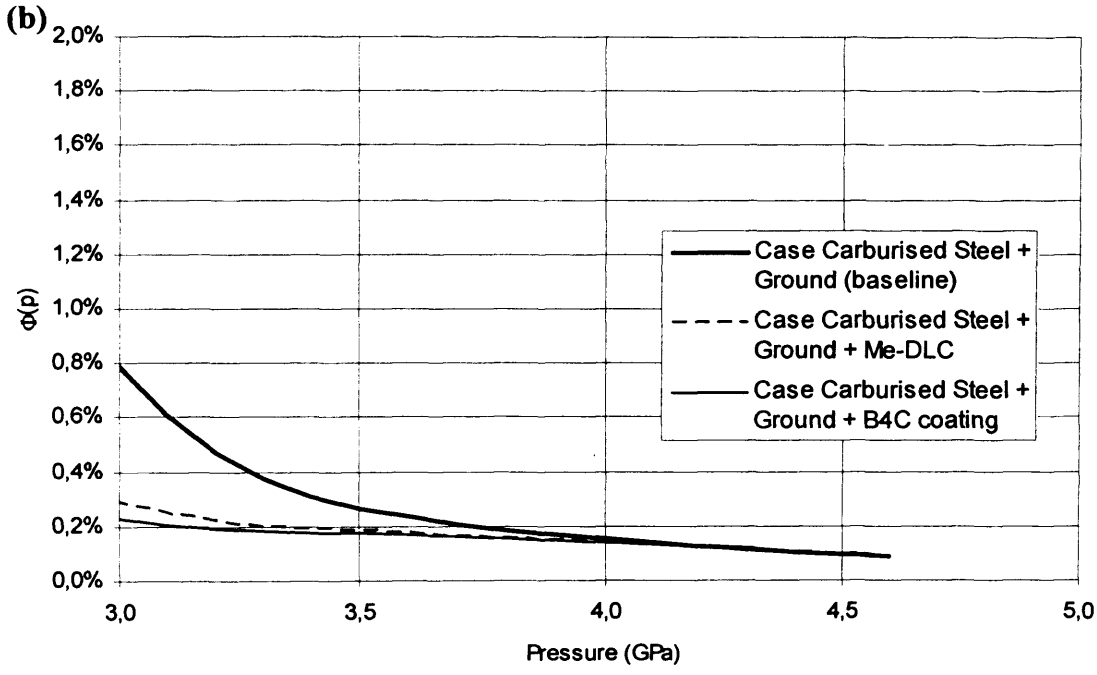

Figure 6.21: High pressure behaviour for the case carburised coated configurations with reference to the baseline configuration
(a) The full spectrum
(b) A close-up of the highest pressure area

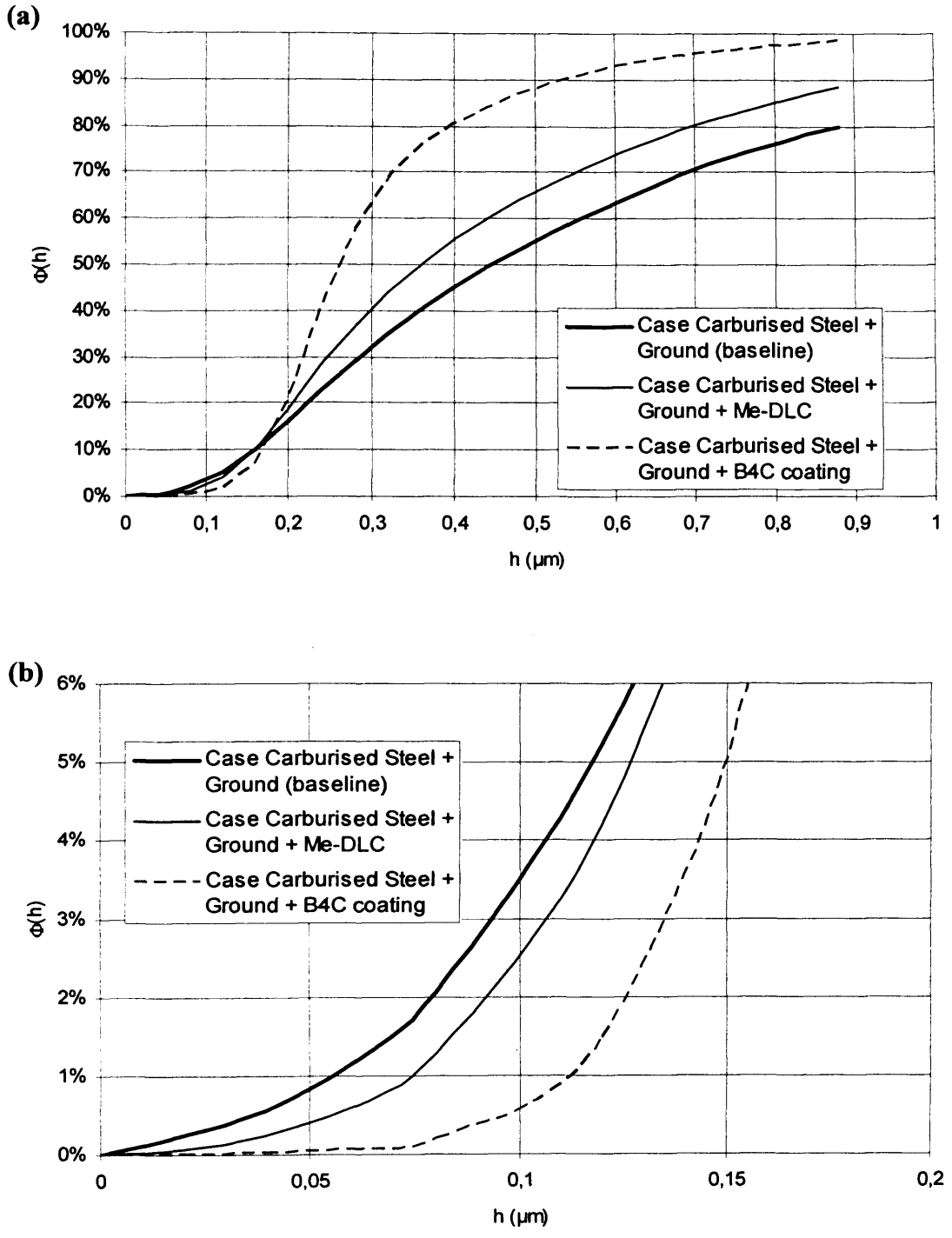

Figure 6.22: Low film thickness behaviour of the case carburised coated configurations with reference to the baseline configuration
(a) The full spectrum
(b) A close-up of the lowest film thickness area

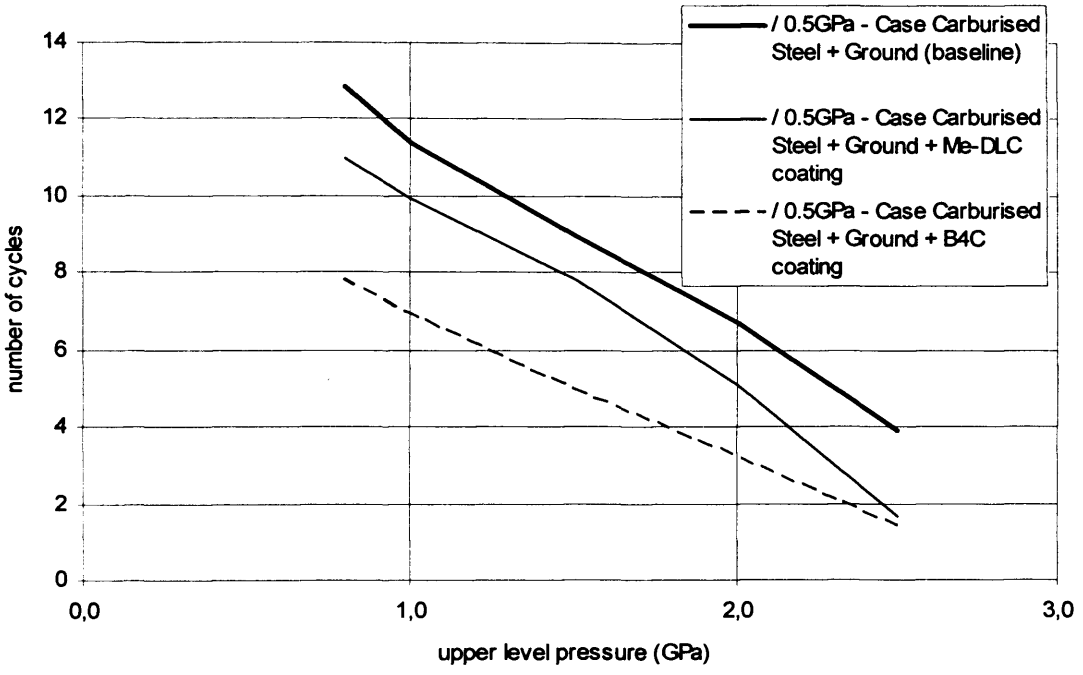

Figure 6.23: **Pressure cycle counts obtained for the case carburised coated configurations with reference to the baseline configuration for a lower pressure cycle limit of 0.5 GPa**

the contact area. From the low film thickness behaviour point of view, the ranking appears even more obvious in favour of the Boron Carbide coating. This is also confirmed from the pressure cycle counts behaviour as illustrated in Figure 6.23. All these simulation results were confirmed by the experiments performed on this coating which gave an excellent scuffing performance as discussed in Chapter 5.

6.5.5 Comparison of the superfinished configurations

The superfinished configurations were compared including the nitrided substrates, and the superfinished and coated configuration. From the high pressure behaviour point of view (see Figure 6.24), there is, as one could have expected, a very noticeable difference in favour of the superfinished configurations. This is not so obvious for the nitrided superfinished and coated substrate which exhibits pressure levels across the contact area fairly similar to the baseline configuration despite a much improved scuffing performance. This could be the result of the behaviour of the coating subjected to these very high pressures which may tend to delaminate and/or transforms itself as already discussed in Chapter 5, resulting in surface roughness features less favourable from a micro-EHL point of view. The two other coatings exhibit a similar behaviour. This trend is confirmed by the film thickness plots (see Figure 6.25) where a similar pattern is found. The uncoated configurations exhibit a near identical behaviour whereby there is hardly any area with low film. On the other hand, the coated configuration reveals a behaviour (in terms of pressure) close to the baseline configuration but with a bearing area much larger than the baseline configuration (flat end of the curve). This could also in part be explained by the coating itself and the changes that are likely to have taken place in its structure. Again, the cycle counts (see Figure 6.26) confirm this trend and are in favour of the superfinished uncoated configurations. This favourable performance of superfinished surfaces was confirmed in the experimental work although discrimination between the coated and uncoated configuration was not feasible as in both cases the scuffing performance was such that the test rig capability was reached.

(a)

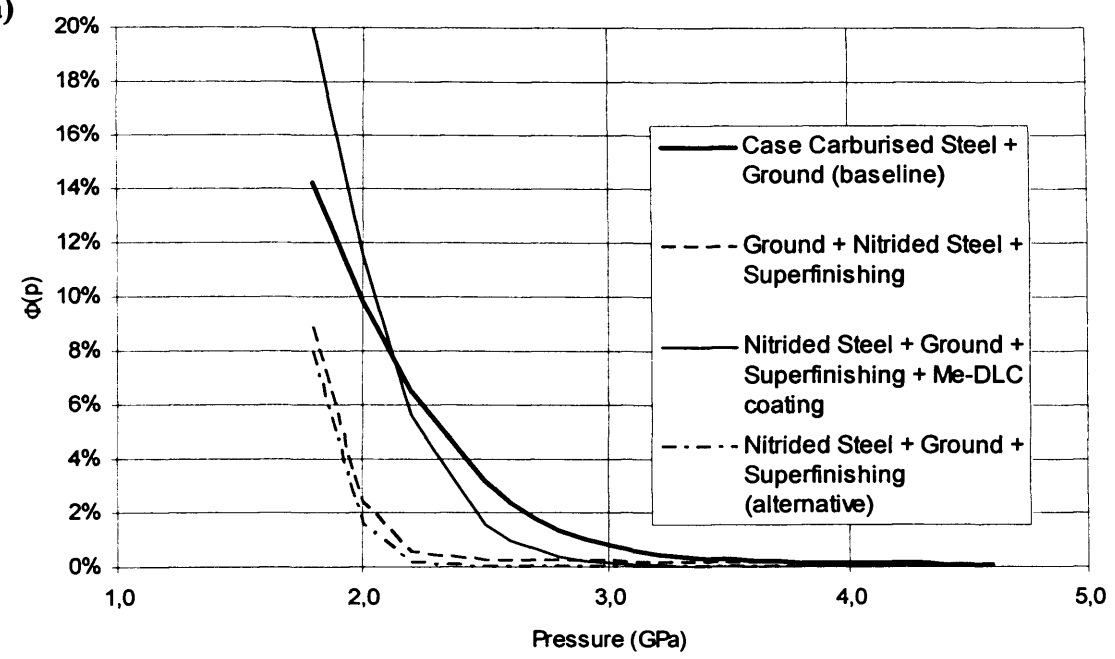

(b)

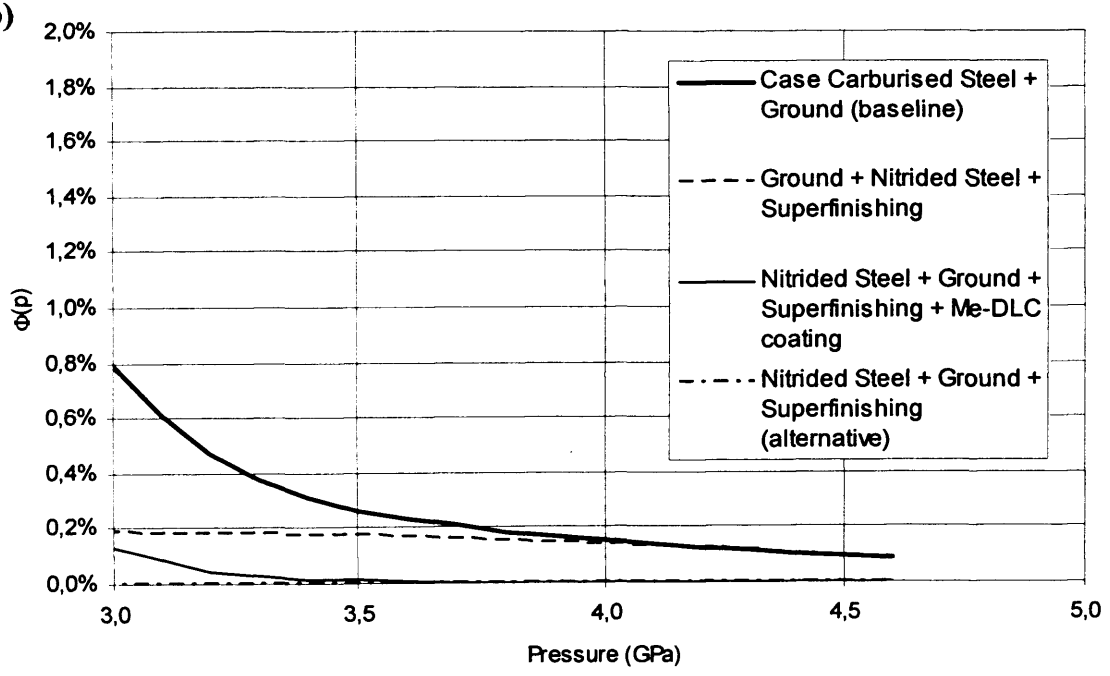

Figure 6.24: **High pressure behaviour for the superfinished configurations with reference to the baseline configuration**
(a) The full spectrum
(b) A close-up of the highest pressure area

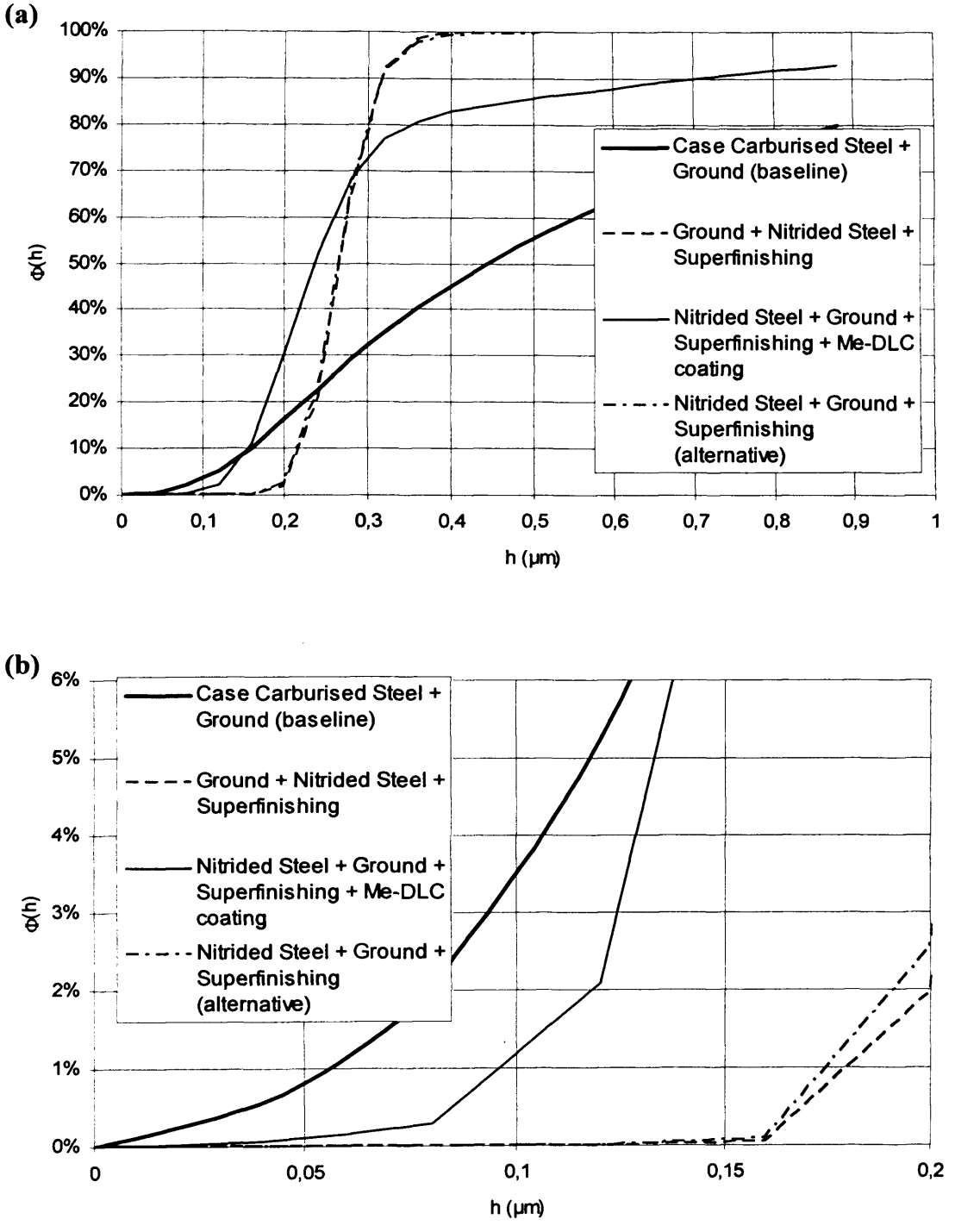

Figure 6.25: **Low film thickness behaviour of the superfinished configurations with reference to the baseline configuration**
(a) The full spectrum
(b) A close-up of the lowest film thickness area

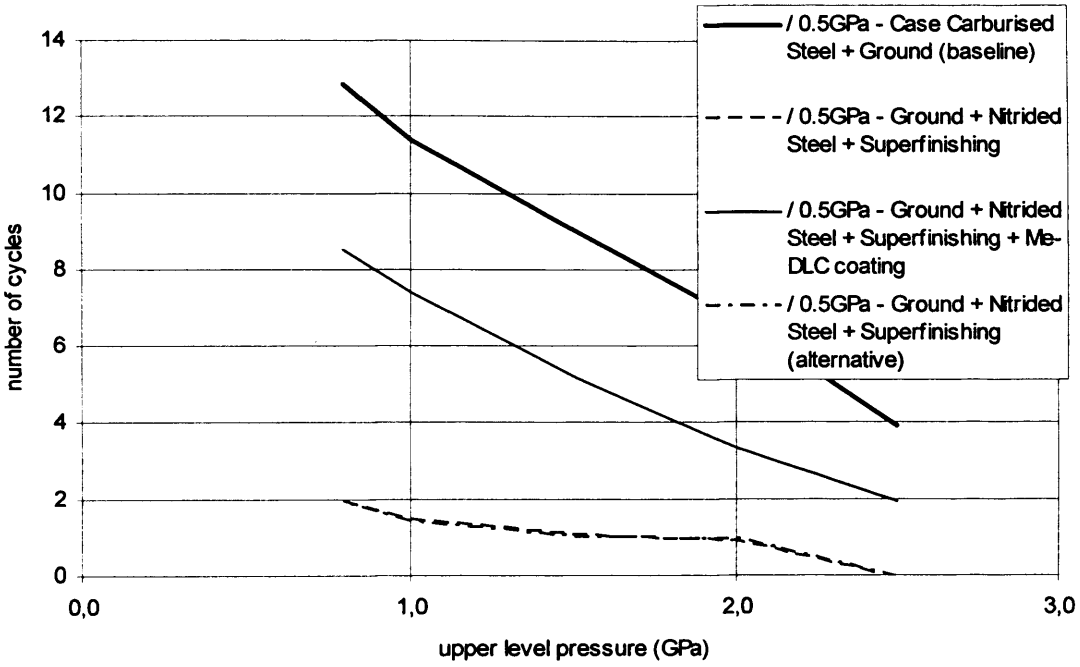

Figure 6.26: Pressure cycle counts obtained for the superfinished configurations with reference to the baseline configuration for a lower pressure cycle limit of 0.5 GPa

CHAPTER 7.

Discussion, conclusions and recommendations for further work

7.1 Experimental work

7.1.1 Work performed on modifying, designing and building rigs

The implementation of a computerised control system on the rig used to perform scuffing tests first used by Patching *et al.* (1994) was judged to be successful. Testing productivity was improved as a result of automatic operation along with the precision of speed and load control as a result of the PID control loop. The speed of the test shafts can now be considered as virtually insensitive to the load, being adjusted instantly when the load varies. The operation is also safer due to the various thresholds in force. Real time data logging allows also for much more flexible processing and presentation of results from the scuffing tests. All these alterations can be judged as successful from the fact that results acquired can be compared directly to the benchmark results as obtained by Patching *et al.* Indeed the "piggy back" approach has allowed the use of the same data acquisition path and the same loading actuator as well as the same electric motor. This advantage was demonstrated when scuffing tests were performed on the baseline ground case carburised steel that exhibited (taking into account the experimental scatter) the same scuffing results for the whole sliding velocity range. This development of the scuffing rig has also aided the design of the control system for the pitting rig.

A new micropitting rig has been designed and built based upon the two discs principle of the scuffing rig. The rig has been design as a fatigue apparatus, capable of sustained operation for many millions of cycles. It includes a heavy duty high speed motor capable of powering high sliding speeds (typically 16 m/s) with typical slide-roll ratios as found in the aerospace industry. The lubrication system which includes exclusively stainless steel piping is capable of running for very long periods of time without inducing any major lubricant pollution. The whole system is mounted with a number of sensors (temperature, speed, resisting torque, load) allowing a precise monitoring of the major test parameters. The whole system is controlled and monitored by a fully computerised control and data acquisition system allowing the full control and data acquisition of the rig through a "Labview" type interface.

To enhance the capabilities of the rig, a new development has taken place allowing in-situ surface texture measurement. This enables acquisition of surface profiles at various stages of a micropitting test so that surface evolution and wear can be monitored as a function of running period.

7.1.2 Experimental investigation of scuffing failure

The first part of the experimental work has added to and confirmed earlier scuffing experiments using axially ground hardened steel surfaces with a gas turbine oil as a lubricant. These were the tests performed by Patching *et al.* (1994). The combination of the new results with Patching's provide a reliable benchmark against which scuffing performance using other substrate materials, substrate coatings and / or surface finish may be assessed.

As in the earlier work of Patching *et al.* (1994) with uncoated case-carburised samples, it was found that in all cases of scuffing with the coated, ground surfaces there was strong evidence of running in of the surfaces before scuffing took place. This effect was particularly evident in the case of the Me-DLC coated samples as outlined in Chapter 5. The surface profiles taken before running and from the un-scuffed parts of the run track show significant modification of the peaks of the surface asperities but with little or no effect on the valley features. In the case of the Me-DLC coated samples the effect produced a near "superfinished" surface which eventually led to scuffing near the centre (rather than at the edges) of the running track which is characteristic of superfinished discs as outlined also previously by Patching *et al.* Evidence of this running in effect is seen during the progress of the test in the behaviour of friction and temperature when running at constant load. In the early stages the friction force remains almost constant during the period of constant load, but at heavier loads there is a tendency for the friction force to decline during the load stage, with a corresponding slight fall in the temperature of both surfaces after the initial rapid increase. With the coated samples running in can produce surfaces of a polished appearance, but the principal mechanism for scuffing for these relatively rough surfaces nevertheless corresponds to side leakage of the lubricant from valley features at the edge of the contact where transverse pressure gradients are high.

A summary of all configurations tested is given in Table 7.1. Sliding speeds, fixed for each test, as mentioned in previous chapters were generally at three levels of 7 m/s, 16 m/s and 20 m/s. This corresponds to a total of nine configurations being tested.

Table 7.1

Summary of configurations tested

Configuration	Substrate	Finish	Coating	No of tests at each sliding speed		
				7 m/s	16 m/s	20 m/s
1*	case carburised	ground	none (reference)	3	1	1
2**	case carburised	superfinished	none	-	2	2
3	case carburised	ground	Me-DLC	3	3	3
4	case-carburised	ground	B_4C	2	4	3
5	nitrided	ground, compound layer off	none	4	3	3
6	nitrided	ground, compound layer on	none	4	3	3
7	nitrided	superfinished	none	-	3	3
8	nitrided	ground	Me-DLC	-	1	-
9	nitrided	superfinished	Me-DLC	-	3	-

* one other test was performed at each of the sliding speeds of 10, 13, 18.5 m/s, plus two other tests at 26 m/s.
** two other tests were performed at each of the sliding speeds of 10, 13, 23 m/s, plus three other tests at 18.5 m/s.

Figure 7.1(a) shows the nine different configurations ranked in terms of average scuffing load capacity at the sliding speed of 16 m/s. In the case of the Me-DLC coating applied to superfinished samples the performance is remarkable as no scuffing occurred under any of the conditions of load and speed investigated. No running in was observed and the mean bulk temperatures of the discs were very low, indicating low friction as shown in Table 7.2 and Figures 7.1(b) and (c).

Table 7.2

Comparison of average mean bulk temperature (T_m) and average traction coefficient (μ) for various selected test configurations at 16 m/s sliding speed (at the scuffing load, W_s, just prior to scuffing).

Config -uration	T_m/°C	μ	W_s/N
(1)	184	0.029	1850
(5)	223	0.031	2387
(8)	236	0.017	4100*
(3)	190	0.017	1648
(4)	157	0.012	3732
(9)	133	0.003	4251*

*maximum load reached without scuffing failure

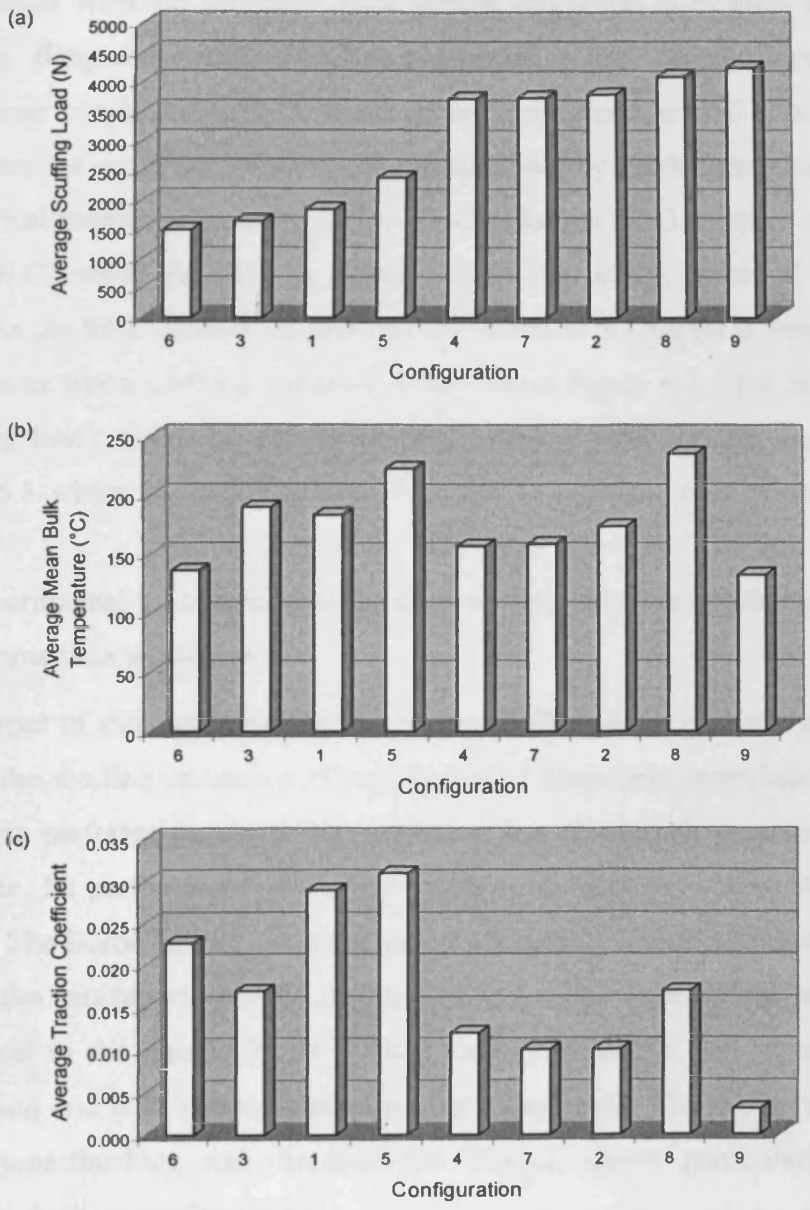

Figure 7.1: **Comparison of performance between the different configurations (defined in Table 7.1) for tests performed at 16 m/s sliding speed. Uncoated configurations added for comparison. (a) scuffing load, (b) average mean bulk temperature at scuffing load; (c) average traction coefficient at scuffing load**

The most outstanding scuffing performance obtained was with the nitrided sample coated with Me-DLC. The adherence of the coating was good and scuffing could not be provoked even at the highest loading available.

As was seen in earlier work on uncoated discs surface roughness is of great importance in relation to scuffing. Jiang and Arnell (2000) as mentioned in previous chapters have studied the effect of substrate roughness on DLC coatings and consider a critical maximum contact pressure that triggers the onset of a wear mode characterised by crack formation and flaking. The suggested critical contact pressure is about 3.7 GPa for the DLC coatings studied. In the case carburised DLC coated samples as considered in this study, levels of peak contact pressure as found in the EHL contact simulations and detailed in Chapter 6 were very similar to this threshold value when scuffing occurred as shown on Figure 6.7. This critical pressure (and corresponding load) could indeed explain the scuffing limit for this configuration as shown in Figure 5.5 where the scuffing load was almost constant over a range of sliding speeds.

In terms of the experimental investigation of scuffing failure, the main conclusions of the study could be summarised as follows:

i. The two types of thin hard coatings investigated show some promise as a means of improving the scuffing resistance of hardened steel discs (and gears) although the Me-DLC coating performs poorly when applied to the benchmark uncoated steel in the ground state. Its performance when applied to a nitrided steel substrate is far more promising. The Boron Carbide coating gave significantly improved performance when applied to the benchmark steel in the ground state. This coating was not tested with nitrided steel in the current study. Boron Carbide coatings also gave significantly lower friction and bulk temperatures than the benchmark. The triple combination of nitriding, superfinishing and diamond-like coating shows particularly impressive performance in these scuffing tests.

ii. The very low traction coefficient and beneficial running in of the Me-DLC coated samples could be explained by a graphitisation process (transformation of sp3 to sp2) of the coating promoted by high contact pressures and flash temperatures at the asperity level and high sliding speeds encountered in these tests. This leads to the coating "wearing out".

iii. From the contact mechanics point of view the greater elastic mismatch between the steel substrate and the coating in the case of the Me-DLC coating compared to Boron

Carbide may explain the fractures and delaminations observed in our tests. Contact pressures at the asperity level as predicted by real, rough contact modelling also suggest that a critical load was reached leading to flaking and delamination type distress. This could explain the relative insensitivity of the scuffing load to sliding speed of Me-DLC coated samples.

7.2 Computer simulations of Micro-elastohydrodynamic lubrication of real rough surfaces

All configurations tested at a sliding speed of 16 m/s were simulated using the solver as developed by Elcoate *et al.* (2001) which included both time-dependent and non-Newtonian behaviour. Digitised real surface data were used obtained from surface profiles taken from samples used in the scuffing tests from an un-scuffed part of the contacting surface. The assumption was made supported by the work of Holmes *et al.*(2003) that the contact can be approximated as a line contact (elliptical ratio in this case of about 4). Results from the smooth configuration are summarised in Table 7.3 in terms of maximum Hertzian pressure, corresponding central film thickness and minimum film thickness. Very low film values of the same order or lower than the average roughness of the contacting surfaces are predicted, except in the case of the superfinished samples. These results confirm the severe nature of EHL under the real conditions in ground gears operating with turbine oils at high temperatures.

The simulations with ground samples exhibit the features of what may be termed "mixed lubrication", i.e. asperity interaction, thin films and intermittent "dry" contact. The severity of these "dry" contacts has been tentatively measured by making a simple count of the number of occurrences of such contacts during a simulation run. Preliminary results of this work show a correlation between contact count and the general severity of conditions as indicated by thin films and high ripple pressures. Maximum pressure peaks encountered and minimum films obtained in the simulations are summarised in Table 7.4. As anticipated by the smooth contact analysis, values of film thickness under rough conditions can be extremely low (or non existent in the case of "dry" contacts) apart from the Me-DLC coated configuration which seems to have failed under a different regime as explained earlier. This is also the case for the Boron carbide coating which exhibited a much better behaviour with no "dry" contact. In all cases pressure peaks under roughness conditions far exceeded the corresponding Hertzian

maximum. In the case of the baseline ground case carburised steel pressure peaks exceeded four times the Hertzian maximum pressure. The high pressure peaks encountered in the case of the Me-DLC coated ground case carburised substrate could have triggered the delamination of the coating as explained earlier. All superfinished configurations showed pressure peaks much lower than the ground counterparts in the simulations. The generation of an effective separating film was also much more effective in the case of the superfinished surfaces and this behaviour was confirmed by lower friction in the actual experiments with superfinished surfaces.

Table 7.3
Simulations results obtained for the smooth case for all tests run at 16 m/s

Test n°	Configuration	P_{max} / GPa	h_{min} / µm	h_{cen} / µm
2	Nitrided steel + Ground + Compound Layer	1.25	0.249	0.285
12	Ground + Nitrided steel	1.40	0.239	0.273
14	Nitrided steel + Ground + Me-DLC coating	1.62	0.232	0.263
17	Case Carburised steel + Ground (baseline)	1.25	0.249	0.285
19	Case Carburised steel + Ground + Me-DLC coating	1.25	0.249	0.285
37	Ground + Nitrided steel + Superfinishing	1.63	0.232	0.263
41	Case Carburised steel + Ground + B_4C coating	1.63	0.232	0.263
46	Ground + Nitrided steel + Superfinishing + Me-DLC coating	1.64	0.232	0.263
48	Ground + Nitrided steel + Superfinishing (alternative)	1.63	0.232	0.263

Table 7.4
Simulations results obtained for the rough case for all tests run at 16 m/s

Test n°	P_{max} / GPa		hmin (µm)
	Value	Corresp h_{min} /µm	Value
2	3.08	-0,975*	-1,540*
12	3.12	0.000	0.000

Table 7.4 (continued)

Test n°	P_{max} / GPa		hmin (μm)
14	3.58	0,063	0,011
17	4.18	0,000	0,000
19	3.85	0,037	0,000
37	2.42	0,156	0,138
41	3.40	0,099	0,016
46	error on slow surface profile		
48	2.38	0,167	0,124

*: denotes limits of the model

The use of objective performance parameters in the simulations such as $\Phi(p)$, $\Phi(h)$ and the pressure cycle counts enables us, in principle, to discriminate between different lubricated, rough surface contacts. For example, these parameters would indicate that the nitrided steel with the compound layer left on will perform better than the baseline case carburised steel. However, this configuration would probably be rejected in practice (certainly in aerospace practice) because of the inherently fragile nature of the white layer.

There is also theoretical support for using an ultra hard coating on the ground substrates particularly for the nitrided substrate, and the Boron Carbide type coating on the case carburised substrate. The exception is the case of the coated, ground nitrided surface that exhibited a higher pressure cycling at the higher pressures. This behaviour may favour the development of micropitting. There is very clear advantage of using a superfinished treatment based on the performance parameters used in this study. It is may be less advantageous to use a coating on an already superfinished surface as the pressure cycling shows an increase. The simulations did not show any significant difference in performance between the baseline superfinishing treatment and the alternative process.

The main contradiction found in the simulation work was between predicted and observed performance of the ground nitrided steel behaviour. The theoretical trend in terms of film formation is relatively poor, and this is at odds with its good scuffing performance in the tests.

7.3 Recommendations for further work

This work has allowed consolidation of an existing benchmark in terms of scuffing behaviour of ground case carburised steel and has initiated a new bench mark in terms of scuffing behaviour for nitrided and coated substrates. This new benchmark also needs to be consolidated and more tests need to be performed to confirm the trends seen in this project. There is a need for more work on the scuffing performance of nitrided material which shows promise, particularly when coated. The relatively mediocre performance of the Me-DLC coated samples also requires further investigation.

Regarding the EHL simulations it would be advantageous to develop a model incorporating the elastic properties (Young modulus, Poisson ratio) and thickness of the coating so as to better understand the physical effect of the coating in terms of pressure and film generation. The simulation solver should also be developed to include the transient heating effect within the contact (flash temperature). This should also include the thermal properties of the coating.

Finally the micropitting bench which was developed as part of this project should be used to carry out parallel studies of micropitting behaviour on the same types of finish and coating used in the present study.

APPENDIX A.

Data conditioning computing program

```
!  CONVDATA.f90
!
!  FUNCTIONS:
!     CONVDATA      - Entry point of console application.
!

!****************************************************************************
!
!  PROGRAM: CONVDATA
!
!  PURPOSE:  Entry point for the console application.
!
!****************************************************************************

!     program CONVDATA

        module globals

! Variables
      real z(1:100000)
      real wf(0:100000)
      real ynew(1:100000)
      character*20 datfile,convfile
        integer i,ncut,j,k,jmin,jmax,ilow,ihigh,numpts,iv,itot2,
     &       istart,iend,istep
      real zscalemm,dxmm,dxmic,zscalemic,numstay,inc,rnum
      real cutmm,a,s,s1,s2,s4,nwf,total,maxpeak,minvalley,hmax,
     &         raval2,sumsq,mline,aby,pi,nt,tlength,slength

        end module globals

!***********************
! Body of CONVDATA
!***********************

        use globals
        implicit none

      print*,'ENTER YOUR .PRF FILE'
      read*, datfile
      print*,'SPECIFY THE NAME OF YOUR CONVERTED FILE'
      read*, convfile
      open (unit=10,file=datfile,status='old')
      open (unit=11,file=convfile,status='unknown')
        open (unit=22,file='temp22.dat',status='unknown')
        open (unit=21,file='temp21.dat',status='unknown')
      read (10,*)
      read (10,*)
      read (10,*)
      read (10,500) rnum,zscalemm
        numpts=rnum
500     format (4X,E14.6,3X,E14.6)
```

```
        read (10,*)
      read (10,*)
      read (10,501) dxmm
501   format (10X,E14.6)
      read (10,*)
      read (10,*)
      read (10,*)
      do 10 i=1,numpts
      read (10,*) z(i)
10    continue
        tlength=numpts*dxmm
      print*,'THE NUMBER OF Z POINTS OF YOUR .MOD FILE IS',numpts
      print*,'THE ASSESSMENT LENGTH WAS',tlength,'mm'
      print*,'Z HEIGTHS WILL APPEAR IN MICRONS IN THE CONVERTED FILE'

!DETERMINE NEAREST NO OF ORDINATE SPACINGS IN THE CUT-OFF
      print*,'INPUT NOW THE CUT-OFF YOU WANT TO USE IN mm'
      read*, cutmm
      dxmic=dxmm*1000
      ncut=1000*cutmm/dxmic
! DETERMINE ORDINATES OF THE FILTER WEIGHTING FUNCTION  (WF)
      pi=4*atan(1.0)
      s=1.0/3.0
      s1=1+s
      s2=1-s
      s4=s1
      wf(ncut) = s1
      do 20 i=1,ncut
      j=i+ncut
      a=i/real(ncut)
      wf(j)=sin(s1*pi*a)*sin(s2*pi*a)/((s2*pi*a)*(s2*pi*a)/s2)
      wf(ncut-i)=wf(j)
20    continue
      total=0
      do 30 j=0,2*ncut
      total=total+wf(j)
30    continue
      nt=0
      do 40 k=0,2*ncut
      nwf=wf(k)/total
      nt=nt+nwf
      wf(k)=nwf
40    continue
      print*,'nt=',nt
      jmin=1
      jmax=numpts
      ilow=jmin+ncut
      ihigh=jmax-ncut
      itot2=ihigh-ilow+1
      maxpeak=0
      minvalley=0
      hmax=0
      raval2=0
      sumsq=0

! ******************* main filtering loop ************************
      do 50 i=ilow,ihigh
      mline=0
      do 60 k=0,2*ncut
      j=i-ncut+k
      mline=mline+wf(k)*zscalemm*z(j)*1000
```

```
60    continue

! DEDUCT MEAN LINE FROM PROFILE
      ynew(i)=zscalemm*z(i)*1000-mline
       aby=abs(ynew(i))
       sumsq=sumsq+aby*aby
      if (aby.gt.hmax) then
      hmax=aby
      endif
      if (ynew(i).gt.maxpeak) then
      maxpeak=ynew(i)
      endif
      if (ynew(i).le.minvalley) then
      minvalley=ynew(i)
      endif
      raval2=raval2+aby
50    continue
      raval2=raval2/itot2
! ***************** end of main filtering loop *****************

      print*,'THE Ra VALUE OF THE PROFILE IS'
      print*,'Ra=',raval2,'microns'

      do i=1,numpts
      write (22,*) z(i)*zscalemm*1000,',',ynew(i)
      enddo

        call input
        call output

      end


        subroutine input
        use globals
        implicit none
        integer :: key1
        print*
        print*,'INPUT LENGTH WANTED TO BE SIMULATED (mm):'
        read(*,*)slength
        print*
        if(slength>tlength) then
          print*,'*** WARNING *** THE TOTAL LENGTH IS ',tlength,' mm'
          print*,'WHICH IS LESS THAN THE LENGTH WISH TO BE SIMULATED'
          print*,'SO THE LENGTH WISHED TO BE SIMULATED IS RESET TO '
          print*,' TOTAL LENGTH i.e. ', tlength,'  mm'
          slength=tlength
          istart=1
          iend=numpts
        else
          print*, 'CHOOSE THE POSITION OF SIMULATED PART'
          print*, '1 --- AT BEGINNING'
          print*, '2 --- IN THE MIDDLE'
          print*, '3 --- AT END'
          read(*,*)key1
          if(key1==1) then
            istart=1
            iend=numpts*slength/tlength
          endif
          if(key1==2) then
            istart=numpts/2-numpts*0.5*slength/tlength
```

```
      iend=numpts/2+numpts*0.5*slength/tlength
    endif
    if(key1==3) then
      istart=numpts-numpts*slength/tlength
      iend=numpts
    endif
  endif
  print*
  print*, 'INTERVAL OF MEASURE POINTS IS ',dxmm, 'mm'
  print*
  print*, 'INPUT MAGNIFICANT FACTOR :'
  print*
  read(*,*) istep
  return
  end

  subroutine output
  use globals
  implicit none
write (11,*)
write (11,*)
write (11,*) dxmic*istep
write (21,*) dxmic*istep
write (11,*) raval2
write (11,*) 1.0
write (11,*) cutmm
do i=1,18
write (11,*)
enddo
write (11,*) (iend-istart)/istep+1
write (21,*) (iend-istart)/istep+1
do i=1,17
write (11,*)
enddo
write (11,*) '*****'
  do i=istart,iend,istep
    write(11,*) ynew(i)
    write(21,*) dxmm*i,ynew(i)
  enddo
write (11,*) '+++++'
  print*
  print*,'ACTUAL ASSESMENT LENGTH IS ',(iend-istart+1)*dxmm,' mm'
  print*,'INTERVAL BETWEEN POINTS IS ',istep*dxmm, 'mm'
  print*, 'THE NUMBER OF POINTS IS ',(iend-istart)/istep+1
  return
  end
```

References.

Archard J. F., 1957, Elastic deformation and the laws of friction, Proceedings of the Royal Society of London, Vol. A243, pp. 190-205.

Bartz W. J., 1993, Lubrication of gearing: lubricants and their properties, design of gears, practical gear lubrication, failure analysis; translated from the German by Pam Chatterley; English translation edited by A.J. Moore. London: Mechanical Engineering Publications.

Bell, J. C., Dyson, A., 1972, The effect of some operating factors on the scuffing of hardened steel discs, Elastohydrodynamic lubrication, 1972 Symposium, Proc. Instn. Mech. Engrs. Paper C11/72, pp. 61-67.

Bell, J. C., Dyson, A., Hadley, J. W., 1975, Effects of rolling and sliding speeds on the scuffing of lubricated steel discs, ASLE Transactions, v 18, n 1, pp. 62-73.

Bell, T., 1973, Survey of the heat treatment of engineering components, London, The Iron and Steel Institute.

Bell, T., 1993, Engineering the Surface to Combat Wear, in Proceedings of the 19th Leeds-Lyon symposium on Tribology: Thin Films in Tribology Leeds 1992, Dowson, D et al. Ed., Elsevier, pp. 27-37.

Berthe, D., Michau, B., Flamand, L. & Godet, M., 1978, Effect of roughness ratio and hertz pressure on micro-pits and spalls in concentrated contacts: theory and experiments, Proceedings of the 4th Leeds-Lyon Symposium on Tribology: Surface Roughness Effects in Lubrication, Lyon 1977, Dowson, D. et al. Ed., MEP Ltd., pp. 233-238.

Berthe, D., Flamand, L., Fouchet, D., Godet, M., 1980, Micropitting in Hertzian contacts, Trans ASME, J. of Lubrication Technology, Vol. 102, pp. 478-89.

Bewilogua K., Cooper, C. V., Specht, C., Schroder, J., Wittorf, R., Grischke, M., 2000, Effect of target material on deposition and properties of metal-containing DLC (Me-DLC) coatings, Surface and Coatings Technology, Vol. 127, pp. 224-232.

Blok, H., 1937, Surface temperature under extreme pressure conditions, proceedings of the 2nd World Petroleum Congress, Paris, France, pp. 471-486.

Blok H., 1937, Theoretical study of temperature rise at surfaces of actual contact under oiliness lubricating oil conditions, Proceedings of the Institution of Mechanical Engineers, Vol. 2, pp. 222-235.

Blok, H., 1939, Seizure Delay Method for Determining the Protection Against Scuffing Afforded by Extreme Pressure Lubricants, Journal of the Society of Automotive Engineers, Vol. 44, No. 5, pp. 193-210 and 220.

Bloyce A., 2001, private communication, Balzers UK.

Braza, J. F., 1992, Rolling contact fatigue and sliding wear performance of ferritic nitrocarburized M-50 steel, Tribology Transactions, Vol. 35, n 1, pp. 89-97.

Britton, R. D., Elcoate, C. D., Alanou, M. P.; Evans, H. P.; Snidle, R. W., 2000, Effect of surface finish on gear tooth friction, Journal of Tribology, Transactions of the ASME, v 122, n 1, pp. 354-360.

Buckingham, E., 1988, Analytical mechanics of gears, New York : Dover.

Cameron, A., 1954, Surface failure of gears, J. Institute of Petroleum, Vol. 40, pp. 191-202.

Cermignani, W., Robinson, M. G., Hu, T., Stiehl, L., Rafaniello, W., Fawcett, T., Marshall, P., Rozeveld, S., 1998, Processing, properties and performance of high volume sputter deposited boron-carbon coatings, Proceedings, 41st Annual Technical Conference - Society of Vacuum Coaters, pp. 66-74.

Cheng, H. S., Dyson, A., 1978, Elastohydrodynamic lubrication of circumferentially ground discs, ASLE Trans., Vol. 21, No. 1, pp. 25-40.

Chittenden, R.J., Dowson, D, Dunn, J.F. and Taylor, C.M, 1985, A theoretical analysis of the isothermal elastohydrodynamic lubrication of concentrated contacts, Proc. Roy. Soc. Lond., A391, pp. 245-269, pp. 271-294.

Conry, T. F., Wang, S., Cusano, C., 1986, Reynolds-Eyring equation for elastohydrodynamic lubrication in line contacts, American Society of Mechanical Engineers (Paper), 86-TRIB-53, 7p.

Coy, J. J., Townsend, D. P., Zaretsky, E. V., 1985, Gearing, NASA Reference Publication 1152, AVSCOM Technical Report 84-C-15.

Cutiongco, E. & Chung, Y. W., 1994, Prediction of scuffing failure based on competitive kinetics of oxide formation and removal application to lubricated sliding of AISI 52100 steel on steel, STLE Tribology transactions, Vol. 37, n°3, pp. 622-628.

Czichos, H., 1977, Influence of asperity contact conditions on the failure of sliding elastohydrodynamic contacts, Wear, v 41, n 1, pp. 1-14.

Davies, D.P. & Gittos, B.C., 1989, Gear Steels for Future Helicopter Transmissions, Proceedings of the IMechE, Vol. 203, pp. 113-121.

DiRusso, R., 1986, Advances and Applications of Pyrowear 53 in Helicopter Transmission Systems, Presented at the Rotary Wing Propulsion System Specialist Meeting, Williamsburg, Virginia, pp. 8: 1-8.

Donnet, C., 1998, Recent progress on the tribology of doped diamond-like and carbon alloy coatings: a review, Surface & Coatings Technology, Vol. 100-101, pp. 180-186.

Dowson, D., Higginson G. R., 1959, A numerical solution to the elasto-hydrodynamic problem, J. Mech. Eng. Sci. Vol. 1(1), pp. 6-15.

Dowson, D., Higginson G. R., 1960, The effect of material properties on the lubrication of elastic rollers, J. Mech. Eng. Sci., Vol. 2(3), pp. 188-194.

Dowson, D. and Higginson, G. R. Elastohydrodynamic Lubrication, Pergamon Press, Oxford, 1966.

Dowson, D., 1992, Engineering at the interface, Proc. Instn. Mech. Engrs., Vol. 206, pp. 149-165.

Dudley, D. W., 1994, Handbook of practical gear design, Lancaster, Pa : Technomic Pub. Co.

Dyson, A., 1975, Scuffing – a review, Tribology International, Vol. 8, Pt. 1, pp. 77-87, Pt. 2, pp.117-122.

Dyson, A., 1977, Elastohydrodynamic lubrication of Rough surfaces with lay in the direction of motion, Surface and roughness effects in lubrication, Proceedings of the 4th Leeds-Lyon symposium on tribology, Lyon, France, Dowson et al. ed. Butterworths, London, pp. 201-209.

Dyson, A., 1976, The failure of elastohydrodynamic Lubrication of circumferentially ground rough discs, Prc. Inst. Mech. Eng., Vol. 190, n°1, pp. 52-76.

Dyson, A., Evans H. P., Snidle R.W., 1992, A simple accurate method for calculations of stresses and deformations in elliptical Hertzian contact, Proc. Instn. Mech. Engrs., Part C, Vol. 206, n 2, pp. 139-141.

Eckardt, T., Bewilogua, K., van der Kolk, G., Hurkmans, T., Trinh, T., Fleischer, W., 2000, Improving tribological properties of sputtered boron carbide coatings by process modifications, Surface and Coatings Technology, Vol. 126, pp. 69-75.

Elcoate, C. D., Evans, H. P., Hughes, T. G., Snidle, R. W., 2001, Transient elastohydrodynamic analysis of rough surfaces using a novel coupled differential deflection method, Proceedings of the Institution of Mechanical Engineers, Part J: Journal of Engineering Tribology, Vol. 215, n 4, pp. 319-338.

Elsharkawy, A. A., Hamrock, B. J., 1991, Subsurface stresses in micro-EHL line contacts, Journal of Tribology, Transactions of the ASME, Vol. 113, n 3, p 645-655.

Enthoven, J.C., Cann, P.M., Spikes, H.A., 1993, Temperature and scuffing, STLE Tribology transactions, Vol. 36, n°2, pp.258-266.

Errichello, R., 2000, State of the art review: Micropitting, Geartech, Presented at the 55th STLE annual meeting, Nashville, May 7-11 2000.

Evans, C. R., Johnson, K. L., 1986, Rheological properties of elastohydrodynamic lubricants, Proceedings of the Institution of Mechanical Engineers, Part C: Mechanical Engineering Science, Vol. 200, n C5, pp. 303-312.

Evans, H. P. and Snidle, R W, 1996, A model for elastohydrodynamic film failure in contacts between surfaces having transverse finish, Trans ASME Jn. of Tribology, Vol. 118, pp. 847-857.

Evans, H. P., Hughes, T.G., 2000, Evaluation of deflection in semi-infinite bodies by a differential method, Proceedings of the Institution of Mechanical Engineers, Part C: Journal of Mechanical Engineering Science, Vol 214, n 4, pp. 563-584.

Goglia P. R., Cusano, C., Conry T. F., 1984, The effects of surface irregularities on the elastohydrodynamic lubrication of circular contacts. Part I – single irregularities; Part II – wavy surfaces, Trans. ASME, Journal of Tribology, v 106 pp. 104-112, 113-119.

Greenwod, J. A., Williamson J. B. P., 1966, Contact of nominally flat surfaces, Proceedings of the Royal Society of London, Vol. A295, pp. 300-319.

Grubin A. N., Vinogradova I. E., 1949, Fundamentals of the hydrodynamic theory of lubrication of heavily loaded cylindrical surfaces, Series Ed. Ketova, K. F., Central Scientific Research Institute for Technology and Mechanical Engineering (Moscow), Book No 30, (DSIR translation No 337).

Halling J., 1978, Principles of Tribology, Houndmills, Basingstoke, Hampshire and London, Macmillan Education Ltd.

Hans M., Buchel R., Grischke M., Hobi R. and Zach M., 2000, High-volume PVD coating of precision components of large volumes at low process costs, Surf. Coat. Technol. 123, pp. 288-293.

Harris, S.J., Weiner, A. M., Meng, Wen-Jin, 1997, Tribology of metal-containing diamond-like carbon coatings, Wear, Vol 211, pp. 208-217.

Hertz, H., 1881, On the contact of elastic solids, J. reine und angrew. Math., 92, 156-171.

Hirst W., Hollander A. E., 1974, Surface finish and damage in sliding, Proc. R. Soc. A 337, pp. 379-394.

Höhn, B-R, Michaelis, K, Kopatsch, F, 2001, Systematic investigations on the influence of Viscosity Index improvers on EHL film thickness, in "Gear Technology", Nov./Dec. 2001, Randall Publishing Ed.

Holmberg, K., Matthews, A., Ronkainen, H., 1998, Coatings tribology - contact mechanisms and surface design, Tribology International, Vol. 31, pp. 107-120.

Holmes, M.J.A., Evans, H.P., Hughes, T.G., Snidle, R.W., 2003, Transient elastohydrodynamic point contact analysis using a new coupled differential deflection method part 2: Results, Proceedings of the Institution of Mechanical Engineers, Part J: Journal of Engineering Tribology, Vol 217, n 4, pp. 305-322.

Hu, T., Steihl, L., Rafaniello, W., Fawcett, T., Hawn, D. D., Mashall, J. G., Rozeveld, S. J., Putzig, C. L., Blackson, J. H., Cermignani, W., Robinson, M. G., 1998, Structures and properties of disordered boron carbide coatings generated by magnetron sputtering, Thin Solid Films, Vol. 332, pp. 80-86.

Hutchings, I. M., 1992, Tribology: friction and wear of engineering materials, London, Edward Arnold.

Jatczak, C. F., 1978, Speciality carburising steels for elevated temperature service, Metal Progress, Vol. 113, n 4, pp. 70-78.

Jiang, Jiaren, Arnell, R. D., 2000, The effect of substrate surface roughness on the wear of DLC coatings, Wear, Vol. 239, pp. 1-9.

Johnson K. L., Greenwood J. A., Higgingson J. G., 1985, The contact of elastic regular wavy surfaces, Int. J. Mech. Sci., 27, pp. 383-396.

Johnson, K. L., 1985, Contact Mechanics, Cambridge University Press.

Ju Y., Farris T. N., 1996, Special analysis of two-dimensional contact problem, Trans. ASME, Journal of Tribology, v 118 pp. 320-328.

Kweh, C. C., Evans, H. P., Snidle R. W., 1989, Micro-elastohydrodynamic lubrication of an elliptical contact with transverse and three dimensional sinusoidal roughness, ASME Journal of Tribology, Vol. 111, pp. 577-583.

Krantz T. L., Alanou M. P., Evans H. P., and Snidle R. W., 2001, Surface fatigue lives of case-carburised gears with an improved surface finish, Trans. ASME, Journal of Tribology, v 123, Issue 4, pp. 709-716.

Le Huu, T., Zaidi, H., Paulmier, D., Voumard, P., 1996, Transformation of sp^3 to sp^2 sites of diamond like carbon coatings during friction in vacuum and under water vapour environment, Thin Solid Films, Vol. 290-291, pp. 126-130.

Lee K. M., Cheng H. S., 1973, Effects of surface asperity on elastohydrodynamic lubrication, NASA CR-2195, Washington, DC.

Littmann, W.E., Widner, R.L., 1966, Propagation of Contact fatigue from Surface and Subsurface Origins. Trans. ASME J. of Basic Engineering, Vol. 88, pp. 624-635.

Liu, E., Blanpain, B., Shi, X., Celis, J. -P., Tan, H. S., Tay, B. -K., Cheah, L. K., Roos, J. R., 1998, Tribological behaviour of different diamond-like carbon materials, Surface & Coatings Technology, Vol. 106, pp. 72-80.

Lubrecht, A. A., ten Napel, W. E., Bosma, R., 1988, The influence of longitudinal and transverse roughness on the elastohydrodynamic lubrication of circular contacts, ASME Journal of Tribology, Vol. 110, pp. 421-426.

Martin, M. J., Alanou, M. P., Evans, H. P., Snidle, R. W., Kawamura, H., Dodd, A., 2001, Scuffing performance of M50 bearing steel lubricated with a gas turbine engine oil at high sliding speeds, Tribology Transactions, Vol. 44, n 3, pp. 465-471.

Merritt, H. E., 1962, Gear tooth contact phenomena, Proc. Instn. Mech. Engrs. London, 176, No. 7., 141.

Meyers N. O., Characterisation of surface roughness, 1962, Wear, 5, p. 182.

Mridha S., Jack D. H., 1982, Characterisation of nitrided 3% chromium steel, Metal Science, Vol. 16, pp. 398-404.

Oliveira, S. A. G., Bower, A. F., 1996, Analysis of fracture and delamination in thin coatings subjected to contact loading, Wear, Vol. 198, pp. 15-32.

Olver, A. V., 1984, Micropitting and asperity deformation, in "Proceedings of the 10th Leeds-Lyon symposium on Tribology: Developments in Numerical and Experimental Methods Applied to Tribology", Lyon 1983, Dowson, D. et al. Ed., Butterworths, pp. 319-324.

Olver, A. V., Spikes, H. A., Macpherson P. B., 1986, Wear in rolling contact, Wear, Vol. 112, pp.121-144.

Olver, A.V, Cole, S.J., Sayles, R.S., 1993, Contact stresses in nitrided steels, in "Proceedings of the 19th Leeds-Lyon Symposium on Tribology: Thin films in Tribology", Leeds 1992, Dowson, D. Ed., Elsevier, pp. 71-80.

Olver, A.V., 1997, Correlation factors for the 2D coated Hertzian contact problem, Wear, Vol. 212, n 2, pp. 265-267.

Onions, R. A., Archard, J. F., 1974, Pitting of gears and discs, Inst Mech Eng (Lond) Proc, Vol. 188, n 54, pp. 673-682.

Patching, M. J., 1994, The effect of surface roughness on the micro-elastohydrodynamic lubrication and scuffing performance of aerospace gear tooth contacts, PhD Thesis, Cardiff University.

Patching, M. J., Kweh C.C., Evans H. P., Snidle R. W., 1995, Conditions for scuffing failure of ground and superfinished steel disks at high sliding speeds using a gas turbine engine oil, Trans. ASME, v 117 pp. 482-489.

Patir, N., Cheng, H. S., (1978), An average flow model for determining effects of three dimensional roughness on partial hydrodynamic lubrication, ASME Journal of Tribology, Vol. 100(1), pp. 12-17.

Petrusevich, A. I., 1951, Fundamental conclusions from the contact-hydrodynamic theory of lubrication, Izvestiya Akademii Nauk SSSR (OTN) 2, 1-11. (Ministry of Defense Translation No. 293).

Plumet, S., Dubourg, M. -C., 1998, A 3-D model for a multilayered body loaded normally and tangentially against a rigid body: Application to specific coatings, Journal of Tribology, Trans. ASME, Vol. 120, pp. 668-675.

Poon C. Y., Sayles R. S., 1989, Frictional transitions in boundary lubrication sliding, 2nd Int. Conf. on Combustion Engines – Reduction of Friction and Wear (London: Institute of Mechanical Engineers).

Reigada D.C., Prioli R., Jacobsohn L. G., Freire Jr. F. L., 2000, Boron carbide films deposited by a magnetron sputter-ion plating process: film composition and tribological properties, Diamond and Related Materials, Vol. 9 pp. 489-493.

Reynolds O., 1886, On the theory of lubrication and its application to Mr Beauchamp Tower's experiments, including an experimental determination of the viscosity of olive oil, Phil Trans. R. Soc., 177, pp. 157-234.

Sadegui F., Sui P. C., 1990, Thermal elastohydrodynamic lubrication of rough surfaces, Trans. ASME, Journal of Tribology, v 111 pp. 56-62.

Sainsot, P., Leroy, JM., Villechaise, B., 1990, Effect of surface coatings in a rough normally loaded contact, in "Proceedings of the 17th Leeds-Lyon Symposium on Tribology", Dowson, D. Ed., Elsevier, pp. 151-156.

Schlicht, H. & Zwirlein, O., 1980, Varying Heat Treatment Parameters to Optimize Material and Rolling Contact Fatigue Strength, Trans. ASME J. Heat Treating, Vol. 1, No.3, pp.73-80.

Seager, D. L., 1976, Separation of gear teeth in approach and recess, and the likelihood of corner contact, ASLE Trans, v 19, n 2, p 164-170.

Sharif K. J., Barragan de Ling FdM, Martin M. J., Alanou M. P., Evans H. P., Snidle R. W., 2000, Film thickness predictions for elastohydrodynamic elliptical contacts over a wide range of radius ratios with consideration of side starvation, Proc. of the Inst. Mech. Eng., Part J, Journal of Engineering Tribology, Vol. 214, pp. 63-78.

Shotter, B. A., 1981, Micro-pitting, its characteristics and implications, Proceedings of the Institute of Petroleum Conference on Performance and Testing of Gear Oils and Transmission Fluids, pp.53-65.

Sproul, W. D., 1996, Physical vapour deposition tool coatings, Surface & Coatings Technology, Vol. 81, pp. 1-7.

Stanley, H. M., Kato, T., 1997, An FFT –based method for rough surface contact, Trans. ASME, Journal of Tribology, Vol. 119, pp. 481-485.

Tao, J., Hughes, T.G., Evans, H.P., Snidle, R.W., Hopkins, N.A., Talks, M., Starbuck, J.M., 2003, Elastohydrodynamic lubrication analysis of gear tooth surfaces from micropitting tests, Journal of Tribology, Vol. 125, n 2, pp. 267-274.

Teeter, F. J., Berger, M., 1996, Wear protection for gears, Gear Technology, Vol. 13, pp. 27-29.

Townsend, D. P., 1983, Status of understanding for gear materials, NASA Conference Publication, v 2, pp. 795-809.

Voevodin, A. A., O'Neill, J. P., Zabinski, J. S., 1999, Tribological performance and tribochemistry of nanocrystalline WC/amorphous diamond-like carbon composites, Thin Solid Films, Vol. 342, pp. 194-200.

Wang, M., Schmidt, K., Reichelt, K., Dimigen, H., Hubsch, H., 1992, Characterization of metal-containing amorphous hydrogenated carbon films, Journal of Materials Research, Vol. 7, pp. 667-676.

Wanstrand, O., Larsson, M., Hedenqvist, P., 1999, Mechanical and tribological evaluation of PVD WC/C coatings, Surface & Coatings Technology, Vol. 111, pp. 247-254.

Webster, M. N., Norbart, C. J. J., 1995, Investigation of micropitting using a roller disk machine, ASME Tribol Trans, Vol. 38, n 4, pp. 883-893.

Webster, M. N., Sayles R. S., 1986, A numerical model for the elastic frictionless contact of real surfaces, Trans. ASME, Journal of Tribology, v 108, pp. 314-320.

Whitehouse D. J., Archard J. F., 1970, The properties of random surfaces of significance in their contact, Proc. R. Soc., A 316, pp.97-121.

Wilkinson, C. M. R., 1998, The durability of highly loaded, lubricated, case hardened steel gears, PhD Thesis, Imperial College of Science, Technology and Medicine, London.

Winter, H., Weiss, T., 1981, Some Factors Influencing the Pitting, Micro-Pitting (Frosted Areas) and Slow Speed Wear of Surface Hardened Gears, ASME J. of Mechanical Design, Vol. 103, pp. 499-505.

Zaidi, H., Frene, J., Senouci, A., Schmitt, M., Paulmier, D., 2000, Carbon surface modifications during sliding test and friction behaviour of carbon thin films against XC 48 steel, Surface and Coatings Technology, Vol. 123, pp. 185-191.